

2007

Geologic and geotechnical characterization for liquefaction-induced deformation

Anne M. Rosinski
San Jose State University

Follow this and additional works at: https://scholarworks.sjsu.edu/etd_theses

Recommended Citation

Rosinski, Anne M., "Geologic and geotechnical characterization for liquefaction-induced deformation" (2007). *Master's Theses*. 3563.
DOI: <https://doi.org/10.31979/etd.an6e-yjer>
https://scholarworks.sjsu.edu/etd_theses/3563

This Thesis is brought to you for free and open access by the Master's Theses and Graduate Research at SJSU ScholarWorks. It has been accepted for inclusion in Master's Theses by an authorized administrator of SJSU ScholarWorks. For more information, please contact scholarworks@sjsu.edu.

INFORMATION TO USERS

This manuscript has been reproduced from the microfilm master. UMI films the text directly from the original or copy submitted. Thus, some thesis and dissertation copies are in typewriter face, while others may be from any type of computer printer.

The quality of this reproduction is dependent upon the quality of the copy submitted. Broken or indistinct print, colored or poor quality illustrations and photographs, print bleedthrough, substandard margins, and improper alignment can adversely affect reproduction.

In the unlikely event that the author did not send UMI a complete manuscript and there are missing pages, these will be noted. Also, if unauthorized copyright material had to be removed, a note will indicate the deletion.

Oversize materials (e.g., maps, drawings, charts) are reproduced by sectioning the original, beginning at the upper left-hand corner and continuing from left to right in equal sections with small overlaps.

ProQuest Information and Learning
300 North Zeeb Road, Ann Arbor, MI 48106-1346 USA
800-521-0600

UMI[®]

**GEOLOGIC AND GEOTECHNICAL CHARACTERIZATION FOR
LIQUEFACTION-INDUCED DEFORMATION**

A Thesis

Presented to

The Faculty of the Department of Geology

San José State University

In Partial Fulfillment

Of the Requirements for the Degree

Master of Science

by

Anne M. Rosinski

December 2007

UMI Number: 1452085

Copyright 2007 by
Rosinski, Anne M.

All rights reserved.

UMI[®]

UMI Microform 1452085

Copyright 2008 by ProQuest Information and Learning Company.
All rights reserved. This microform edition is protected against
unauthorized copying under Title 17, United States Code.

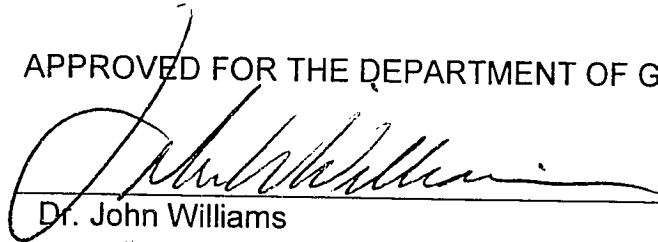
ProQuest Information and Learning Company
300 North Zeeb Road
P.O. Box 1346
Ann Arbor, MI 48106-1346

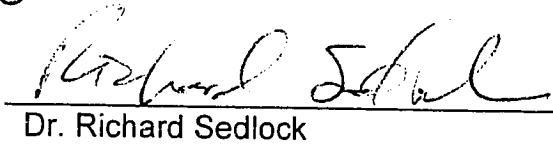
© 2007

Anne M. Rosinski

ALL RIGHTS RESERVED


APPROVED FOR THE DEPARTMENT OF GEOLOGY


Dr. John Williams


Dr. Richard Sedlock


Keith L. Knudsen, California Geological Survey

APPROVED FOR THE UNIVERSITY

 01/09/08

ABSTRACT

GEOLOGIC AND GEOTECHNICAL CHARACTERIZATION FOR LIQUEFACTION-INDUCED DEFORMATION

By Anne M. Rosinski

The focus of this research is to provide a geotechnical and geologic characterization of the tectonically active northern Santa Clara Valley, California. This characterization is combined with new models for predicting strain to develop 1:24,000-scale hazard maps based on laboratory testing and improved understanding of processes that affect prediction of surface deformation resulting from liquefaction.

Qualitative geologic information and quantitative geotechnical boring log information are linked together; each layer in each boring is assigned a geologic map unit designation thereby, expanding the description of each geologic unit to include quantifiable geotechnical characteristics. Maps produced in this study group geologic map units with similar amounts of estimated volumetric and shear strain. The maps produced in this study reveal that late Holocene deposits are likely to experience the greatest liquefaction-induced strain, whereas older deposits are likely to experience significantly less horizontal and vertical strain in future earthquakes.

ACKNOWLEDGMENTS

This project was sponsored in part by the University of California at Berkeley's Pacific Earthquake Engineering Research Center's Program of Applied Earthquake Engineering Research of Lifeline Systems supported by the State Energy Resources Conservation and Development Commission and the Pacific Gas & Electric Company. The financial support of the PEARL sponsor organizations, including Pacific Gas & Electric Company, the California Energy Commission, and the California Department of Transportation, is acknowledged. This work made use of the Earthquake Engineering Research Center's Shared Facilities supported by the National Science Foundation under Award #EEC-9701568. The author wishes to thank Keith Knudsen, Dr. Raymond Seed, Dr. Jiaer Wu, Cliff Roblee, Michael Riemer and Tom Shantz for their guidance and support. In addition, the author wishes to thank Dr. John Williams, Dr. Richard Sedlock, Dr. Rhea Williamson, Dr. Carl Wentworth, Dr. John Tinsley, Seena Hoose, and Tom Moore. A number of California Geological Survey personnel have provided support, including Charles Real, Teri McGuire, Diane Vaughn, Marvin Woods, and Elise Mattison. Geotechnical borings were obtained from a variety of organizations and jurisdictions, including: Santa Clara Valley Water District, City of San Jose, City of Milpitas, URS Corporation, William Lettis & Associates, and Cal Trans. Finally, the author wishes to thank a number of family and friends for their continued support, including my parents Gene and

Anne, my friends Eva and Elise for their help, patience and advice editing, as well as Pete, Katie, Terry, Katita, Marshall, Chris, Rob, Kit, Shelly, Rick and Cindy.

TABLE OF CONTENTS

	Page
INTRODUCTION	1
Purpose of Study.....	1
Geologic and Geotechnical Characterization of Holocene to Late Pleistocene Sedimentary Deposits.....	2
Liquefaction-Induced Deformation Hazard Analysis.....	4
BACKGROUND	6
Previous Studies	6
Liquefaction.....	7
Study Area	8
Geologic and Geomorphic Setting	9
Seismicity	12
Subsidence	13
Historical Liquefaction	16
METHODS.....	21
Data Collection.....	22
Assignment of Geologic Map Units to Each Boring Layer.....	23
Liquefaction Analysis	33
Deformation Analysis for Level-Ground Conditions.....	40
RESULTS	46

Nearest Neighbor Statistics.....	47
Pleistocene Surface Elevation Map (Interpreted).....	48
Liquefiable Textures.....	50
(N_1) _{60, cs} , Factor of Safety, and Cyclic Resistance Ratio.....	51
Liquefaction Potential Index.....	55
Estimating Strain for Each Geologic Map Unit.....	58
Observed vs. Predicted Deformation.....	66
CONCLUSIONS.....	69
REFERENCES.....	72
APPENDICES (on compact disc)	
Appendix 1: Database	
Deformation Calculation Spreadsheet (Wu, 2002)	
Liquefaction Analysis Summary for Borehole Data (Calculated Data Only) (California Geological Survey, unpublished)	
Liquefaction Analysis Summary for Layer Data (Calculated Data Only) (California Geological Survey, unpublished)	
Appendix 2: (N_1) ₆₀ Quality Ranking (California Geological Survey, unpublished)	
Appendix 3: Unit Weight Data (California Geological Survey, unpublished)	
Appendix 4: Comparison Of Predicted Vs. Observed Deformation	

LIST OF ILLUSTRATIONS

Figure	Page
1. Loma Prieta, California, Earthquake October 17, 1989	5
2. Subsidence in the Santa Clara Valley	15
3. Deterministic Correlation for Evaluation of Liquefaction Potential	37
4. Probabilistic Correlation for Evaluation of Liquefaction Potential.....	38
5. Methods of Predicting Liquefaction-Induced Deformation	41
6. Proposed Correlations Between CSR, $(N_1)_{60, cs}$, and Reconsolidation Volumetric Strain	43
7. Proposed Correlations Between CSR, $(N_1)_{60, cs}$, and Limiting Shear Strain	43
8. Nearest Neighbor Semi-Variogram.....	48
9. Histograms of Penetration Resistance	54
10. Box and Whisker Plot of Fines Corrected Penetration Resistance Measurements.....	56
11. Liquefaction Potential Index	57
12. Histogram Showing the Number of Borings that Plot in the Map Polygon with the Corresponding Volumetric Strain (%).....	62
13. Histogram Showing the Number of Borings that Plot in the Map Polygon with the Corresponding Shear Strain (%)	63
14. Histogram Showing the Percent of Borings that Plot in the Map Polygon with the Corresponding Volumetric Strain (%) as well as the Polygon with the next Higher and Lower Volumetric Strain Category....	64

15. Histogram Showing the Percent of Borings that Plot in the Map Polygon with the Corresponding Shear Strain (%) as well as Polygon with the next Higher and Lower Shear Strain Category 65

LIST OF PLATES

Plates in back pocket:

1. Index Plate of study area
2. Historic Ground Failure
3. Cross Section for Milpitas 7.5-Minute Quadrangle
4. Top of Pleistocene Map
5. Histograms Showing Fines Corrected Penetration Resistance
6. Map of Volumetric Strain Calculated for each Boring and Grouped by Median Strain of Geologic Map Unit
7. Map of Limiting Shear Strain Calculated for each Boring and Grouped by Median Strain of Geologic Map Unit

LIST OF TABLES

Table	PAGE
1. Quaternary Geologic Map Units.....	11
2. Criteria for Assigning Layers to Geologic Map Units.....	26
3. Fines Content Assigned to Samples with Liquefiable Textures for Which No Textural Data Was Provided on Boring Logs	35
4. Percentage of Each Geologic Map Unit with Textures that Are Potentially Liquefiable	50
5. Fines Corrected Penetration Resistance, Factor of Safety and Cyclic Resistance Ratio	52
6. Calculated Volumetric and Limiting Shear Strain Along with Volumetric Settlement and Horizontal Displacement for each Geologic Map Unit	58

INTRODUCTION

Purpose of Study

Geotechnical and geologic characterization of sedimentary deposits in the northern Santa Clara Valley, California is the goal of this research. Interpretation of the Holocene-late Pleistocene boundary in the subsurface and characterization of sediment in the Santa Clara Valley is conducted and used to produce regional (1:24,000-scale) hazard maps based on predicted surface deformation resulting from liquefaction. Any attempt to produce maps of future liquefaction-induced deformation must take into account the nature and variability of geologic deposits in the area to be mapped. This task is complicated by the limited subsurface data (geotechnical boring logs) that are generally available in most areas. In this study, 668 boring logs are used to characterize the geology of the northern Santa Clara Valley (Plate 1). Maps of liquefaction-induced deformation based upon the geotechnical and geologic characterization of the sediment in the northern Santa Clara Valley can be used to supplement classical liquefaction susceptibility or liquefaction potential maps. In addition, deformation potential maps may provide information to serve emergency response planning, mitigation prioritization, and assessments of vulnerability of lifeline systems.

In the past, predictions of liquefaction potential have identified areas expected to experience earthquake-induced ground failure such as the maps showing Zones of Required Investigation for Liquefaction produced by the

California Geological Survey (CGS). Construction on artificial fill over San Francisco Bay mud (afbm) in the Marina district in San Francisco resulted in tremendous structural damage and the loss of several lives following the 1989 Loma Prieta earthquake (Harris and Egan 1992), and this damage is an illustration of liquefaction-induced ground failure. Although the cause of ground deformation was well understood, predictions of estimated amounts of ground deformation were not available at the time of the earthquake.

Geologic and Geotechnical Characterization of Holocene to Late Pleistocene Sedimentary Deposits

Knowledge of the distribution of layered cohesionless sediment deposits such as gravel, sand, and silt is an important element for mapping the liquefaction hazard in a given area (Martin and Lew 1999). Most liquefaction-hazard maps are based on an evaluation of sediment type and the likelihood that materials will liquefy, or that liquefaction will be “triggered” during future earthquakes. Typically, categories of very high to low or very low are assigned to each Quaternary geologic map polygon. Deviations from a one-to-one correspondence between Quaternary map unit and liquefaction susceptibility category are typically based on differences across the region in depth to ground water and expected levels of earthquake ground shaking (Knudsen et al. 2004). Geotechnical information is collected during sub-surface investigations for liquefaction analysis using the Simplified Seed Procedure (Seed and Idriss 1971)

and plotted on a map. The final stage of the mapping process involves comparing the results of the susceptibility analysis with the outcome of the triggering analysis performed on the geotechnical boring data. Saturated, liquefiable sediments deposited in areas where ground shaking is expected from earthquakes on nearby active faults are mapped as areas with the potential for liquefaction.

The susceptibility of a soil to liquefaction is commonly examined in the context of a criteria matrix that accounts for the qualitative characteristics of a soil such as age of the deposit and environment of deposition. Descriptive features of the sediment, such as particle size, which may be unique to a particular setting, can be used as keys to recognize liquefaction susceptibility in other similar environments. In addition, quantifiable geotechnical characteristics such as density and grain size distribution are reviewed. The range of values for quantitative characteristics for which liquefaction is known to occur can be established and used as a basis for comparison with measurement of quantitative data collected from other sites.

When a geologic investigation is carried out, the study of the geologic environment is conducted independently of the measurement of the geotechnical parameters. Geotechnical parameters are considered in relation to the Unified Soils Classification System (USCS) designation assigned to the layer in which the measurement was taken. The USCS only describes the physical properties of each layer and considers each layer as existing independently of the layers

above and below it. It is common in geologic investigations that, after the geotechnical properties have been measured, the data are analyzed using the Simplified Seed Procedure (Seed and Idriss 1971). As a consequence, the geotechnical properties become separated from geologic context responsible for their development.

The goal of this research is to combine both types of data to take advantage of both the qualitative and quantitative factors that contribute to liquefaction susceptibility in order to develop a more detailed picture of the liquefaction-induced deformation potential of the region. In this study, 668 boring logs and recent Quaternary mapping by Witter et al. (2006) are used to characterize the geology of the northern Santa Clara Valley. Qualitative geologic information and quantitative geotechnical boring log information are linked together; each layer in each boring is assigned a geologic map unit designation, thereby expanding the description of each geologic unit, and the quantifiable geotechnical characteristics are further inferred to apply to every occurrence of each geologic unit even where not tested by borings.

Liquefaction-Induced Deformation Hazard Analysis

Advance knowledge of where liquefaction-induced ground deformation is likely to occur may provide an opportunity to retrofit structures prior to a damaging, large-scale earthquake (Fig. 1). Most previous efforts to map potential liquefaction-induced deformation on a regional scale have been based

on predictions of lateral spread displacements (e.g. Youd and Jones 1993). To formulate a more complete picture of hazards due to liquefaction-induced ground deformation, the geologic characterization developed in this research may in the



Figure 1. "Loma Prieta, California, Earthquake October 17, 1989. Structures damaged in the Marina District of San Francisco. The first story of this three-story building was damaged because of liquefaction; the second story collapsed. What is seen is the third story." Figure 24B, U.S. Geological Survey Circular 1045. Image file: </htmlib/batch88/batch88j/batch88z/batch88/pla00049.jpg>

future be used in combination with new models for predicting liquefaction-induced strain (Wu 2002; Wu and Seed 2004) to develop regional maps of liquefaction-induced volumetric and shear strain (Knudsen et al. 2004).

BACKGROUND

Previous Studies

This research follows earlier research conducted for the City of San Jose by Cooper, Clark & Associates (1974) and Falls (1988). In addition to data collected by the California Geological Survey, the present research uses the same data from the city of San Jose used by both Cooper, Clark & Associates and Falls, and relies on the Simplified Seed procedure (Seed and Idriss 1971) to analyze the data to determine where liquefaction is likely to occur. Cooper, Clark & Associates and Falls both estimated liquefaction potential based upon analysis of factors contributing to liquefaction susceptibility combined with an investigation of opportunity for the material in each individual boring to liquefy. The present study estimates liquefaction potential using the Simplified Seed procedure (Seed and Idriss 1971) to calculate the soil resistance to liquefaction (Cyclic Resisting Ratio, CRR) which is then compared to calculated earthquake driving forces (Cyclic Stress Ratio, CSR). Like the report produced for the City of San Jose by Cooper, Clark & Associates, the present research includes maps showing the distribution and potential for earthquake-induced ground failure. However, the hazard maps produced by Cooper, Clark & Associates are based on qualitative data, namely the susceptibility ranking of each geologic map unit, and not on quantitative analysis of liquefaction-induced deformation performed for specific

bore hole locations. In addition, the boundaries on the maps produced by Cooper, Clark & Associates do not follow geologic contacts.

Liquefaction

Estimates of liquefaction potential are the result of analysis of a combination of factors (CGS 1997). In order for liquefaction to occur, susceptible, saturated, unconsolidated, granular material must be present (CGS 1997). In addition, opportunity, i.e. cyclic loading from a nearby active fault source (faults that have ruptured in the last 11,000 years; CGS 2007) must be possible. The result of cyclic loading of saturated, unconsolidated, granular material can be the fluidization of sediment. When earthquake shaking occurs, grains shift into a denser configuration by rearranging to fill in void spaces, which may be occupied by water. As the volume of void space available for water to occupy decreases, water pressure increases. As densification continues, pore space decreases to the point that water pressure rapidly passes a critical threshold and water is expelled from the void spaces. As water is expelled, it forces sediment grains apart, resulting in liquefaction.

Regional geology and depositional environment influence the development of characteristics of a particular sedimentary deposit. In fluvial environments for example, uplift and erosion contribute source material that is deposited downstream, and the type of unconsolidated granular material in sediment plays a key role in liquefaction. Sphericity and roundness affect the

efficiency of grain packing, which in turn influences the volume of void space that can be occupied by water. Composition of the material influences whether or not the soil will behave plastically. Clay-sized quartz particles are liquefiable because they are non-plastic and under earthquake loading will behave as a cohesionless material (Seed et al. 2003; Boulanger and Idriss 2006). Gravelly soil, although liable to liquefy, generally has larger pore spaces and therefore is better able to attenuate pore pressure. In addition, due to the energy required to transport larger particles, gravelly material, unlike finer-grained material, tends not to be deposited loosely (Seed et al. 2003).

Study Area

The study area, located in the southern San Francisco Bay region of northern California, includes approximately 390 square kilometers in the northern Santa Clara Valley (Plate 1). The study area includes the Milpitas, San Jose East, San Jose West and portions of Calaveras Reservoir 7.5-minute quadrangles. The majority of the study area is heavily urbanized. The City of San Jose covers a large percentage of northern Santa Clara Valley, and portions of the cities of Alviso, Campbell, Los Gatos, Milpitas, Santa Clara, Saratoga, and Sunnyvale are also included.

The northern end of the study area along the margin of San Francisco Bay is occupied by salt evaporation ponds and associated levees. The San Jose International Airport is located in the north-central part of the study area.

Numerous fluvial systems flow through the northern Santa Clara Valley. The two largest systems are Guadalupe River and Coyote Creek. Guadalupe River is supplied by Saratoga, San Tomas Aquinas, Calabazas and Los Gatos creeks, all of which originate outside the study area in the Santa Cruz Mountains to the west. Coyote Creek is supplied by Berryessa, Penitencia, Tularcitos, Scott, Arroyo de los Coches, Piedmont, Calara, Miguelita, Silver, Babb and Thompson creeks, all of which originate in the Diablo Range to the east (Plate 1).

Six major freeways and several smaller arterial roadways cross the study area. Northwest-trending U.S. Highway 101 (Bayshore Freeway) connects the northern Santa Clara Valley to the San Francisco Peninsula, and northeast-trending Interstate 680 closely parallels the foothills of the Diablo Range and connects the northern Santa Clara Valley to major cities along the east side of San Francisco Bay. State Highway 17/ Interstate 880 extends southward in the western portion of the study area. Trending roughly east-west, State Highway 237 and Interstate 280 span the northern portion of the study area.

Geologic and Geomorphic Setting

The northwest-trending, northern Santa Clara Valley, part of the Coast Range geomorphic province, is situated between the Santa Cruz Mountains to the west outside the study area and the Diablo Range to the east. Outside of the study area, the northern Santa Clara Valley is bordered on the west by the San Andreas fault, and within the study area, on the east by the Hayward and

Calaveras faults. There are 27, primarily non-marine, Quaternary and pre-Quaternary bedrock map units in the northern Santa Clara Valley study area (Table 1 and Plate 1). The margins of the northern Santa Clara Valley are asymmetrically framed by broad alluvial fans that slope gently northward toward San Francisco Bay. Along the west and southwest sides of the valley, at the base of the Santa Cruz Mountains, latest Pleistocene alluvial fans (Qpf) are overlain by thin Holocene alluvial fan deposits (Qhf) (Witter et al. 2006). Along the east and northeast sides of the valley, at the base of the Diablo Range, latest Pleistocene (Qpf) and Holocene alluvial fans (Qhf) are smaller than fans on the west side of the valley, and only minor levees (Qhl) have developed. Holocene alluvial fans generally are composed of poorly sorted mixtures of gravel, sand, silt, and clay. At the upstream end of the alluvial fans, where gradients are steeper, fan deposits typically are composed of coarse-grained material (Qhf), and grade into finer-grained material (Qhff) downstream. Where the fans terminate at the edge of San Francisco Bay, fine-grained material transitions into Holocene fine grained alluvial fan-estuarine complex deposits (Qhfe), Holocene San Francisco Bay Mud (Qhbm) and artificial fill (af) over Bay Mud (afbm). Down the northwest-trending axis of the valley, both Guadalupe River and Coyote Creek contain Holocene stream channel deposits (Qhc), and artificial channel (ac) deposits, and are flanked by Holocene alluvial fan levee deposits (Qhl) and Holocene stream terrace deposits (Qht). Artificial fill (af) is associated with large-scale transportation infrastructure, including highways and railroads, such as the

TABLE 1. QUATERNARY GEOLOGIC MAP UNITS (Modified from Knudsen et al. 2000)

Environment of deposition		Environment of deposition	
<u>Modern</u>			
af	Artificial fill	gq	Gravel quarry
afbm	Artificial fill over Bay Mud	ac	Artificial stream channel
aff	Artificial fill, levee	Qhc	Modern stream channel
<u>Latest Holocene</u>			
Qhfy	Alluvial fan	Qhty	Stream terrace
Qhly	Alluvial fan levee		
<u>Holocene</u>			
Qhbm	San Francisco Bay mud	Qhff	Alluvial fan, fine facies
Qhb	Basin	Qhl	Alluvial fan levee deposits
Qhfe	Fine grained alluvial fan-estuarine complex	Qht	Stream terrace
Qhf	Alluvial fan	Qha	Alluvium, undifferentiated
<u>Latest Pleistocene to Holocene</u>			
Qf	Alluvial fan	Qt	Stream terrace
Ql	Alluvial fan levee	Qa	Alluvium, undifferentiated
<u>Latest Pleistocene</u>			
Qpb	Basin	Qpa	Alluvium, undifferentiated
Qpf	Alluvial fan		
<u>Early to late Pleistocene</u>			
Qof	Alluvial fan	Qoa	Alluvium, undifferentiated
<u>Pre-Quaternary</u>			
br	Bedrock		

interchange for U.S. Route 101 with Interstate Routes 280 and 680 near the center of the study area.

Bedrock geology in the vicinity of the study area is divided into individual, fault-bounded structural blocks recognized on the basis of differing stratigraphic sequences and geologic histories (Wentworth et al. 1999). Rocks from the Silver Creek, Alum Rock and Mt. Hamilton blocks are within the four quadrangles included in the study area. At the southeastern end of the study area, rocks of the Franciscan Complex (KJf) are juxtaposed against Jurassic rocks of the Coast Range Ophiolite (Jsp) along a low-angle thrust fault in the Silver Creek structural block (Wentworth et al. 1999). Rocks of the Silver Creek block are found along

the hills drained by Silver Creek and in the vicinity of Yerba Buena Ridge. The Alum Rock block, composed of Jurassic to Quaternary age rocks, is exposed along the eastern margin of the northern Santa Clara Valley. The Alum Rock block is separated from the Mt. Hamilton block to the east by the Calaveras fault and from the Silver Creek block to the south by a concealed fault (Wentworth et al. 1999). *Cretaceous and Jurassic rocks of the Eastern Belt of the Franciscan Complex* are exposed in the northeast portion of the study area.

Seismicity

The study area is the northern Santa Clara Valley. The San Andreas fault system lies to the west just outside the study area, and the Calaveras and the southern end of the Hayward fault systems are mapped in the north east margins of the study area (Plate 1). Among the more significant historic earthquakes in the region are the M7.0 Hayward earthquake of October 21, 1868 (Berkeley Seismological Laboratory, http://seismo.berkeley.edu/faq/1868_0.html), the M7.9 San Francisco earthquake of April 18, 1906, and the M_w 6.9 Loma Prieta earthquake of October 17, 1989. Each of these earthquakes caused liquefaction-induced ground failure(s) in the northern Santa Clara Valley.

The level of seismic excitation used for this study is the level of peak ground acceleration (PGA) with a 10% probability of being exceeded over a 50-year period. The statewide probabilistic seismic hazard analysis (Peterson et al. 1996) indicates that peak ground accelerations with a 10% probability of being

exceeded in 50 years are expected to range from about 0.5 g near the margin of San Francisco Bay to about 0.8 g in the foothills of the Diablo Range at the northeast corner of the study area (Peterson et al. 1996). Deaggregation of the seismic hazard model yields the magnitude and distance of the earthquake that contributes most to the probabilistic estimate of ground motion at a particular location. The deaggregation indicates that the seismic hazard in the southwest part of the study area is dominated by a $M_w7.9$ earthquake on the San Andreas fault at a distance ranging from about 18 to 24 km (CGS 2002). The seismic hazard in the northeast part of the study area is dominated by a $M_w7.1$ earthquake on the Hayward fault at a distance ranging from about 2 to 7 km (CGS 2001). The hazard in the southeast part of the map area is dominated by a $M_w6.4$ earthquake on the southeast extension of the Hayward fault system at a distance of about 7 km (CGS 2000).

Subsidence

Subsidence due to ground-water withdrawal is well documented in the northern Santa Clara Valley. The alluvial fill in the northern Santa Clara Valley consists primarily of Pliocene to Holocene deposits up to approximately 300 m thick, with sand and gravel more prevalent on alluvial fans that line the margins, transitioning to silt and clay toward the San Francisco Bay (Poland 1984). In the early part of the last century, ground-water withdrawal was primarily for agricultural use; however, by the middle of the last century agriculture in the

valley declined while urban development increased the demand on municipal water supplies (Poland 1971). As ground-water levels decreased, the effective overburden pressure on the water-bearing sediments increased, causing compaction and land subsidence. Most of the subsidence in the northern Santa Clara Valley was accommodated by compaction of fine grained sediment (Ingebritsen and Jones 1999).

Between approximately 1915 and 1967, as much as 2.4 m of subsidence occurred, and overall, approximately 260 km² subsided more than 1 m within the limits of the study area (Poland 1984) (Fig. 2). Careful monitoring and management of the basin, including importation of surface water, has led to the recovery of small amounts of subsidence. The Santa Clara Valley Water District has observed an increasing number of artesian wells, which reflects rising ground-water levels (Seena Hoose, SCVWD, oral communication 2000). Within the study area, historical ground water levels range from less than approximately 3.5 m below land surface near the San Francisco Bay to approximately 10-25 m throughout the rest of the study area (CGS 2004). As ground-water levels rise, vertical effective stress is reduced, causing regional uplift (Schmidt and Bürgmann 2002). InSAR time-series data record net uplift in the study area averaging approximately 15-20 mm and as high as approximately 40 mm on the east side of the south end of Coyote Creek between 1992 and 1998 (Schmidt and Bürgmann 2002). The InSAR data also show that uplift in

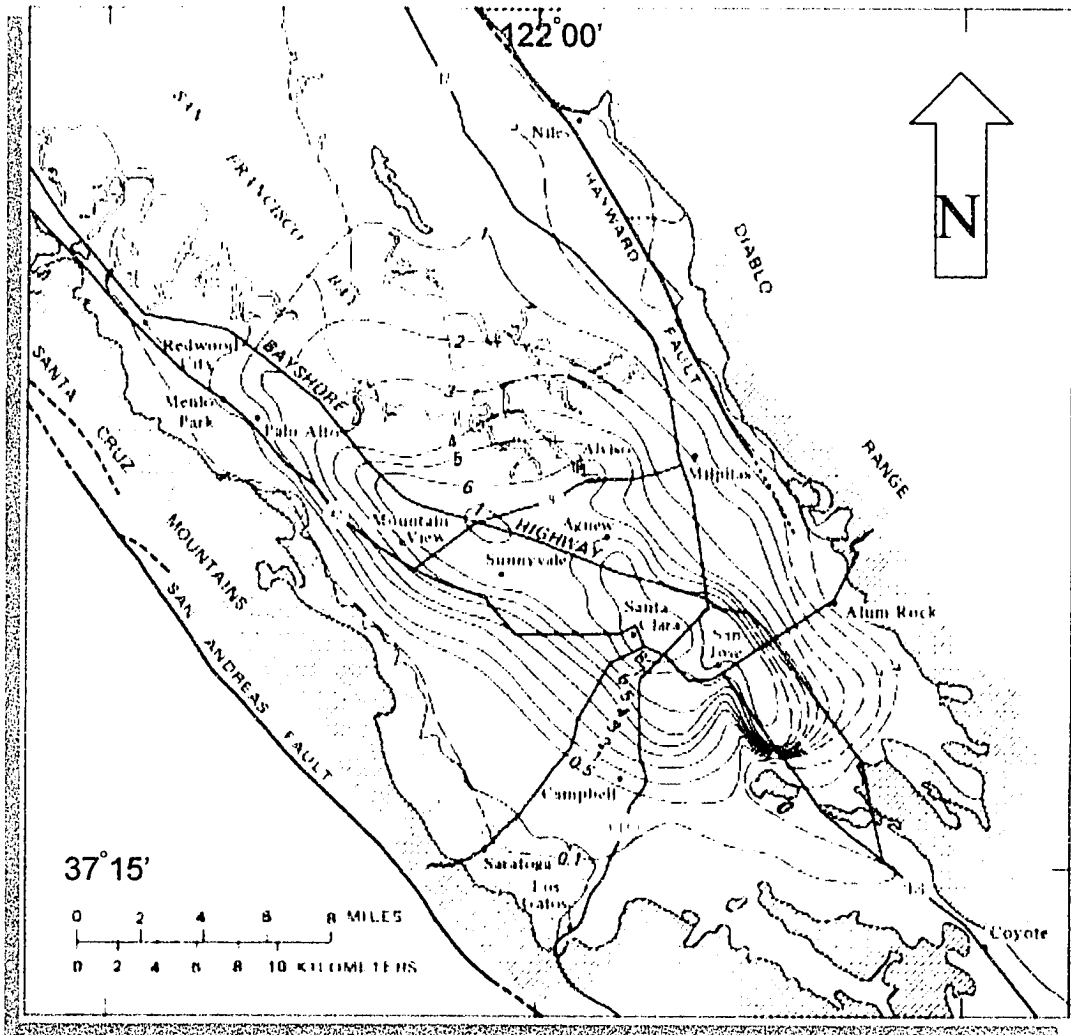
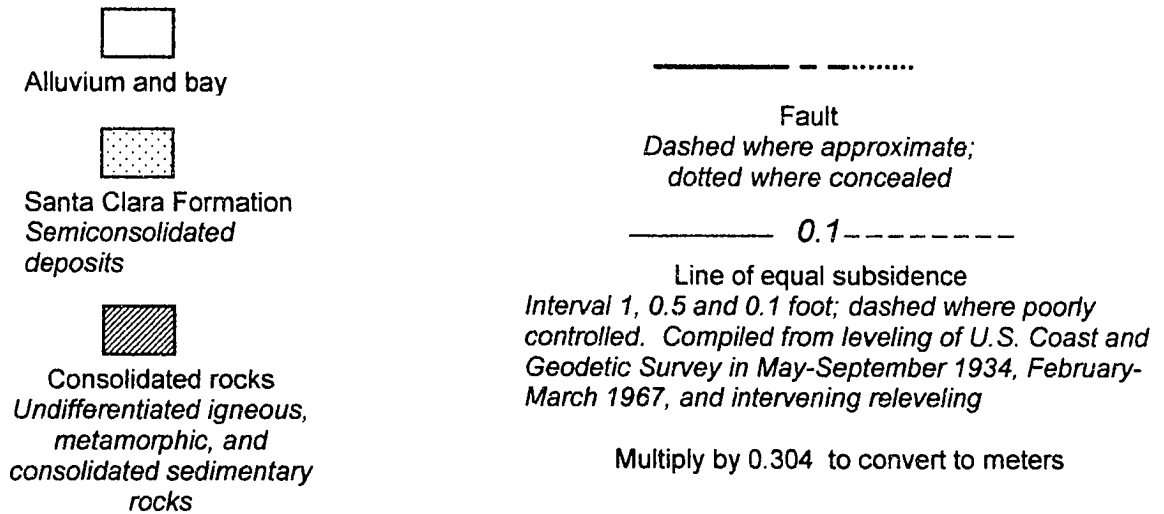


Figure 2. Subsidence in the Santa Clara Valley, California (after Poland 1969).



the Santa Clara Valley is a seasonal phenomenon (Schmidt and Bürgmann 2002).

Historical Liquefaction

Ground failure associated with the 1868 Hayward, 1906 San Francisco, and 1989 Loma Prieta earthquakes includes sand boils, disturbed wells, settlement, lateral spread, stream-bank failure and ground cracks (Youd and Hoose 1978). The majority of ground-failure phenomena observed in the study area caused by the 1868, 1906 and 1989 earthquakes is concentrated in the northern half of the study area near the margin of the San Francisco Bay, where ground water levels are typically within 3-4 m of ground surface (Plate 2).

Ground failure associated with the 1868 Hayward earthquake includes lateral spreading and sand boils. Lateral spreading was observed at station 149 (Knudsen et al. 2000) (Plate 2). Accounts of lateral spread describe the banks of Coyote Creek being "shaken together" and cracks with water pouring out along the bay side of the creek (Youd and Hoose 1978). Sand boils were observed at station 149 as well (Knudsen et al. 2000). Reports of sand boils relate that cracks flowed with water for 48 hours following the earthquake, and water spurted "...to the height of several feet" (Youd and Hoose 1978).

Reported ground failure associated with the 1906 San Francisco earthquake was more varied and more widespread than that associated with the 1868 Hayward earthquake, and included stream bank land sliding, lateral

spreading, ground settlement, ground cracks, sand boils and disturbed wells. Lateral spread was observed at stations 148, 149, 150 and 155 (Knudsen et al. 2000). Reports of lateral spread at station 148 relate that "...two rows of trees in an orchard had parted off and slid into the slough" (Youd and Hoose 1978). At station 149, reports of lateral spread include descriptions of a bridge that "...was shifted on its concrete supports, the two ends moving in opposite directions" and "...cracks on both sides of the Coyote River at intervals all the way to San Jose" (Youd and Hoose 1978). At station 150, it was reported that fissures were observed near a ranch house and that .3 m (1 foot) of "downthrow" was measured on the east side of the fracture (Youd and Hoose 1978). Finally, at station 155, it was reported that "heave of the land" occurred "in a northwesterly direction 1.3 m (4 feet) from its original position" (Youd and Hoose 1978).

Ground settlement as a result of the 1906 San Francisco earthquake was documented at stations 148, 149, 150, 151 and 152 (Knudsen et al. 2000). At station 148, settlement was observed along the train tracks leading out of the north end of the town of Alviso, and a well casing was driven out of the ground (Youd and Hoose 1978). At station 149, reports of ground settlement describe the west side of a 3.7-m-diameter pool being lifted higher than the east side of the pool (Youd and Hoose 1978). Details of settlement are sparse for stations 150 and 151; however, it was documented that at these stations a ranch house settled slightly on its northwest side, and that there was a "slump in soft ground"

respectively (Youd and Hoose 1978). Finally, at station 152, settlement occurred in front of the principal hotel in Alviso (Youd and Hoose 1978).

The 1906 San Francisco earthquake caused sand boils to occur at numerous locations, including stations 148, 149, 150, 151 and 153. (Knudsen et al. 2000). A report of sand boils for station 148 notes that “cracks formed from which muddy and sandy water flowed” (Youd and Hoose 1978). A report of sand boils associated with station 149 notes that “water flowed from cracks in the yard and piled up sand .15 m (6 inches) on both sides” and also record “many craterlets of sand” (Youd and Hoose 1978). Further, a report of sand boils associated with station 150 recounts that “considerable sand was brought up by water flowing from the cracks” in an orchard (Youd and Hoose 1978). At station 151, it was reported that “cracks in the vicinity of Milpitas flowed artesian water for 48 hours after the shock” (Youd and Hoose 1978). Finally, at station 153, a report of sand boils describes water spouting into the air “to the height of several feet” (Youd and Hoose 1978).

Miscellaneous effects of ground failure associated with the 1906 San Francisco earthquake include reports of disturbed wells at stations 148, 155 and 158 (Knudsen et al. 2000). The report of a disturbed well at station 148 records that prior to the earthquake the well in question “required a wind-mill to pump the water. At the time of the earthquake the casing was driven .6 m (2 feet) out of the ground, wrecking the pump, and since that time the well has been flowing under a heavy pressure” (Youd and Hoose 1978). At station 155, it was reported

that, "On the farm of Mr. Fox, 4.8 km (3 mi.) north of San Jose, the water pipe of an artesian well was broken off 18.2 m (60 ft.) below the surface and carried by the heave of the land in a northwesterly direction 1.3 m (4 ft.) from its original position" (Youd and Hoose 1978). Finally, at station 158, "water and mud in many instances are reported as having spurted from the artesian wells, but in a few days they resumed their normal condition" (Youd and Hoose 1978).

Ground failure associated with the Loma Prieta earthquake of 1989 was limited in scope compared to the earthquakes of 1868 and 1906; however, lateral spread and settlement were observed. At station 51E, south of San Jose Municipal Airport, "minor lateral spreading" and settlement caused "minor cracking" along a frontage road (Seed and Harder 1990). In addition, at station 51D approximately 1 km north of San Jose Municipal Airport, "minor settlement" of a tower foundation was observed (Seed and Harder 1990). Finally, settlement was observed at station 51B in Alviso in the approach fills of the Gold Street Bridge (Tinsley et al. 1998).

The absence of ground failure in areas that are susceptible to liquefaction is also important because, among other reasons, non-failure can provide information about shaking intensity. Reports of the absence of ground failure associated with the 1906 earthquake in the study area are recorded for stations 156 and 157 (Knudsen et al. 2000). No ground failure was reported at station 156 "between Coyote Creek and the mountains" (Youd and Hoose 1978). At station 157, south of State Highway 280 in the vicinity of W. William Street, no

damage was reported at San Jose Water Works or the city's gas mains (Youd and Hoose 1978). Further, following the 1989 Loma Prieta earthquake at station 51C, the absence of liquefaction was reported "from the shoreline of the bay to State Highway 237" (Tinsley et al. 1998) where numerous instances had been reported following the 1868 and 1906 earthquakes at station 149 (Youd and Hoose 1978).

METHODS

Data from geotechnical boring logs were used to characterize the geotechnical properties of the geologic units mapped in the northern Santa Clara Valley for the purpose of evaluating the liquefaction-induced ground deformation hazard of each geologic unit. All of the layers in each boring log were reviewed, and each layer was assigned to a geologic map unit. While completing this task, particular attention was paid to identifying a change with depth in the measurable geotechnical properties of sediment. After each layer in each boring was assigned a geologic map unit, liquefaction potential analysis was performed on each of the layers in each boring. Liquefaction potential analysis for each layer was calculated deterministically using the methods of Youd et al. (2001) and probabilistically using the methods originally developed by Seed and Idriss (1971) and modified by Seed et al. (2003). The liquefaction analysis was carried out using a program developed by the California Geological Survey (Unpublished). Finally, using the Cyclic Stress Ratio (CSR) and corrected penetration test results produced by the liquefaction analysis, post-liquefaction deformation potential analysis was performed on all saturated layers composed of liquefiable textures for which penetration test data are available, and the total amount of potential volumetric and shear strain for each boring was summed using the methods of Wu et al. 2004 (volumetric strain) and Wu 2002 (shear strain).

These geotechnical properties infer the position and shape of a three-dimensional surface at shallow depth that can be broadly characterized as a boundary between shallower low-density materials and deeper higher-density materials. In many areas, this surface probably coincides with the top of the Pleistocene section, i.e., with a specific stratigraphic surface. However, in other areas evidence indicates that the density boundary does not coincide with the top of the Pleistocene. The focus of this paper is the density boundary defined by geotechnical properties, but for convenience the boundary is often referred to as the top of the Pleistocene.

Data Collection

To assess the potential for liquefaction-induced ground failure, an understanding of this area's late Quaternary history and deposits was developed by interpreting logs of geotechnical borings and relating the stratigraphy depicted in the borings to geologic map units. The information collected and used to interpret the geologic setting in this project includes: (a) detailed Quaternary geological map for the northern Santa Clara Valley area produced at 1:24,000 scale by Witter et al. (2006), (b) 668 geotechnical borings, (c) probabilistic earthquake shaking information, and (d) ground-water levels. Data used in this study are from the Milpitas, Calaveras Reservoir, San Jose East and San Jose West 7.5-minute quadrangles (Plate 1). The boring data were collected from local government files and entered into a Geographic Information System during

previous seismic hazard mapping efforts conducted by the California Geological Survey (<http://gmw.consrv.ca.gov/shmp/index.htm>).

The boring logs collected for this study range in depth from 3.1 to 45.7 m (10 to 150 feet), with 40% reaching a depth of 12.2 m (40 feet) or more. In a study like this in which only existing geotechnical borings are used, the quality of the borehole data varies. The logs should provide thorough documentation of how and where each boring was advanced. Of primary importance on the boring log is the penetration test data, which are standard data needed when calculating liquefaction potential. Laboratory studies of texture, grain-size distribution and fines content (FC) provide information needed in several of the methods used to estimate liquefaction-induced deformation. Data are stored in a database according to whether the information was measured, calculated or assigned for a sample or layer, or summed for the boring as a whole (Appendix 1).

Assignment of Geologic Map Units to Each Boring Layer

Layers in each boring were assigned to a geologic map unit based on both the descriptive geologic characteristics and the geotechnical properties of the material encountered and recorded on individual boring logs. Effort was first placed on determining whether layers are Pleistocene or Holocene in age. The Pleistocene surface is important because most researchers believe that sediment greater than 11,000 years old is unlikely to liquefy.

The study area includes two major drainages discharging into the San

Francisco Bay and is characterized by unconsolidated sedimentary deposits that are highly variable, both vertically and laterally, over short distances. Because the data used in this study consist of boring logs collected from a variety of outside sources, and no new data were collected, dating of samples was not possible. Further, no attempt was made to locate age-dated soil samples from outside sources. Logs collected for this study are from borings distributed randomly across the study area, and the separation between borings is large (typically >300 m) compared to layer thickness (85% < 3 m thick), making it difficult to correlate discontinuous layers between borings.

Ideally, the same class of data would be available for every layer in every boring. But, because the same data were not available for every layer in every boring, the most important type of information reviewed was the penetration test data, because it may be used as a proxy for the density of the layer. Contrasts in penetration resistance are particularly important for identifying the boundary between the Holocene and latest Pleistocene. As sediment ages and becomes more lithified, the density of the sediment increases, and the increase in density is reflected in a higher penetration resistance (Powers et al. 1992; Hitchcock and Helley 2000, 2003).

Penetration resistance also was reviewed in the context of the lithologic description recorded for each layer. Lithologic descriptions that include words such as "organics," "roots," or "carbonaceous" may also indicate the presence of a buried late Pleistocene soil horizon. As sea level rose at the end of the latest

Pleistocene the depositional environment of the northern Santa Clara Valley changed. In the study area the change in depositional environment is preserved in some borings as a textural change at the inferred boundary between the late Pleistocene and Holocene (Hitchcock and Helley 2000, 2003). Other researchers have interpreted the “top of Pleistocene” to represent a former land surface that existed prior to the rise of seawater through the Golden Gate at the beginning of the Holocene (Helley and Lajoie 1979; Atwater, Hedel and Helley 1977).

In the northern Santa Clara Valley, repeated fluctuations in the depth of groundwater due to the influence of the nearby San Francisco Bay may cause sediment to consolidate, resulting in higher penetration resistance.

In some borings, it is easier to discriminate one geologic unit from another based upon the texture of the sediment layers sampled in the boring. For instance, silt (ML) is a fine-grained material that is a component of many of the geologic units found in the map area, such as Holocene alluvial fan levee deposits (Qhl) and Holocene alluvial fan deposits (Qhf). Each geologic map unit represents a different depositional environment; however, silt contained in different units may be described on different boring logs using similar terms such as “fine, brown, medium stiff, moist”. By carefully reviewing the textural composition of a given layer in the context of the other layers in the boring in which it is sampled as well as in the context of surrounding borings, it may be possible to discern the geologic setting in which the sediment was deposited, and

ultimately, the geologic unit to which the sediment belongs. Table 2 lists criteria that are compared to assign layers to specific geologic units. It is important to note that some of the descriptive characteristics listed in Table 2 may not be noted in the description of every sediment layer on a boring log; however, several layers together may display a combination of characteristics that make it possible to interpret the geologic setting for a series of layers.

TABLE 2. CRITERIA FOR ASSIGNING LAYERS TO GEOLOGIC MAP UNITS (Clahan et al. 2002)

Are there features that suggest the presence of a soil (rootlets, caliche, and pedogenesis)?

Are there regionally correlatable discontinuities?

Is there a change in penetration resistance within/between layers in borings?

Are regionally identifiable units (e.g. Merritt Sand, Bay Mud) present?

Does the color change (mottling, oxidation at the Top of Pleistocene)?

Does the texture change (grain size, gradation, sorting) laterally and/or vertically?

For example, in boring 000051_00142 (Appendix 1), layers 1 through 4 are composed primarily of silt, clay, and fine-grained sand, and are interpreted as geologic unit Holocene alluvial fan levee deposits (Qhl). According to Helley and Wesling, (1989) "levee deposits are loose, moderately to well sorted sand, silt and clay." In contrast, although the textures of layers 5 through 8 in boring 000051_00142 are similar to the textures of layers 1 through 4 (sand, silt and clay), layer 8 contains gravel, and the descriptions for layers 5 and 8 include modifying phrases such as "discontinuous sand lenses" and "interbedded

streaks of sand” respectively. Layers 5 through 8 in boring 000051_00142 are interpreted as geologic unit Holocene alluvial fan deposits (Qhf) rather than Qhi because according to Witter et al. (2006), Qhf consists of “sand, gravel, silt and clay, and is moderately to poorly sorted, and moderately to poorly bedded.” The subtle change in the textural composition and continuity of bedding between layers 1 through 4 and layers 5 through 8 is interpreted to be the result of a change in depositional environment, and therefore layers 1 through 4 are interpreted as belonging to a different geologic map unit than layers 5 through 8.

Due to the paucity of useful descriptive terminology on boring logs, it is difficult to differentiate among Holocene or latest Pleistocene sub-units in most cases. In many cases the shallowest sub-surface layers are assigned to the geologic map unit mapped at the ground surface on the Quaternary map produced by Witter et al. (2006). However, in some borings an effort was made to identify sub-units for subsurface layers. In addition to the criteria listed in Table 2, for borings advanced into artificial fill, levee deposits (alf), the elevation of the top of the levee was compared to the elevation of the natural ground surface adjacent to the artificial levee. All layers in the boring with appropriate physical properties and with elevation equal to or below the elevation of the natural ground surface, but above the layers identified as Pleistocene (where present), were assigned to the geologic map unit upon which the levee was constructed.

In addition, an effort was made to recognize borings where the geologic unit assigned to the uppermost layer in a boring was different from the geologic

unit(s) assigned to underlying layers in the same boring, especially for borings located near a geologic contact. Because it is common for sedimentary layers of adjacent geologic units to interfinger, an attempt was made to determine whether subsurface layers in borings near geologic contacts should be assigned to the geologic unit mapped at the surface of the boring, or assigned to the geologic unit in contact with the geologic unit mapped at the surface of the boring. The boring log was reviewed and differences in the characteristics of sedimentary layers including penetration resistance, color, grain size, and lithology were used to determine to which geologic unit a layer should be assigned. For example, boring 2009B1 (Plate 1) near the intersection of Senter Road and Phelan Avenue on the San Jose East quadrangle, is located near the geologic contact between Holocene stream terrace deposits (Qht) and Holocene alluvial fan levee deposits (Qhl). Layers 1 (clay) and 2 (poorly sorted sand) are interpreted to belong to geologic map unit Qht, the unit mapped at the surface on the Quaternary geologic map used for this project, whereas layers 3 through 6 (silt, clay, silty sand, and clay respectively) are interpreted to belong to geologic map unit Qhl. Witter et al. (2006) describe Qht deposits as including sand, gravel, silt, and minor clay. However, Helley and Wesling (1989) describe Qhl deposits as including moderately to well-sorted sand, silt, and clay. Layers 2 through 6 are described as fine-grained silty sand, silt, or clay with no mention of coarser material.

The following criteria were used as keys to identify layers of different ages in the northern Santa Clara Valley:

Modern

Where not specifically noted on boring logs, artificial fill deposits (af), artificial fill over Bay Mud (afbm), and artificial fill, levee (alf) are identified where the layer description on the boring log indicates the presence of man-made historical debris such as bits of glass or broken concrete typically in a well-sorted matrix (Witter et al. 2006). Commonly, modern deposits are tan to light brown (Witter et al. 2006). In addition, the location of the boring may help identify the presence of fill deposits. Large-scale infrastructure such as bridges and major highways commonly require placement of fill during construction, and therefore, borings in the vicinity of infrastructure often encounter fill deposits. Layers that are not composed of fill but are considered Modern, including artificial stream channel (ac) and modern stream channel (Qhc), are most easily identified based upon their geographic location in existing streams. The median penetration resistance was calculated for each of the geologic map units and the median penetration resistance of all the Modern deposits in the northern Santa Clara Valley ranged from 6 to 11 blows per foot.

Latest Holocene

Youngest Holocene deposits are typically unconsolidated, very loose to loose granular deposits, or very soft to soft, fine-grained deposits (Witter et al. 2006). Youngest Holocene deposits are most easily identified based upon their geographic location adjacent to existing streams. Layers that are identified as Youngest Holocene include alluvial fan (Qhfy), alluvial fan levee (Qhly), and stream terrace (Qhty) deposits. The median penetration resistance was calculated for each of the geologic map units and the median penetration resistance of all the Holocene deposits in the northern Santa Clara Valley ranged from 6 to 11 blows per foot.

Holocene

Holocene deposits tend to be slightly consolidated clay, silt, and fine sand, as well as mixtures of slightly consolidated sand, silt and clay (Witter et al. 2006). Holocene deposits are most easily identified based upon their geographic location in the distal areas of active fans and downstream portions of active fluvial systems. Layers identified as Holocene include San Francisco Bay mud (Qhbm), basin (Qhb), and stream terrace (Qht) deposits, and deposits associated with alluvial fan environments including fine grained alluvial fan estuarine complex (Qhfe), alluvial fan (Qhf), alluvial fan fine facies (Qhff), and alluvial fan levee (Qhl) deposits. The median penetration resistance was calculated for each of the geologic

map units and the median penetration resistance of all the Holocene deposits in the northern Santa Clara Valley ranged from 4 to 25 blows per foot.

Pleistocene

Pleistocene deposits of a given texture, such as silt, have a higher density than those of the same texture in a younger deposit. Pleistocene deposits are typically mapped at the surface in the proximal portions of alluvial fans located along the margins of the Santa Clara Valley, and are commonly dissected by Holocene stream channels. It is not uncommon to note a coarsening-upward sequence in Pleistocene sediment within a single boring, although the coarsening-upward sequence, if present, may be subtle, such as a transition from clay to sandy silt. Where only a single source is contributing sediment to a portion of the study area it may be possible to discern a sediment sequence or layer that marks the change from latest Pleistocene to Holocene. Because there are many source areas contributing sediment to the northern Santa Clara Valley, particularly toward the downstream axis of the study area, unique sedimentary sequences, if present, are most likely to be observed in borings at the margins of the valley where streams from single source areas emanate from the base of either the Santa Cruz Mountains on the western margin of the valley, or along the base of the Diablo Range on the eastern margin of the valley. Sediment from a single source may be identified by the consistent use of descriptive terminology such as "gray-brown silty gravel" regardless of when or by whom the subsurface investigation was conducted. Layers identified as Pleistocene include late Pleistocene to Holocene alluvial fan (Qf), Late Pleistocene to Holocene alluvial fan levee (Ql), Late Pleistocene to Holocene stream terrace (Qt), Late Pleistocene to Holocene alluvium, undifferentiated (Qa), Late Pleistocene basin (Qpb), alluvial fan (Qpf), Late Pleistocene alluvium, undifferentiated (Qpa), Early to middle Pleistocene undifferentiated alluvium (Qoa) and Early to middle Pleistocene alluvial fan (Qof). The median penetration resistance was calculated for each of the geologic map units and the median penetration resistance of all the latest Pleistocene sediment in the northern Santa Clara Valley ranged from 8 to 28 blows per foot.

Cross sections were constructed after each layer was initially assigned to a geologic map unit. Borings were critically reviewed in the context of surrounding borings, with particular attention paid to differences in density as measured by blow count values and lateral and vertical textural changes

observed in layers at similar depths, and in some cases, the name of the geologic map unit assigned to a particular layer was revised. Plate 3 is a cross section constructed along the northern edge of the study area. The process of scrutinizing layer descriptions in the context of layers in surrounding borings as they appear on cross sections and then revising the name of the geologic unit assigned to each layer was repeated numerous times. Cross sections were constructed both parallel and normal to the northwest-trending axis of the study area. Borings that appear on more than one cross section were reviewed to ensure consistency in assignment.

On Plate 3, the top of Pleistocene is depicted as a solid line through the top of the shallowest layer identified as latest Pleistocene and as a queried dashed line at the estimated depth of the top-of-Pleistocene surface through borings in which Pleistocene is uncertain or not identified. For example, at the east end of the cross section in Plate 3, the top-of-Pleistocene surface is identified in borings 000057_00138 and 000057_00121, but not in boring 000057_00140. The surface is projected through the middle of layer 3 in boring 000057_00140 because that is the expected depth based on the known depth to Pleistocene in the adjacent borings. For shallow borings, such as those at the west end of the cross section, the top-of-Pleistocene surface is projected as a queried dashed line below the boring at the depth at which Pleistocene might be expected.

The top-of-Pleistocene surface may be identified based upon different

criteria in different borings. In boring 000057_00100 on Plate 3, it is inferred based on an increase in penetration resistance and a coarsening-upwards sequence of layers 8, 7, and 6, recorded as a change from clay in layer 8 to sand in overlying layers 6 and 7. In contrast, for boring 000057_00139, the top-of-Pleistocene surface is inferred from an increase in penetration resistance with depth for layers with the same USCS classification. Clay layer 3 in boring 000057_00139 has penetration resistance values of 39 and 33 blows per foot; however, clay layer 5 in the same boring has a penetration resistance of 61 blows per foot, and the log states that the sediment is "very hard below 7 feet." Further, it should be noted that the characteristics that are used to identify the top-of-Pleistocene surface in the northern Santa Clara Valley may not be valid for other regions of the valley or elsewhere. The characteristics that are used to identify the top-of-Pleistocene surface may vary from region to region based on factors such as number and type of source areas, regional tectonics, climate, and depositional environment.

After each layer was assigned to a geologic map unit, a contour map showing the elevation of the top of the Pleistocene was constructed. The contours on the map were constructed through the elevation of the top of the uppermost layer in each boring identified as latest Pleistocene. The contour map was reviewed to make sure that the surface depicted by the map was consistent with a land surface that would be expected to develop during a period of low sea level. Remnants of Pleistocene fans exposed along the margins of the present-

day northern Santa Clara Valley were compared to the contour surface constructed using the elevations of the top of the Pleistocene as interpreted from boring logs. The exposed surfaces of Pleistocene fans are places where the elevation of the top of the Pleistocene is known with confidence and can be used as control points when constructing a contour. In particular, borings that caused contour lines to be deflected or drawn in a manner inconsistent with the expected land surface were reviewed and reinterpreted in the context of surrounding borings, and the emerging contour surface of the elevation of the top of Pleistocene was subsequently revised.

During the late Pleistocene, sea level is interpreted to have been as much as 130 m below the current level, resulting in a prolonged period of subaerial exposure, weathering and consolidation (Helley and Lajoie 1979). As sea level dropped, the center of the basin that was once filled with water became exposed. The period at the end of the Pleistocene when sediment was exposed allowed for the development of a distinct pedogenic horizon that has been identified in excavations by Hitchcock and Helley (2003) as defined by a marked increase in density as well as identifiable changes in color and texture.

Liquefaction Analysis

To perform liquefaction analysis, information from individual boring logs was entered into a database without modification (whenever possible). However in some cases, professional judgment was necessary to clarify information

recorded on the log. In particular, the quality of the standard penetration test (SPT) varies considerably from one boring and operator to the next. Non-SPT values add additional variation to liquefaction analysis. Recorded blow counts for non-SPT sampling, where the sampler diameter, hammer weight, drop distance, and energy delivery differ from those specified for an SPT are converted to SPT-equivalent blow count values, when appropriate.

To characterize the quality of each SPT value, each penetration test compiled in the database was ranked from 1 to 29 (CGS unpublished) based upon how closely the sampling matches ASTM D1586-99 standards (ASTM 1999) and whether or not the recorded blow counts can reasonably approximate those of an SPT. For example, a penetration test for which the diameter of the sampler is not known is assigned a quality ranking of 13 if the blow counts have been converted to the SPT equivalent. Penetration tests with a quality ranking lower than 12 were not used (Appendix 2) (CGS unpublished). Where no analysis of laboratory fines content is provided for layers with liquefiable textures, a default (fc) for liquefiable materials was assigned based upon the Unified Soil Classification System (USCS) designation for the layer (Table 3). Similarly, if unit weight data are not provided on the boring logs, then values for each layer based on the layer's soil type must be assumed (Appendix 3) (CGS unpublished). The actual and converted SPT blow counts are normalized using a common reference effective overburden pressure of 1 atmosphere (approximately 1 ton per square foot), and a hammer efficiency of 60% using a method described by

Seed and Idriss (1971, 1982, with updates by Seed, Idriss and Arango 1983, 1985; Seed and De Alba 1986; and Seed and Harder 1990) and updated according to the

TABLE 3. FINES CONTENT (FC) ASSIGNED TO SAMPLES WITH LIQUEFIABLE TEXTURES FOR WHICH NO TEXTURAL DATA WERE PROVIDED ON BORING LOGS (Knudsen et al. 2004)

	Curve used in triggering evaluation [†]	FC used in $(N_1)_{60,cs}$ calculation [‡]
<u>Standard/conforming USCS categories</u>		
GW, GP, SW, SP	SD	2.5
GW-GM, GW-GC, GP-GC, SW-SM, SW-SC, SP-SM, SP-SC	SM	8.5
GM, SM	SM	24
GC-GM, SC-SM	ML	30
GC, SC, ML	ML	35
<u>Other non-USCS categories found on boring logs[§]</u>		
GP-SP, GW-GP, SW-SP "cobbles & boulders", "gravel", "gravel and sand", "sand"	SD	2.5
"artificial fill", "soil"	SM	12
GP-SM, SM-SP	SM	14
SC-SP, SC-GP	SM	19
GM-SM, "alluvium", "loess"	SM	24
ML-SM, SM-SC	ML	30
ML-CL, SC-CL, SC-ML, SM-CL, SM-ML	ML	35

[†] curve assigned for use in Simplified Procedure triggering analysis (SD- 5%, SM - 15%, ML - 35% fines content)

[‡] fines content in percent assigned (when no laboratory textural data are available) for use in calculating $(N_1)_{60,cs}$

[§] soil descriptions found on boring logs that do not conform with USCS categories; these categories are not recommended for use in logging borings

recommendations of Youd et al. (2001) and Seed et al. (2003). This normalized blow count is referred to as $(N_1)_{60}$. Some of the methods for evaluating the susceptibility of deposits to liquefaction and the potential for deformation include adjusting the $(N_1)_{60}$ value for the fines content of the sample; this adjusted "clean-sand equivalent" value is referred to as $(N_1)_{60,cs}$. Finally, the liquefaction potential of each layer in every boring is evaluated deterministically using the methods of Youd et al. (2001) and probabilistically using the methods of Seed et al. (2003).

The deterministic model proposed by Seed et al. (1984, 1985) uses SPT-based correlations. With minor modifications proposed by the NCEER Working

Group (NCEER 1997; Youd et al. 2001), this correlation is one of the most widely accepted correlations that is still used in practice (Fig. 3) (Cetin et al. 2004).

Figure 3 shows the relationship between the standard penetration test $(N_1)_{60}$ measured for a soil, with respect to intensity of cyclic loading, expressed as a magnitude-weighted equivalent uniform cyclic stress ratio (CSR_{eq}) approximating earthquakes with magnitudes of 7.5 (Cetin et al. 2004).

The cyclic stress ratio for a soil layer is calculated by using the equation developed by Seed and Idriss (1971).

$$CSR = .65(a_{max}/g) (\sigma_{vo} / \sigma'_{vo}) r_d \quad (\text{equation 1})$$

CSR = Cyclic Stress Ratio

a_{max} = Peak horizontal ground acceleration

g = acceleration of gravity

σ_{vo} = vertical overburden stress

σ'_{vo} = vertical overburden stress minus pore pressure

r_d = non-linear shear mass participation factor minus stress reduction coefficient to account for flexibility in the soil

Peak horizontal ground acceleration (a_{max}) is derived from the statewide probabilistic seismic hazard evaluation released cooperatively by the California Department of Conservation, California Geological Survey, and the U.S. Geological Survey (Petersen et al. 1996).

In contrast, probabilistic models include data from a growing set of field observed liquefaction case history data from earthquakes that have occurred since 1984 (Seed et al. 2003). The term probabilistic refers to “triggering” of liquefaction, not the consequences (resulting from deformation). Probabilistic

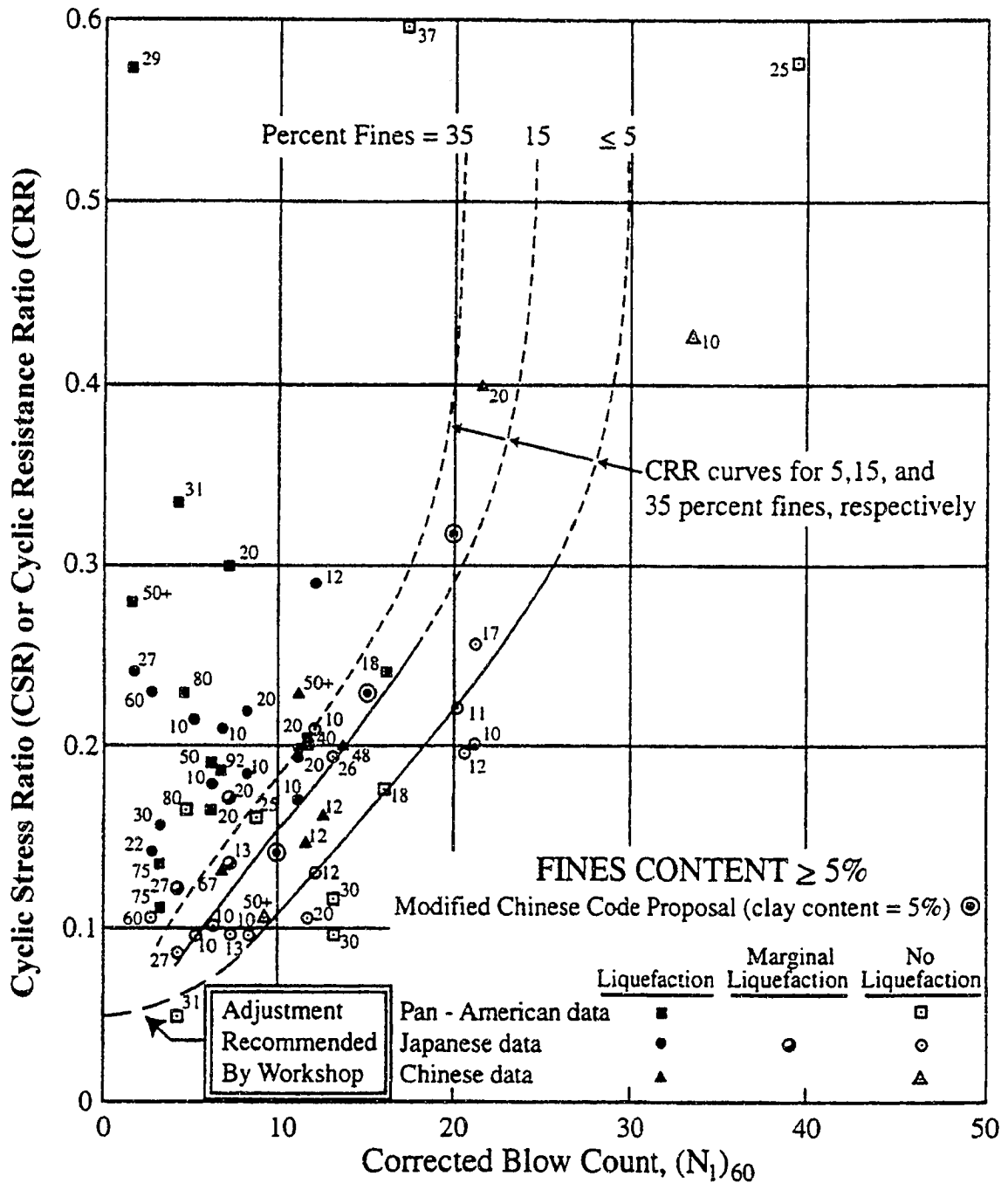


Figure 3. Deterministic correlation for evaluation of liquefaction potential. The chart shows CRR curves for clean sand (5% fines), silty sand (15% fines), and silt (35% fines). Given a corrected blow count value $[(N_1)_{60}]$ from a valid penetration test and the fines content of the soil, the CRR value is read off the y-axis (Seed et al. 1984; Youd et al. 2001).

charts (Fig. 4) commonly are plotted with the deterministic curves derived by Seed et al. (1984) from Figure 3.

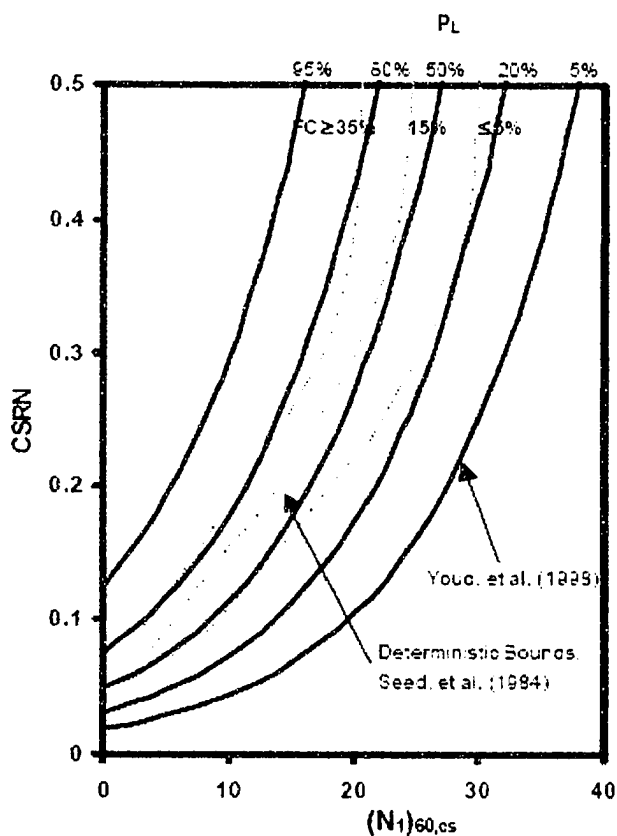


Figure 4. Probabilistic correlation for evaluation of liquefaction potential (Youd et al. 1997). This chart shows probability of liquefaction curves plotted in same space as deterministic correlations of Seed et al. (1984).

To use the chart in Figure 3, the corrected SPT value is plotted in the CSR - $(N_1)_{60}$ space and then the results are reviewed to see whether the point falls to the left or right of the appropriate empirically determined curve. The liquefaction curves are calibrated for liquefiable textures that describe clean sand (5% fines), silty sands (15% fines) and silt (35% fines). Similarly, to use the chart in Figure 4

the corrected SPT values are plotted in the CSR - $(N_1)_{60}$ space and then the results are reviewed to see whether the point falls to the left or right of the appropriate curve denoting probability of liquefaction. The Factor of Safety against liquefaction (FS), an estimate of whether liquefaction will occur, is the ratio of a soil's resistance to liquefaction (CRR), to the cyclic seismic loading imposed on the soil (CSR) (Seed and Idriss 1982):

$$\text{Factor of Safety} = \text{CRR/CSR} \quad (\text{equation 2})$$

The CGS liquefaction analysis program calculates a FS for each geotechnical sample where blow counts were collected. Typically, multiple samples are collected for each borehole. The program then independently calculates a FS for each non-clay layer that includes at least one penetration test using the minimum $(N_1)_{60}$ value for that layer. The minimum FS value of the layers penetrated by the borehole is used to evaluate the liquefaction potential for each borehole location. The reliability of FS values varies according to the quality of the geotechnical data (CGS 2006).

The liquefaction potential index (LPI) defined by Iwasaki et al. (1982) provides an estimate of the severity of liquefaction at a specific location. The purpose is not to predict the occurrence of liquefaction, but rather to indicate the potential for ground failure manifested by occurrences of sand boils or other similar phenomena as a result of liquefaction. The LPI calculation takes into

account the thickness of the liquefied layer, the proximity of the liquefied layer to the ground surface, and the degree to which the Factor of Safety for a particular boring is less than 1.0 (Iwasaki et al. 1982). The calculation requires a maximum depth of 20 m. LPI values calculated for borings that penetrate the subsurface to a depth shallower than the required depth are considered minimum values.

Deformation Analysis For Level-Ground Conditions

Two classes of methods for estimating quantities of post-liquefaction ground deformation, both of which are typically used in site investigations, not in regional mapping, are (1) empirical predictions of lateral spread displacements, and (2) predictions of volumetric and shear strains (Knudsen et al. 2004) (Fig. 5). This study deals only with predictions of volumetric and shear strain, which can be predicted using either semi-empirical formulations or numerical simulations. Semi-empirical methods for predicting shear and volumetric strain are based on a growing set of laboratory data and improved understanding of processes; some of these methods have been calibrated against the growing database of historical ground failure case histories. Probabilistic liquefaction triggering analysis and analysis of volumetric strain for non-saturated soils also may be incorporated into these methods. The major disadvantages of applying the semi-empirical methods to estimate shear and volumetric strain are that these methods require detailed geotechnical data (for best results laboratory data

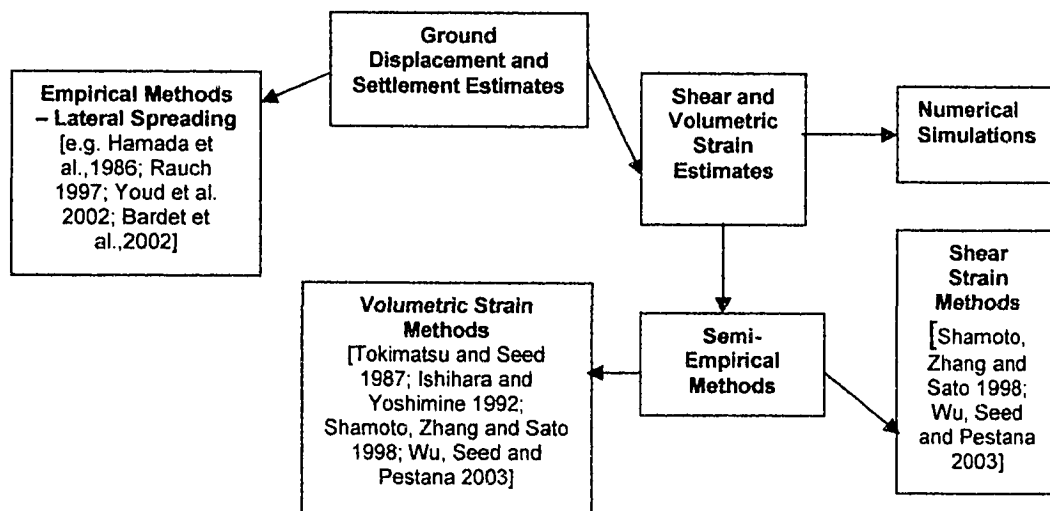


Figure 5. Methods of predicting liquefaction-induced deformation (Knudsen et al., 2004)

are used) that can be expensive to collect (Knudsen et al. 2004).

The methods of Wu (2002), Wu and Seed (2004), and Wu et al. (2003) are based on laboratory testing, specifically cyclic simple shear testing of undrained samples of fully saturated sand. Wu (2002) conducted tests using Monterey No. 0/30 sand, with strain measured at 15 cycles (approximating an M 7.5 earthquake), pressures of 40kPa, 80kPa, and 180kPa, and relative densities ranging from 35% to 80%. The results of the testing show that measured strain (for level ground conditions) falls within the ranges predicted by the limiting strain charts formulated by Tokimatsu and Seed (1987). Among the benefits of this method is that, in addition to providing an estimate of probability of liquefaction (P_L), it includes updates to previously developed tools including a new nonlinear

shear mass participation factor (R_d) and new fines correction factor (C_{fines}) (Knudsen et al. 2004).

There are four steps required to apply the method of Wu (2002) and Wu et al. (2003): (1) evaluate liquefaction susceptibility for each saturated layer as described earlier in this section; (2) use the values of $(N_1)_{60, \text{cs}}$ and CSR estimated in step one in conjunction with a new family of curves (Fig. 6) to estimate the post-liquefaction reconsolidation volumetric strain (settlement) of each saturated, liquefiable layer; (3) calculate volumetric compression of non-saturated sandy layers according to the procedures of Tokimatsu and Seed (1987); and (4) sum the volumetric changes of all saturated and unsaturated soil layers. The new procedure was shown by Wu and Seed (2004) to perform well for a suite of field performance case histories with small to moderate ground settlements.

Wu (2002) also proposed a new pragmatic chart (Fig. 7) for prediction of limiting shear strain (displacement). This chart, however, is preliminary because it has yet to be thoroughly calibrated against field performance case histories, so it may be updated or modified in the future.

The methods for estimating volumetric strain yield results that can be thought of as “predicted” or as “within-a-factor-of-two,” whereas the relationships used to estimate future shear strain should be thought of as “limiting” or “potential” values (Knudsen et al. 2004). Because shear strain amplitude

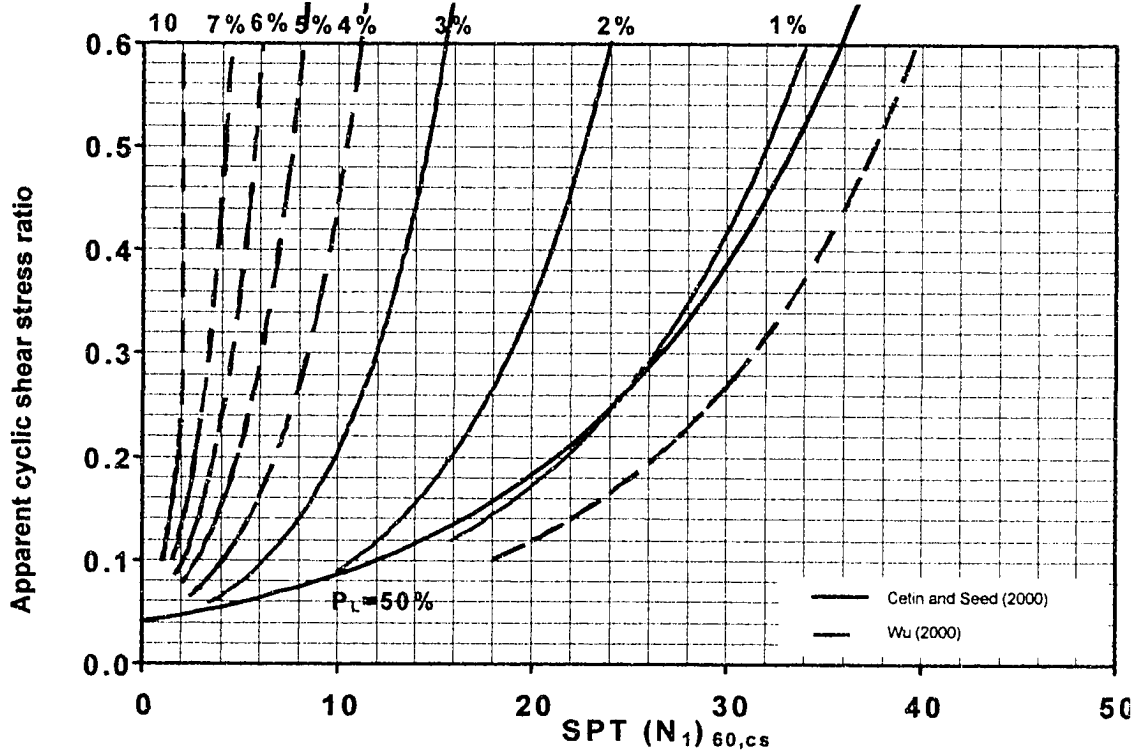


Figure 6. Proposed correlations between CSR, $(N_1)_{60,cs}$ and reconsolidation volumetric strain (Wu et al. 2003).

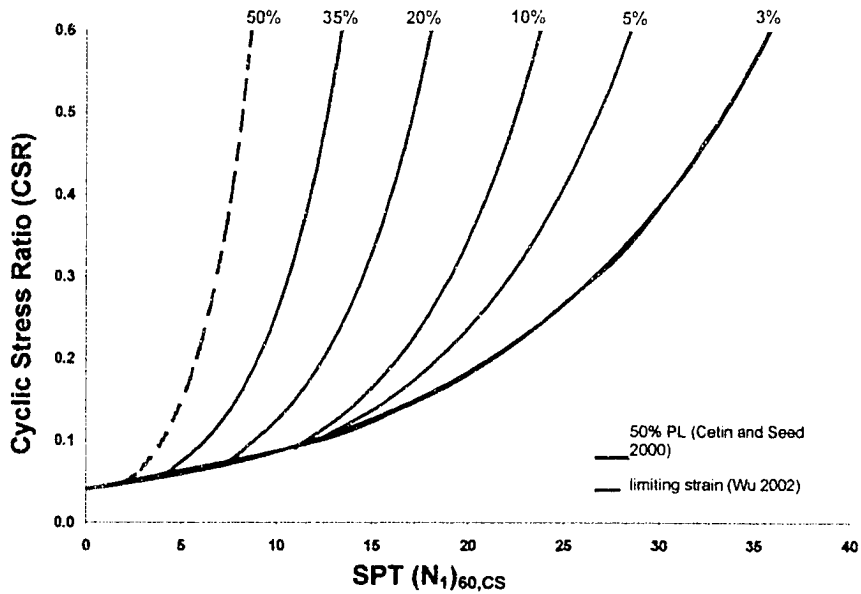


Figure 7. Proposed correlations between CSR, $(N_1)_{60,cs}$ and limiting shear strain (Wu et al. 2003).

continues to accumulate in liquefied sands under constant shear load conditions, liquefaction-induced shear strain is uniquely defined by selection of a pre-determined number of cycles (Knudsen et al. 2004). For the Wu (2002) method, liquefaction-induced limiting shear strain is defined as the single amplitude shear strain at the 15th loading cycle, which is the approximate number of uniform loading cycles in a typical M_w 7.5 earthquake.

Finally, the potential volumetric and shear strain that can be expected in deposits from different geologic environments and of different ages is characterized using the results of the post-liquefaction deformation analysis. The predicted strain of individual geologic map units is estimated by multiplying the calculated strain (for each combination of CSR and corrected penetration resistance) by the thickness of each layer containing saturated sediment with liquefiable textures and then summing the calculated deformation amounts for all of the layers for each map unit.

Deformation potential calculations are carried out only for layers with liquefiable textures (Table 3) and are then summed over the entire length of the boring. A value of zero is assigned to a layer for which either (1) the particular combination of N-value and CSR for that layer does not result in measurable strain, or (2) the particular combination of N-value and CSR for the layer results in measurable strain but the liquefiable textures in the layer are not saturated. The depths to first-encountered unconfined ground water were plotted onto a map of the project area and contoured to constrain the estimate of historically

shallowest ground water. An anticipated high ground-water level is estimated based on historical ground-water data. In areas where ground water is either currently near-surface or could return to near-surface levels within a land-use planning interval of 50 years, CGS constructs regional contour maps that depict these levels (CGS 2006). A null value means that either no liquefiable textures are present and/or that no penetration test data are available, and therefore strain could not be calculated. Thus, where data are not available, calculated values must be considered minima.

RESULTS

Each layer in each of the 668 boring logs was assigned to Quaternary map units and used to characterize the geology of the northern Santa Clara Valley and interpret the Holocene-late Pleistocene boundary in the subsurface. The geotechnical data were grouped and analyzed with respect to the geologic map unit to which each layer was assigned, and with respect to the age of the geologic unit mapped at the surface of each boring.

Trends in the data revealed during the analysis, such as an increase or decrease in a given geotechnical parameter interpreted as the result of an increase or decrease in the age of sediment, are used to validate the methods used in this project. For instance, penetration resistance is expected to increase as a result of increasing age because the sediment has been subjected to consolidation for a longer period of time. If the results of the analysis do not conform to the expected outcome, it may be an indication that errors were made in the interpretation and assignment of the layers in the borings to a particular geologic map unit.

A range of geotechnical parameters is recorded and calculated for each of the layers within each boring and for the boring as a whole. The liquefaction potential of each layer is evaluated deterministically using the methods of Youd et al. (2001) and probabilistically using the methods of Seed et al. (2003). Other parameters calculated for each layer include factor of safety (FS) and probability

of liquefaction (P_L). Parameters calculated for each boring include the thickness of sediment with liquefiable textures, the thickness of saturated liquefiable sediment, and the liquefaction potential index (LPI). The results of the various analyses are used to create maps of liquefaction-induced deformation based upon the geotechnical and geologic characterization of the sediments in the northern Santa Clara Valley.

Nearest Neighbor Statistics

A geostatistical approach is adopted to evaluate the variability in sediment properties from boring to boring. Figure 8 uses the T_{15} parameter, a parameter introduced by Youd, Hansen and Bartlett (2002) and Bardet et al. (2002) in their lateral spread predictive models, to describe the thickness of saturated sediment with liquefiable textures and penetration resistance values of less than 15. In a setting with "layer cake" geology, T_{15} values should be similar from boring to boring. Figure 8 shows that 900 m is the maximum distance for which there is a relationship between adjacent borings (in the T_{15} parameter) (Knudsen et al. 2004). However, the median separation distance between any two borings in the study area is approximately 1,044 m. This means that caution is warranted for estimates of geotechnical and geologic properties made for areas that are more than 900 m from the nearest boring and between borings more than 900 m apart. The conclusion that can be drawn from this information is that a greater density

of borings would improve understanding of the geologic variability in this area (Knudsen et al. 2004).

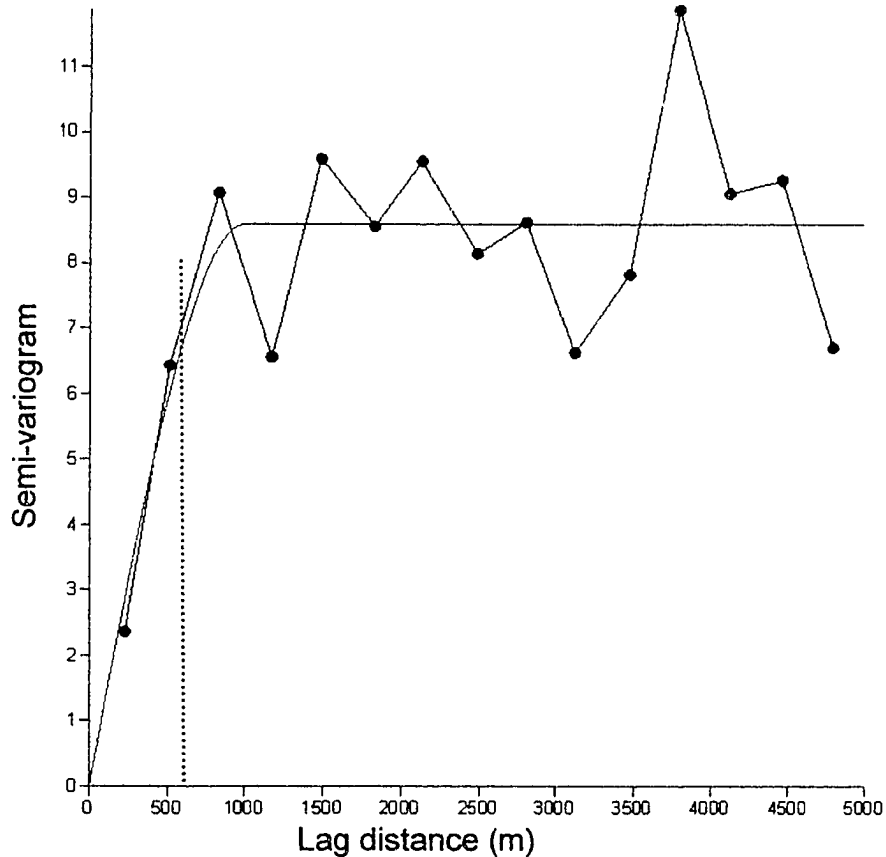


Figure 8. Nearest neighbor semi-variogram. Semi variance is a measure of the degree of spatial dependence between samples (Clark and Harper 2000). A semi-variogram measures the variance between data as a function of distance. The maximum separation distance for borings in the study area for which there is a relationship between adjacent borings is approximately 900 m (Knudsen et al. 2004).

Pleistocene Surface Elevation Map (Interpreted)

As mentioned at the outset of the Methods section, the geotechnical properties of materials in the borings were used to infer a three-dimensional

surface that broadly defines a boundary based on density differences. For the purposes of this study, that surface is generally interpreted as the Holocene-Pleistocene boundary (Plate 4). However, evidence indicates that the two surfaces do not coincide in some areas. In any event, for the purposes of liquefaction hazard mapping, it is more important to identify the change in the geotechnical properties of sediment than the age of sediment.

It was possible to identify a change in the measurable geotechnical properties of sediment such as penetration resistance in 215 of 668 borings used in this study. Approximately 272 borings penetrate to significant depths in the center of the valley where the Pleistocene surface is deepest, so contours in the center of the valley are constructed with much less confidence than those near the valley edges. It appears that during the late Pleistocene a significant volume of the Santa Clara Valley was drained by one primary source oriented roughly parallel to the present day location of Coyote Creek, or that two large streams were flowing parallel and in close proximity to one another like Guadalupe River and Coyote Creek are today.

Mapping the elevation at which the change in the penetration resistance of sediment occurs results in the depiction of a surface that is a reasonable representation of a natural land surface. The surface depicted on the map suggests an environment where the land surface was stable for a period of time long enough for it to begin to be incised by numerous small drainages, and depicts a surface that closely resembles the topography of the modern land

surface. Dates obtained for sediment in eight deep wells in the northern Santa Clara Valley collected by Carl Wentworth and John Tinsley of the USGS indicate that the elevation of the top of Pleistocene based on dates is somewhat lower than the surface depicted on Plate 4 (Carl Wentworth oral communication 2007) indicating imperfect correlation of geotechnical and stratigraphic boundaries. Wentworth (oral communication 2007) notes that "the latest pulse of sedimentation started before the end of the Pleistocene, and therefore, one may argue that the geotechnical boundary coincides with the top of the Pleistocene".

Liquefiable Textures

Table 4 shows that for many of the geologic map units fewer than half of

TABLE 4. PERCENTAGE OF EACH GEOLOGIC MAP UNIT WITH TEXTURES THAT ARE POTENTIALLY LIQUEFIABLE

Geologic map unit	Number of layers		Layer thickness	
	# of layers	% of layers with liquefiable texture (%)	Cumulative thickness of all layers (m)	% of total with liquefiable textures
af	223	26	329	14
alf	11	55	21	57
Qhc	20	65	53	55
Qhfy	46	22	78	13
Qhly	169	37	323	28
Qhty	87	44	129	31
Qhbm	29	7	51	9
Qhb	17	18	35	7
Qhfe	103	31	160	18
Qhf	1700	47	2925	42
Qhff	267	14	488	10
Qhl	357	53	611	48
Qht	8	88	8	92
Qf	116	46	415	37
Ql	12	50	17	39
Qt	2	100	2	100
Qpf	561	59	1304	58

See Table 1 for geologic map unit definitions, units are listed in order of increasing age

the sediment layers described on the compiled boring logs are coarse enough to liquefy. Calculations of liquefaction-induced strain are made only for the layers with granular textures (thus not USCS classes CL, CH, MH, ML-CL, OH, OL, Pt) because fine-grained soils are not expected to liquefy. Map units that are expected to be fine grained (e.g. Qhb – Holocene basin deposits, Qhff – Holocene alluvial fan, fine facies, Qhbm – Holocene Bay mud) all consist of more than 80 to 85% fine sediment.

$(N_1)_{60,cs}$, Factor of Safety, and Cyclic Resistance Ratio

Table 5 shows several trends are evident. (1) $(N_1)_{60,cs}$ values for sediment with liquefiable textures are generally low; in most cases the median values are less than 15, a value previous researchers have considered an upper bound for sediment likely to experience large-scale liquefaction-related deformation. (2) The method of Youd et al. (2001) results in median $(N_1)_{60,cs}$ values that tend to be 2 to 3 blows/ft higher than the values calculated using the method of Seed et al. (2003). The methods of Youd et al. (2001) and Seed et al. (2003) are identical except in the input value for the non-linear shear mass participation factor (r_d). The non-linear shear mass participation factor is used to account for the fact that a column of soil does not act like a rigid body, so the peak shear stress calculated using equation 1 decreases with depth (Cetin and Seed 2000). The stress reduction coefficient r_d is a function of site stratigraphy, soil properties, and the characteristics of the "input" motions (excitations). By definition, it has a value of 1.0 at the ground surface (Cetin and Seed 2000). The methods of Seed et al.

(2003) use improved correlations for estimation of r_d as calculated by Cetin and Seed (2000). Cetin and Seed (2000) performed 2,153 seismic site response analyses to examine the change in r_d for a range of site conditions and ground motion excitation characteristics (Seed et al. 2003). Cetin and Seed (2000) found that the r_d suggested by Seed and Idriss (1971) (and used by Youd et al.,

TABLE 5. FINES CORRECTED PENETRATION RESISTANCE, FACTOR OF SAFETY AND CYCLIC RESISTANCE RATIO (SUMMARIZED BY LAYER FOR ALL GEOLOGIC MAP UNITS)

Geologic map unit	Penetration Resistance (N_1) _{60,cs}				Factor of Safety (only liquefiable textures)				Cyclic Resistance Ratio (CRR)		standard deviation
	# of layers	median [Seed et al., 2003]	median [Youd et al., 2001]	% of layers	median [Seed et al., 2003]	# of FS values	mean FS	median FS	mean	median	
af	48	10.4	13.1	163	11.9	42	0.7	0.3	0.27	0.15	0.29
alf	5	6.3	9.8	75	8.5	5	0.2	0.2	0.12	0.09	0.05
Qhc	11	11.2	11.6	100	11.2	11	0.5	0.4	0.36	0.23	0.36
Qhfy	7	11.1	14.8	100	11.1	7	0.6	0.4	0.16	0.17	0.04
Qhly	54	6.5	9.5	95	6.5	51	0.4	0.3	0.21	0.17	0.19
Qhty	28	7.0	9.4	100	7.0	27	0.3	0.2	0.20	0.15	0.19
Qhbm	1	8.5	12.1	0	na	na	na	na	na	na	na
Qhb	4	6.2	9.7	50	7.9	4	0.2	0.2	0.15	0.15	na
Qhfe	15	4.8	7.9	100	4.8	15	0.2	0.2	0.18	0.12	0.24
Qhf	598	11.2	14.2	89	11.6	553	0.5	0.3	0.35	0.20	0.33
Qhff	35	8.7	12.3	55	9.5	31	0.4	0.3	0.24	0.18	0.24
Qhl	137	10.3	13.8	90	10.3	135	0.4	0.3	0.27	0.17	0.27
Qht	4	28.9	31.1	100	25.3	4	1.0	1.2	1.00	1.00	na
Qf	41	10.8	13.6	100	10.8	40	0.4	0.3	0.23	0.22	0.17
Qi	4	8.5	12.1	100	8.5	4	0.2	0.2	0.15	0.14	
Qt	2	26.3	28.8	100	26.3	2	0.7	0.7	na	na	na
Qpf	227	19.2	21.5	93	19.8	222	0.9	0.7	0.56	0.35	0.39

See Table 1 for unit definitions. Units are listed in order of increasing age. Textures that are not subject to liquefaction include CL, CH, MH, ML-CL, OH, OL, Pt.

2001) underestimates the degree to which r_d may vary with changes in site conditions and ground motion characteristics, and results in overestimates of r_d between depths of 10 and 50 feet, the depth range for which liquefaction potential is calculated (Seed et al. 2003). It is likely that the difference in r_d values accounts for the difference in corrected blow count values. (3) The median factor of safety (FS) value for most geologic map units is much less than 1. Where the FS value is less than 1, layers with potentially liquefiable textures are prone to liquefaction when subjected to a level of shaking that has only a 10% probability of being exceeded in 50 years. However, it is important to remember that a significant fraction of the sediment in the study area is composed of fine-grained materials – materials that are too fine to be likely to liquefy. For instance, Table 5 shows that the median FS value for latest Holocene alluvial fan deposits (Qhfy) is 0.17. However, Table 4 shows that only 22% out of a total of 46 layers, and only 13% out of the total thickness of 78 meters of sediment, are composed of liquefiable textures. This means that although the composition of Qhfy includes sediment that is liquefiable, the relative abundance of the liquefiable fraction of Qhfy is low.

Figure 9 summarizes some of the geologic characteristics of the liquefiable deposits found in the study area. Because geologic characteristics are often complex and difficult to model, data distributions are frequently non-ideal, although some interpretation is possible. Figure 9 illustrates a range of measured penetration resistance values for layers as grouped according to age

for latest Holocene (Qhfy, Qhly, Qhty, and Qhfe), Holocene (Qhb, Qhc, Qhf, Qhff, Qhl, and Qht) and latest Pleistocene (Qf, Ql, Qt, and Qpf) ages. The x axis

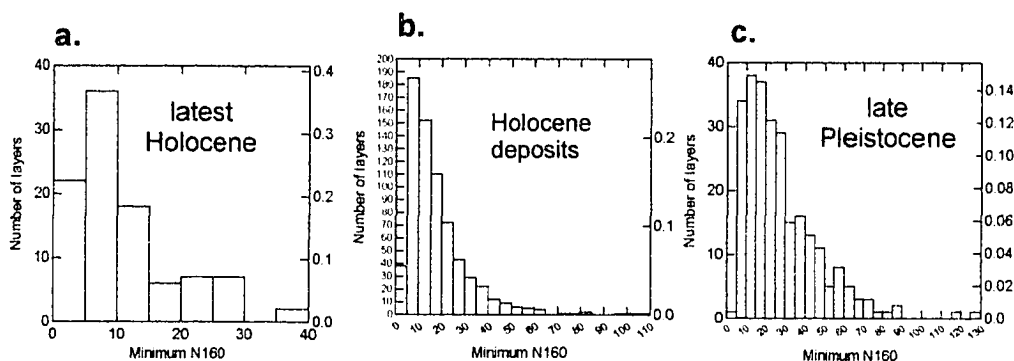


Figure 9. Histograms of penetration resistance (by layer, only liquefiable textures are included). From a. Latest Holocene [number of layers = 98, mean=11.5, median=8.9]; b. Holocene deposits [number of layers = 693, mean=17.7, median=14.1]; and c. Latest Pleistocene deposits [number of layers = 255, mean=28, median=23].

records the minimum penetration resistance of each layer, and the y axis records the number of layers for each $(N_1)_{60}$ value. Late Pleistocene layers (Fig. 9c) have the highest penetration resistance, with a median value of 23, followed by Holocene (Fig. 9b) layers with a median value of 14.1, and latest Holocene deposits (Fig. 9a) with a median value of 8.9. The overall increase in density with increasing age of the deposit is likely a reflection of the fact that older deposits have been subjected to compaction and lithification processes longer.

Plate 5 shows histograms of all penetration resistance measurements (from layers with liquefiable textures) collected for this research. Each layer has been assigned a geologic map unit based on interpretation of the stratigraphy depicted in the boring logs as described above. The histograms for map units for

which there are a sufficient number of samples (e.g. Qhly, Qhfe, Qhf, Qhl) suggest that $(N_1)_{60,cs}$ populations are not normally distributed, but are more likely to be log-normally distributed. There appears to be a general trend of increasing penetration resistance with increasing age of deposits, as observed in Table 5. A “box and whisker” plot of these same data (Fig. 10) shows that the properties of the map units overlap. The results depicted on Figure 10 underscore an important point: if the methods used in this research are to be applied in other geographic regions, the minimum number of borings necessary to produce meaningful results will vary based upon the complexity of the geology of the region under investigation.

Liquefaction Potential Index

LPI has been calculated for all borings in the study area with saturated, loose, granular deposits for which penetration test data are available. Figure 11 shows that many geologic map units have calculated median LPI values in the range of 10 to 15. Toprak and Holzer (2001) found that the surface manifestation of liquefaction-induced deformation is 93% for LPI values of near 15 and 58% for values near 5. Because sediment becomes increasingly resistant to liquefaction with age, LPI should decrease with increasing age. However, calculated LPI values for Holocene and late Pleistocene deposits in this study do not follow the expected trend. The reason for this difference may be that the LPI parameter expresses only the probability of surface manifestations of liquefaction and not

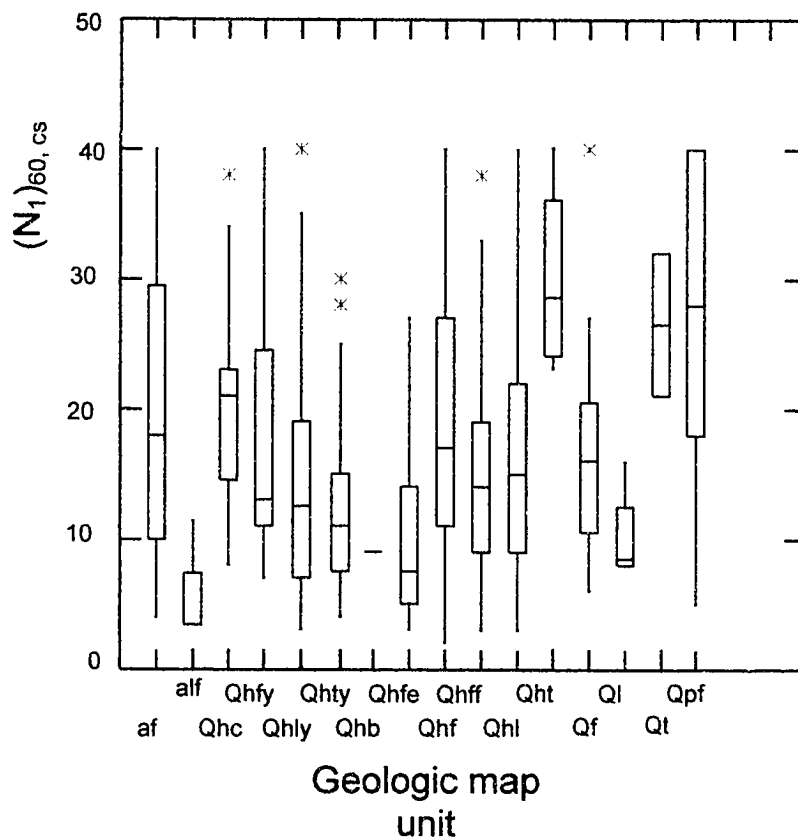


Figure 10. Box and whisker plot of fines corrected penetration resistance measurements for every layer in the project geotechnical boring database. The length of the box shows inter-quartile range (the median of the upper part of the data minus the median of the lower part of the data) and larger box lengths indicate greater variability in the data set; the line through the box shows the median value. The "whiskers" show the overall range of the data. Outliers in the data set are represented by stars at either end of the whiskers. Geologic map units are listed in order of increasing age from left to right.

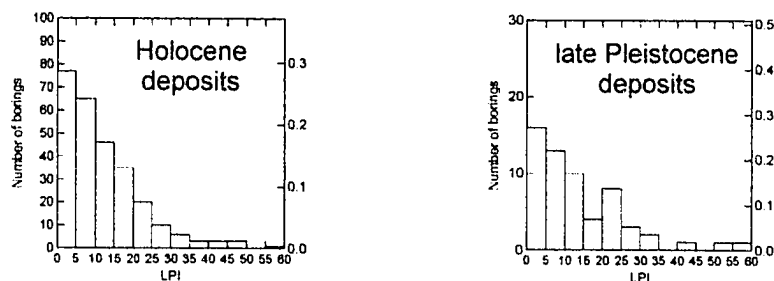


Figure 11. Liquefaction Potential Index calculated for borings aggregated to the representative age of the majority of deposits (Holocene or Late Pleistocene) in the boring; Holocene deposits [number of borings = 269, median = 9.6], Late Pleistocene deposits [number of borings = 59, median = 10.4].

magnitudes of deformation. Toprak and Holzer (2003) noted that pockets of potentially liquefiable material that are not laterally continuous might yield a high LPI value but no surface manifestations of liquefaction, whereas a thin but widely distributed potentially liquefiable layer that is deeply buried might yield a low LPI yet produce significant liquefaction-related surface features. Sedimentary deposits in the northern Santa Clara Valley are highly variable both laterally and vertically over a short distance. It is possible that sediment that is identified as late Pleistocene contains discontinuous lenses of potentially liquefiable material, that are not likely to produce deformation features at the ground surface.

Deviation from expected results may also be due to the fact that not all of the borings in this study reach the minimum required depth of 20 m (Iwasaki et al. 1982) and/or that more data are needed.

Estimating Strain for Each Geologic Map Unit

Table 6 summarizes data generated by the methods of Wu et al. (2004) (volumetric strain) and Wu (2002) (limiting shear strain) liquefaction-induced ground deformation models used in this study. The table shows strain calculations for borings grouped according to surficial geologic map unit.

TABLE 6. CALCULATED VOLUMETRIC AND LIMITING SHEAR STRAIN ALONG WITH SETTLEMENT AND HORIZONTAL DISPLACEMENT FOR BORINGS INITIATED IN EACH GEOLOGIC MAP UNIT

	#	Volumetric strain (%)			Settlement (meters)			Shear strain (%)			Displacement (meters)		
		μ	med	σ	μ	med	σ	μ	med	σ	μ	med	σ
afbm	6	4.5	4.8	0.6	0.1	0.1	0.1	42.1	43.0	5.4	1.2	1.0	0.7
alf	24	3.1	3.0	1.7	0.1	0.1	0.2	26.5	27.1	16.8	1.0	0.5	1.3
ac	2	2.7	2.7	0.9	0.2	0.2	0.1	26.8	26.8	9.0	1.9	1.9	1.5
Qhc	3	1.0	0.5	1.3	0.0	0.0	0.1	7.9	0.0	13.7	0.4	0.0	0.6
Qhfy	21	3.1	3.0	1.4	0.1	0.1	0.1	28.6	27.2	15.6	0.9	0.7	0.7
Qhly	28	2.7	2.9	1.6	0.1	0.1	0.1	24.9	24.2	17.7	1.1	0.8	1.2
Qhty	18	3.2	3.2	1.3	0.1	0.1	0.1	30.0	27.5	16.0	0.9	0.8	0.7
Qhfe	11	4.2	4.1	2.0	0.2	0.1	0.2	33.8	30.3	15.1	1.6	1.1	1.4
Qhf	183	1.4	0.8	1.7	0.0	0.0	0.1	11.7	0.6	16.3	0.3	0.0	0.8
Qhff	72	2.2	2.1	1.6	0.1	0.0	0.1	18.9	14.7	16.8	0.5	0.3	0.7
Qhl	87	2.4	2.6	1.8	0.1	0.0	0.1	21.7	20.9	17.9	0.6	0.4	0.7
Qht	4	2.3	2.3	1.5	0.2	0.2	0.1	20.1	19.3	15.4	1.6	1.5	1.5
Qf	6	1.2	1.3	0.8	0.0	0.0	0.0	5.3	6.1	4.8	0.1	0.0	0.1
Qt	1	0.9	--	--	0.1	-	-	1.0	--	--	0.2	-	-
Qpf	23	0.2	0.0	0.4	0.0	0.0	0.0	0.5	0.0	1.3	0.0	0.0	0.1

"Predicted" volumetric strain is calculated and shown here using the Wu et al. (2004) approach. This method assumes nearly level ground and, based on comparison with case studies yields estimates that should be within a factor of two of future settlement.

See Table 1 for listing of names of geologic map units.

"Limiting" shear strain is calculated and shown here using the preliminary correlations by Wu (2002). This method assumes nearly level ground and yields estimates that should be considered maxima.

- number of borings; μ mean; med - median; σ - standard deviation.

To estimate amounts of volumetric strain or limiting shear strain, the calculated strain is multiplied by the thickness of saturated sediment with potentially liquefiable textures. Table 6 reveals that there is an inverse correlation between the age of the deposit mapped at the ground surface and estimated strain – generally, the younger the deposit the larger the estimated strain. The younger deposits (e.g. the late Holocene units Qhfy, Qhly, Qhty and

Qhfe) generally are less dense and thus more susceptible to liquefaction triggering and the subsequent deformation. As noted in the methods section, the methods for estimating volumetric strain yield results that can be thought of as "predicted" or as "within-a-factor-of-two," whereas the relationships used to estimate future shear strain should be thought of as "limiting" or "potential" values.

The median strain values for each geologic map unit are grouped into five categories (ranging from Very Low to High) according to the median strain value for all borings that penetrate a given geologic unit at the ground surface. Plates 6 and 7 show where these units occur at the land surface. The colored dots on each map represent the locations of borings for which strain was calculated, where the color of each dot correlates to the total amount of strain for all layers composed of saturated, liquefiable textures summed for the entire length of each boring. The higher values of both volumetric and shear strain tend to be located adjacent to Guadalupe River and Coyote Creek (the two largest water courses in the study area), and where these water courses discharge into the San Francisco Bay. Areas adjacent to active water courses where thick accumulations of loose, saturated and granular material are more susceptible to liquefaction (Witter et al. 2006) appear to have a correspondingly higher susceptibility to liquefaction-induced strain. In contrast, older sediment that has been subjected to consolidation over a longer period of time is less susceptible to liquefaction

(Witter et al. 2006) and appears to have a correspondingly lower susceptibility to liquefaction-induced strain.

On Plates 6 and 7, the geologic map unit artificial fill over Bay Mud (afbm) is assigned to the category with the highest median strain value. Clay is not considered a liquefiable texture because cohesive fines such as clays (a primary component of mud) do not liquefy during undrained cyclic loading, i.e., earthquake shaking (Boulanger and Idriss 2004). However, because fill associated with afbm is less likely to be engineered and in many locations was dredged from sandy areas (Witter et al. 2006), even though the unit includes a high percentage of clay, the liquefaction susceptibility of afbm is considered Very High and the potential for liquefaction-induced strain for afbm is likely to be high as well.

Strain results summed for all saturated, liquefiable textures for which penetration test data are available in each boring suggest that for borings near Guadalupe River and Coyote Creek there is limited agreement between the amount of volumetric or limiting shear strain per boring and median strain value for the geologic map unit in which the boring is located. However, overall it appears that borings located near Guadalupe River and Coyote Creek tend to have the highest strain values (categories High, Moderate-High, and Moderate) regardless of whether or not the amount of strain for an individual boring falls into the same strain category as the map unit in which it is located.

Figures 12 and 13 show the number of individual borings assigned to each

strain category that plot in the correspondingly colored polygon representing the same amount of deformation on the strain maps. Of the 668 borings reviewed for this research, percent strain was summed for 489 borings that record penetration test data and contain layers composed of saturated, liquefiable textures. Figures 12 and 13 show that a small number of the borings plot within the map polygon that represents the same strain category. Figures 14 and 15 show the percent of borings that plot within the map polygon that represents the same strain category, as well as the percent of borings that plot within the polygon with the next higher and lower strain category. The relatively low correlation between mapped strain category and the strain category for each individual boring is most likely due to the fact that sedimentary deposits in the map area vary vertically and laterally over a short distance. Variability in distribution of sedimentary deposits results in variation in susceptibility to liquefaction, and subsequent liquefaction-induced strain.

The purpose of this study is to try to understand how well the range of variability in strain that is likely to occur within a given geologic map unit may be predicted by the environment in which the sediment was deposited. For instance, distal fan areas such as Holocene alluvial fan, fine facies (Qhff) are typically low-energy environments characterized by deposition of fine sediments such as silts and clays. The relative percent of silt and clay sampled in multiple boring advanced into Qhff sediment may vary. One boring may include a larger

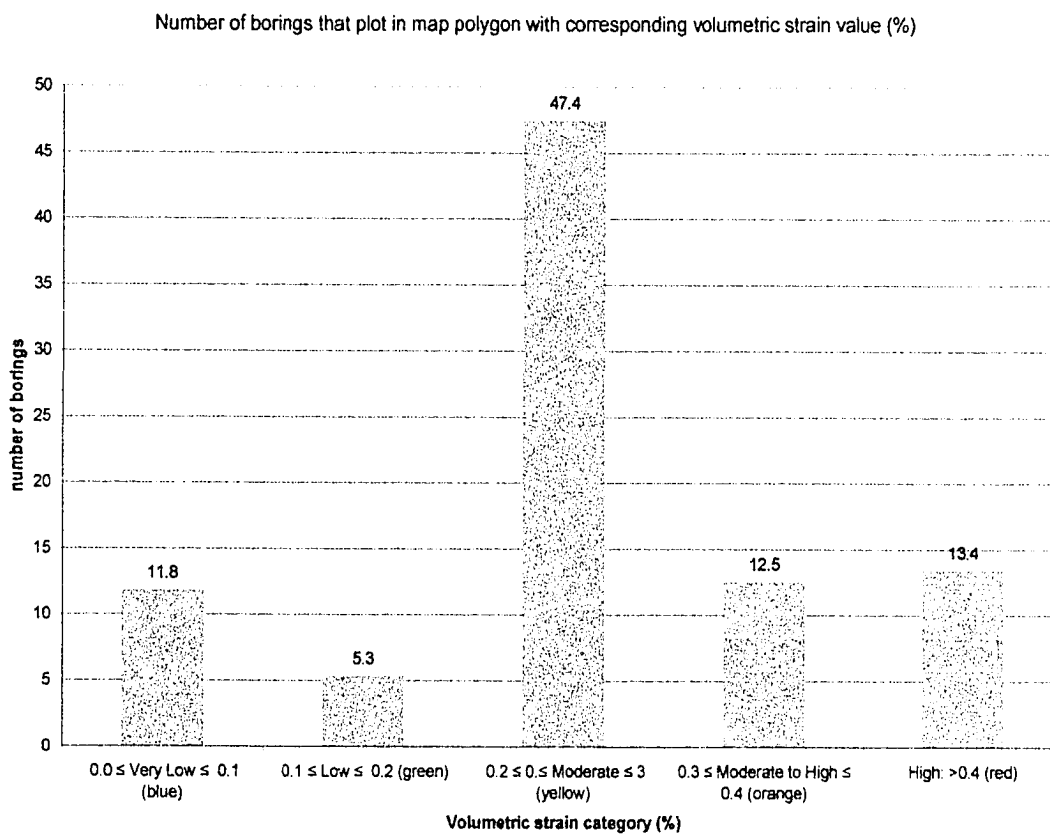


Figure 12: Histogram showing the number of borings that plot in the map polygon with the corresponding volumetric strain (%). The color noted on the x axis corresponds to the strain category for the dots and the shaded polygons on the map.

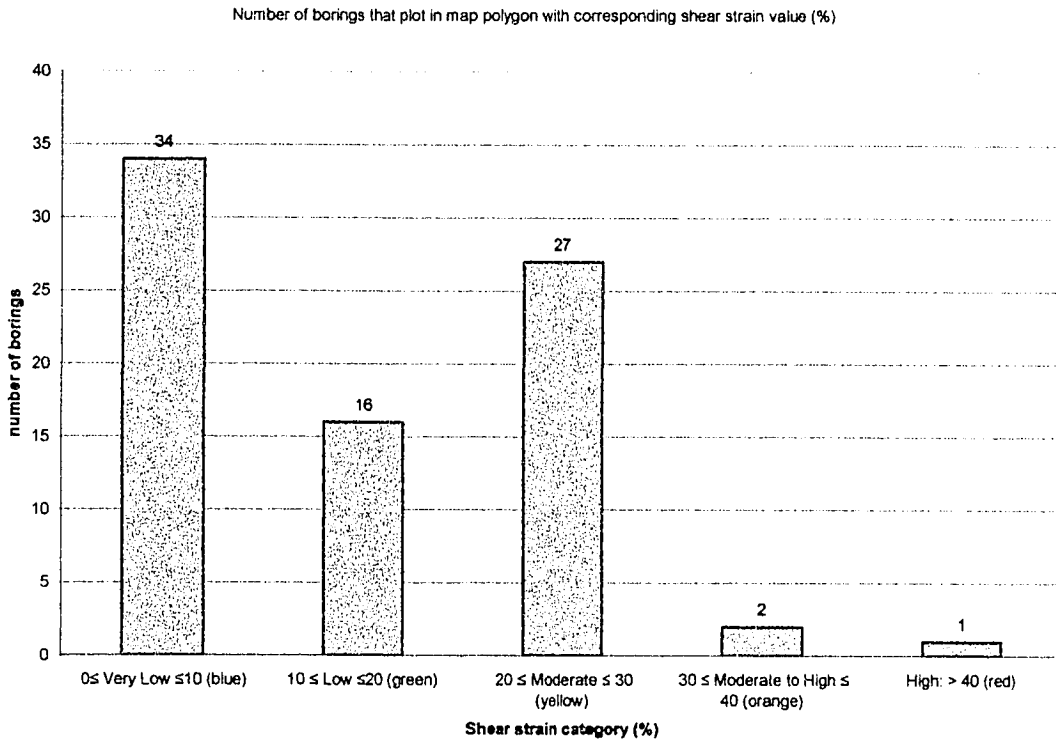


Figure 13: Histogram showing the number of borings that plot in the map polygon with the corresponding shear strain (%). The color noted on the x axis corresponds to the strain category for the dots and the shaded polygons on the map.

Percent of borings that plot in polygon with same volumetric strain value, polygon with next higher volumetric strain value, and polygon with next lower volumetric strain value

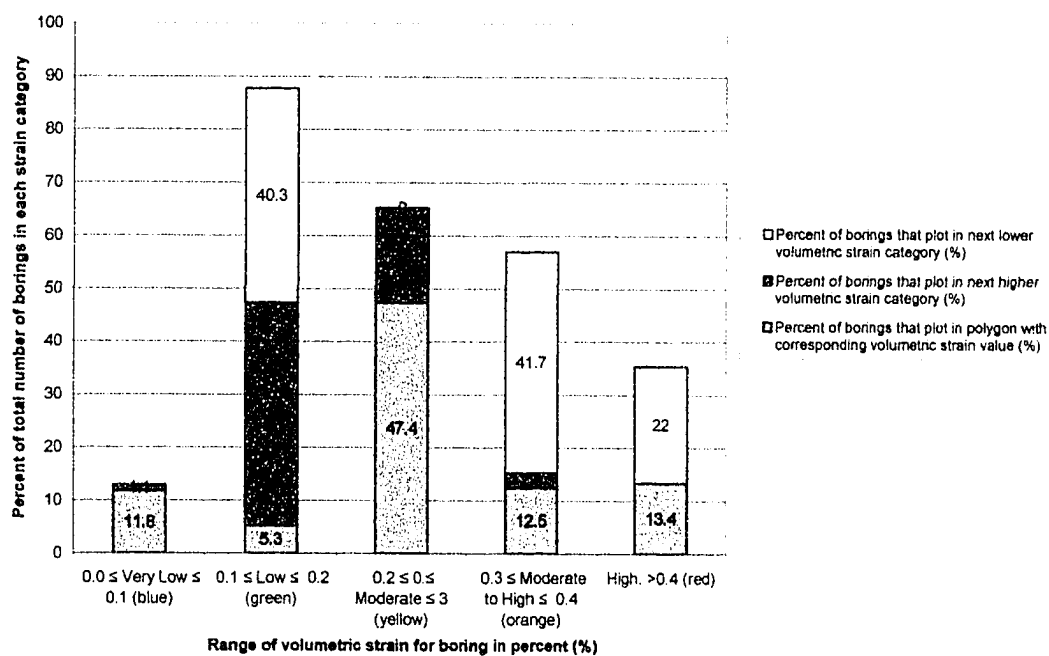


Figure 14: Histogram showing the percent of borings that plot in the map polygon with the corresponding volumetric strain (%) as well as the polygon with the next higher and lower volumetric strain category. The color noted on the x axis corresponds to the strain category for the dots and the shaded polygons on the map.

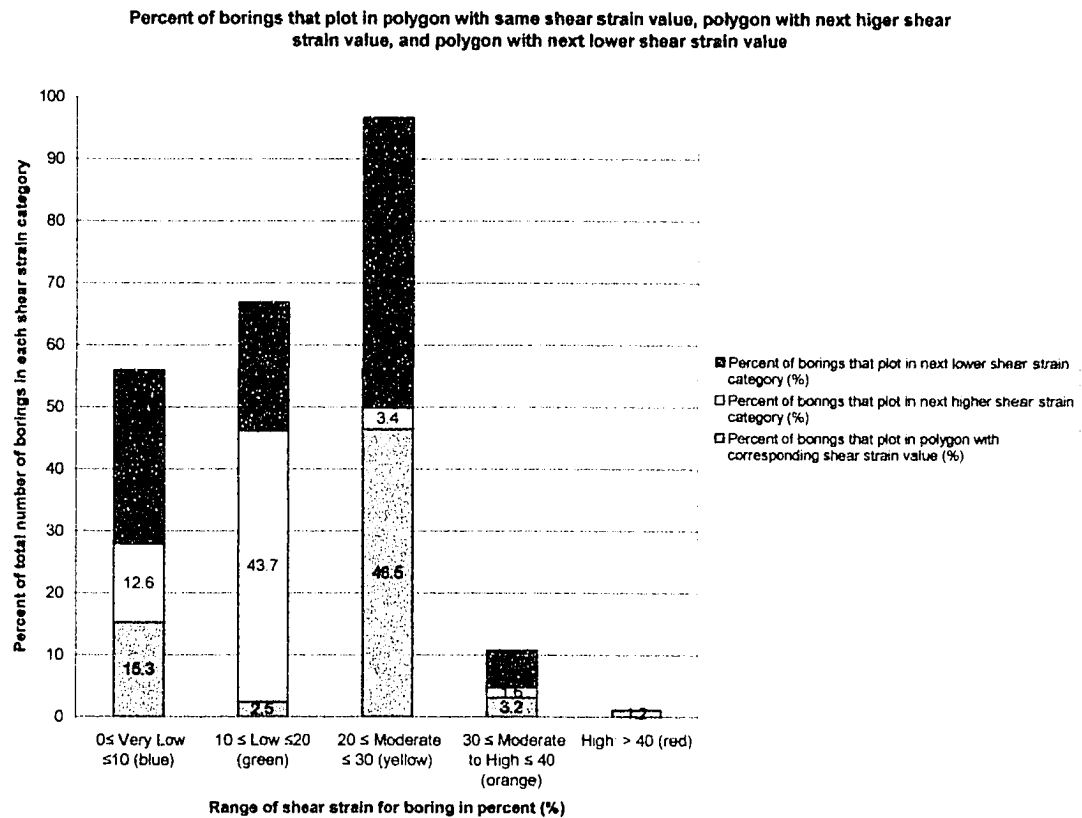


Figure 15: Histogram showing the percent of borings that plot in the map polygon with the corresponding shear strain (%) as well as the polygon with the next higher and lower shear strain category. The color noted on the x axis corresponds to the strain category for the dots and the shaded polygons on the map.

percentage of silt and therefore be relatively more susceptible to liquefaction and likely to experience a relatively greater amount of strain compared to other nearby borings in Qhff with more clay. However, even though the liquefaction susceptibility and subsequent strain may vary for adjacent borings, overall the range of variability will be limited because the type of sediment deposited in Qhff is limited by the low-energy depositional processes that operate in that environment. Geotechnical data recorded on boring logs such as penetration

resistance provide quantifiable data that can be used to calculate liquefaction potential and the potential for liquefaction-induced strain. Grouping the geologic map units according to the median strain value for all of the borings that penetrate that unit allows for the production of a regional-scale map that illustrates characteristic liquefaction-induced strain based on specific geologic environment. The boundaries of the strain polygons correspond to boundaries of geologic map units, and Plates 6 and 7 show that environments with the highest predicted amounts of strain are nearest to higher-energy stream environments where young, loose, coarser-grained sediments are deposited.

Observed vs. Predicted Deformation

Because it was not possible to calibrate deformation predicted by this study using primary data (in-situ measurements from preserved historical ground failure features), an attempt to calibrate results using descriptions of historical ground failure from the 1868 Hayward, 1906 San Francisco and 1989 Loma Prieta earthquakes was conducted instead. Accounts of ground deformation compiled by Youd and Hoose (1978) include descriptions with quantified estimates of ground failure.

An attempt was made to compare the amounts of liquefaction-induced ground deformation predicted using data compiled in this study with measured amounts of historical deformation within the study area caused by the 1868, 1906 and 1989 earthquakes. In the fall of 2003, William Lettis and Associates, Inc.

excavated a 93-m-long trench at Cilker Orchards, just west of Coyote Creek, approximately 4 km south of San Francisco Bay (Thompson et al. 2004). The purpose of their study was to investigate whether lateral spreads occur repeatedly in the same location. Youd and Hoose (1978) compiled several accounts of lateral spread adjacent, and in close proximity, to Coyote Creek in the vicinity of the trench, including fissures, offset rows of trees in the adjacent orchards, and settlement caused by both the 1868 Hayward and 1906 San Francisco earthquakes. Unfortunately reconstruction of a levee adjacent to Coyote Creek in 1993 made it impossible to locate a trench in the area where the majority of ground failure features were reported. Only two small sand dikes (3-5 mm wide) were visible in the trench, and they did not provide enough information to calibrate the results of this study.

These written accounts were reviewed and a table containing an estimate of the type of ground failure to occur at each site (displacement or settlement) and the amount of deformation that occurred at each site was compiled (Appendix 4). After each site was located, the estimated amount of predicted ground failure was compared to the observed amount of ground failure within each geologic map unit. For settlement, the predicted amount exceeds the observed amount of ground failure, while for displacement the observed amounts of ground failure are somewhat higher than predicted. Although there are many reports of earthquake-induced ground failure following the 1906 earthquake, some features are not well documented. Youd and Hoose caution that "most

post-earthquake investigative efforts were applied to assessing the extent of structural and other damage or tracing out ruptured faults; hence notations concerning ground failures are commonly of incidental nature," e.g., no distinction is made between ground failures due to liquefaction and those caused by deformation of soft clay.

CONCLUSIONS

The surface elevation of the boundary that is interpreted as the top of the Pleistocene shows a central topographic low aligned down the center of the northern Santa Clara Valley that corresponds to the present-day location of *Guadalupe River and Coyote Creek*. Identification of this paleo-land surface is accomplished through an iterative process that includes collecting and reviewing geotechnical data recorded on boring logs and constructing cross sections through the study area. The most important type of information reviewed was the penetration test data because it may be used as a proxy for the density of the layer. As sediment ages and lithifies, its density and penetration resistance increase. The top of the Pleistocene was inferred from penetration test data, laboratory test results including grain size analysis, moisture content, and dry density, and descriptive comments that mention changes in color, lateral and vertical textural changes, or presence of organic matter. All borings that contained layers interpreted as Pleistocene were plotted and a contour map was constructed. Borings that caused contour lines to be deflected or drawn in a manner inconsistent with the expected land surface were reviewed and reinterpreted in the context of surrounding borings, and the emerging contour surface of the elevation of the top of Pleistocene was subsequently revised. The contours delineating the center of the northern Santa Clara Valley are constructed with much less confidence than those along the margins of the

valley. Holocene sediment increases in thickness both toward the center of the northern Santa Clara Valley and downstream. Most of the geotechnical borings used in this study are not deep enough to penetrate the Pleistocene surface in the center of the study area.

The following conclusions are reached about sediment layers described in geotechnical boring logs collected in the northern Santa Clara Valley: 1) fewer than half of the sediment layers described are coarse enough to liquefy, whether analyzed by the total number of layers or the total boring length assigned to each map unit; 2) the median corrected penetration resistance ($(N_1)_{60,cs}$) value for sediment with liquefiable textures in most cases is less than 15, a value previous researchers have considered an upper bound for sediment likely to experience large-scale liquefaction-related deformation; 3) the method of Youd et al. (2001) results in median $(N_1)_{60,cs}$ values that tend to be 2 to 3 blows/ft higher than the values calculated using the method of Seed et al. (2003); 4) where the Factor of Safety value is less than 1, layers with granular textures are prone to liquefaction when subjected to a level of shaking that has only a 10% probability of being exceeded in 50 years, although a high percentage of the sediment in the study area consists of fine-grained materials that probably are too fine to liquefy; 5) liquefaction potential index values for younger deposits tend to be lower than for older deposits; and 6) the maximum distance for which there is a relationship between adjacent borings is approximately 900 m, while the median separation distance between any two borings in the study area is approximately 1,044 m,

indicating that additional data are required to adequately characterize geologic variability in the northern Santa Clara Valley.

Because the descriptions for sediment layers on boring logs often lack sufficient detail, it is often not possible to distinguish sub-units for sub-surface layers. For the purposes of liquefaction and liquefaction-induced deformation analysis it is sufficient to identify the paleo-land surface boundary, or the depth at which the sediments are sufficiently dense that they will not liquefy.

The northern Santa Clara Valley is characterized by the highly variable nature of its late Quaternary geology. This variability makes it difficult to differentiate areas likely to experience large liquefaction-related deformation from areas with less hazard. Resolution of this problem might occur with the acquisition of additional geotechnical boring data. The data available for this project (668 boring logs) do not include a uniform number of borings from every potentially liquefiable geologic map unit. Geotechnical data recorded on boring logs such as penetration resistance, fines content, or USCS classification provide quantifiable data that can be used to calculate liquefaction potential and the potential for liquefaction-induced strain. Grouping the geologic map units according to the median strain value for all of the borings that penetrate that unit allows for the production of a regional-scale map that illustrates characteristic liquefaction-induced strain based on specific geologic environment.

REFERENCES

- American Society for Testing and Materials D1586-99, 1999, Standard Test Method for Penetration Test and Split-Barrel Sampling of Soils.
- American Society for Testing and Materials D2487-93, Standard Test Method for Classification of Soils for Engineering Purposes, approved September 15, 1993.
- Atwater, B. F., Hedel, C. W., and Helley, E. J., 1977, Late Quaternary depositional history, Holocene sea-level changes, and vertical crustal movement, southern San Francisco Bay, California: United States Geological Survey Professional Paper 1014, 15 p.
- Bardet, J. P., Tobita, T., Mace, N., and Hu, J., 2002, Regional modeling of liquefaction-induced ground deformation: *Earthquake Spectra*, v. 18, no. 1, p. 19-46.
- Boulanger, R. W., and Idriss, I. M., 2004, Evaluating the potential for liquefaction or cyclic failure of silts and clay: Center for Geotechnical Modeling, Department of Civil and Environmental Engineering, University of California, Davis, report CGM - 04/01, 130 p.
- California Department of Conservation, California Geological Survey, Liquefy program, n.p., n.d.
- California Department of Conservation, California Geological Survey, Penetration test quality ranking, n.p., n.d.
- California Department of Conservation, California Geological Survey, 2000, Seismic Hazard Zone Report for the San Jose East 7.5-Minute Quadrangle, Santa Clara County, California Seismic Hazard Zone Report 044, 55 p.
- California Department of Conservation, California Geological Survey, 2001, Seismic Hazard Zone Report for the Calaveras Reservoir 7.5-Minute Quadrangle, Santa Clara County, California Seismic Hazard Zone Report 048, 55 p.

- California Department of Conservation, California Geological Survey, 2001, Seismic Hazard Zone Report for the Milpitas 7.5-Minute Quadrangle, Santa Clara County, California Seismic Hazard Zone Report 051, 55 p.
- California Department of Conservation, California Geological Survey, 2002, Seismic Hazard Zone Report for the San Jose West 7.5-Minute Quadrangle, Santa Clara County, California Seismic Hazard Zone Report 058, 51 p.
- California Department of Conservation, California Geological Survey, 2006, Seismic Hazard Zone Report for the Palo Alto 7.5-Minute Quadrangle, Santa Clara County, California Seismic Hazard Zone Report 111, 58 p.
- California Department of Conservation, California Geological Survey, Interim Revision 2007, Fault-Rupture Hazard Zones in California, Special Publication 42, 46 p.
- California Department of Conservation, Division of Mines and Geology, 1997, Guidelines for evaluating and mitigating seismic hazards in California: Special Publication 117, 74 p.
- Cetin, O. K., and Seed, R. B., 2000, Earthquake-induced nonlinear shear mass participation factor (r_d) for cyclic stress ratio evaluation: Department of Civil and Environmental Engineering, University of California, Berkeley, Geotechnical Research Report No. GT-2000/08, 41 p.
- Cetin, O. K., Seed, R. B., Der Kiureghain, A., Tokimatsu, K., Harder, L. F., Kayen, R. E., and Moss, R. E. S., 2004, Standard penetration test-based probabilistic and deterministic assessment of seismic soil liquefaction potential: *Journal of Geotechnical and Geoenvironmental Engineering*, v. 130, no. 12, December 1, 2004, p. 1314-1340.
- Clahan, K. B., Mattison, M. E., Rosinski, A. M., Bott, J. D. J., and Knudsen, K. L., 2002, Preliminary maps of (1) Pleistocene alluvial surface, (2) depth to historical high groundwater, and (3) thickness of Holocene alluvium – and their use in liquefaction hazard mapping, Santa Clara Valley and the East San Francisco Bay Plain, California: *EOS, Transactions, American Geophysical Union*, v. 83, no. 47, p. F1312.
- Clark, I., and Harper, B., 2000, *Practical Geostatistics 2000*: Geostakos, (Ecosse) Limited, Scotland, 416 p.

- Cooper-Clark and Associates, 1974, City of San Jose's sphere of influence for the city of San Jose: San Jose, CA, Department of Public Works, 185 p., and plates 4-A and 4-B (ground failure).
- Falls, J. N., 1988, The development of a liquefaction hazard map for the city of San Jose, California: San Jose, California State University, Masters Thesis, 80 p.
- Hamada, M., Yasuda, S., Isoyama, R., and Emoto, K. 1986, Study on liquefaction induced permanent ground displacements: Report of the Association for the Development of Earthquake Prediction in Japan, Tokyo, p. 221-229.
- Harris, S. K., and Egan, J. A., 1992, Effects of ground conditions on the damage to four-story corner apartment buildings *in* O'Rourke, T. D., ed., The Loma Prieta, California Earthquake of October 17, 1989 – Marina District: United States Geological Survey Professional Paper 1551-F, p. F181-F194.
- Helley, E. J., and Lajoie, K. R., 1979, Flatland deposits of the San Francisco Bay Region, California – Their geology and engineering properties, and their importance to comprehensive planning: United States Geological Survey Professional Paper 943, 88 p.
- Helley, E. J., and Wesling, J. R., 1990, Quaternary geologic map of the San Jose East Quadrangle, Santa Clara County, California: United States Geological Survey Open-File Report 90-427.
- Hitchcock, C. S., and Helley, E. J., 2000, Characterization of subsurface sediments, southern San Francisco Bay Area: Preliminary Technical Report, United States Geological Survey National Earthquake Hazards Reduction Program Grant 99-HQ-GR-0097, 27 p.
- Hitchcock, C. S., and Helley, E. J., 2003, Characterization of subsurface sediments, Southern San Francisco Bay Area: Final Technical Report, United States Geological Survey National Earthquake Hazards Reduction Program Grant 99-HQ-GR-0097, 26 p.
- Ingebritsen, S. E., and Jones, D. R. 1999, Santa Clara Valley, California – a case of arrested subsidence, *in* Galloway, D., Jones, D.R., and Ingebritsen, S. E., eds., Land subsidence in the United States, United States Geological Survey Circular 1182, p. 15-22.

- Ishihara, K., and Yoshimine, M., 1992, Evaluation of settlements in sand deposits following liquefaction during earthquakes: *Soils and Foundations*, v. 32, no. 1, p. 173-188.
- Iwasaki, I., Tokida, K., Tatsuoka, F., Watanabe, S., Yasuda, S., and Sato, S., 1982, Microzonation for soil liquefaction potential using simplified methods *in Proceedings, 3rd International Conference On Microzonation*, Seattle, WA, v. 3, p. 1319-1330.
- Knudsen, K. L., Sowers, J. M., Witter, R. C., Wentworth, C. M., and Helley, E. J. 2000, Preliminary maps of Quaternary deposits and liquefaction susceptibility, nine-county San Francisco Bay Region, California: A digital database: United States Geological Survey Open-File Report 2000-444, 26 p.
- Knudsen, K. L., Rosinski, A. M., Wu, J., and Seed, R. B., 2004, Production of regional liquefaction-induced deformation maps, *in Doolin, D., Kammerer, A., Ogami, T., Seed, R. B., and Towhata, I., eds., Proceedings, The 11th International Conference on Soil Dynamics and Earthquake Engineering and the 3rd International Conference on Earthquake Geotechnical Engineering*, Berkeley, CA, p. 318-325.
- Martin, G. R., and Lew, M, eds., 1999, Recommended procedures for implementation of the California Division of Mines and Geology Special Publication 117 – Guidelines for analyzing and mitigating liquefaction in California: Southern California Earthquake Center, University of Southern California, 62 p.
- National Center for Earthquake Engineering Research, 1997, Proceedings of the National Center for Earthquake Engineering Research Workshop on Evaluation of Liquefaction Resistance of Soils, Youd, T. L., and Idriss, I. M., eds., Technical Report No. 97-0022, December 31, 1997, p. 297-313.
- Petersen, M. D., Bryant, W. A., Cramer, C. H., Cao, T., Reichle, M. S., Frankel, A. D., Lienkaemper, J. J., McCrory, P. A., and Schwartz, D. P., 1996, Probabilistic seismic hazard assessment for the State of California: California Department of Conservation, Division of Mines and Geology Open-File Report 96-08, 33 p; also United States Geological Survey Open-File Report 96-706, 33 p.
- Poland, J. F., 1969, Land subsidence in the western United States: Office of Emergency Preparedness, Geologic Problems and Hazards section, p. 77-96.

- Poland, J.F., 1971, Land subsidence in the Santa Clara Valley, Alameda, San Mateo, and Santa Clara counties, California: United States Geological Survey Miscellaneous Field Studies Map MF-336, scale 1:125,000.
- Poland, J.F., 1984, Mechanics of land subsidence due to fluid withdrawal, *in* Poland, J.F., ed., Guidebook to studies of land subsidence due to groundwater withdrawal: Studies and Reports in Hydrology 40, prepared for the International Hydrological Programme, Working Group 8.4, United Nations Educational, Scientific, and Cultural Organization, Paris, France, p. 37-54.
- Powers, M. S., Wesling, J. R., Perman, R. C., and Disilvestro, L. A., 1992, Evaluation of liquefaction potential in San Jose, California: Unpublished Technical Report to the United States Geological Survey National Earthquake Hazards Reduction Program, San Francisco, Geomatrix Consultants, 65 p.
- Rauch, A. F., 1997, EPOLLS: An empirical method for predicting surface displacement due to liquefaction-induced lateral spreading in earthquakes: Blacksburg, Virginia Polytechnic Institution, Ph.D. dissertation, 333 p.
- Rosinski, A. M., Knudsen, K. L., Wu, J., Seed, R. B., and Real, C. R., 2004, Development of regional liquefaction-induced deformation hazard maps, *in* Yegian, M. K., and Kavazanjian, E., eds., Proceedings, Geo-Trans, Los Angeles, California: Geo-Institute of the American Society of Civil Engineers, p. 797-806.
- Schmidt, D., and Bürgmann, R., 2002, Land uplift and subsidence in the Santa Clara Valley, *in* Berkeley Seismological Laboratory Annual Report 2001-2002, University of California, Berkeley, 180 p.
- Seed, H. B., and Idriss, I. M., 1971, Simplified procedures for evaluating soil liquefaction potential: Journal of Soil Mechanics and Foundations Division, American Society of Civil Engineers, v. 97, no. SM9, p. 1249-1273.
- Seed, H.B., and Idriss, I.M., 1982, Ground motions and soil liquefaction during earthquakes: Earthquake Engineering Research Institute, Berkeley, CA, Monograph Series, 134 p.
- Seed, H.B., Idriss, I.M., and Arango, I., 1983, Evaluation of liquefaction potential using field performance data: Journal of Geotechnical Engineering, American Society of Civil Engineers, v. 109, no.3, p. 458-482.

- Seed, H. B., Tokimatsu, Kohji, Harder, L. H., and Chung, R. M., 1984, The influence of SPT procedures in soil liquefaction evaluations: Earthquake Engineering Research Center, University of California, Berkeley, Report 90/05, 50 p.
- Seed, H. B., Tokimatsu, Kohji, Harder, L. H., and Chung, R. M., 1985, Influence of SPT procedures in soil liquefaction resistance evaluations: Journal of Geotechnical Engineering, American Society of Civil Engineers, v. 111, no.12, p. 1425-1445.
- Seed, H. B., and de Alba, Pedro: 1986, Use of SPT and CPT tests for evaluating the liquefaction resistance of sands, *in* S. P. Clemence ed., Use of In-Situ Tests in Geotechnical Engineering, American Society of Civil Engineers, New York, p. 281-302.
- Seed, R. B., Dickenson, S. E., Riemer, M. F., Bray, J. D., Sitar, N., Mitchell, J. K., Idriss, I. M., Kayen, R. E., Kropp, A., Harder, L. F., and Power, M. S., 1990, Preliminary report on the principal geotechnical aspects of the October 17, 1989 Loma Prieta earthquake: Earthquake Engineering Research Center, University of California, Berkeley, Report v. 90, no. 5, 137 p.
- Seed, R.B., and L.F. Harder. 1990, SPT-based analysis of cyclic pore pressure generation and undrained residual strength, *in* J.M. Duncan, ed., Proceedings H. Bolton Seed Memorial Symposium, v. 2, p. 351-376.
- Seed, R. B., Cetin, K. O., Moss, R. E. S., Kammerer, A. M., Wu, J., Pestana, J. M., and Riemer, M. F., 2003, Recent advances in soil liquefaction engineering and seismic site response evaluation, *in* International Conference and Symposium on Recent Advances in Geotechnical Earthquake Engineering and Soil Dynamics, San Diego, CA, p. 71.
- Shamoto, Y., Zhang, J. M., and Sato, M., 1998, Methods for evaluating residual post-liquefaction ground settlement and horizontal displacement: Soils and Foundations, Special Issue 2, p. 69-83.
- Tinsley, J. C., III, Egan, J. A., Kayen, R. E., Bennett, M. J., Kropp, A., and Holzer, T. L., 1998, Appendix: maps and descriptions of liquefaction and associated effects, *in* Holzer, T.L, ed., The Loma Prieta, California, Earthquake of October 17, 1989: liquefaction, strong ground motion and ground failure: United States Geological Survey Professional Paper 1551-B, p. B287-314, scale 1:100,000.

- Thompson, S. C. and Witter, R. C., Givler, R.W., Hitchcock, C.S., and Lettis, W.R., 2004, Evaluating the repeatability of lateral spreading: Final Technical Report, United States Geological Survey National Earthquake Hazard Reduction Program Award 03-HQ-GR-0075, 54 p.
- Tokimatsu, K., and Seed, H. B., 1984, Simplified procedures of the evaluation of settlements in clean sands: University of California, Berkeley, GT v. 84, no. 16, 34 p.
- Tokimatsu, K., and Seed, H. B. 1987, Evaluation of settlement in sands due to earthquake shaking: *Journal of Geotechnical Engineering*, American Society of Civil Engineers, v. 113, no. 8, p. 861-878.
- Toprak, S., and Holzer, T. L., 2003, Liquefaction Potential Index field assessment: *Journal of Geotechnical and Geoenvironmental Engineering*, American Society of Civil Engineers 1090-024, v. 129, no. 4, p. 315-322.
- Wentworth, C. M., Blake, M. C. Jr., McLaughlin, R. J., and Graymer, R. W., 1999, Preliminary geologic map of the San Jose 30 X 60-minute Quadrangle, California: A digital database: United States Geological Survey Open-File Report 98-795, 14 p., scale 1:24,000.
- Witter, R. C., Knudsen, K. L, Sowers, J. M., Wentworth, C. M., Koehler, R. D., and Randolph, C. E., 2006, Maps of Quaternary deposits and liquefaction susceptibility in the central San Francisco Bay region, California: United States Geological Survey Open-File Report 2006-1037, 12 p., scale 1:24,000.
- Wu, J., 2002, Liquefaction triggering and post liquefaction deformations of Monterey 0/30 sand under uni-directional cyclic simple shear loading: Department of Civil and Environmental Engineering, Berkeley, University of California, Ph.D. dissertation, 509 p.
- Wu, J., and Seed, R. B., 2004, Estimation of liquefaction-induced ground settlement (case studies), *in* Prakask, S., ed., Proceedings Fifth International Conference on Case Histories in Geotechnical Engineering, Paper no. 3.09, New York, NY, 14 p.
- Wu, J., Seed, R. B., and Pestana, J. M., 2003, Liquefaction triggering and post liquefaction deformations of Monterey 0/30 sand under uni-directional cyclic simple shear loading: University of California, Berkeley, Geotechnical Engineering Research Report, 279 p.

- Youd, T.L., and Hoose, S.N., 1978, Historic ground failures in northern California triggered by earthquakes: United States Geological Survey Professional Paper 993, 180 p., map scales 1:250,000 and 1:24,000.
- Youd, T.L., and Jones, C.F., 1993, Liquefaction hazard maps for the Portland quadrangle, Oregon: Oregon Department of Geology and Mineral Industries, Geological Map Series, Map GMS-79, 17 p. scale 1:24,000.
- Youd, T. L., Idriss, I. M., Andrus, R. D., Arango, I., Castro, G., Christian, J. T., Dobry, R., Finn, W. D. L., Harder, L. F., Hynes, M. E., Ishihara, K., Koester, J. P., Liao, S. C., Marcuson, W. F., Martin, G. R., Mitchell, J. K., Moriwaki, Y., Power, M. S., Robertson, P. K., Seed, R. B., and Stokoe, K. H., 2001, Liquefaction resistance of soils: Summary Report from the 1996 National Center for Earthquake Engineering Research and 1998 National Center for Earthquake Engineering Research/National Science Foundation Workshops on Evaluation of Liquefaction Resistance of Soils: Journal of Geotechnical and Geoenvironmental Engineering, v. 127, no. 10, p. 817-833.
- Youd, T. L., Hansen, C. M., and Bartlett, S. F. 2002, Revised MLR equations for prediction of lateral spread displacement: Journal of Geotechnical and Geoenvironmental Engineering, v. 128, no. 12, p. 1007-1017.

NOTE TO USERS

Oversize maps and charts are microfilmed in sections in the following manner:

LEFT TO RIGHT, TOP TO BOTTOM, WITH SMALL OVERLAPS

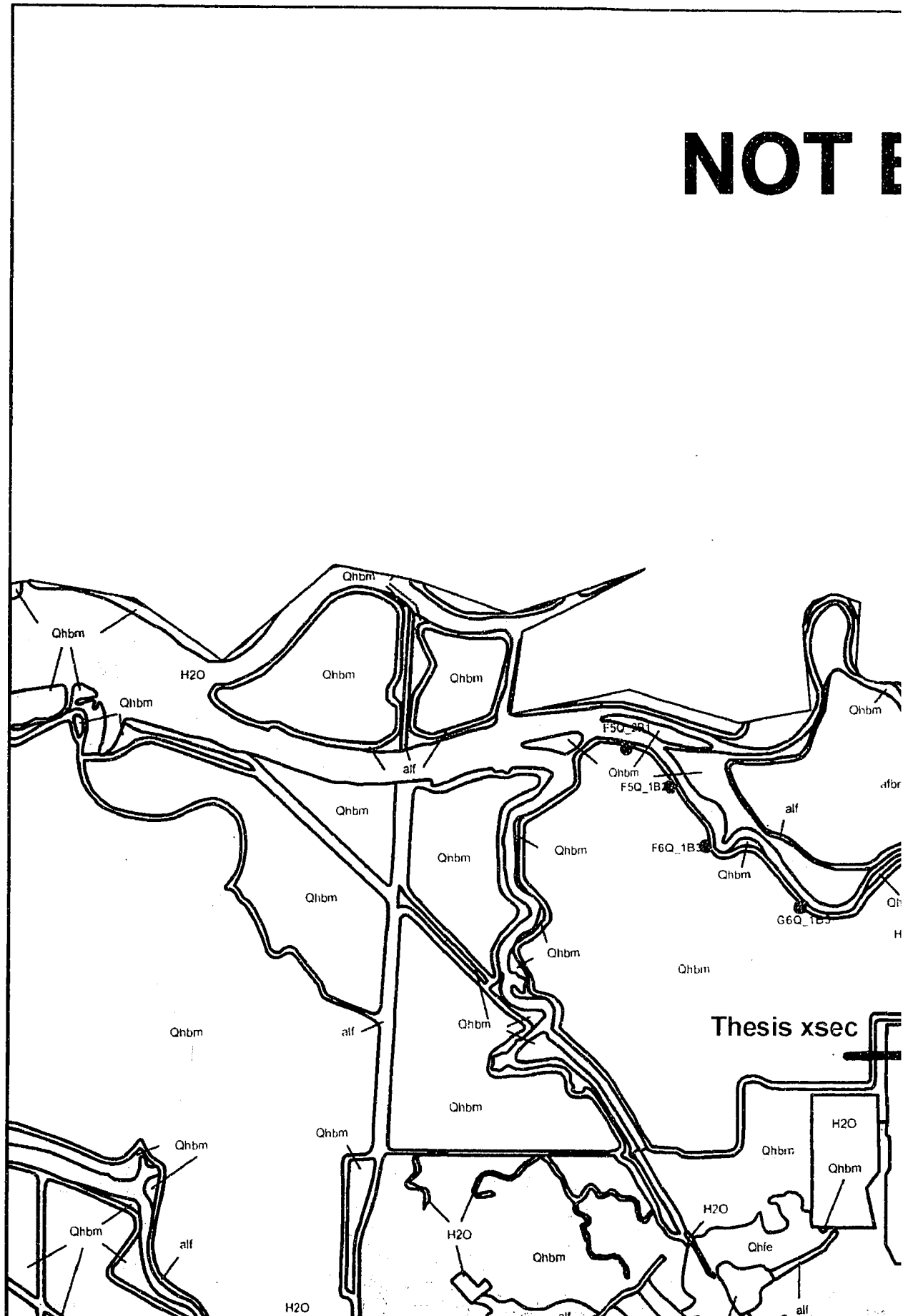
This reproduction is the best copy available.

UMI[®]

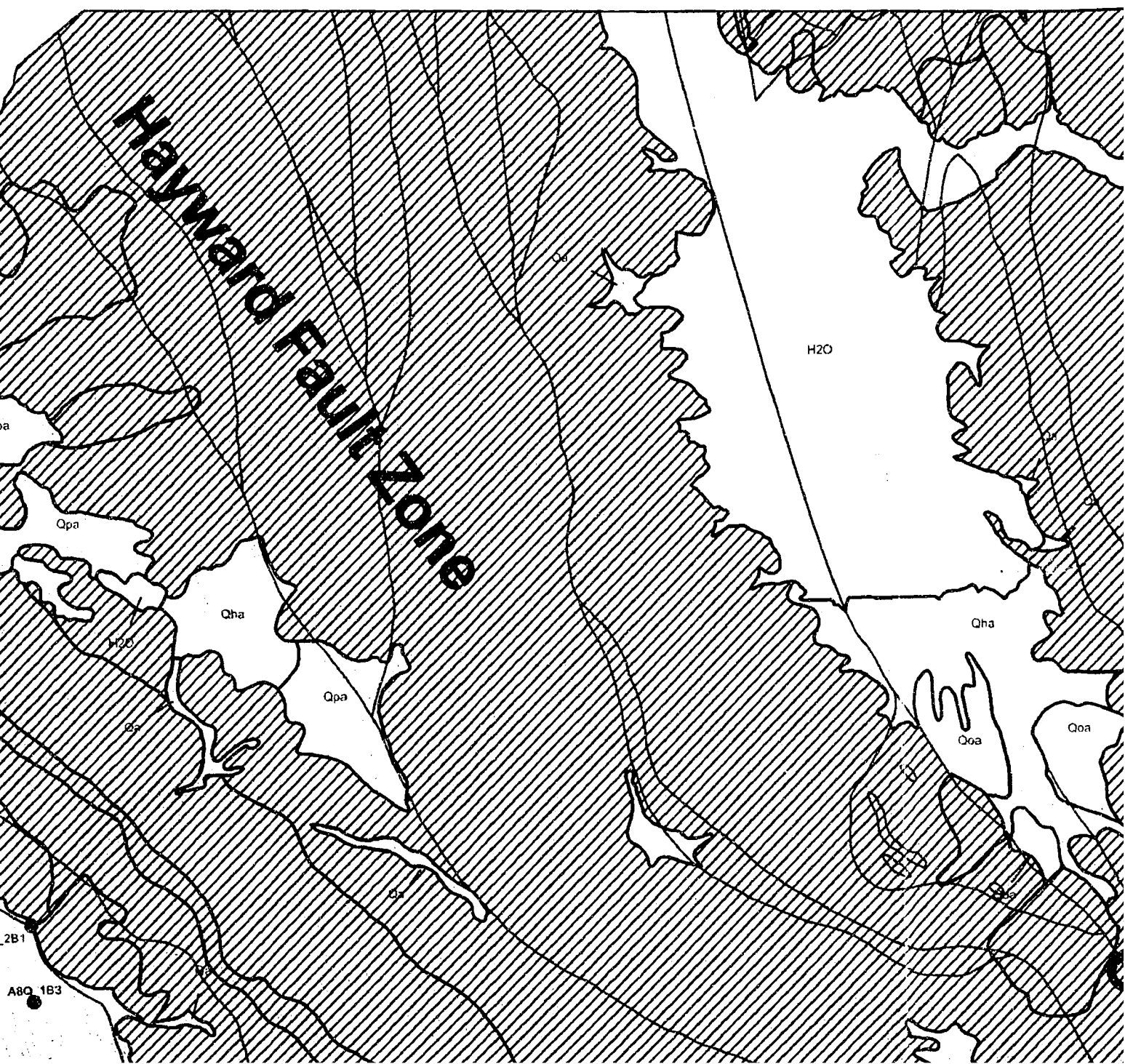
122° 00'

37° 30' 00"

NOT E

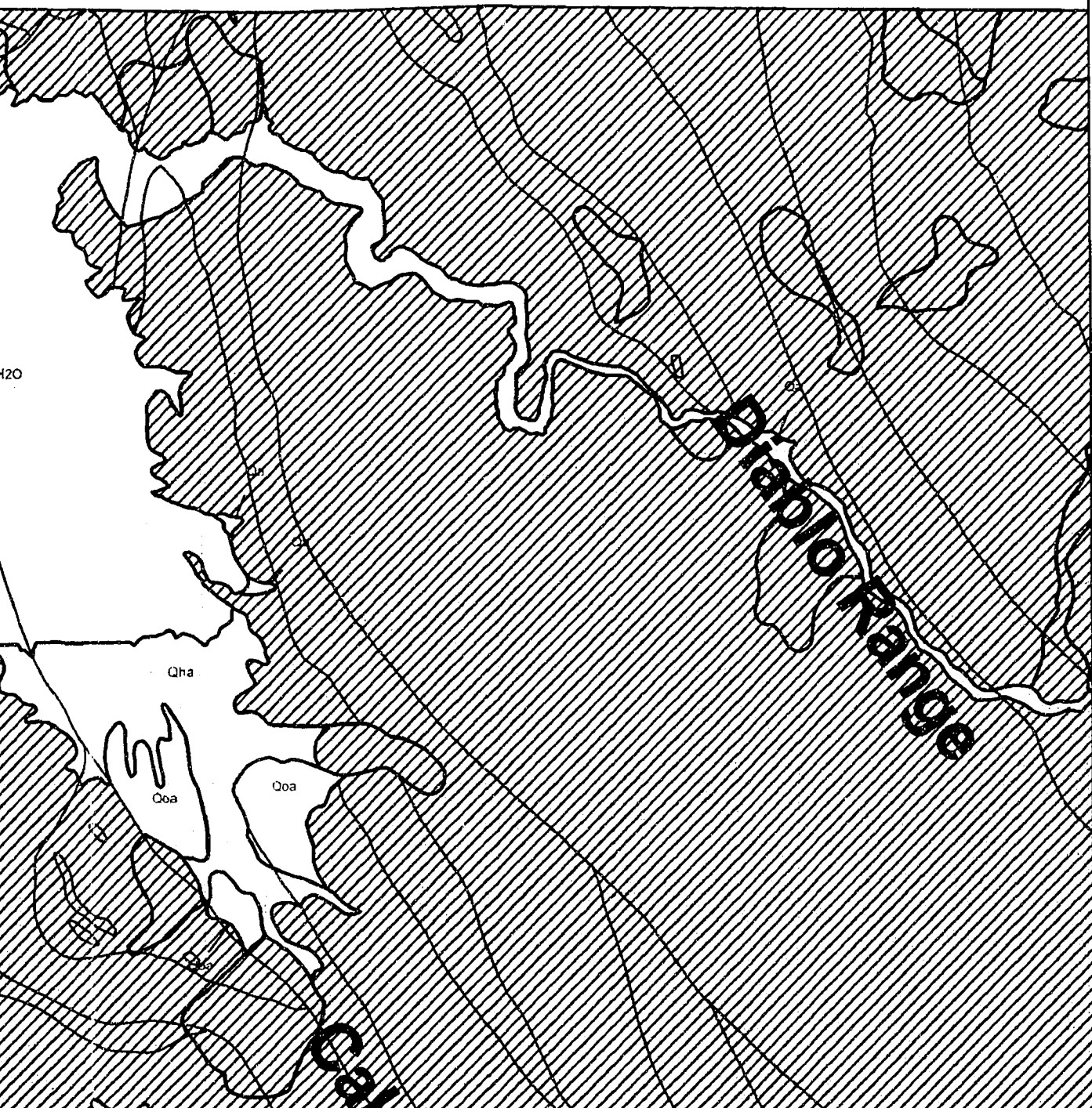


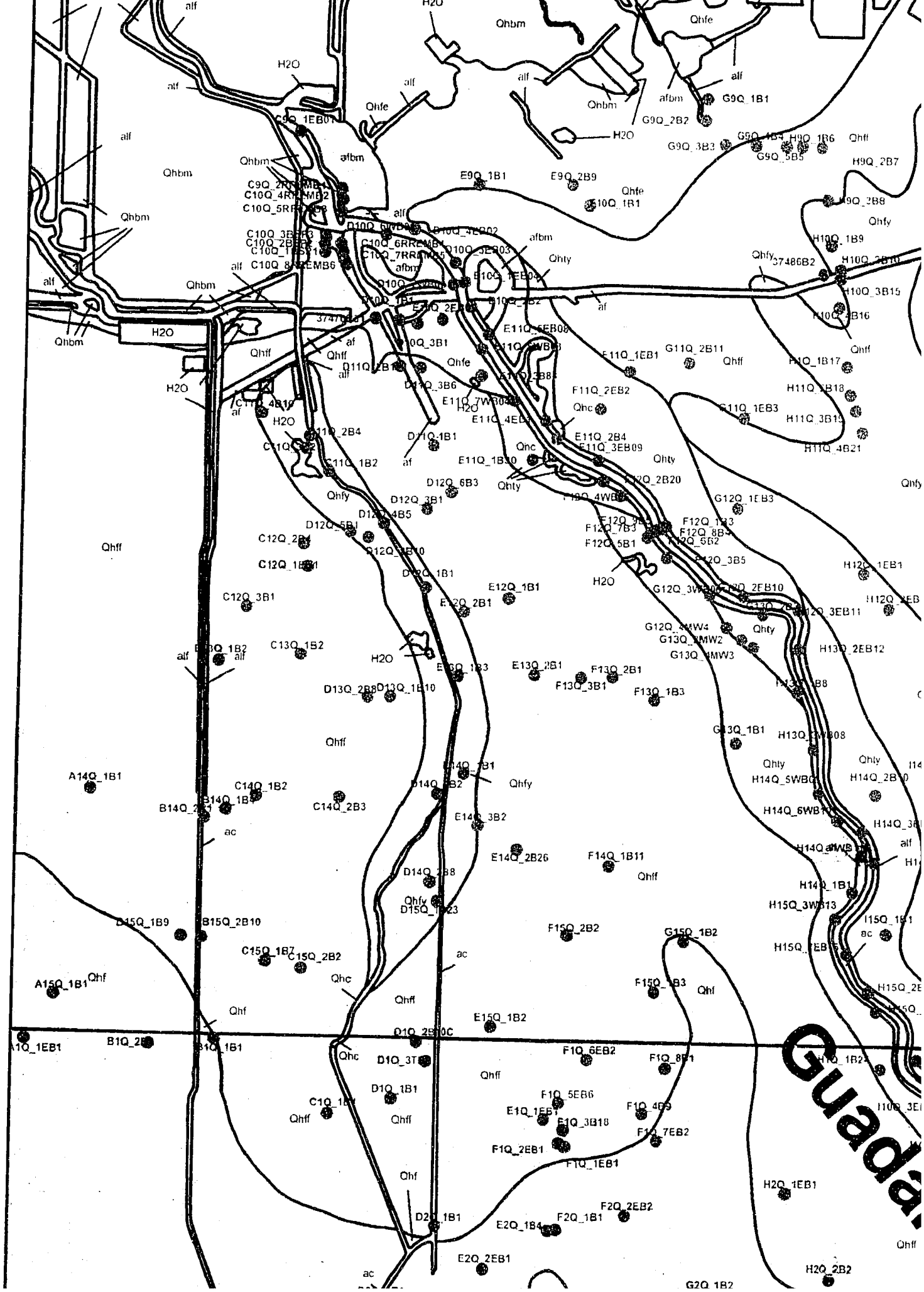
STUDY AREA



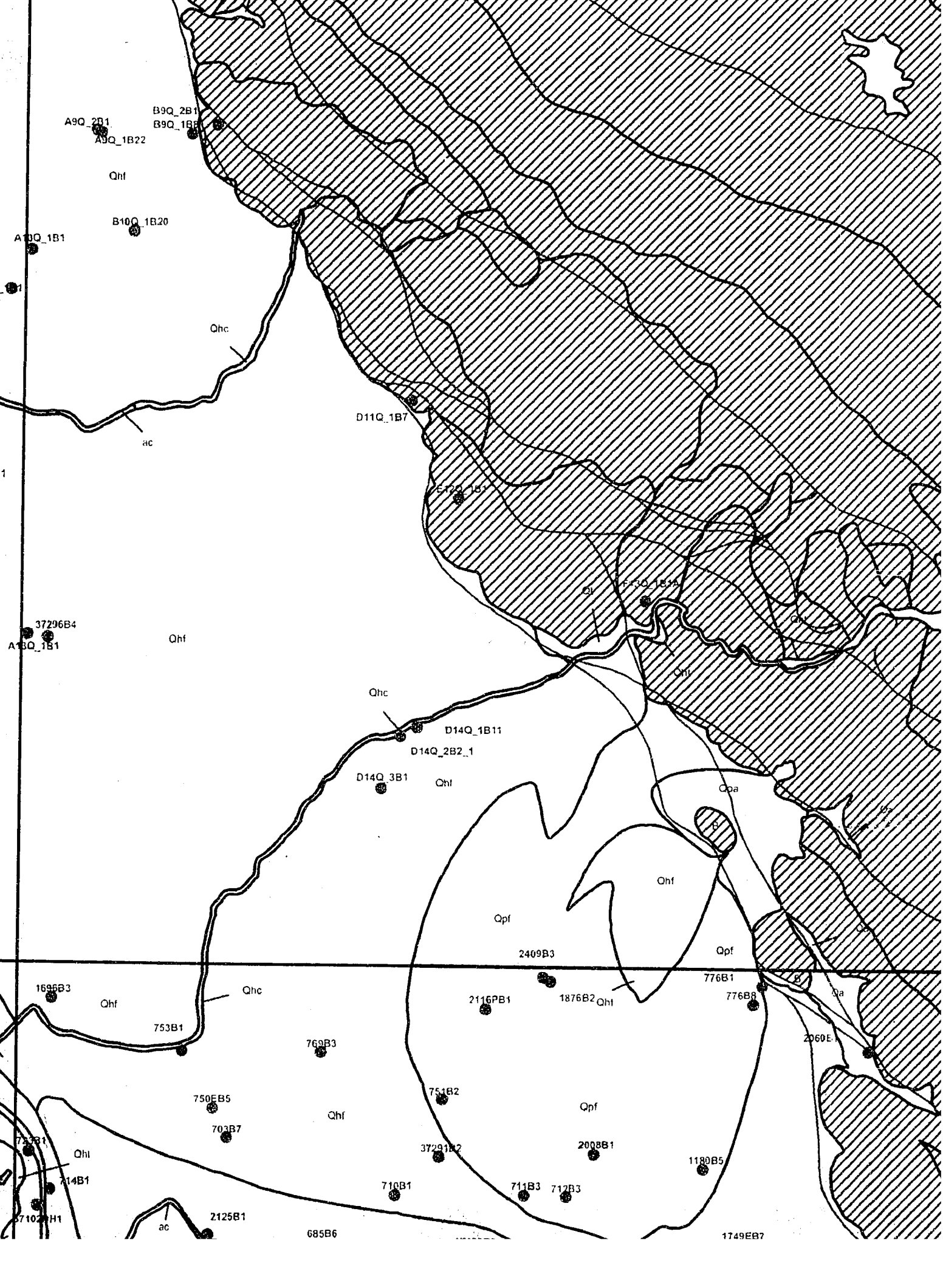
121° 45'

37° 30'





Quadrant



A9Q_2B1
A9Q_1B22

B9Q_2B1
B9Q_1B1

Qhf

B10Q_1B20

A10Q_1B1

Qhc

D11Q_1B7

E12Q_1B1

F15Q_1B1

Qhf

37296B4
A13Q_1B1

Qhc

D14Q_1B11

D14Q_2B2_1

D14Q_3B1

Qhf

Qpa

Qhf

Qpf

Qpf

1695B3

Qhf

Qhc

753B1

769B3

Qhf

750EB5

703B7

751B2

Qpf

2409B3

2116PB1

1876B2

Qhf

776B1

776B2

2060E

37291B2

2008B1

1180B5

710B1

711B3

712B3

7102B1

Qhf

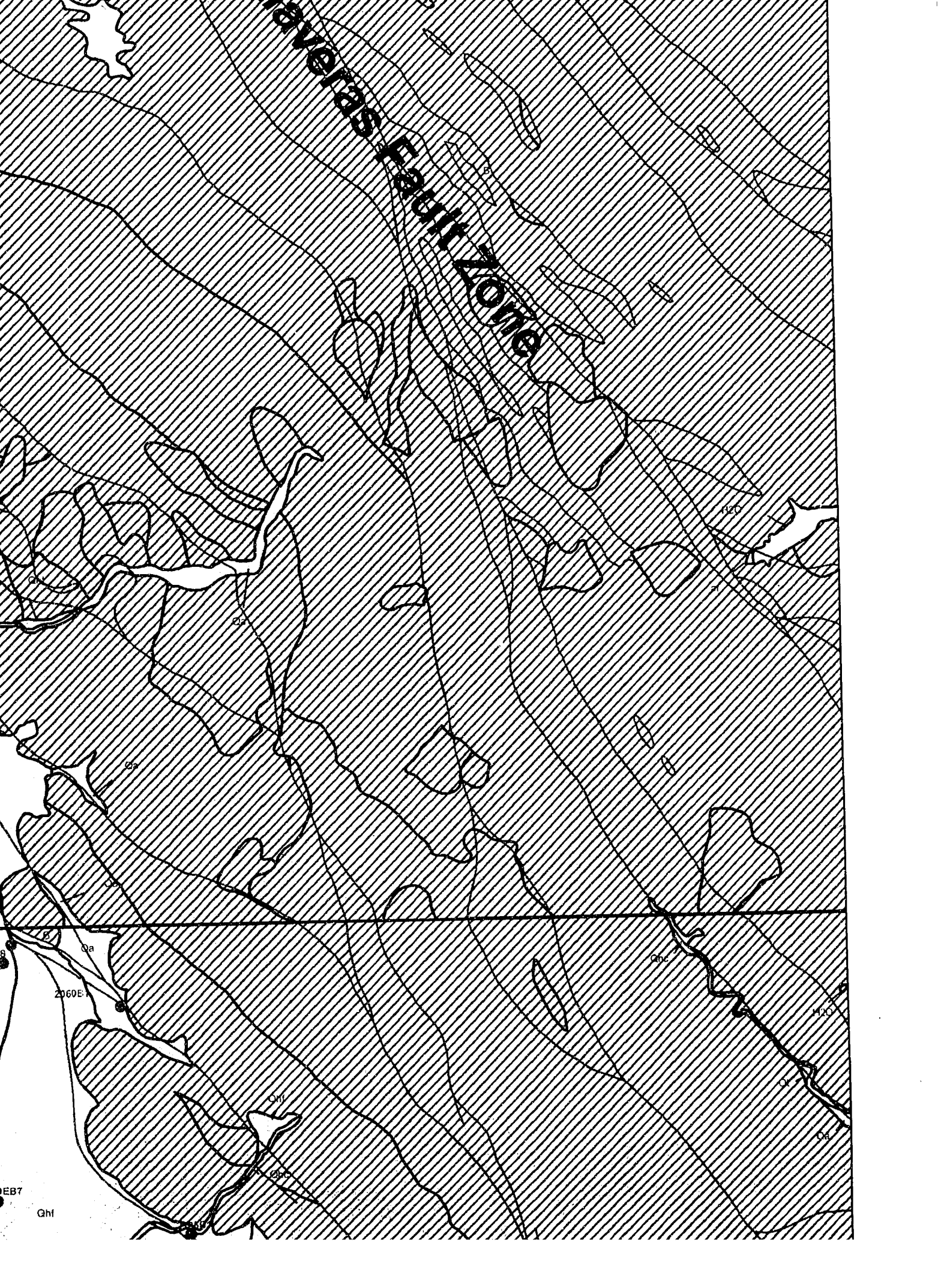
14B1

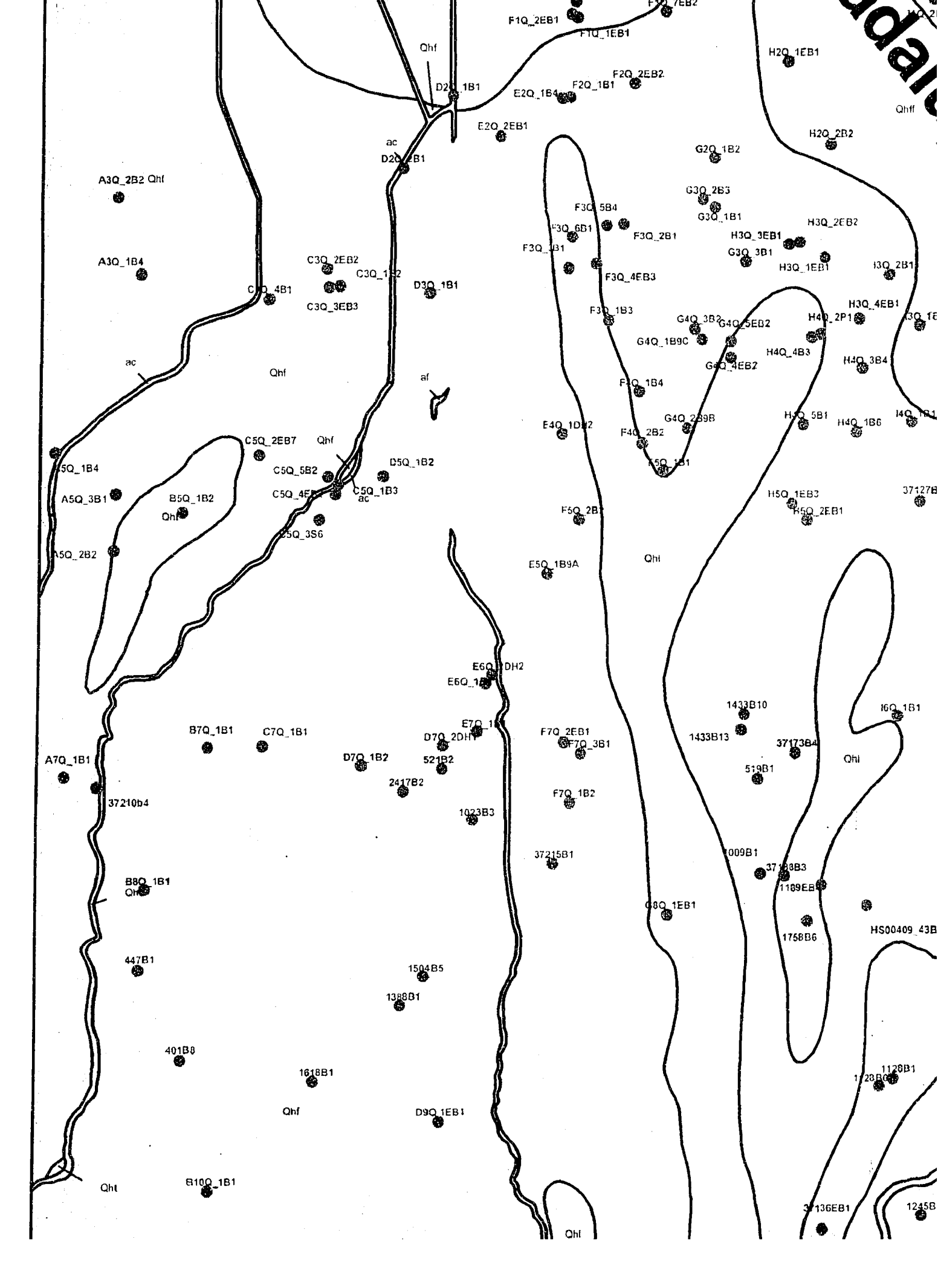
ac

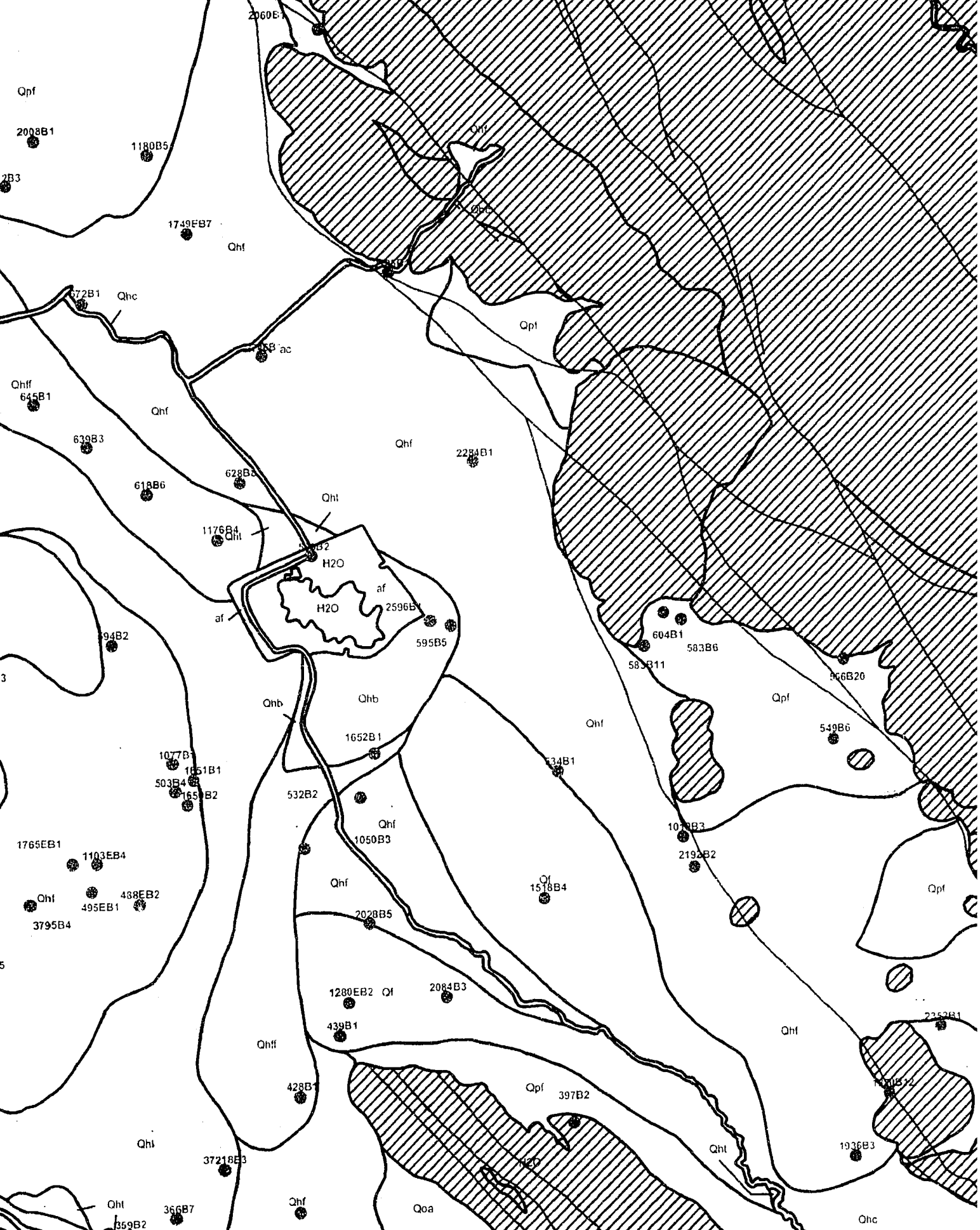
2125B1

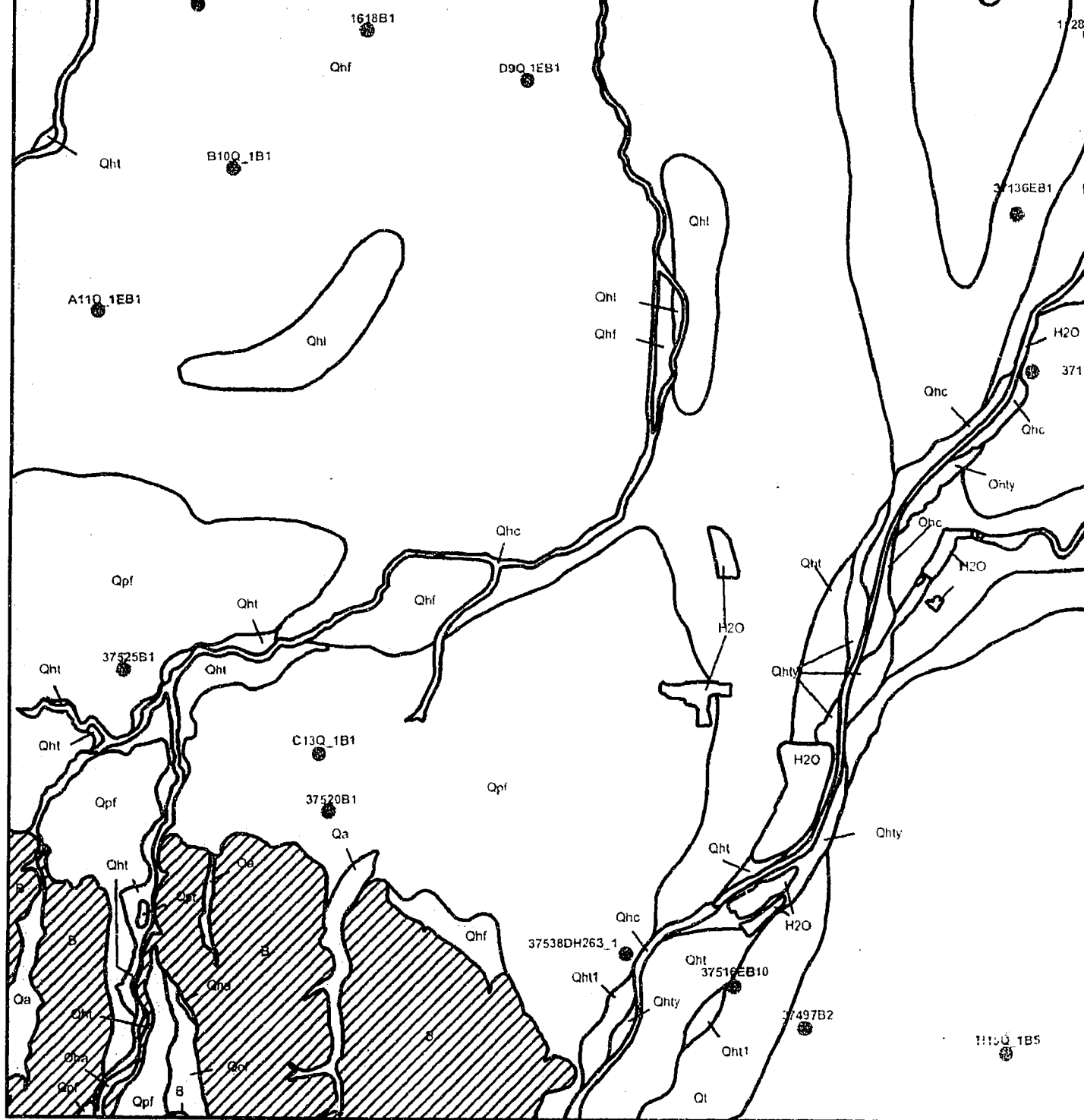
685B6

1749EB7









Milpitas base map prepared by the U. S. Geological Survey , 1961, photorevised 1991
 Calaveras Reservoir base map prepared by the U. S. Geological Survey, 1961, photorevised 1991
 San Jose East base map prepared by the U. S. Geological Survey, 1961, photorevised 1991
 San Jose West base map prepared by the U. S. Geological Survey, 1961, photorevised 1991

Quaternary Geologic maps of the Milpitas, Calaveras Reservoir, San Jose East and San Jose West
 modified from Witter et al. (2006)

Legend

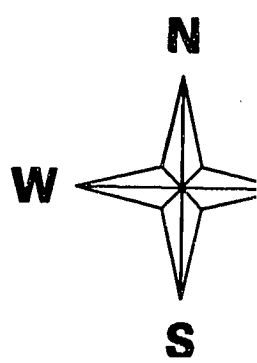
Well location

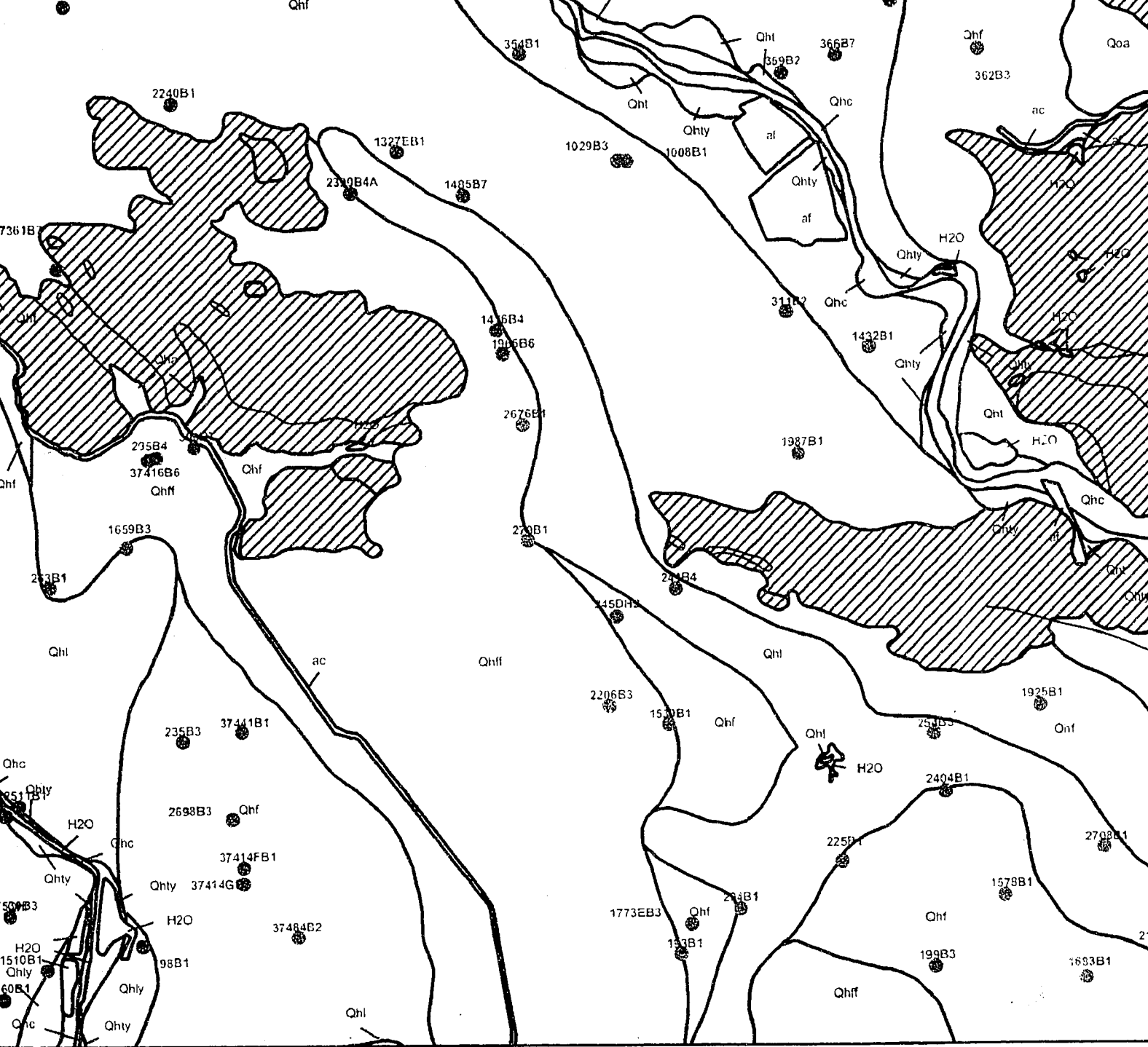


1980.
 Photorevised 1980.
 Revised 1980.
 Revised 1980.

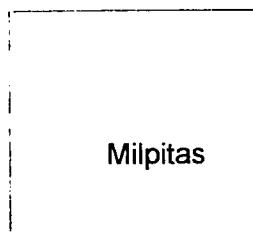
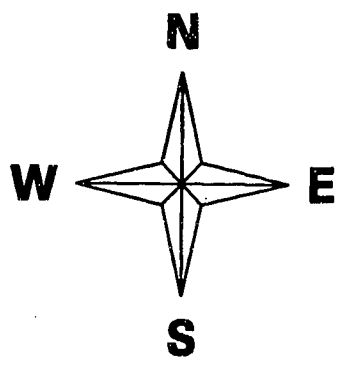
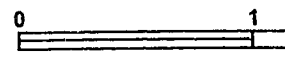
Index Map of the North

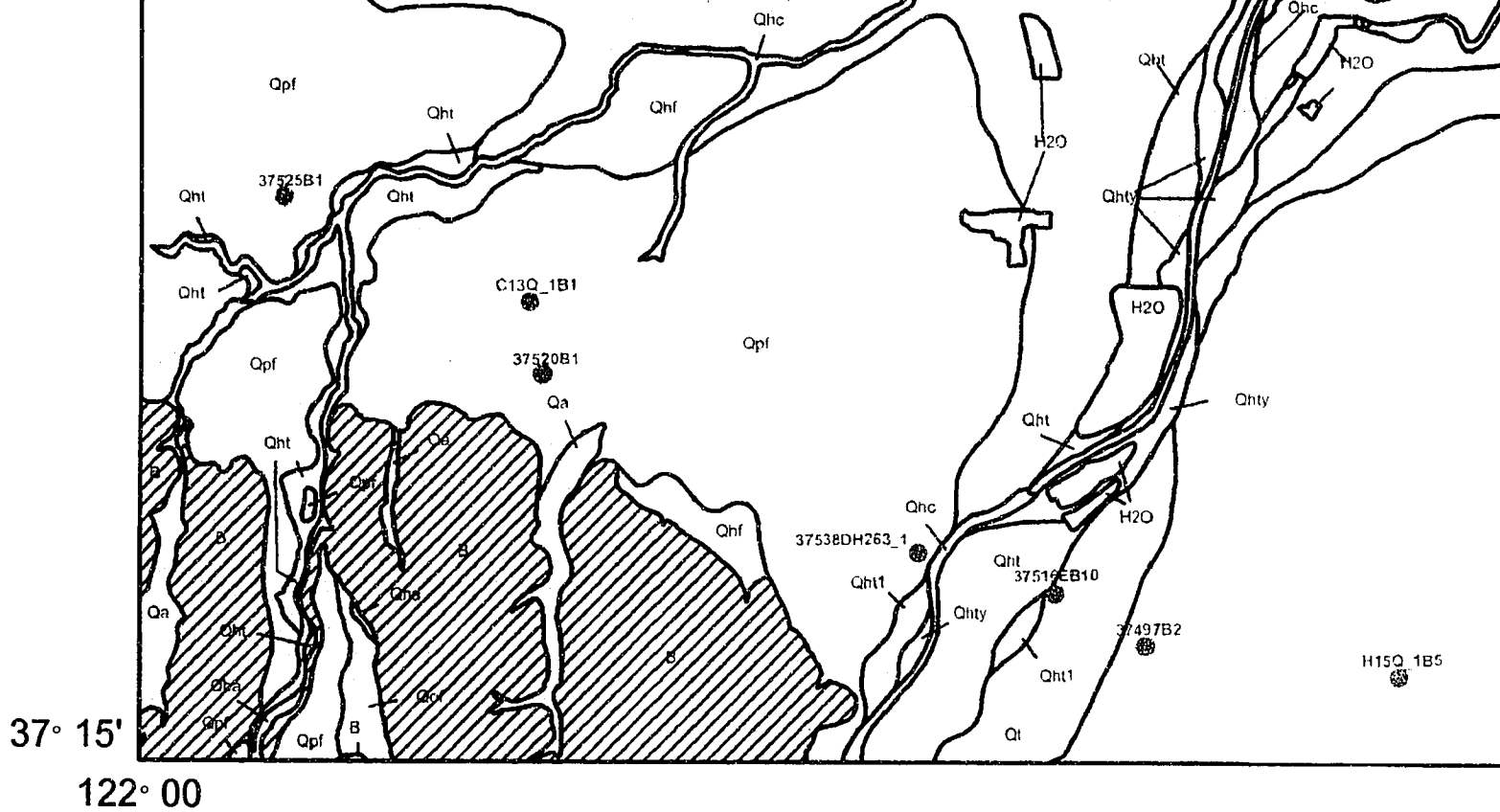
and San Jose West Quadrangles





The Northern Santa Clara Valley, California

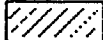


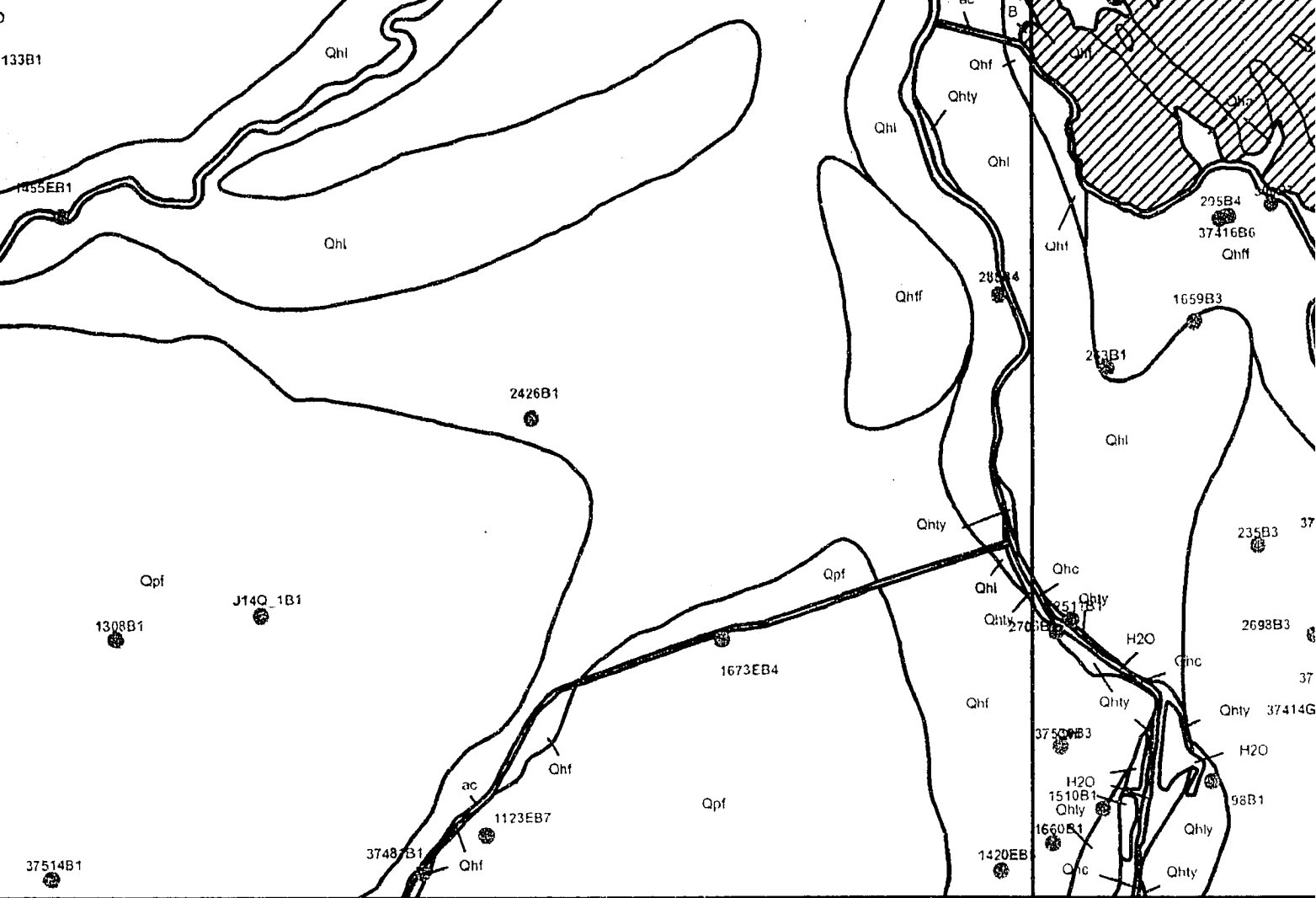


Milpitas base map prepared by the U. S. Geological Survey , 1961, photorevised 1991
 Calaveras Reservoir base map prepared by the U. S. Geological Survey, 1961, photorevised 1991
 San Jose East base map prepared by the U. S. Geological Survey, 1961, photorevised 1991
 San Jose West base map prepared by the U. S. Geological Survey, 1961, photorevised 1991

Quaternary Geologic maps of the Milpitas, Calaveras Reservoir, San Jose East and San Jose West
 modified from Witter et al. (2006)

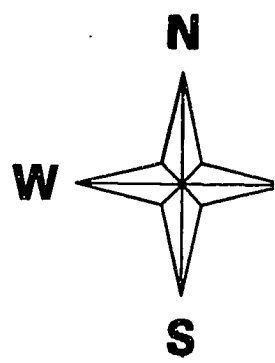
Legend

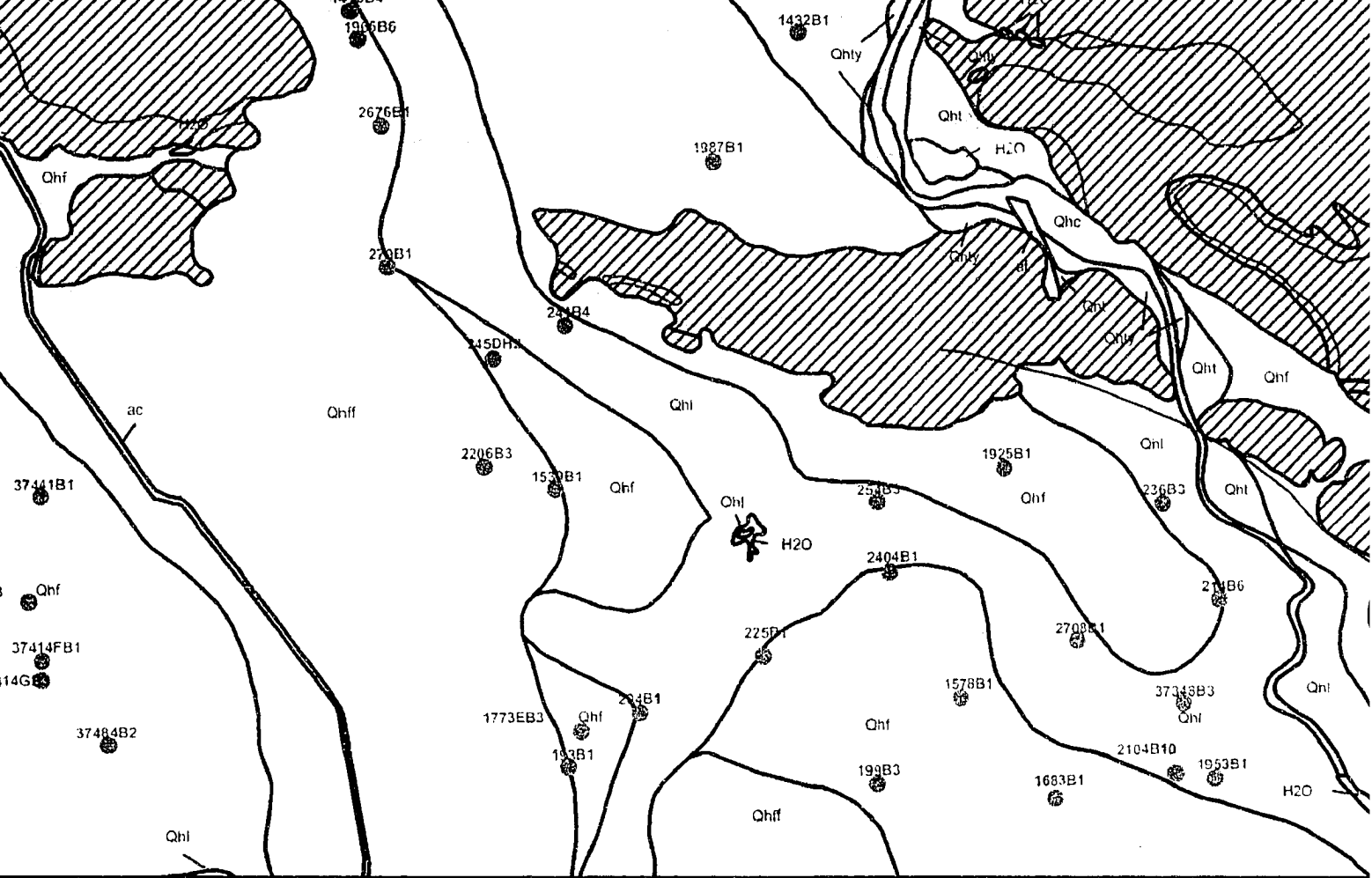
- Borehole location
- I6Q_1B1 Boring name
- Section line location
- THEISIS XSEC Section line label
- Geologic map unit boundary
- Qhff Geologic map unit name (see Table 1 in text for explanation)
-  bedrock
- Faults



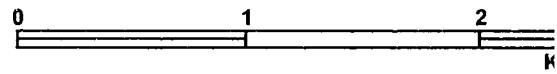
1980.
 photorevised 1980.
 revised 1980.
 revised 1980.
 and San Jose West Quadrangles

Index Map of the Northern

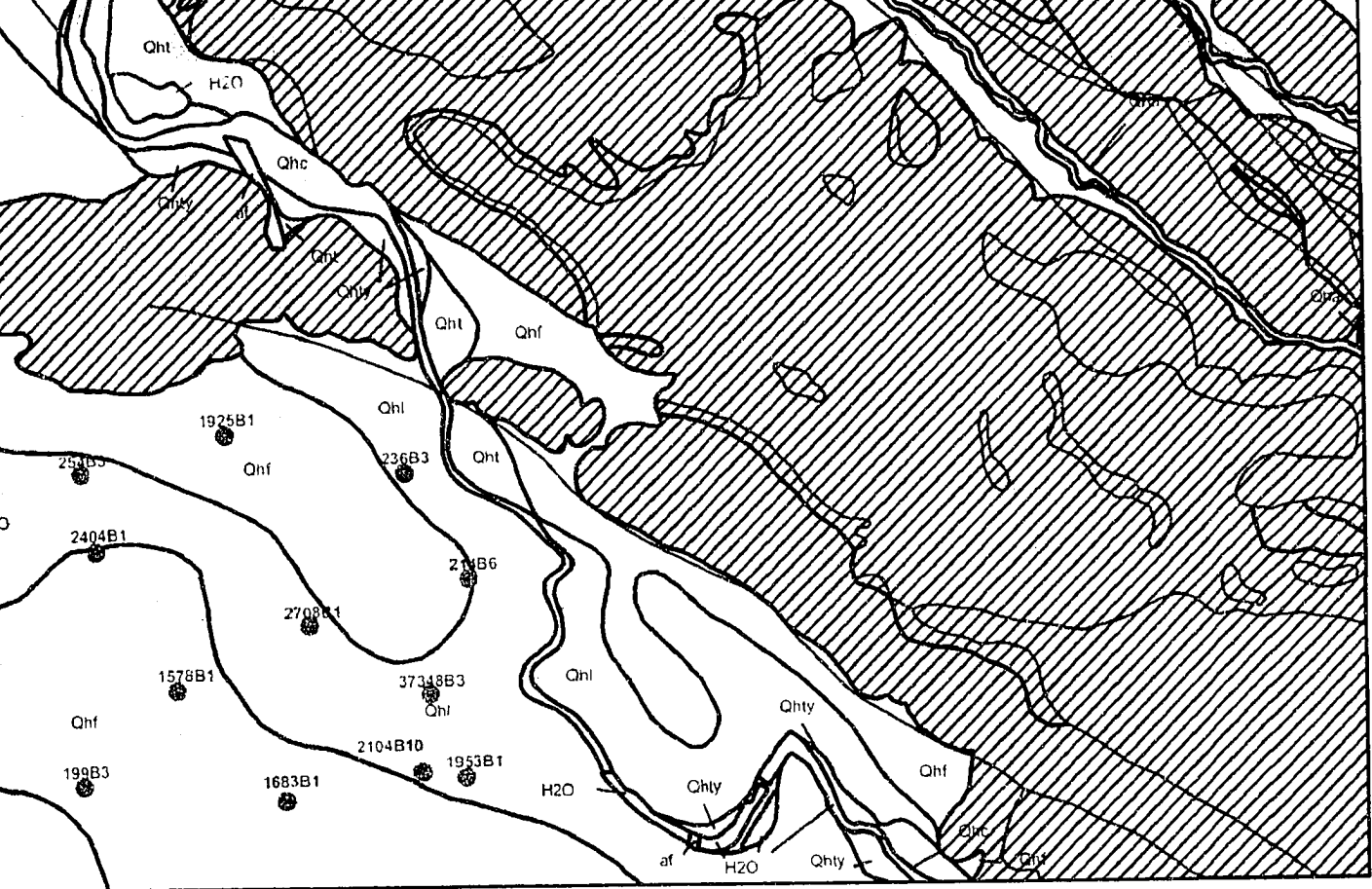




Northern Santa Clara Valley, California



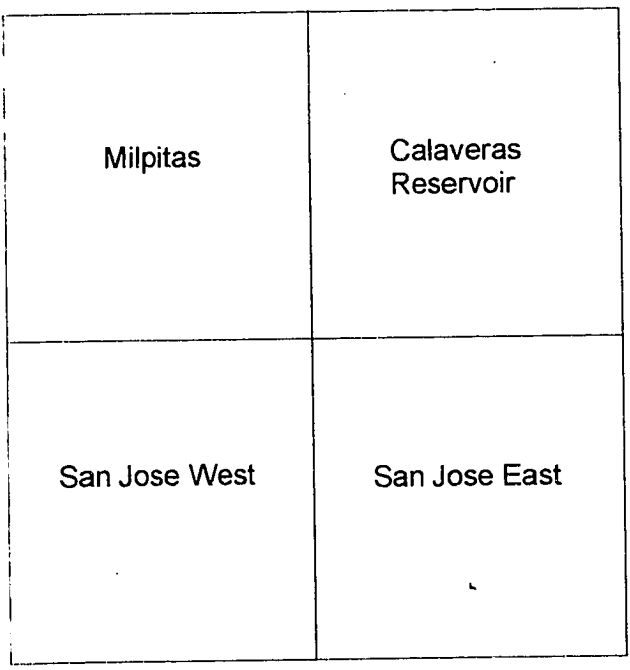
Milpitas	Calaveras Reservoir
San Jose West	San Jose East



37° 15'

121° 45'

California



THESIS PLATE 1 - Index Map
Anne Rosinski

NOTE TO USERS

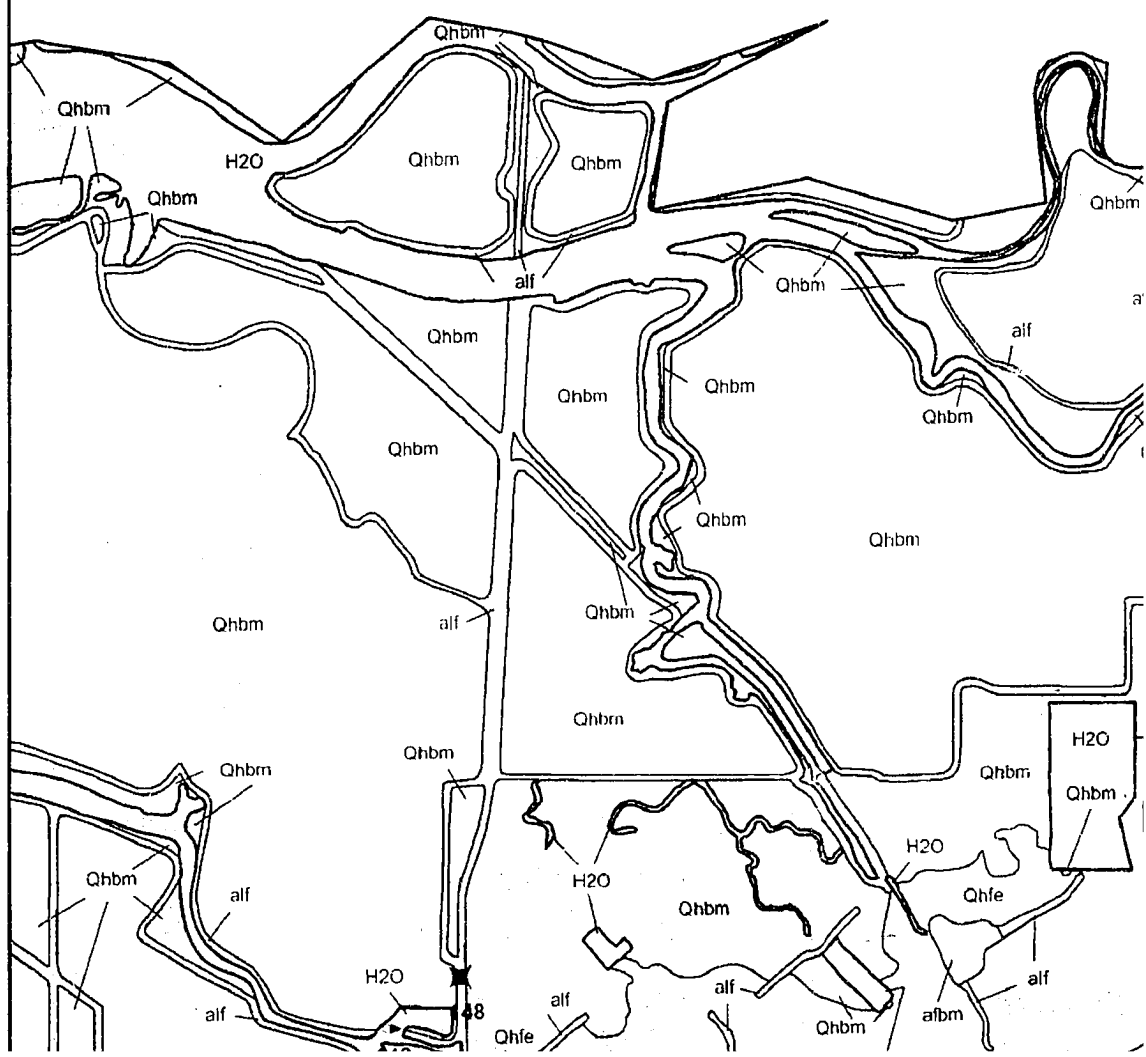
Oversize maps and charts are microfilmed in sections in the following manner:

LEFT TO RIGHT, TOP TO BOTTOM, WITH SMALL OVERLAPS

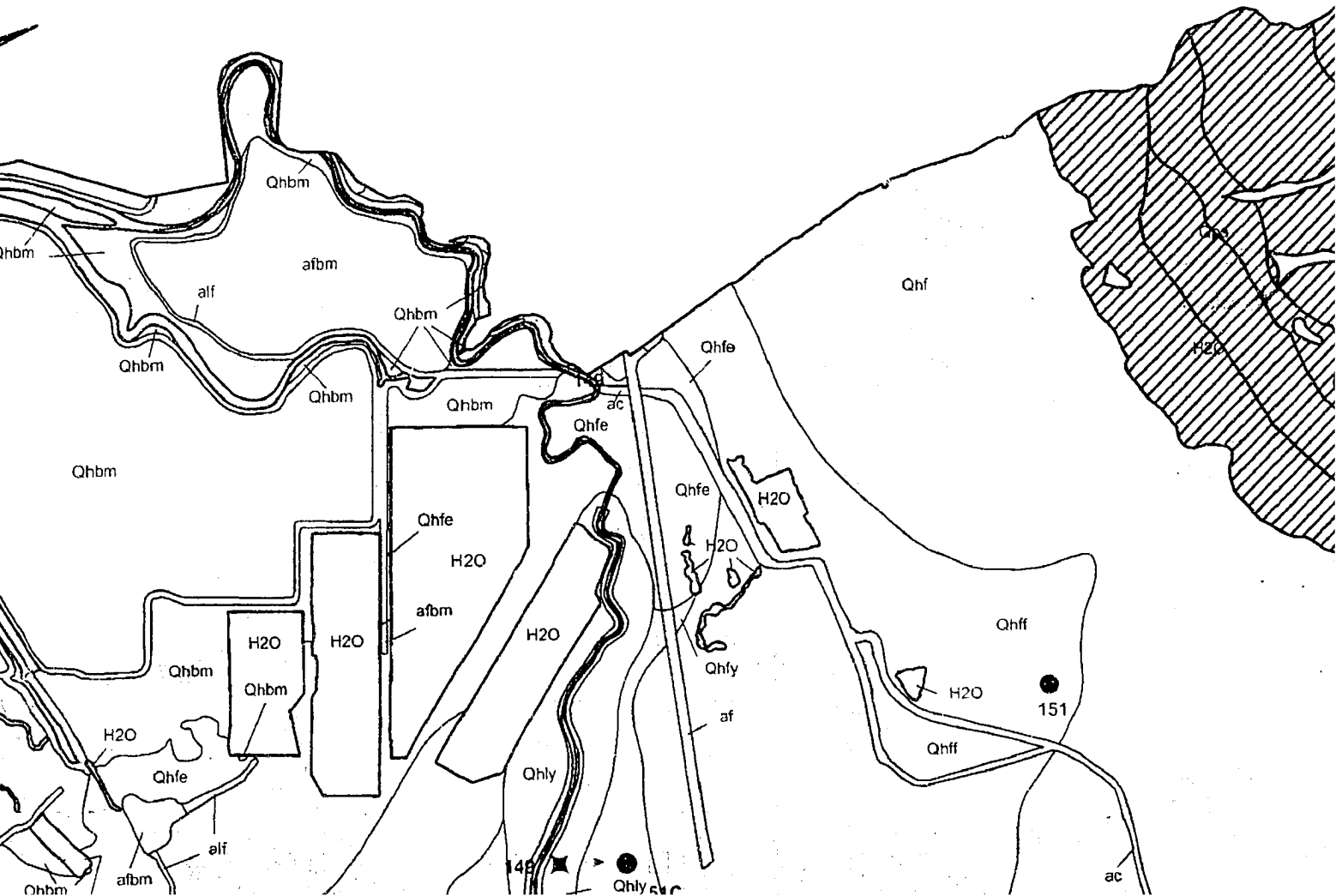
This reproduction is the best copy available.

UMI[®]

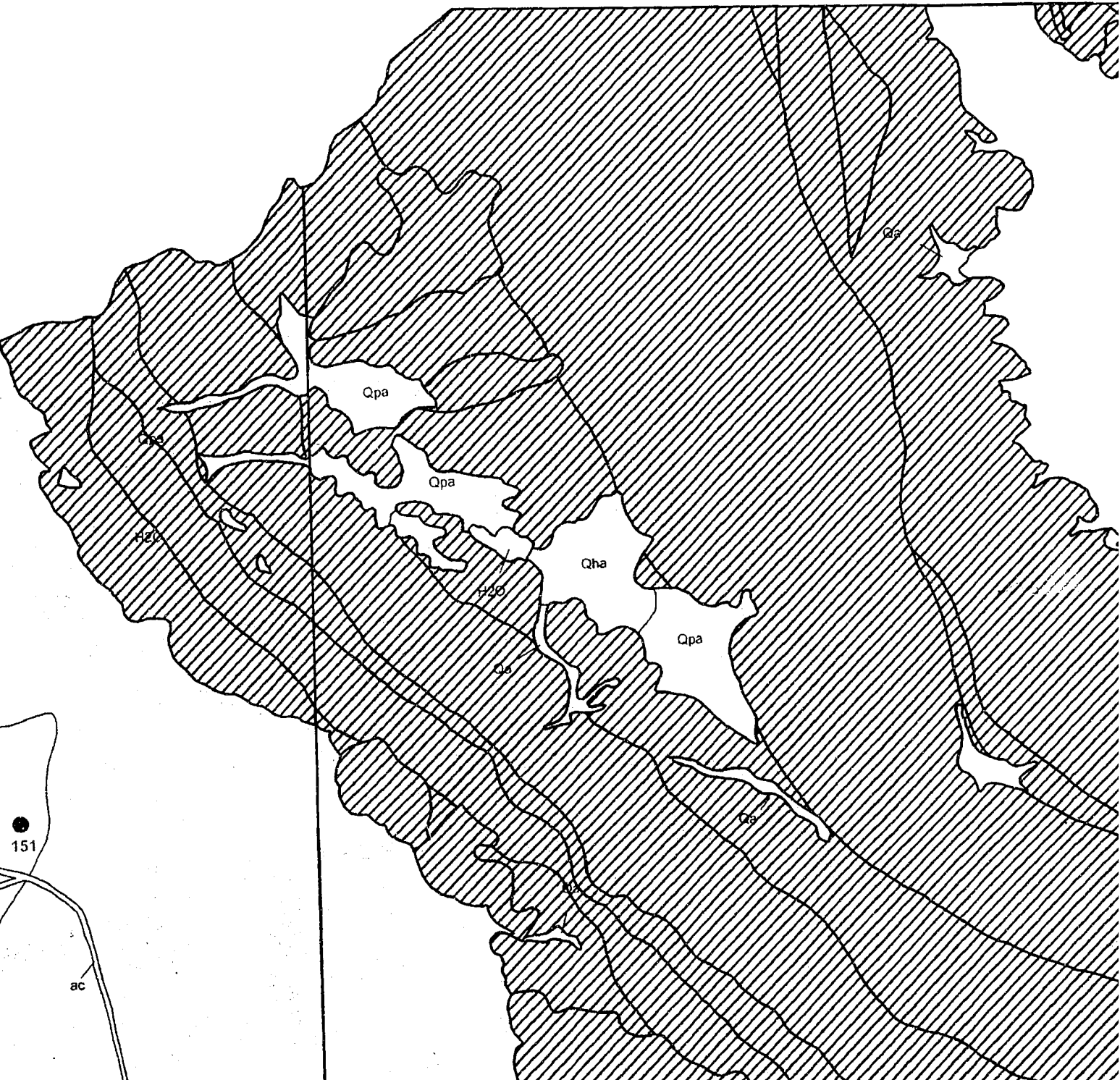
122° 00'
37° 30'



NOT EVALUATED - OU



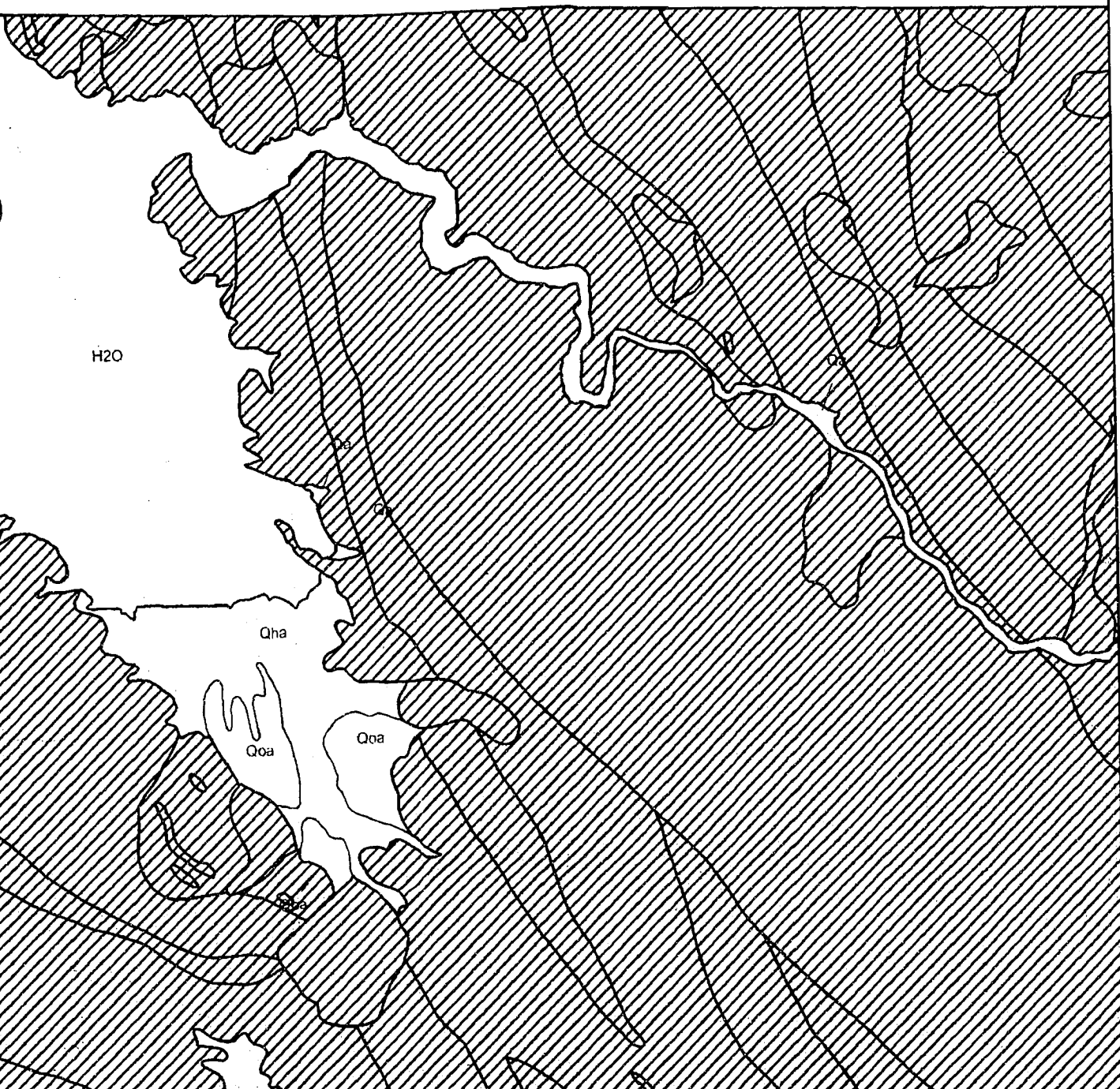
D - OUTSIDE STUDY AREA

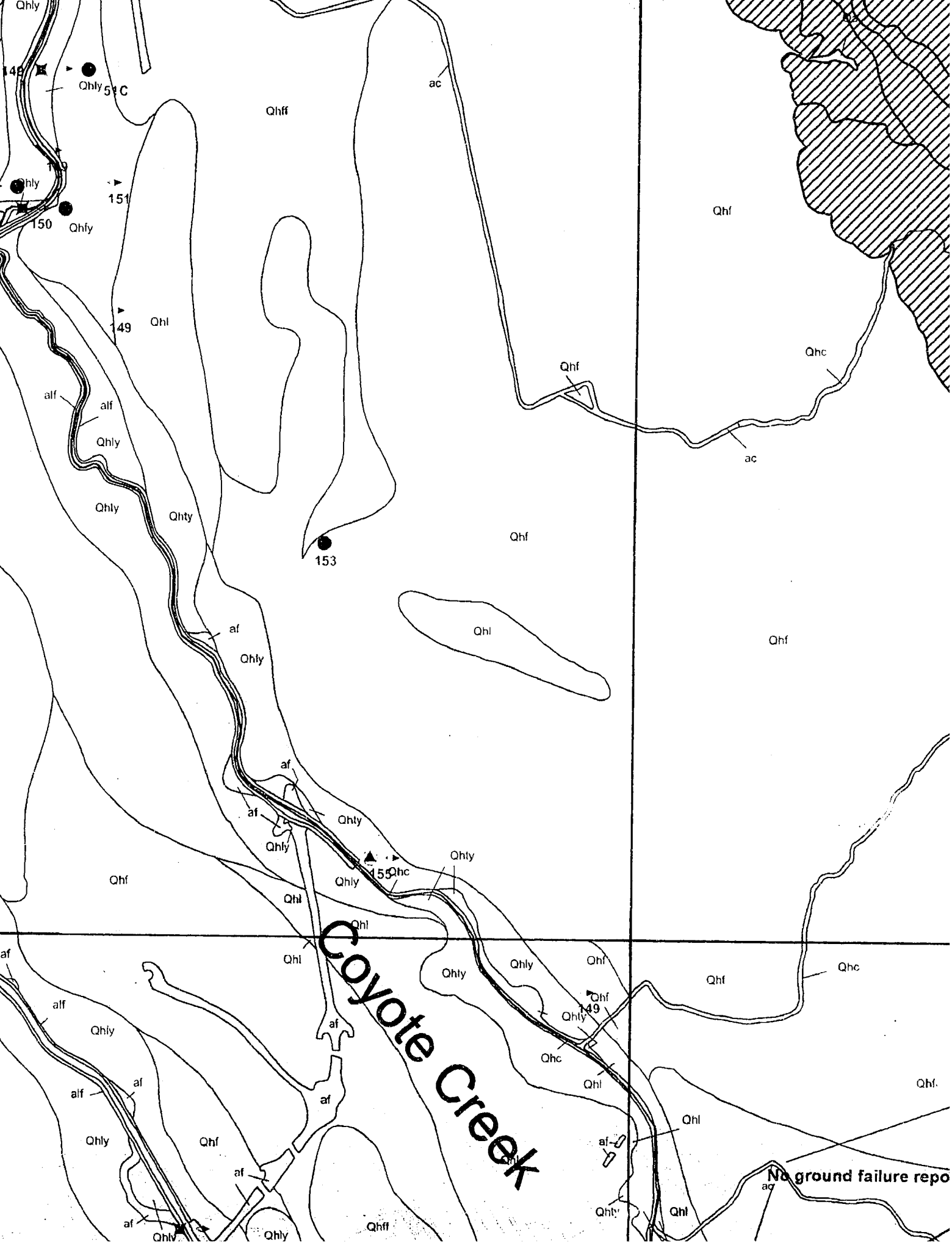


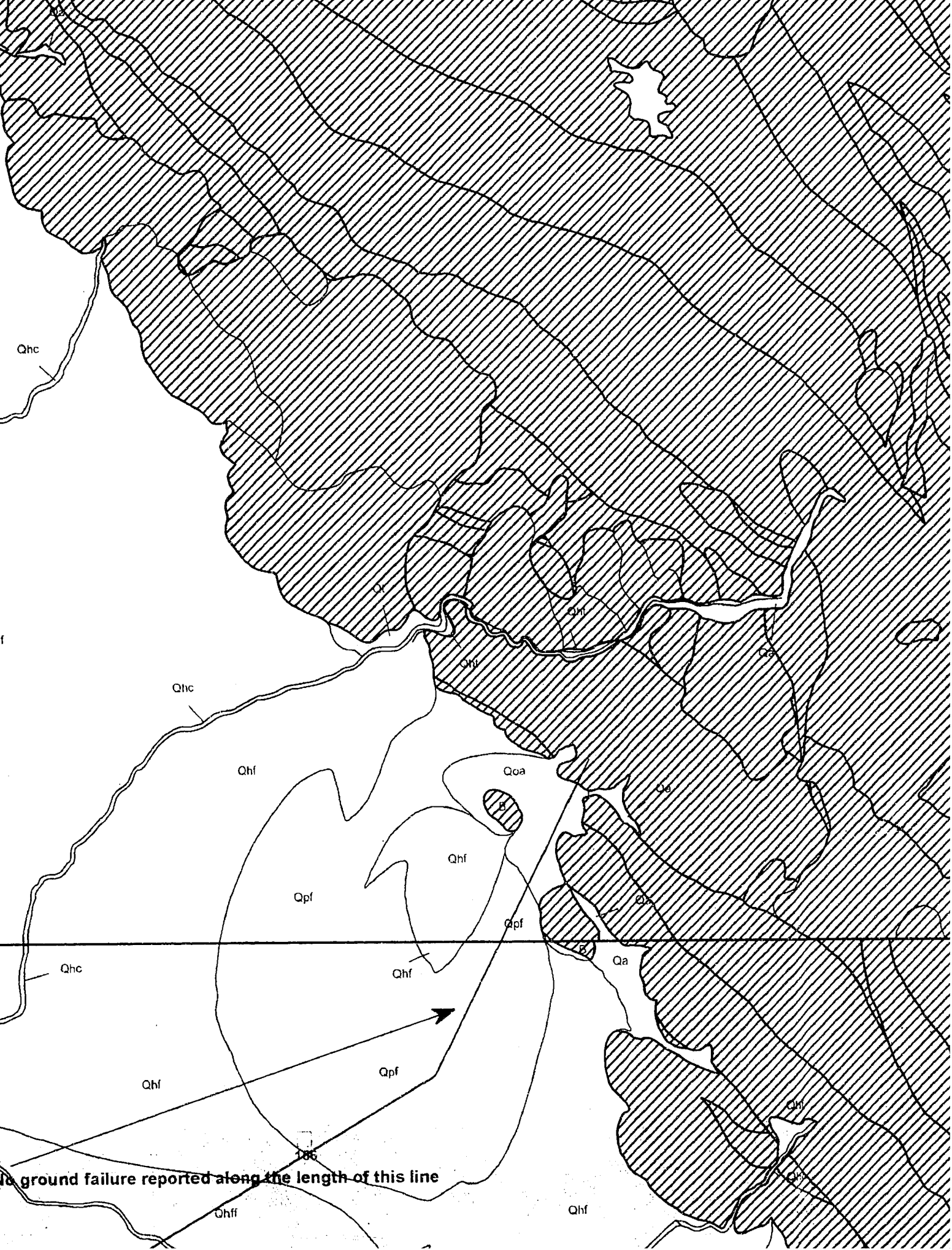
121° 45'

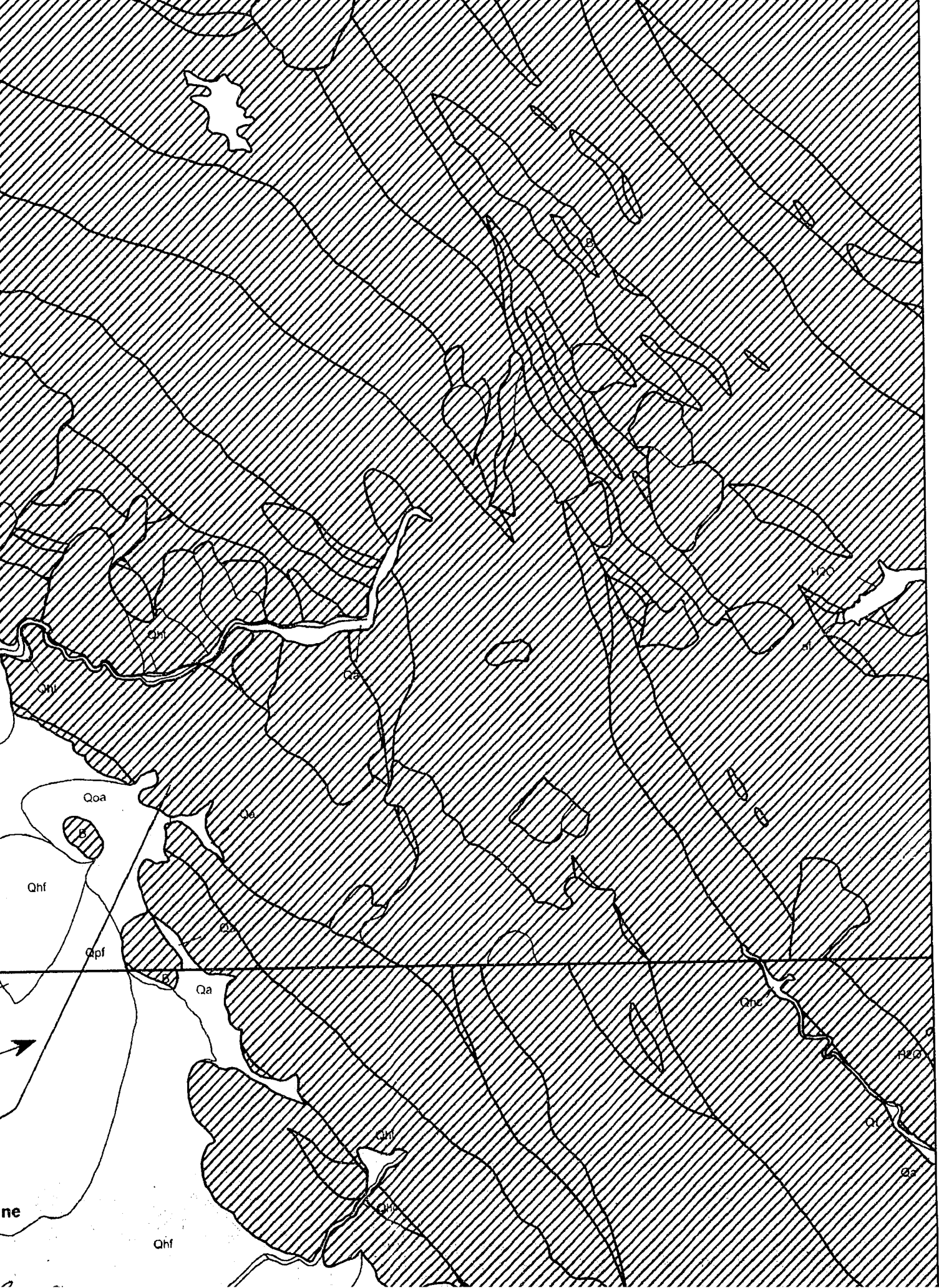
37° 30'

A











Creek

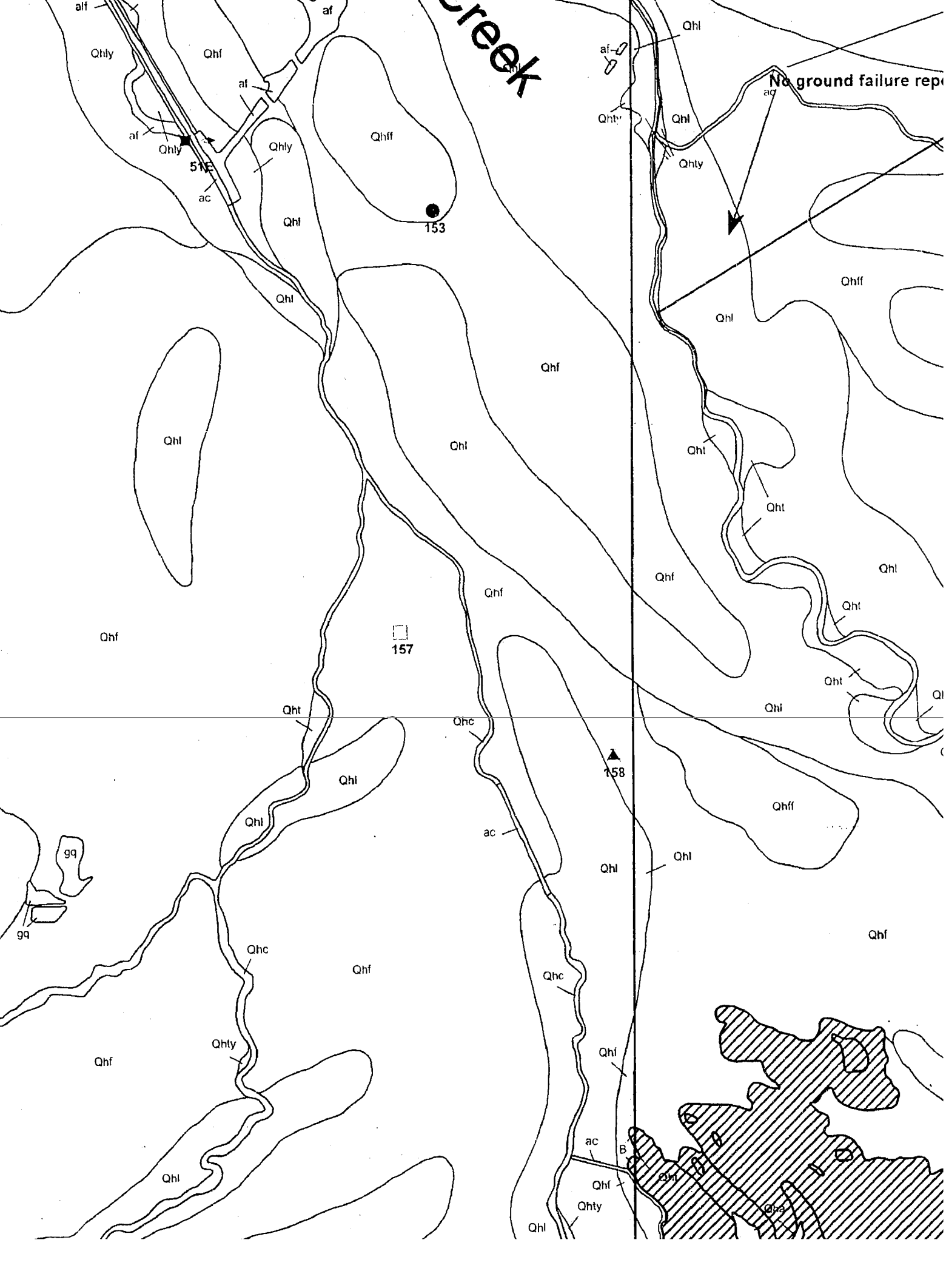
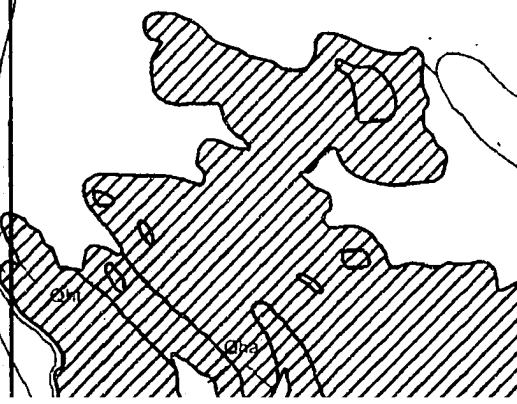
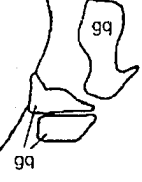
No ground failure reported

51E

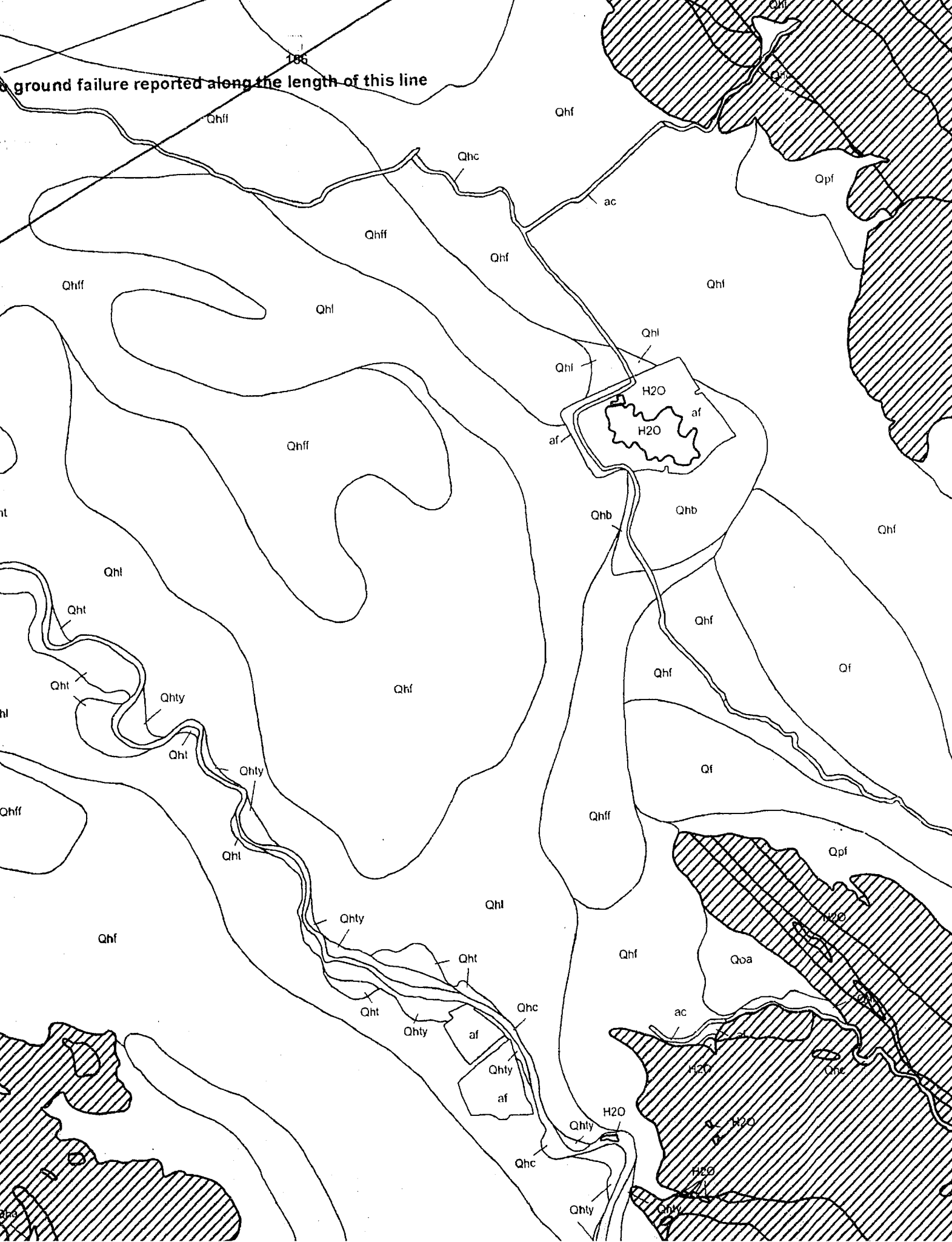
153

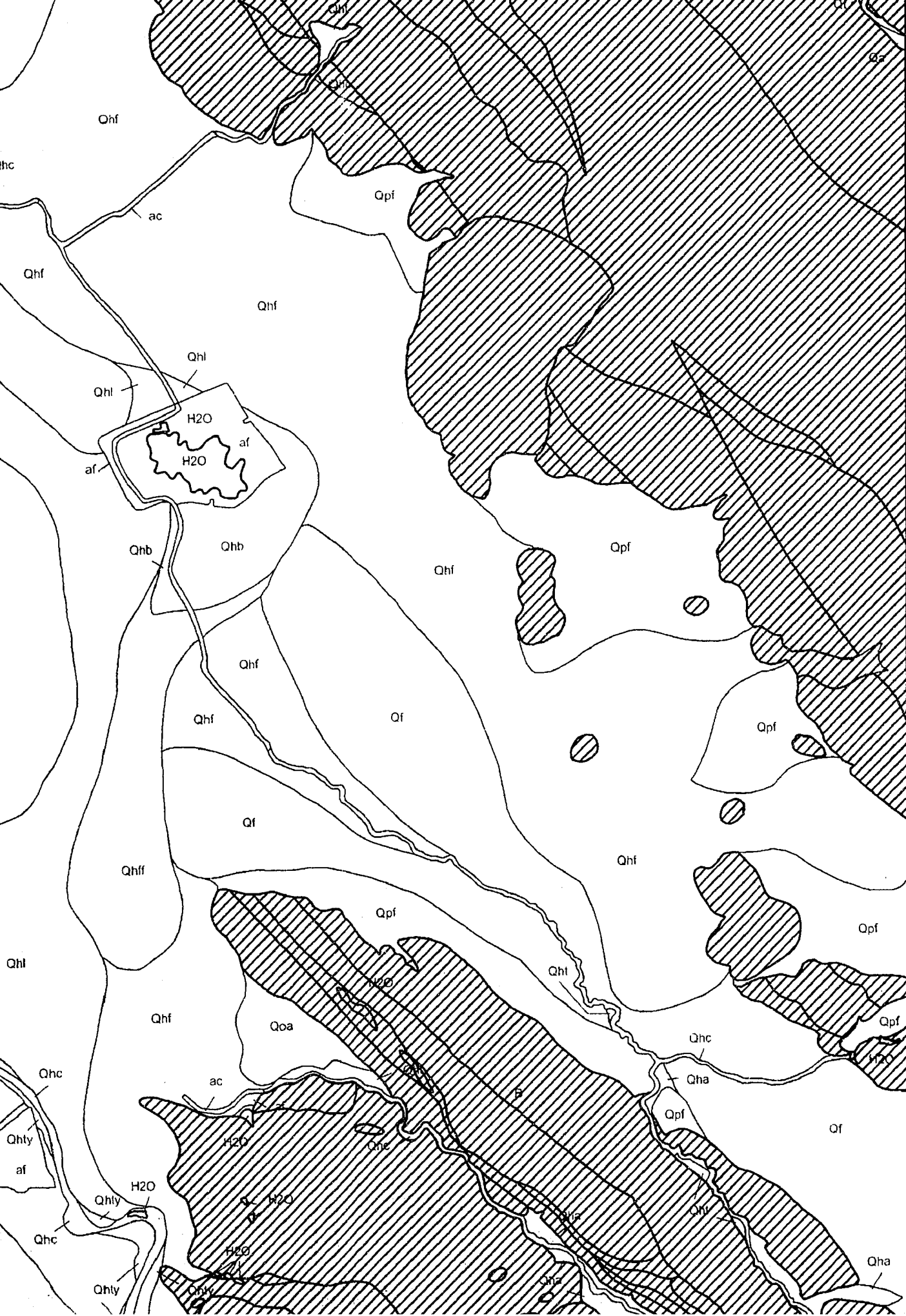
157

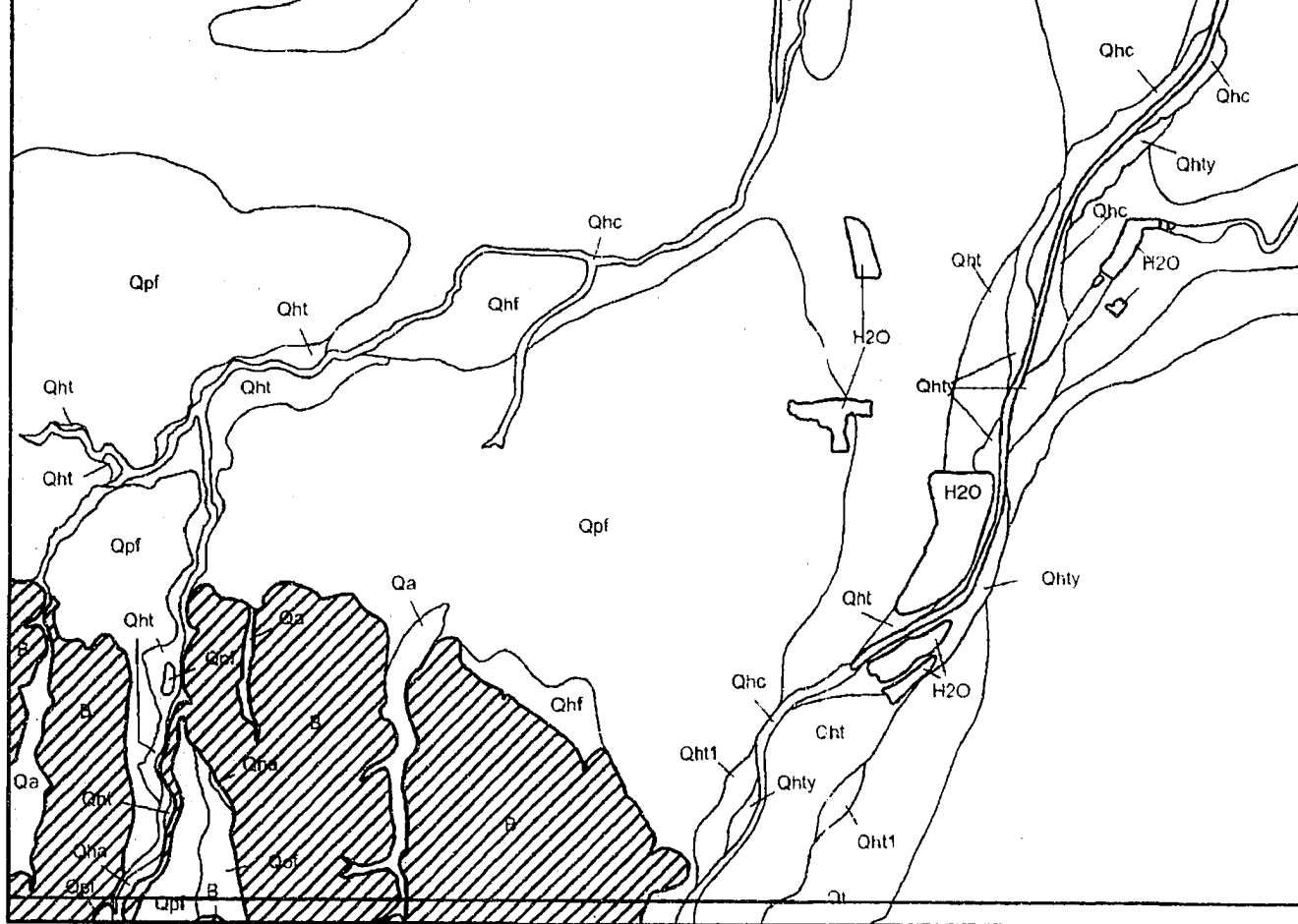
158



186
A ground failure reported along the length of this line







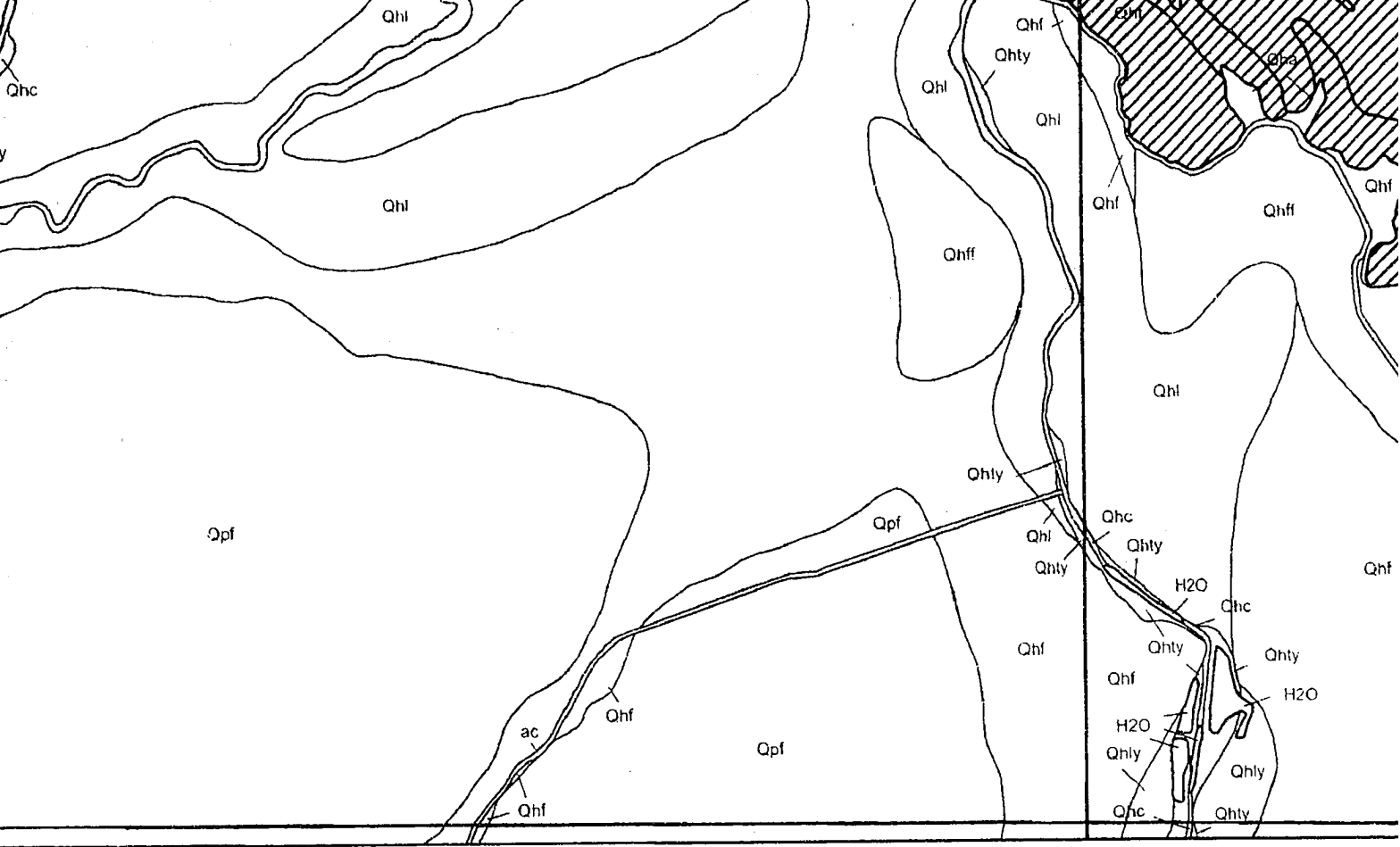
37° 15'
122° 00'

Milpitas base map prepared by the U. S. Geological Survey, 1961, photorevised 1980.
 Calaveras Reservoir base map prepared by the U. S. Geological Survey, 1961, photorevised 1980.
 San Jose East base map prepared by the U. S. Geological Survey, 1961, photorevised 1980.
 San Jose West base map prepared by the U. S. Geological Survey, 1961, photorevised 1980.

REFERENCE:

Quaternary geologic maps of the Milpitas, Calaveras Reservoir, San Jose East and San Jose West Quadrangles modified after Witter et al., (2006)
 Historical ground failure data from Youd and Hoose, 1978; Tinsley, 1998; Knudsen et al., 2000.

Milpitas	Calaveras Reservoir
San Jose West	San Jose East

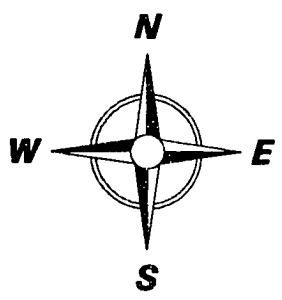
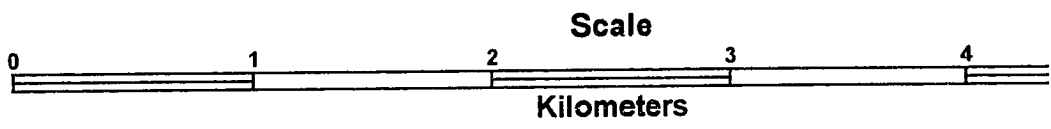


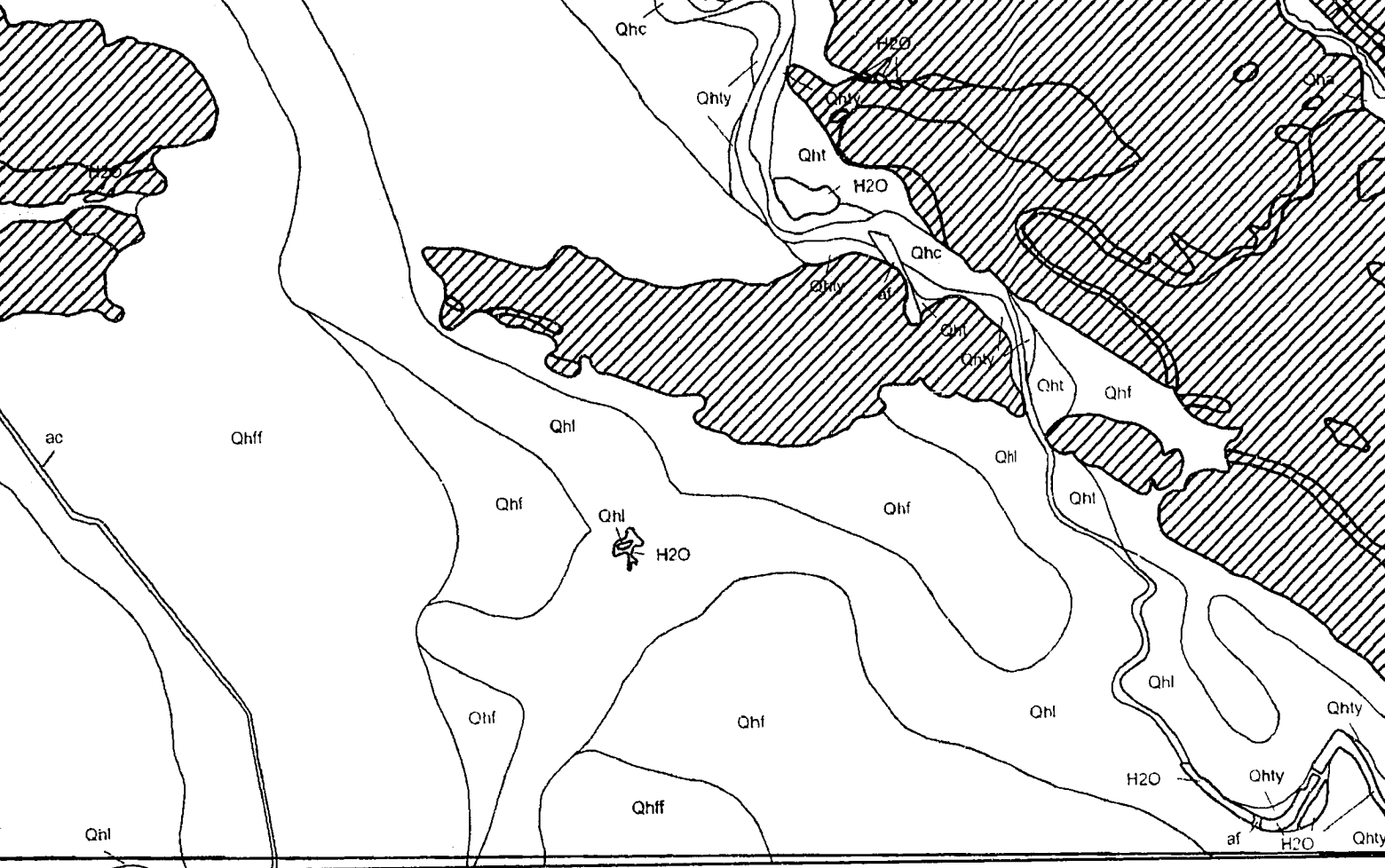
Historical Ground Failure

1980.
 0.

West

00.



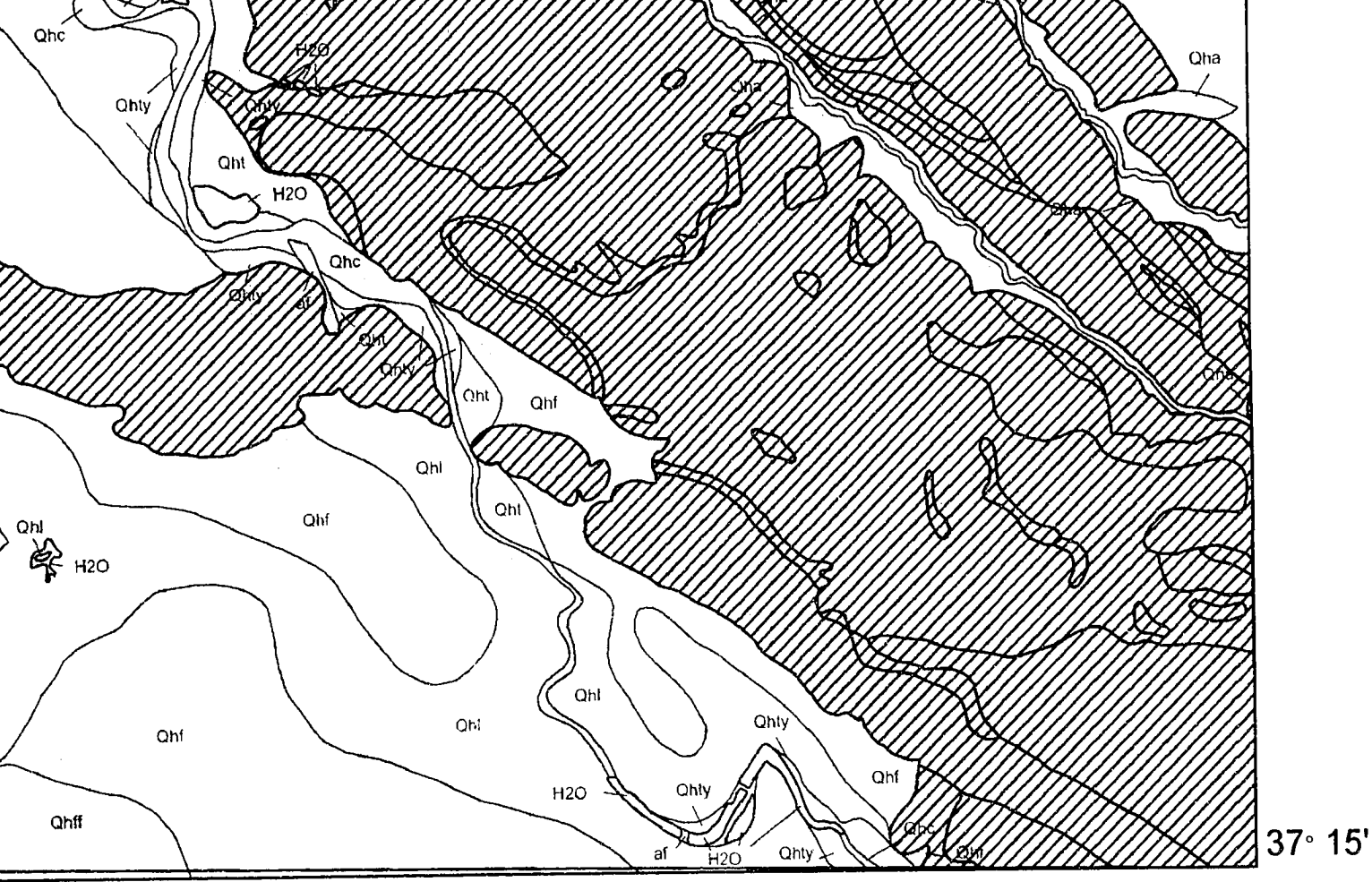


e



Legend

- Geologic map unit boundary
- 148 Ground failure site number (see Appen
- Absence of ground failure reported
- ▲ Disturbed well
- ▶ Lateral spread
- Sand boil
- ✱ Settlement
- Qhff Geologic map unit (see Table 1 in te
- H2O
- ▨ Bedrock



Legend

- Geologic map unit boundary
- 148 Ground failure site number (see Appendix 4 for details)
- Absence of ground failure reported
- ▲ Disturbed well
- ▶ Lateral spread
- Sand boil
- ✱ Settlement
- Qhff Geologic map unit (see Table 1 in text for explanation)
- H2O
- ▨ Bedrock

NOTE TO USERS

Oversize maps and charts are microfilmed in sections in the following manner:

LEFT TO RIGHT, TOP TO BOTTOM, WITH SMALL OVERLAPS

This reproduction is the best copy available.

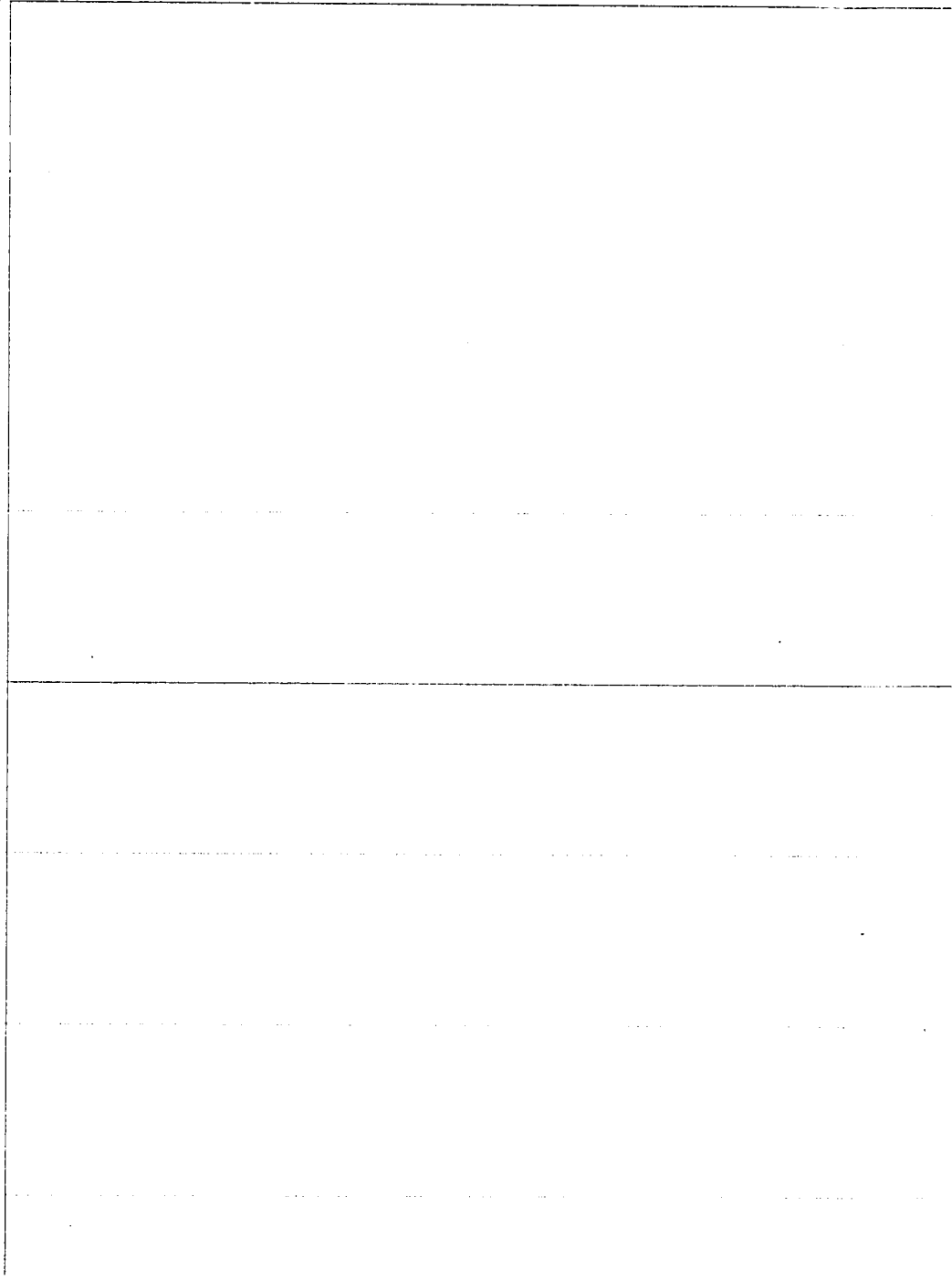
UMI[®]

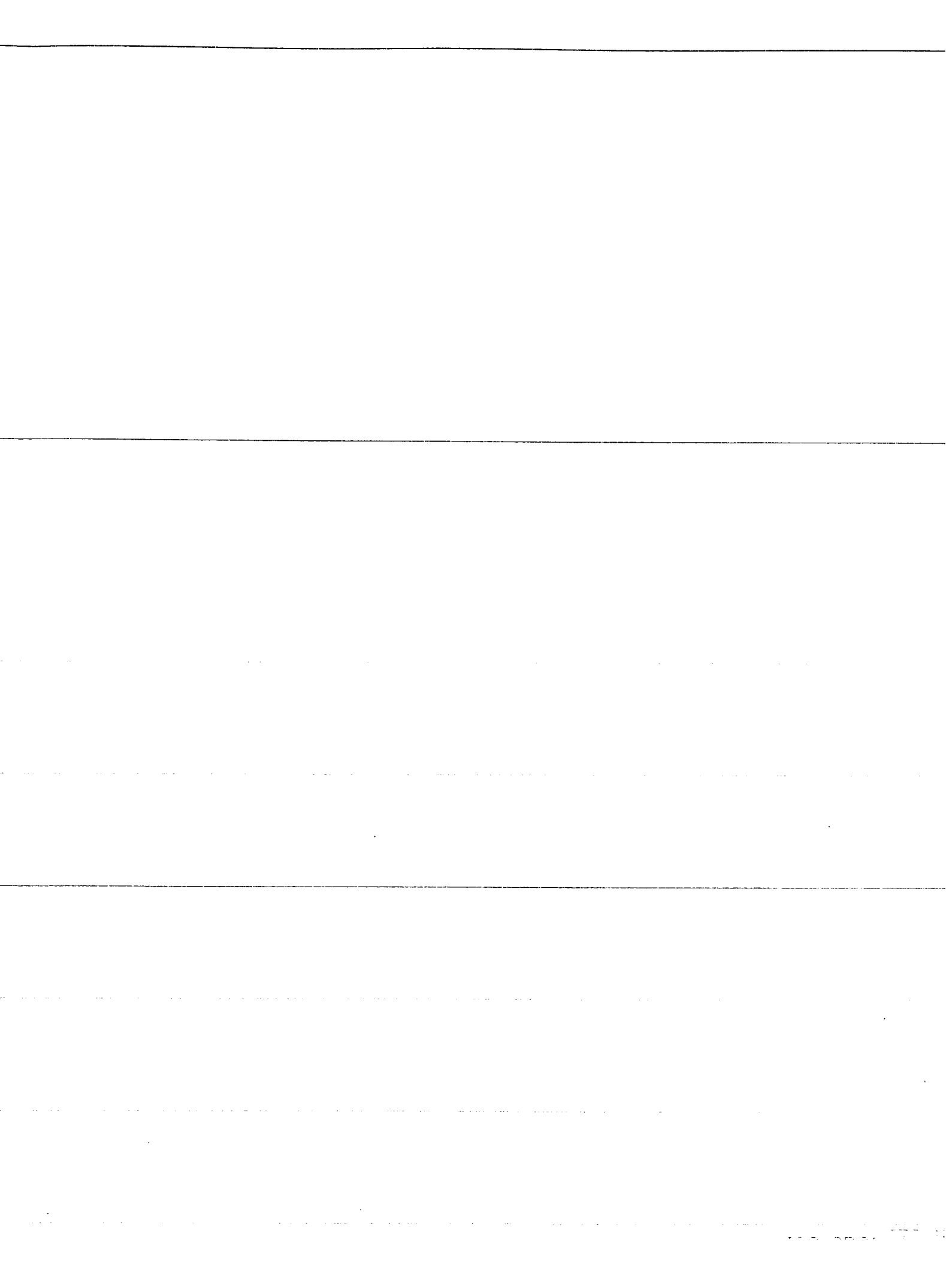
WEST

16A0005, 347526

tion in feet

100
90
80
70
60
50
40
30
20
10
0





Coyote Creek

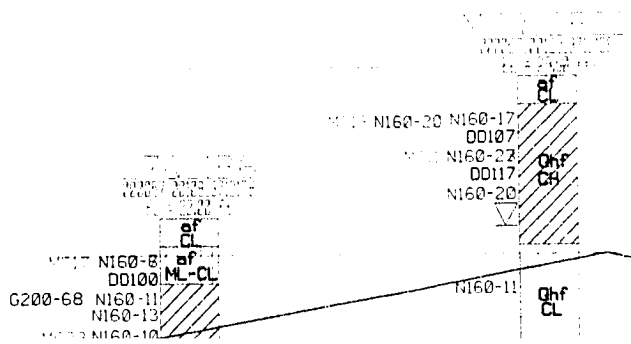
Highway 880

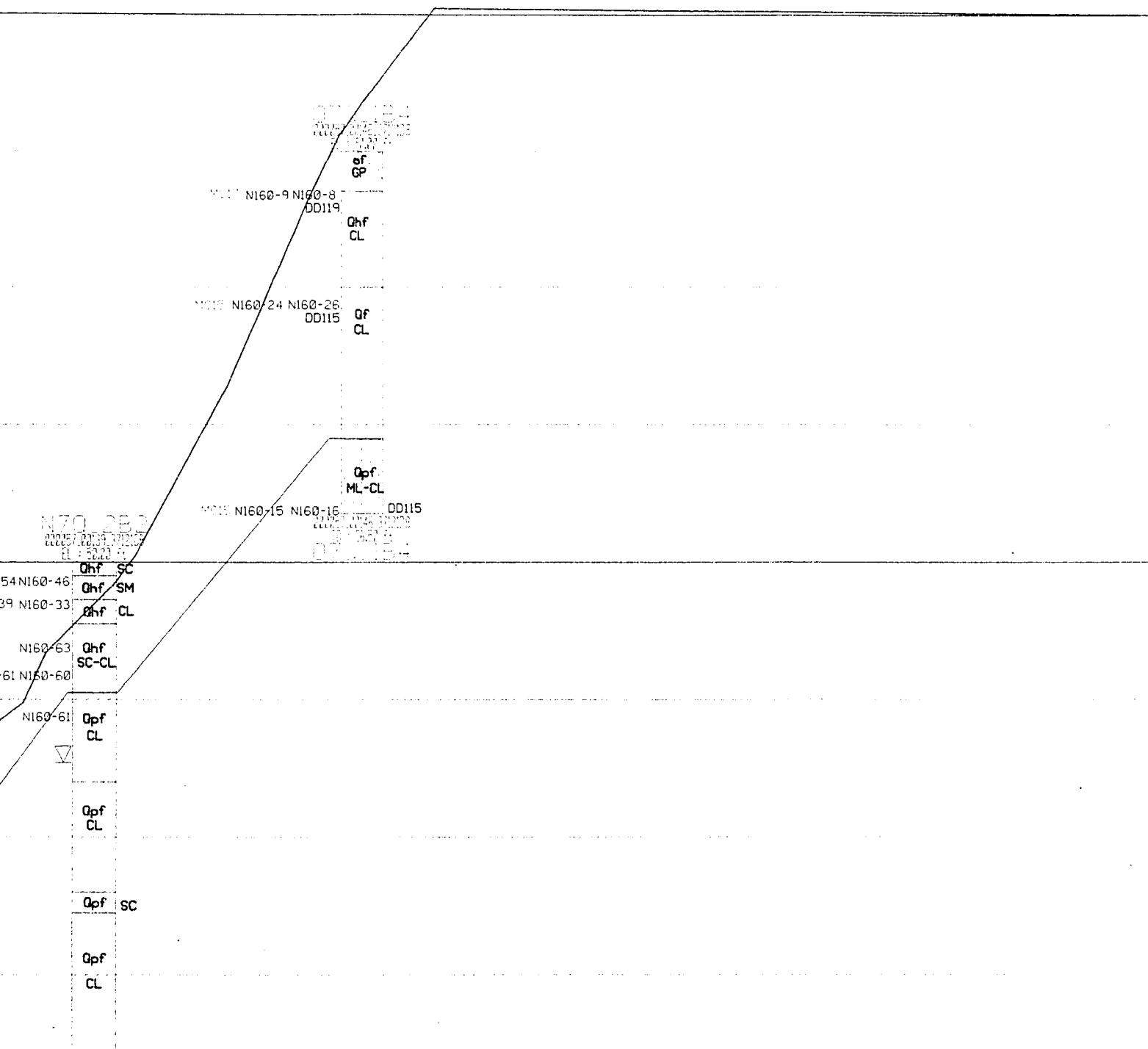
Southern Pacific Rail Road

Approximate ground surface elevation
Note that borings are projected to
cross section line, and therefore, the
top of the boring may not correspond to
ground surface.

Southern Pacific Rail Road

North Main Street





N160-9 N160-8
DD119

Qf
GP

Qhf
CL

N160-24 N160-26
DD115

Qf
CL

Qpf
ML-CL

N160-15 N160-16
DD115

N70-283
0015/0019/0020
0021/0022/0023
0024/0025/0026
0027/0028/0029
0030/0031/0032
0033/0034/0035
0036/0037/0038
0039/0040/0041
0042/0043/0044
0045/0046/0047
0048/0049/0050
0051/0052/0053
0054/0055/0056
0057/0058/0059
0060/0061/0062
0063/0064/0065
0066/0067/0068
0069/0070/0071
0072/0073/0074
0075/0076/0077
0078/0079/0080
0081/0082/0083
0084/0085/0086
0087/0088/0089
0090/0091/0092
0093/0094/0095
0096/0097/0098
0099/0100/0101
0102/0103/0104
0105/0106/0107
0108/0109/0110
0111/0112/0113
0114/0115/0116
0117/0118/0119
0120/0121/0122
0123/0124/0125
0126/0127/0128
0129/0130/0131
0132/0133/0134
0135/0136/0137
0138/0139/0140
0141/0142/0143
0144/0145/0146
0147/0148/0149
0150/0151/0152
0153/0154/0155
0156/0157/0158
0159/0160/0161
0162/0163/0164
0165/0166/0167
0168/0169/0170
0171/0172/0173
0174/0175/0176
0177/0178/0179
0180/0181/0182
0183/0184/0185
0186/0187/0188
0189/0190/0191
0192/0193/0194
0195/0196/0197
0198/0199/0200

Qhf SC

54 N160-46

Qhf SM

39 N160-33

Qhf CL

N160-63

Qhf

61 N160-60

SC-CL

N160-61

Qpf

CL

Qpf

CL

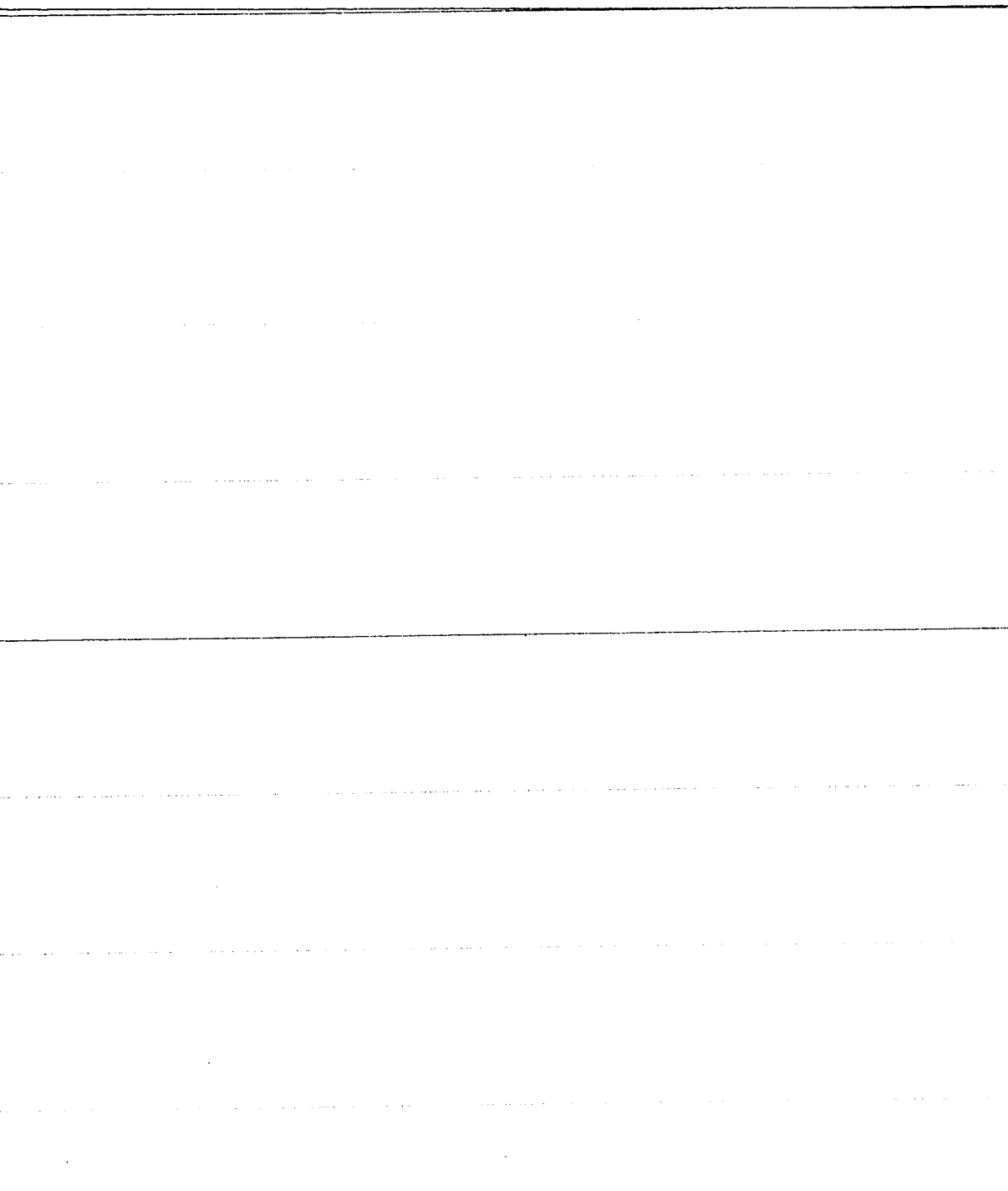
Qpf SC

Qpf

CL

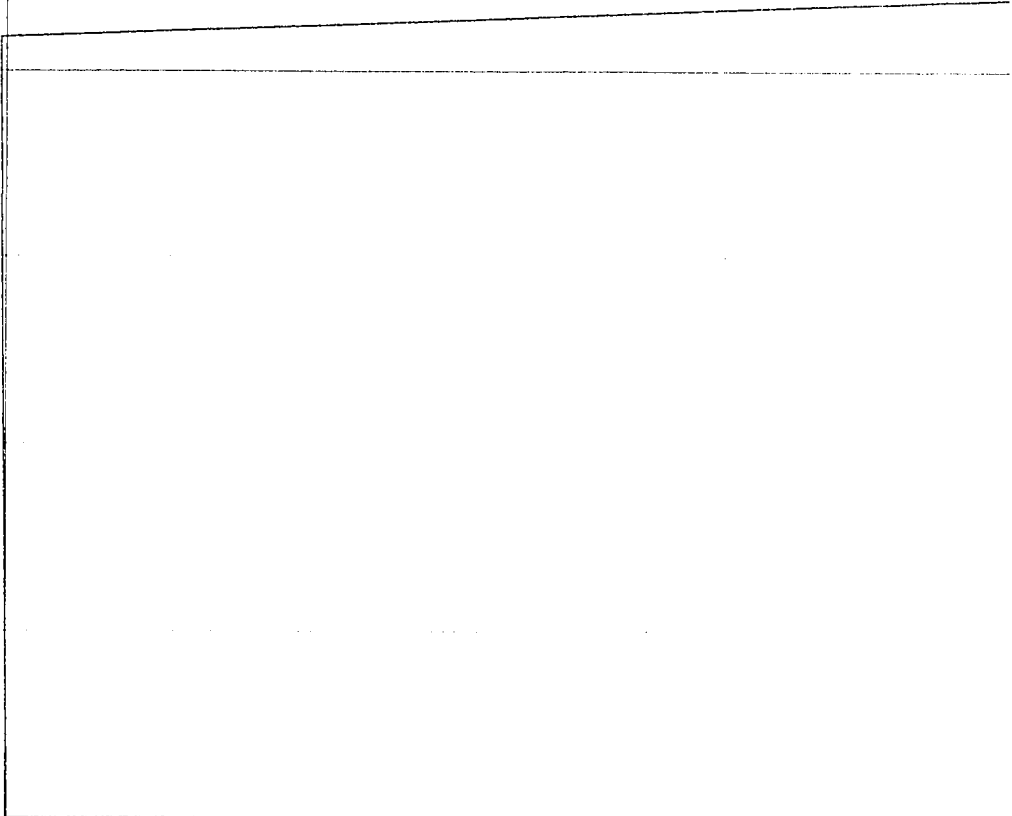
EAST

SECTION



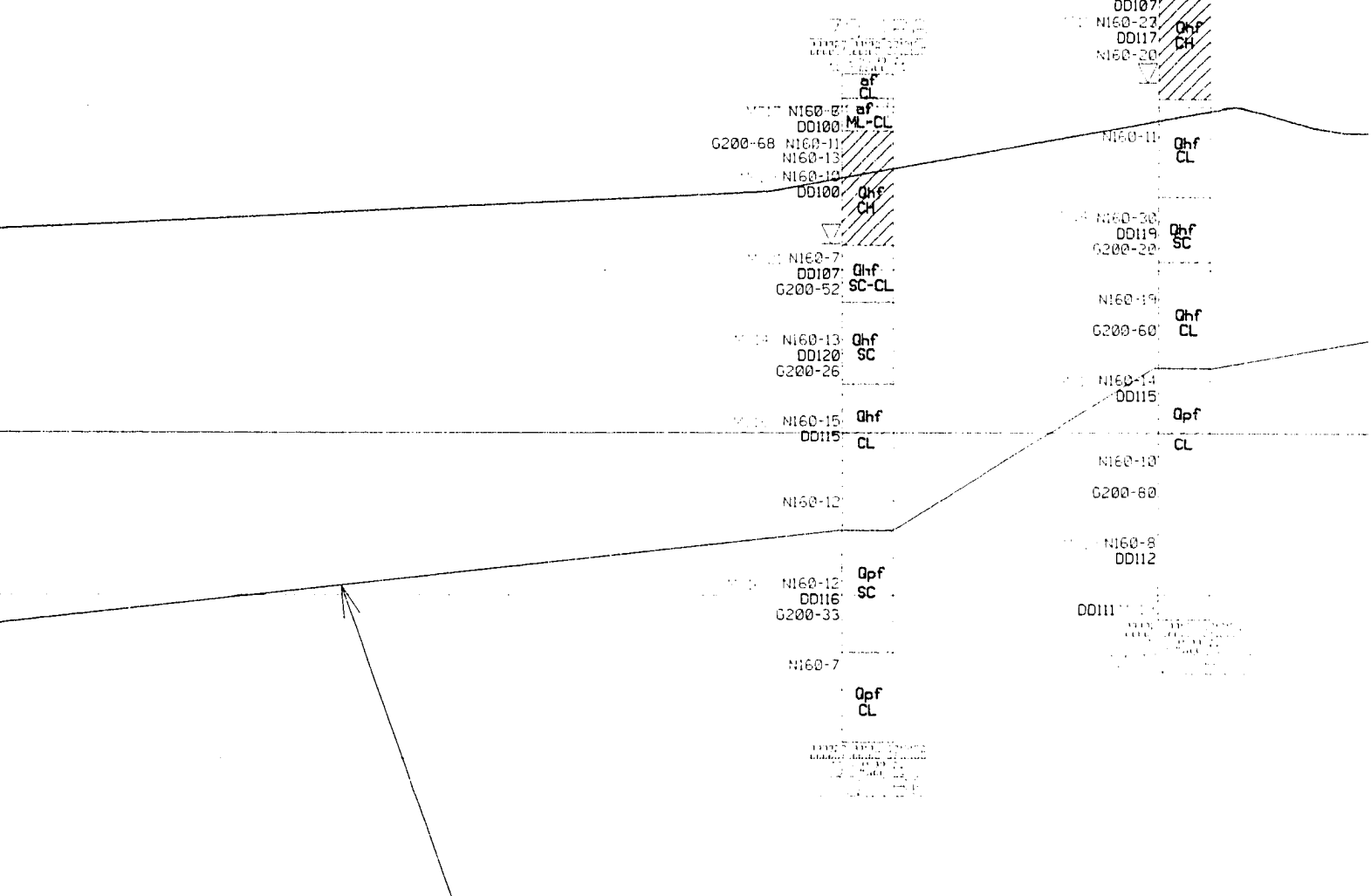
Elevation

11
10
9
8
7
6
5
4
3
2
1



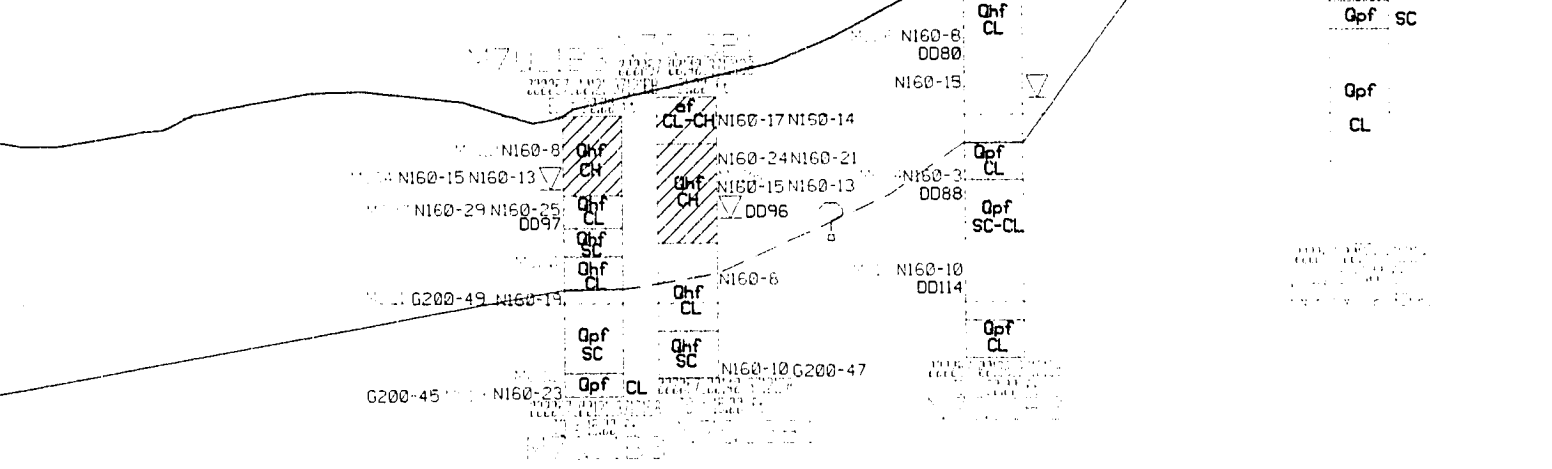
N160-13	N160-13	of	N160-17	of	N160-11
DD110	DD110	CL	DD113	CL-ML	DD120
			N160-30		N160-2
			DD113		DD104
	N160-26		N160-28		N160-11
	DD111		DD112		DD105
	N160-32		N160-6	Only	N160-1
	DD113		DD98	CL-ML	DD98
	N160-19				
	DD118				
	N160-6		N160-9	Only	N160-1
	DD82	Only	DD97	CH	DD99
		CL-ML			
			N160-14		N160-1
				Only	DD101
	N160-19			CL-CH	
			N160-14		N160-1
			N160-7	Only SM	N160-1

----- ? ----- ? ----- ? -----



Top of Pleistocene inferred from
 (actual stratigraphic boundary)

202257.0000.3/1209	Official Boring Name
K7C1B ⁹	Alternate Boring Name
10 - 41.52 ft	Total depth of boring
Qhfy	Stratigraphic Unit - See Appendix 1 for layer description
ML	Lithology (USCS)
N160-11	Penetration Resistance
N160-13	Moisture Content (%)
DD136	Dry Density (pounds per cubic foot)
G200-38	Grain Size Analysis (percent of silt and clay particles finer than 0.074 mm)
▽	Water Level Measured In Boring



from geotechnical properties
 (may differ)

HORIZONTAL SCALE

1000 Feet

VERTICAL SCALE

10 Feet

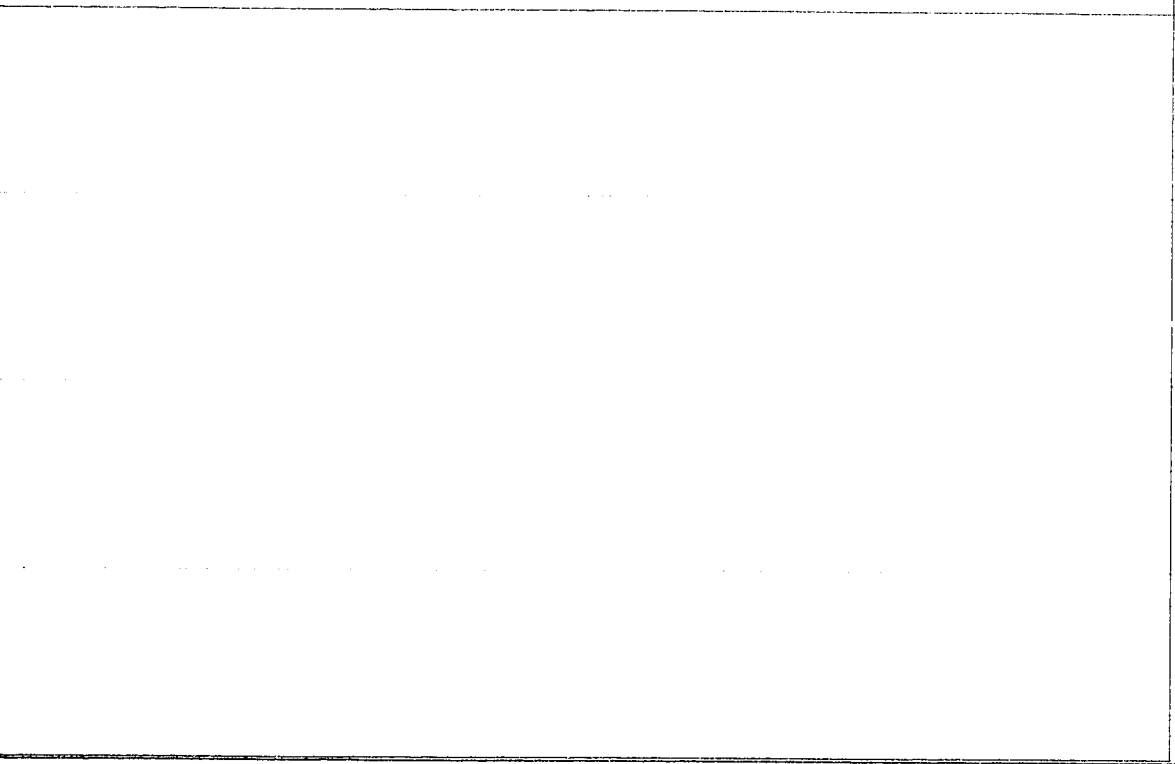
74 mm)

VERTICAL ENLARGEMENT

Feet

et

2. THESIS PLATE 3 - Cross



SIS PLATE 3 - Cross Section

NOTE TO USERS

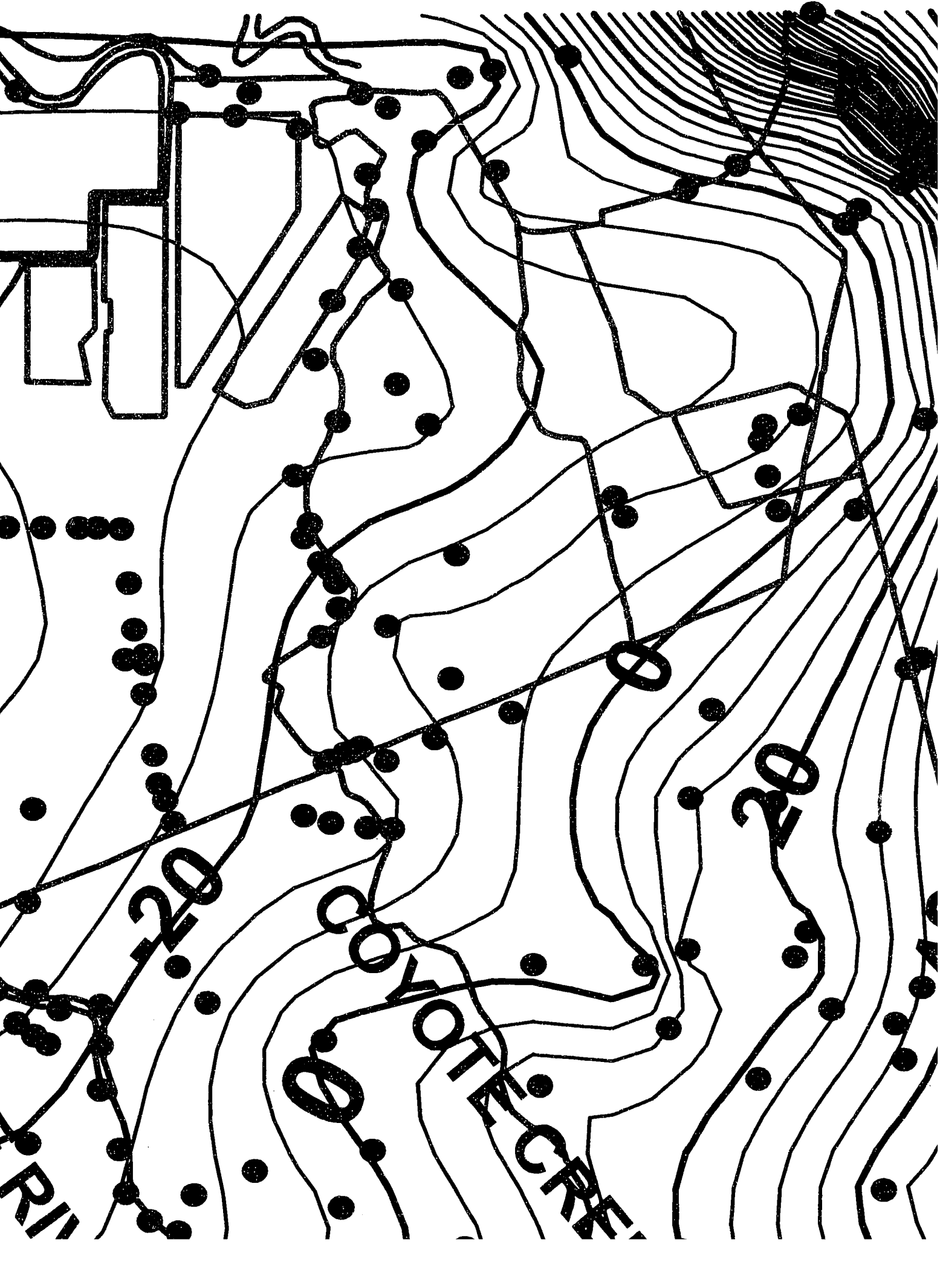
Oversize maps and charts are microfilmed in sections in the following manner:

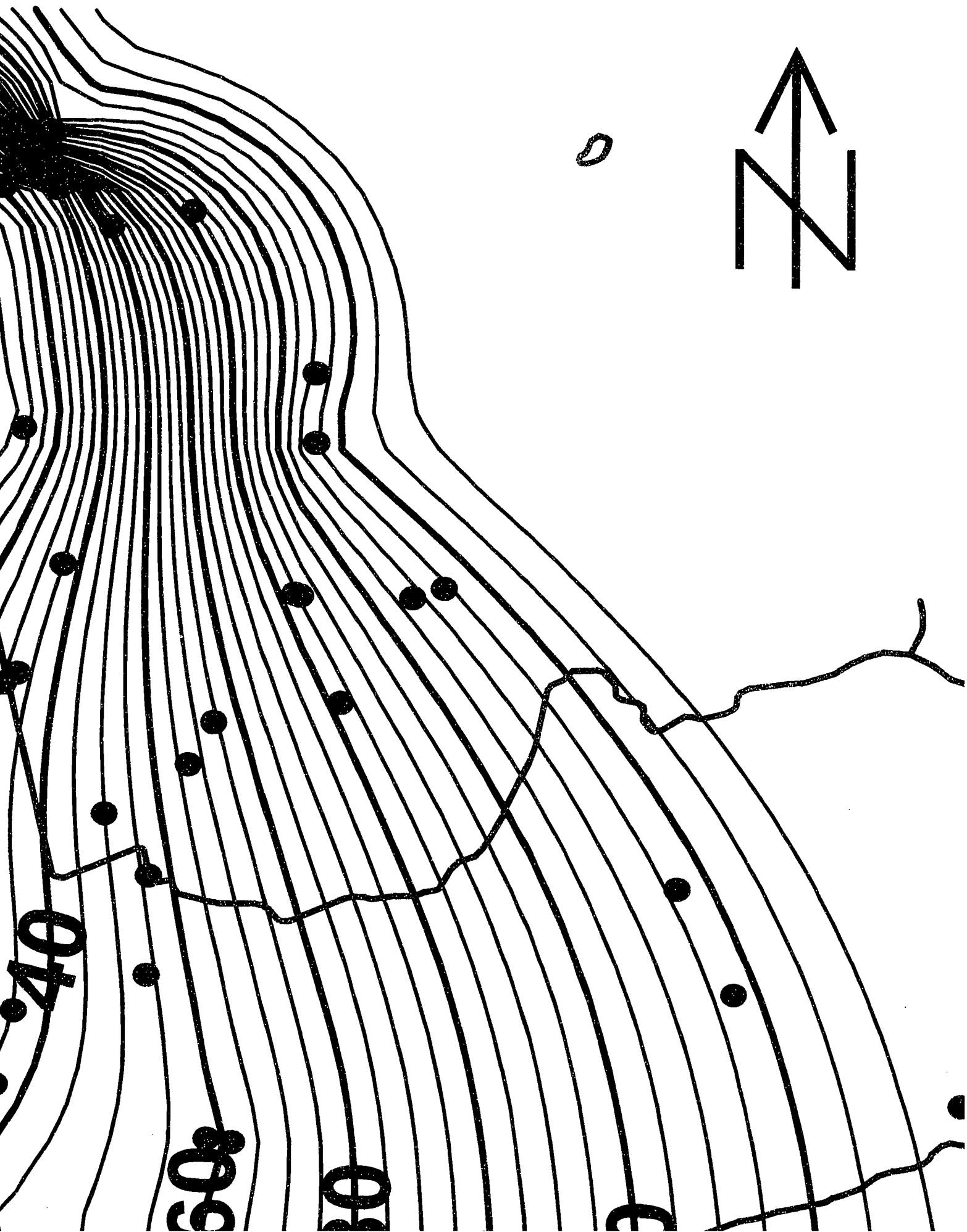
LEFT TO RIGHT, TOP TO BOTTOM, WITH SMALL OVERLAPS

This reproduction is the best copy available.

UMI[®]

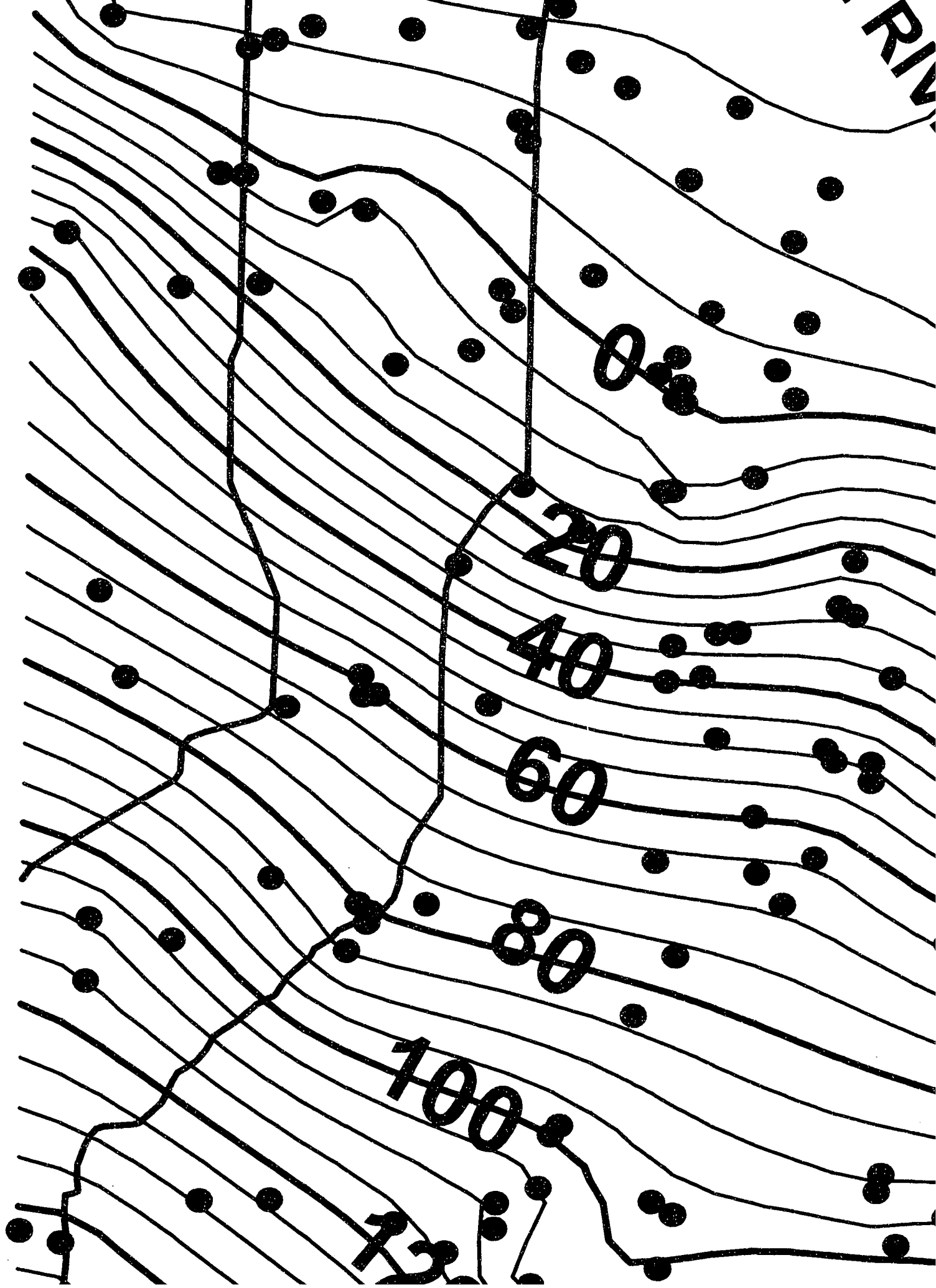








RIM

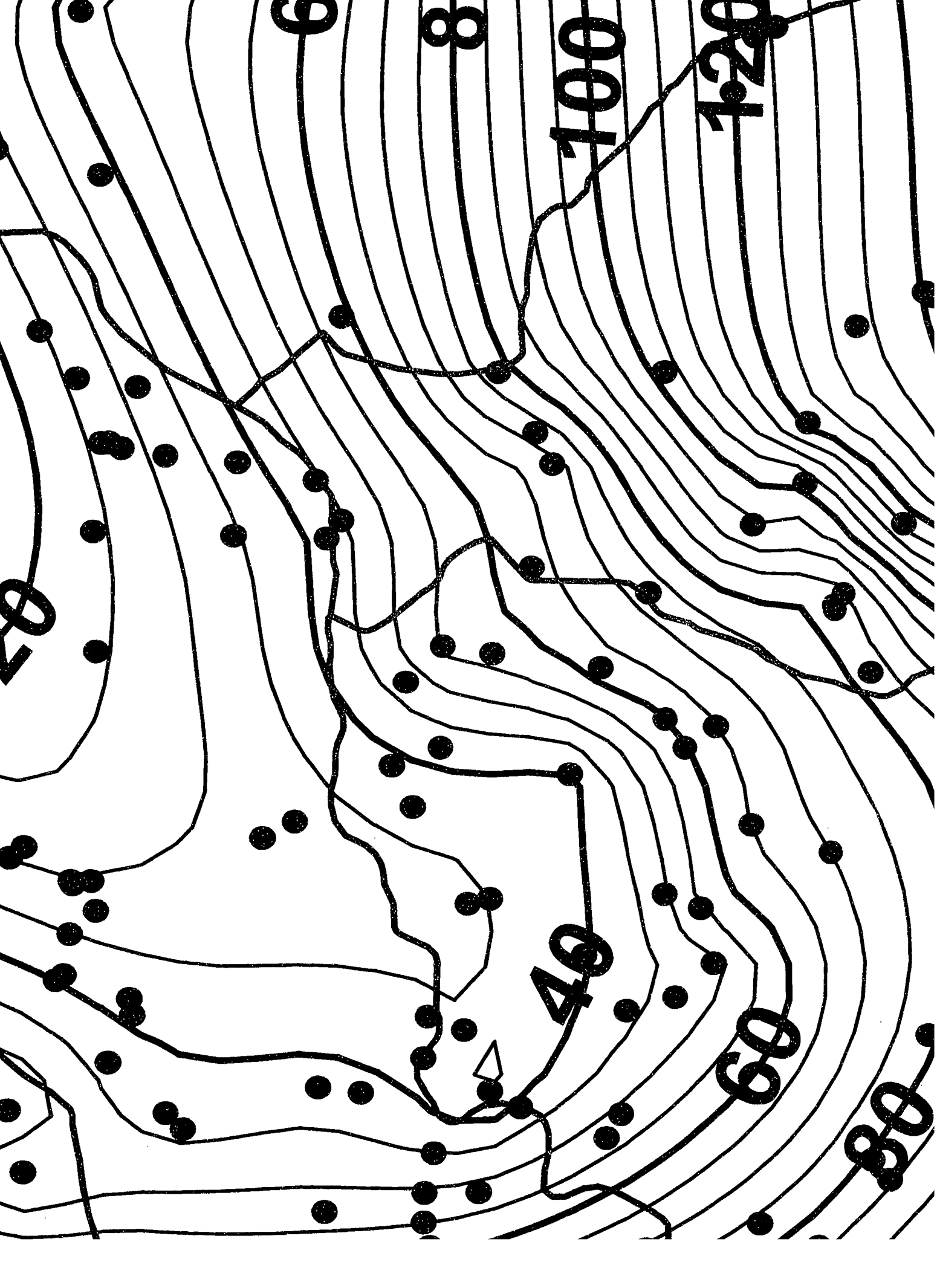


RIVER

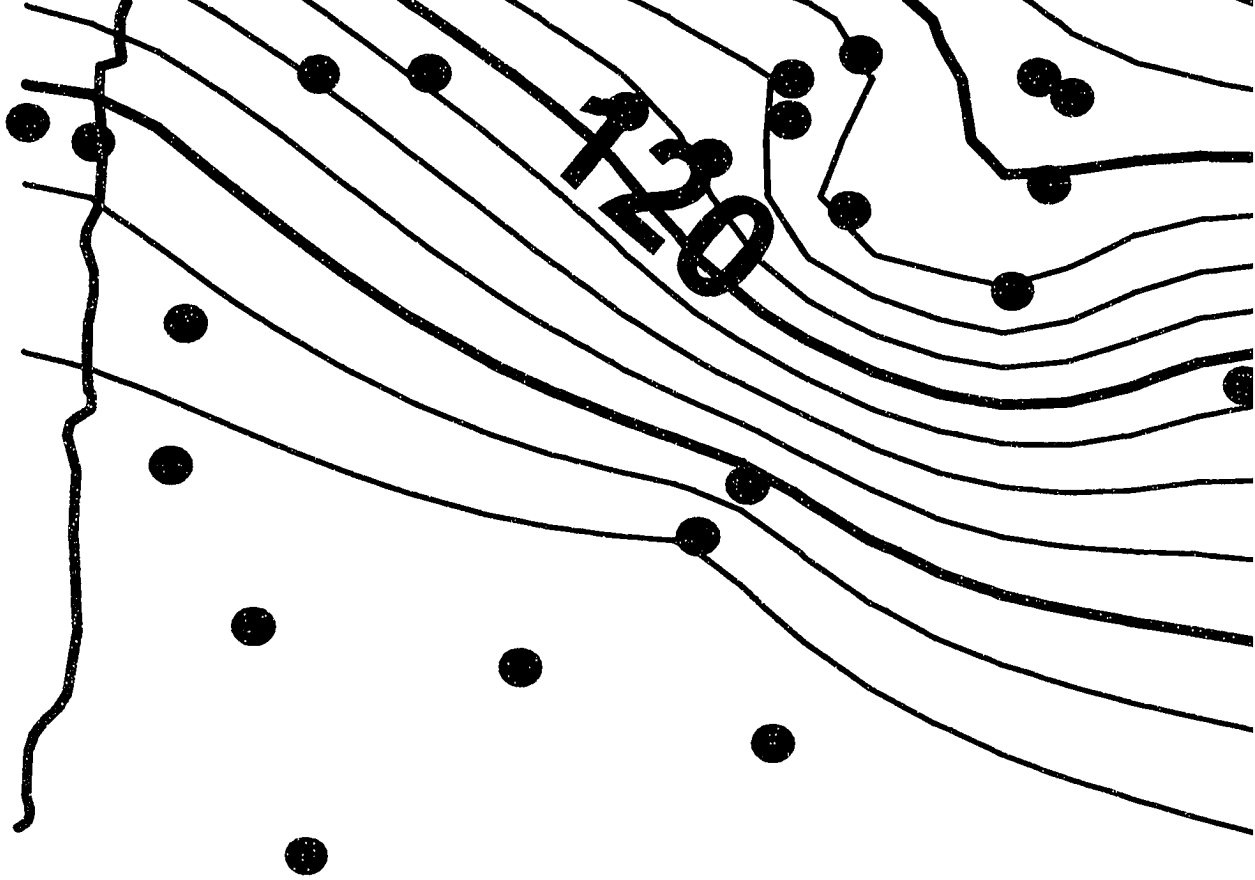
CR

20

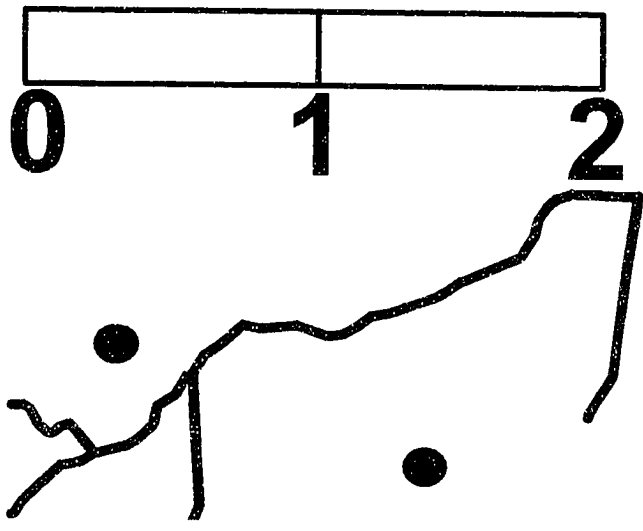




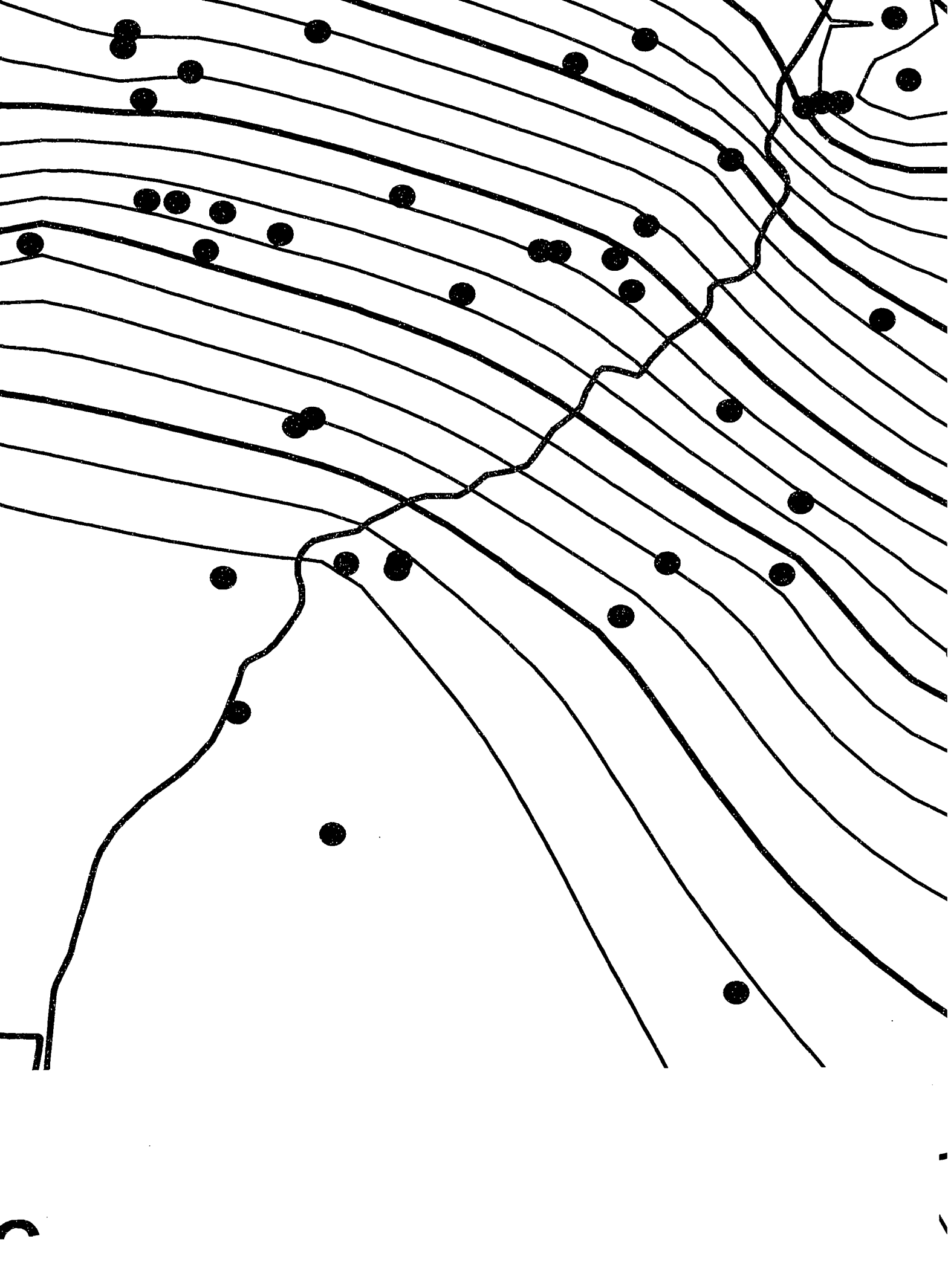


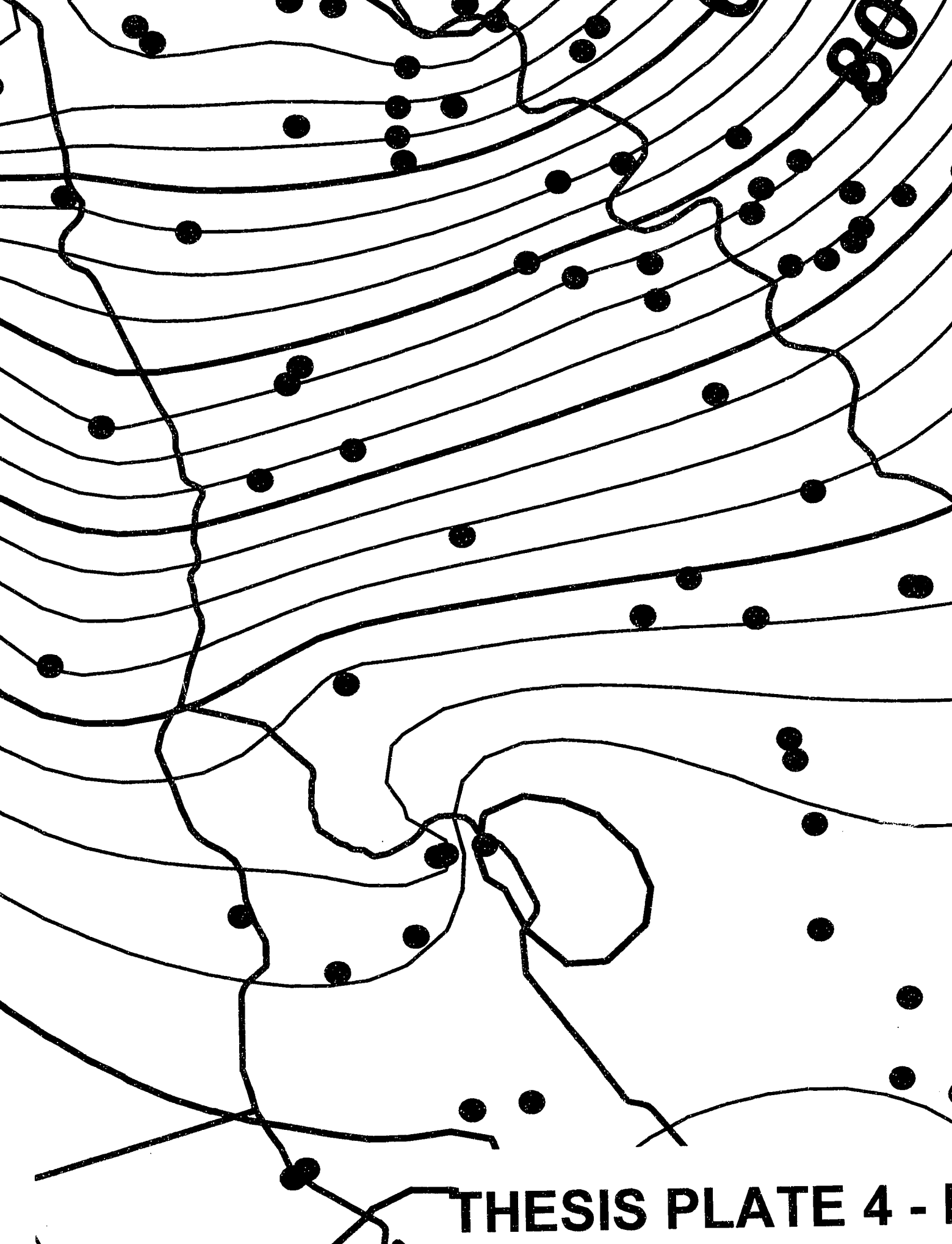


SCALE IN KILOMETERS



GEOTECHNICAL BORING

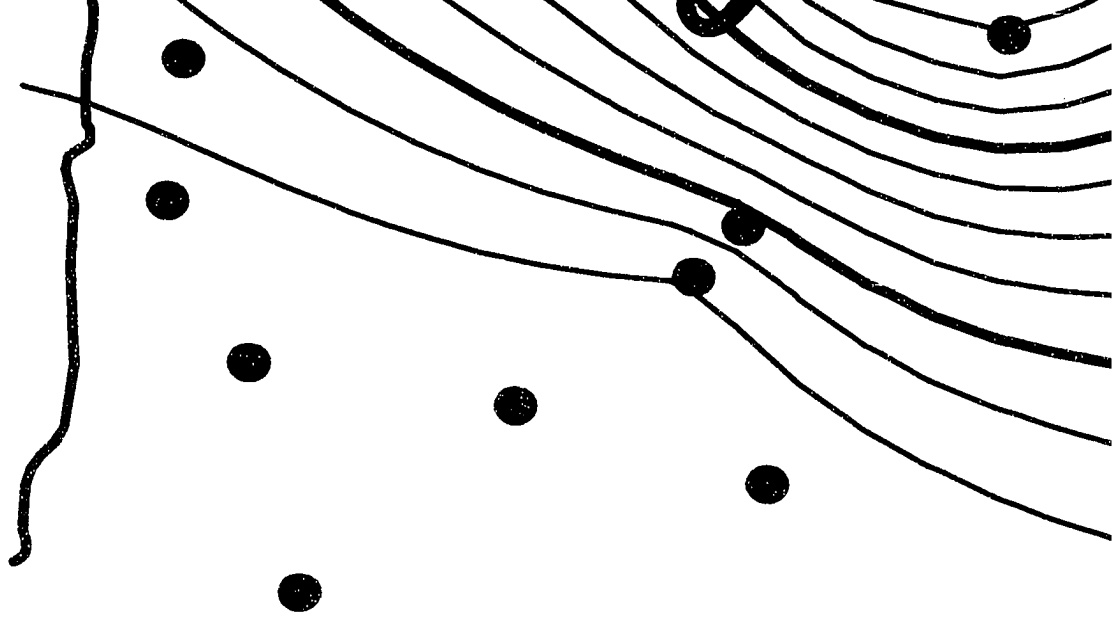




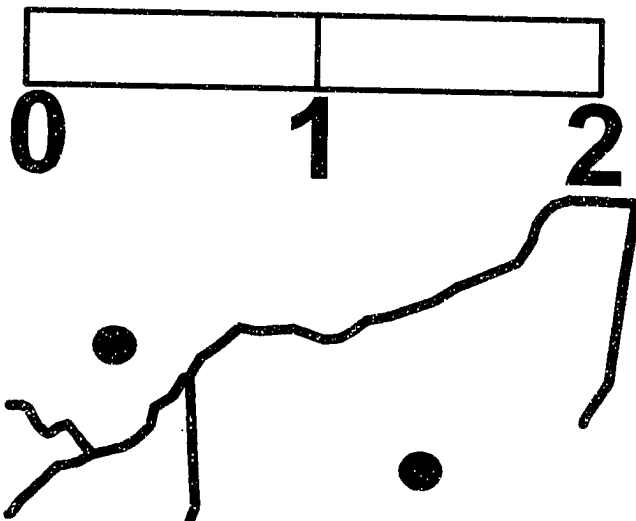
THESIS PLATE 4 - I



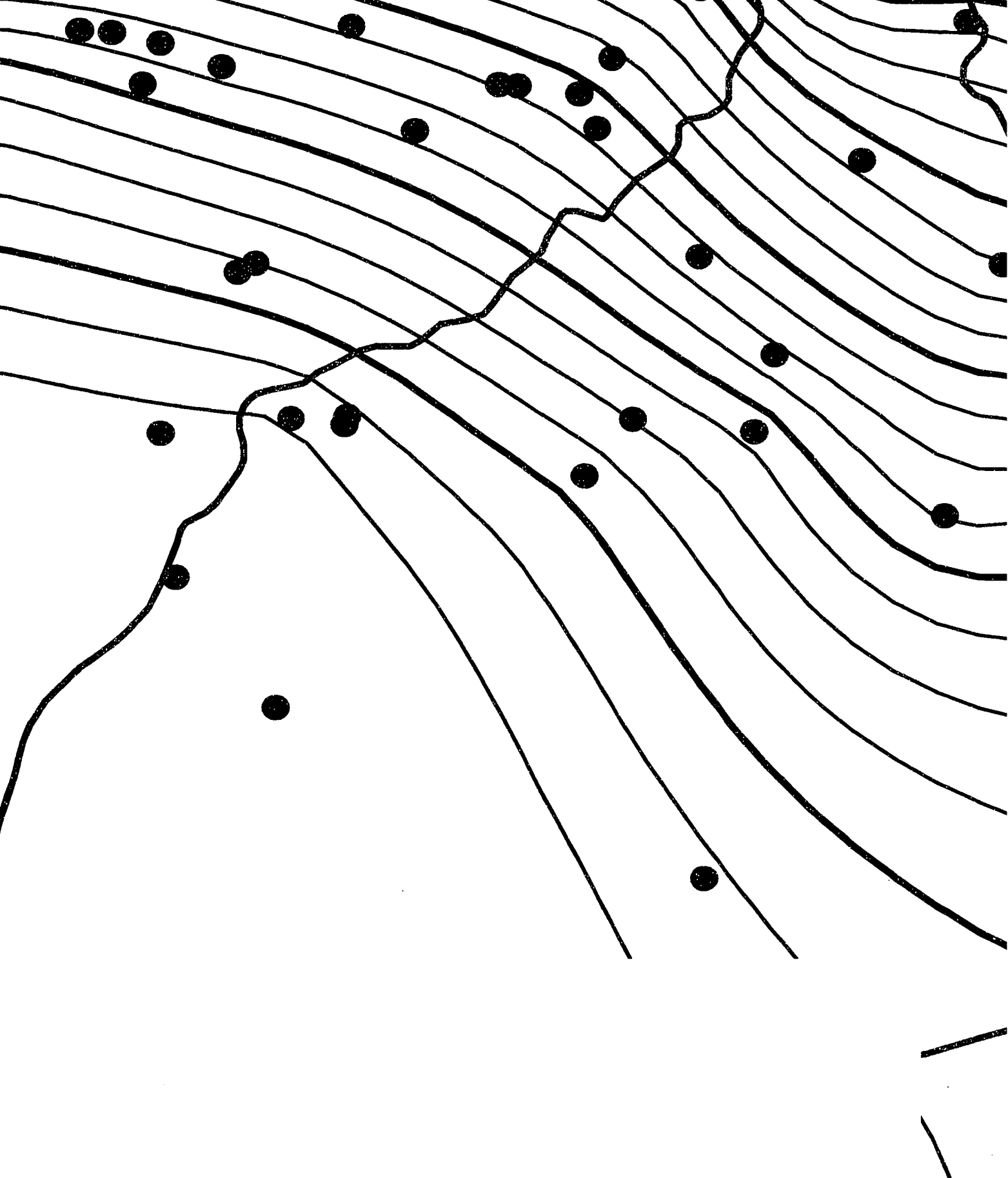
Pleistocene surface elevation map
(interpreted) in feet (modified after



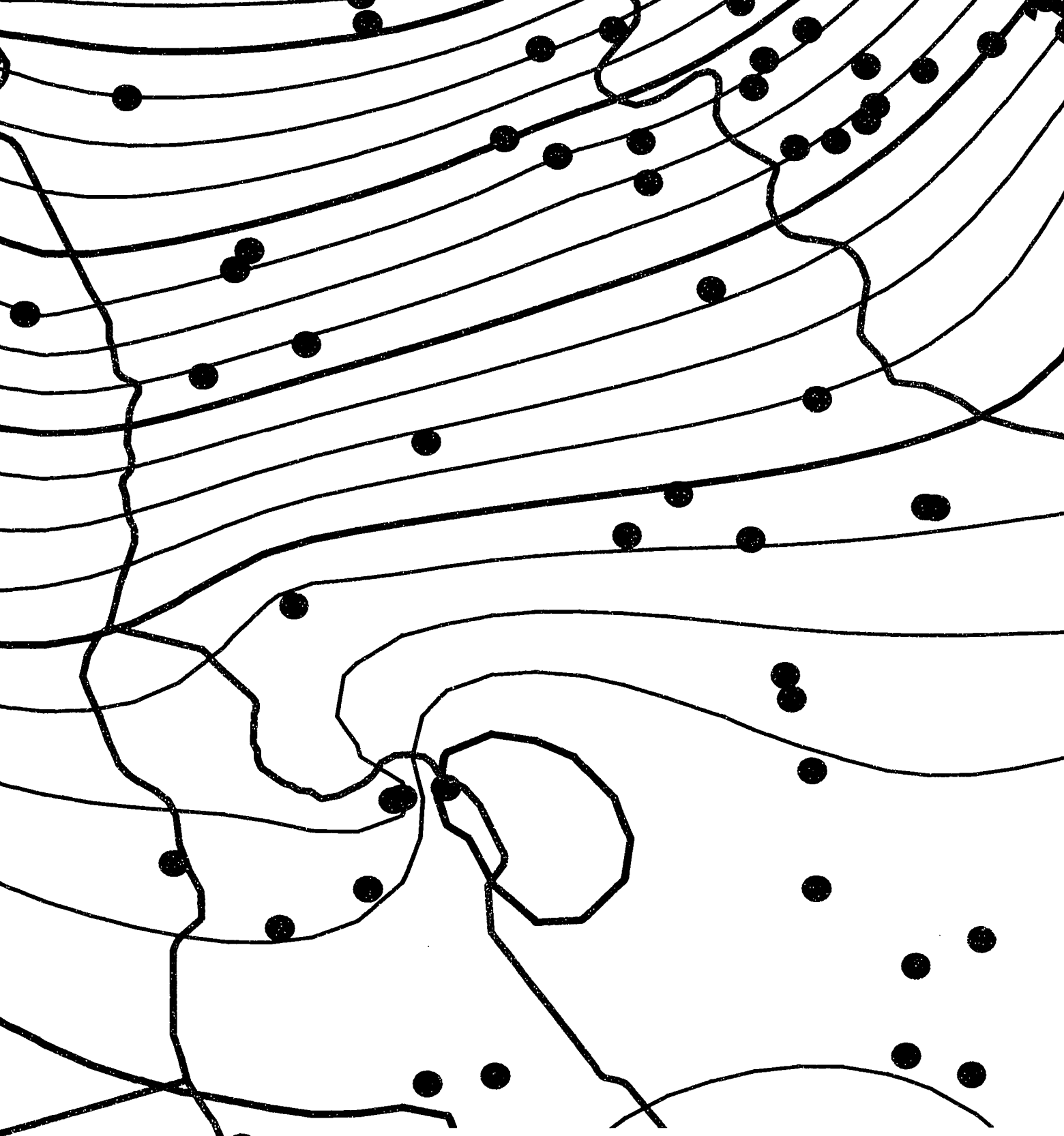
●
SCALE IN KILOMETERS



● **GEOTECHNICAL BORING**
— **PLEISTOCENE SURFACE**



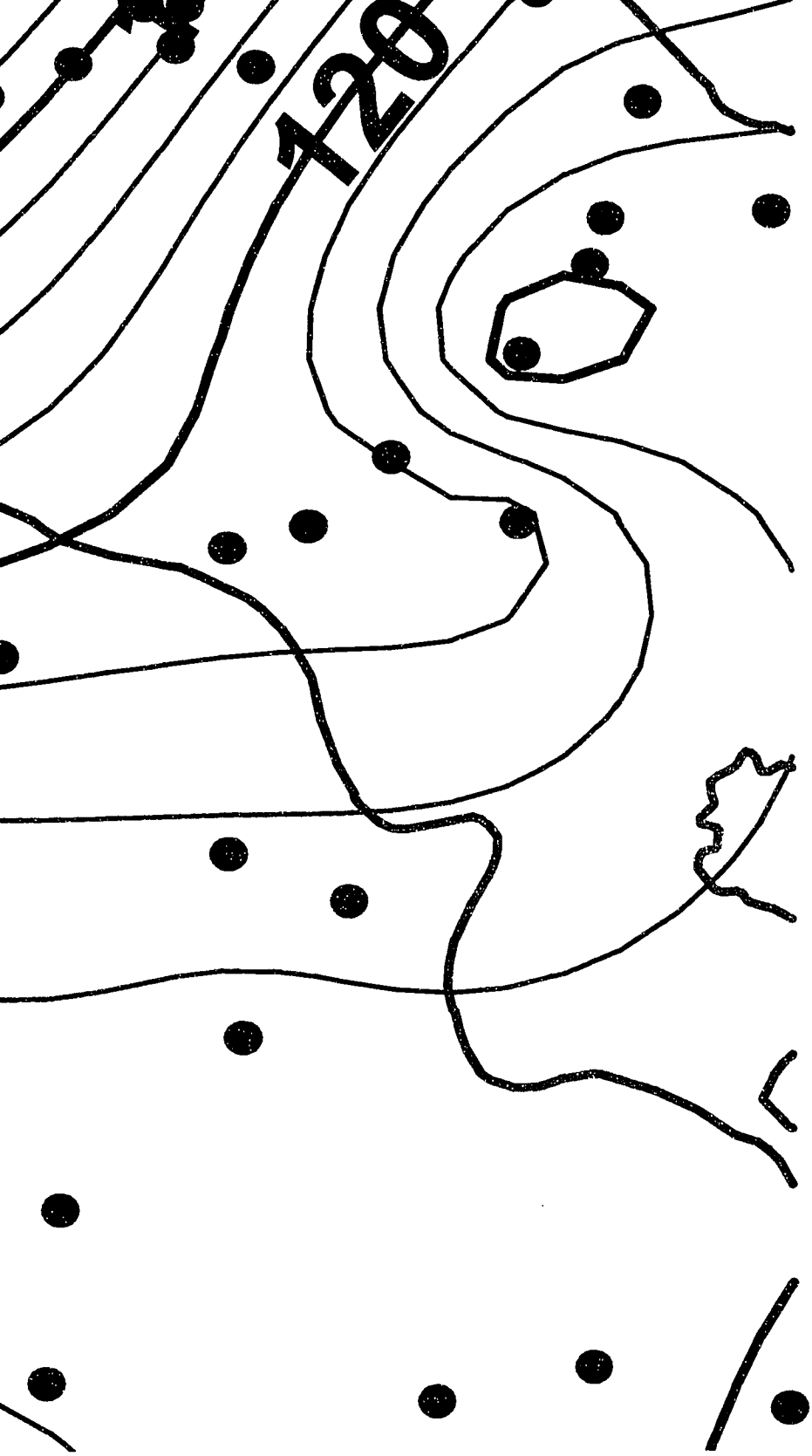
ELEVATION CONTOURS



MS

THESIS PLATE 4 - Pleis

(in
C



**Pleistocene surface elevation map
(interpreted) in feet (modified after
Clahan et al., 2002)**

NOTE TO USERS

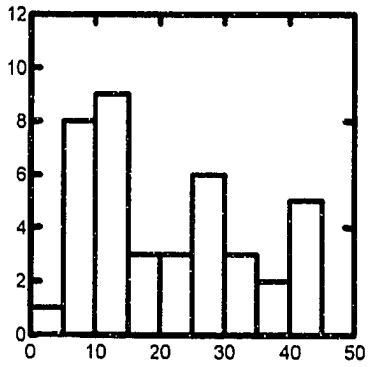
Oversize maps and charts are microfilmed in sections in the following manner:

LEFT TO RIGHT, TOP TO BOTTOM, WITH SMALL OVERLAPS

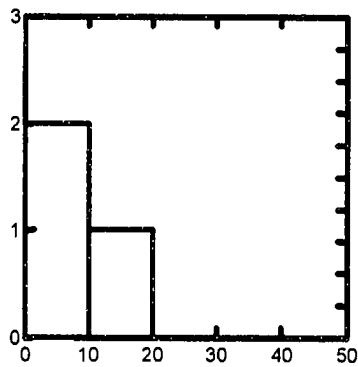
This reproduction is the best copy available.

UMI[®]

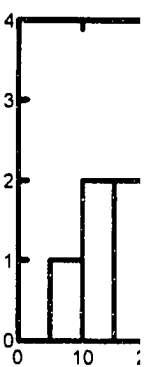
af



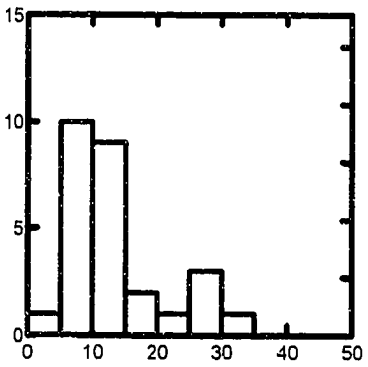
alf



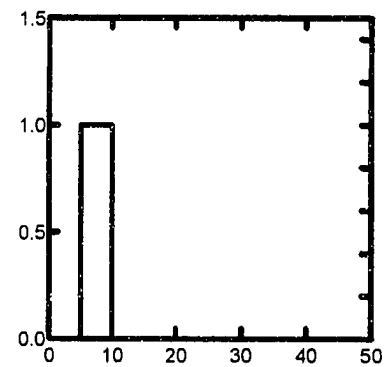
Q



Qhty



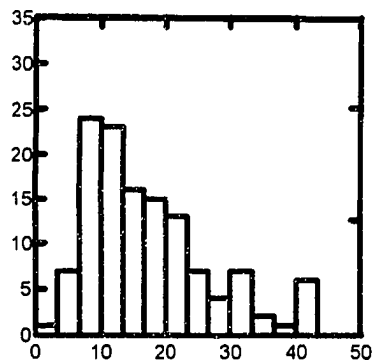
Qhb



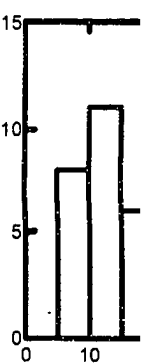
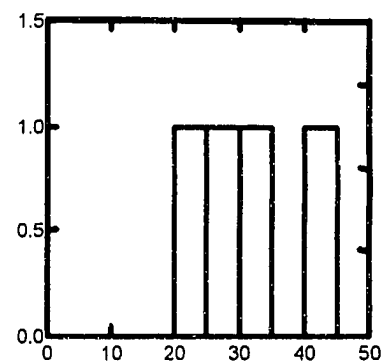
Q



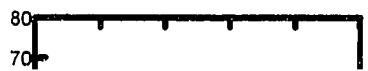
Qhl



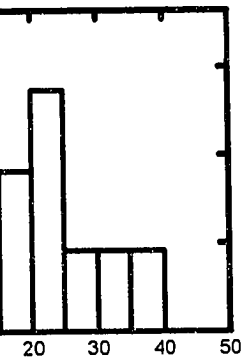
Qht



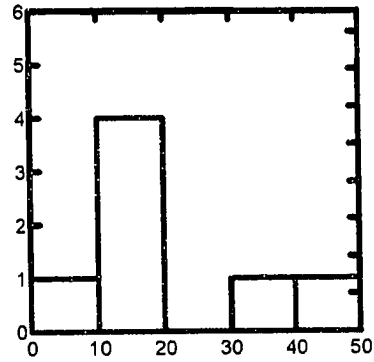
Qpf



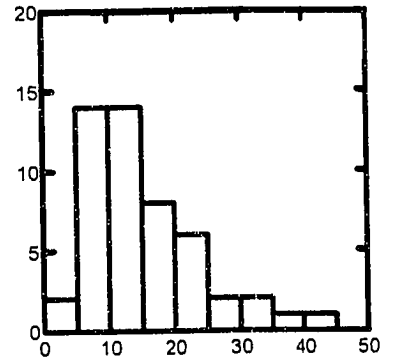
Qhc



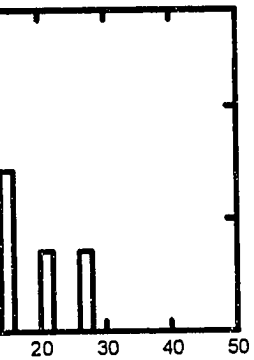
Qhfy



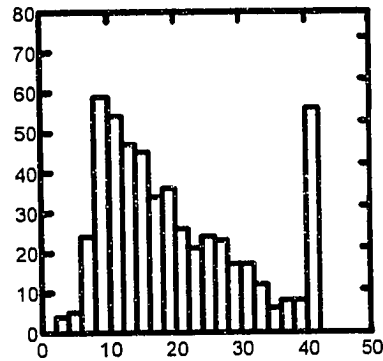
Qhly



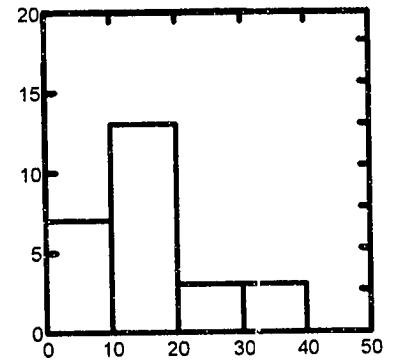
Qhfe



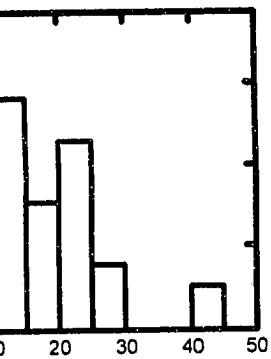
Qhf



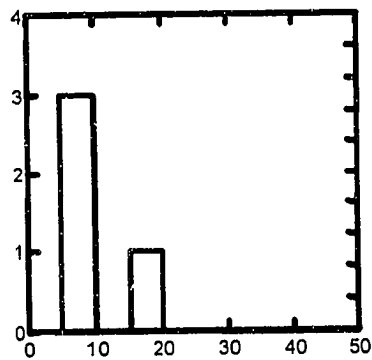
Qhff



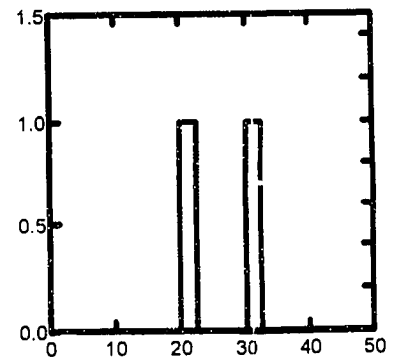
Qf



Ql



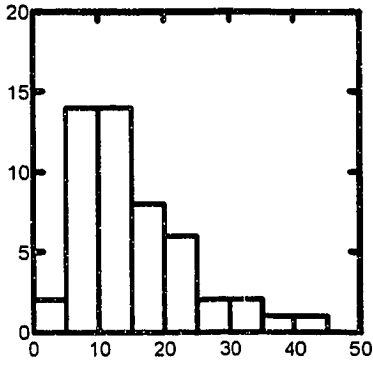
Qt



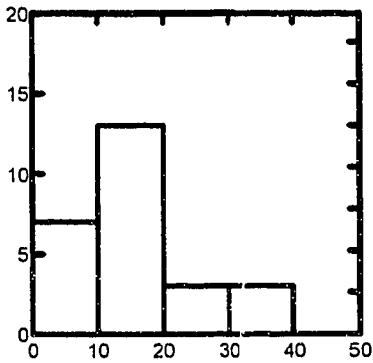
Legend

T
F

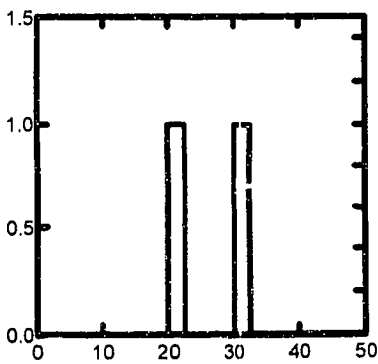
Qmly



Qhff

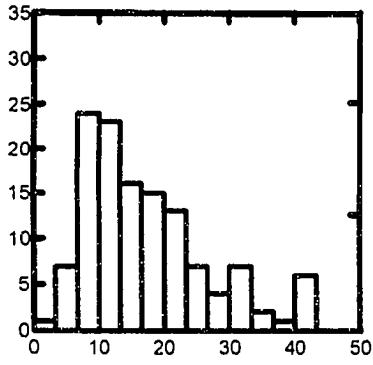


Qt

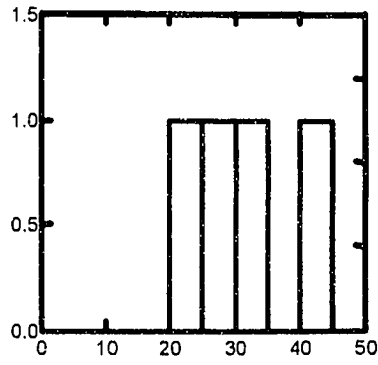


THESIS PLATE 5 -
Histograms showing

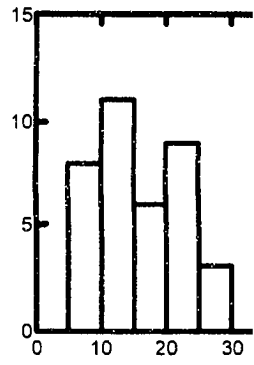
Qhl



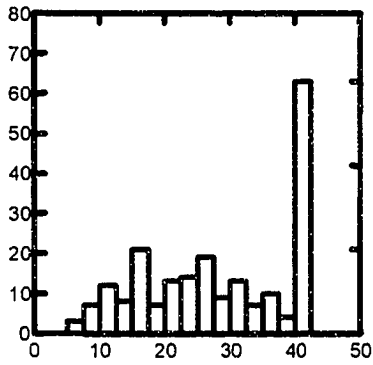
Qht



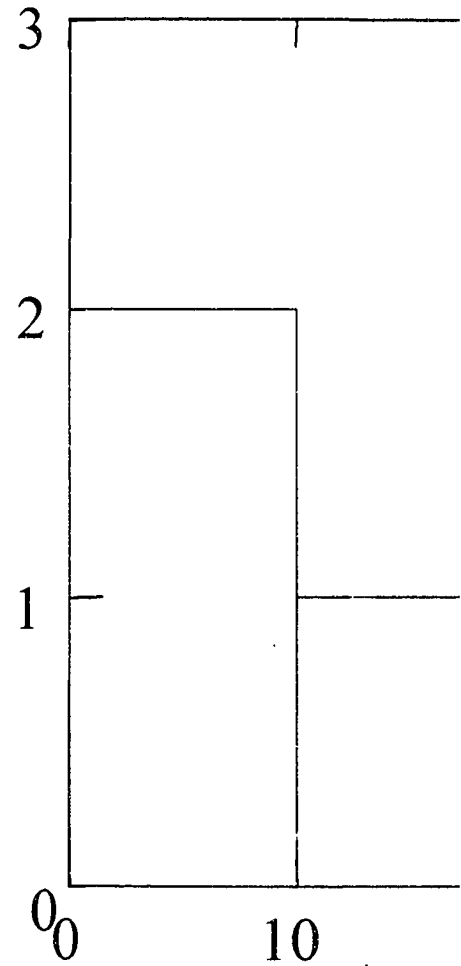
Qf



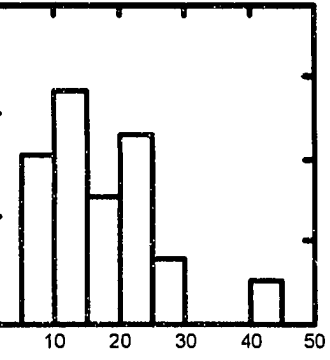
Qpf



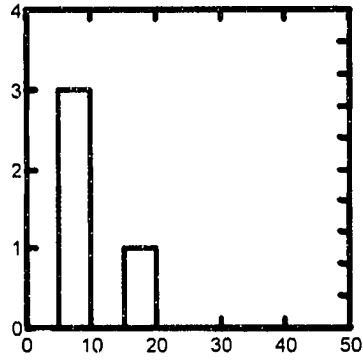
Count



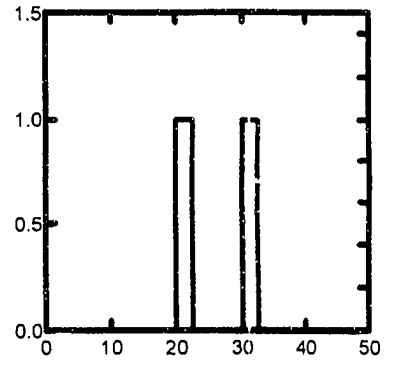
Qf



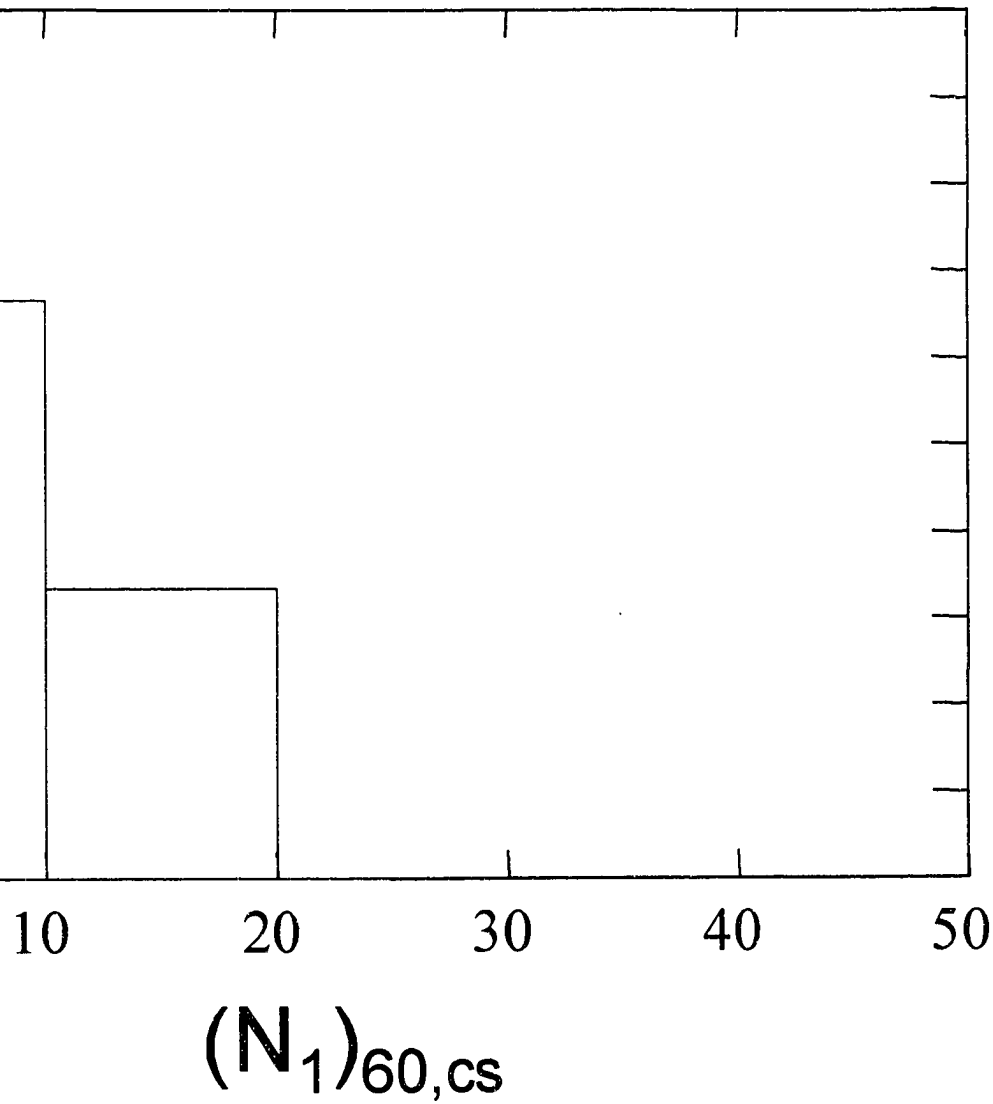
Ql



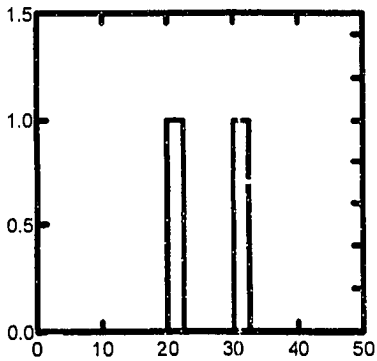
Qt



Legend



Qt



THESIS PLATE 5 -

Histograms showing
fines corrected
penetration
resistance for every
layer in the project
database of
geotechnical boring
logs. (Knudsen et al.
2004)

NOTE TO USERS

Oversize maps and charts are microfilmed in sections in the following manner:

LEFT TO RIGHT, TOP TO BOTTOM, WITH SMALL OVERLAPS

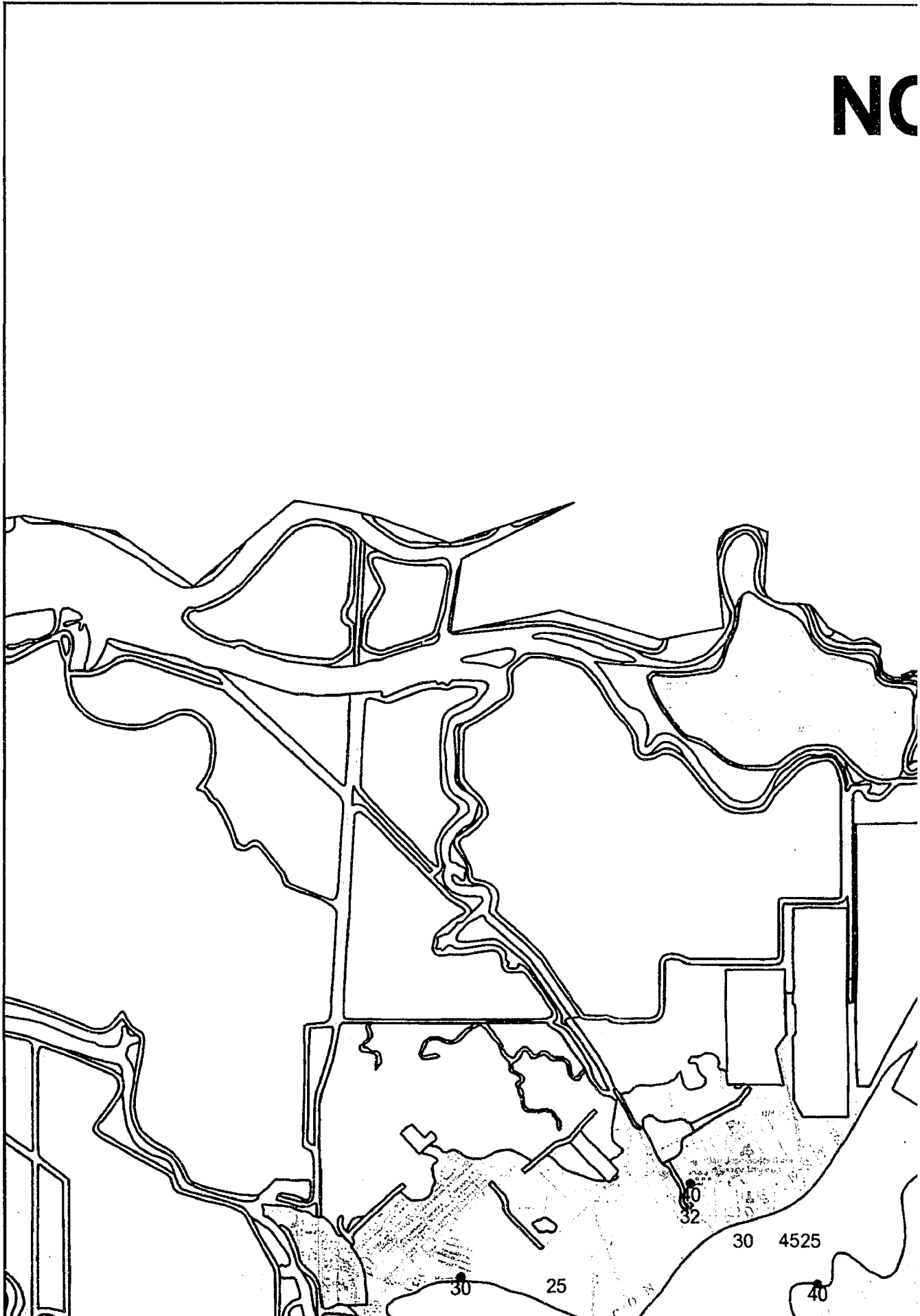
This reproduction is the best copy available.

UMI[®]

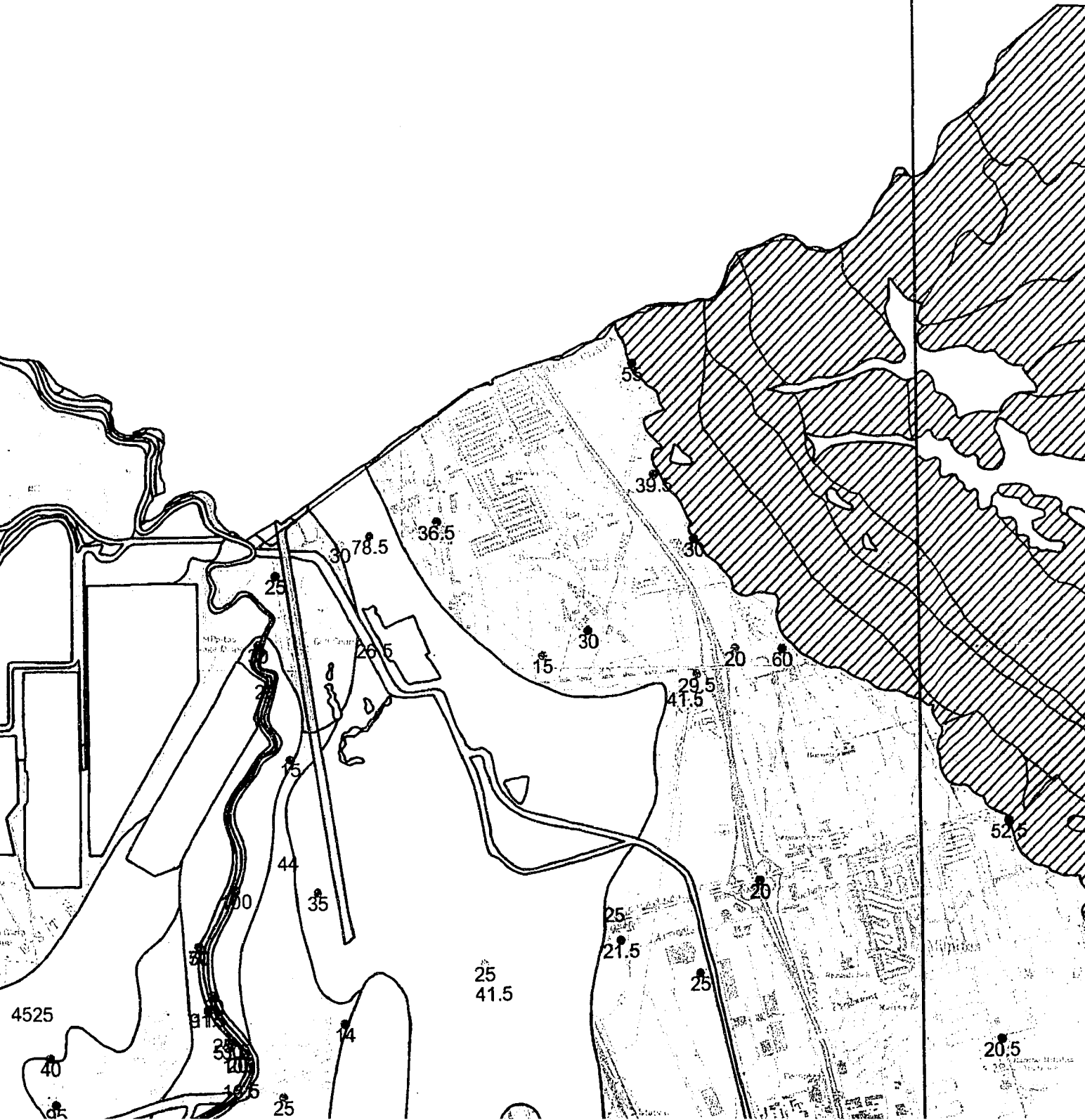
122° 00'

37° 30'

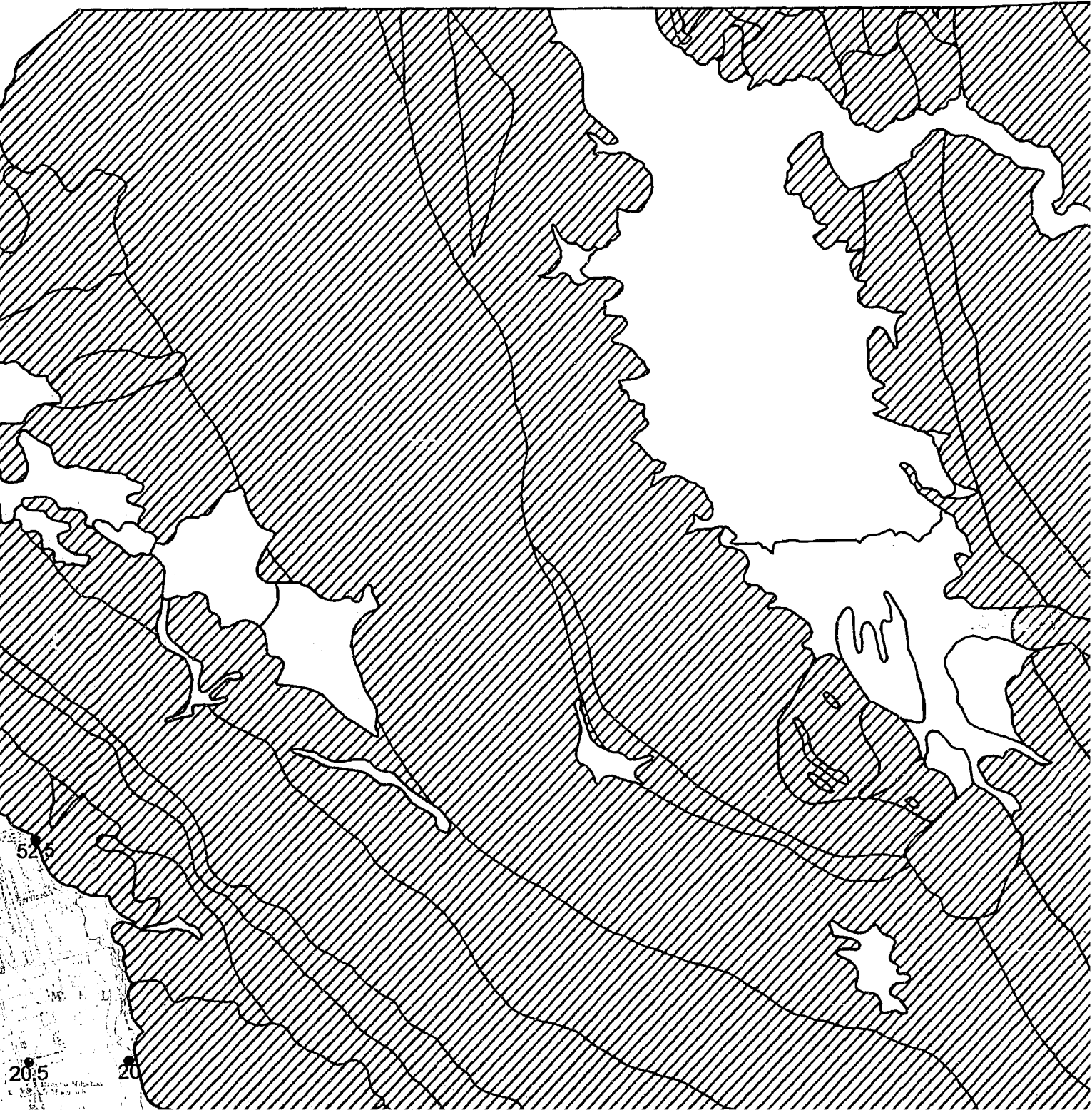
NC



NOT EVALUATED - OUTSIDE

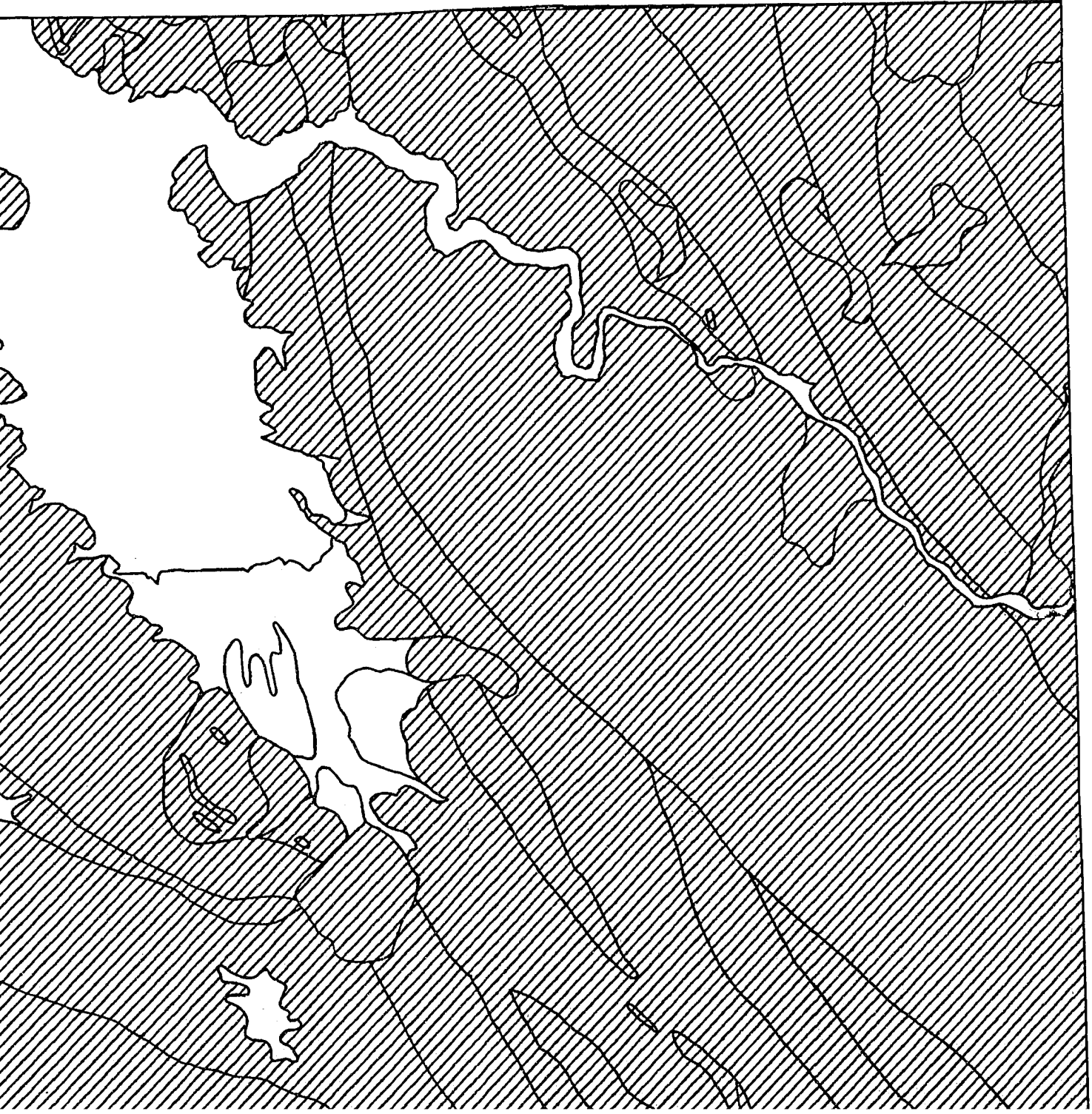


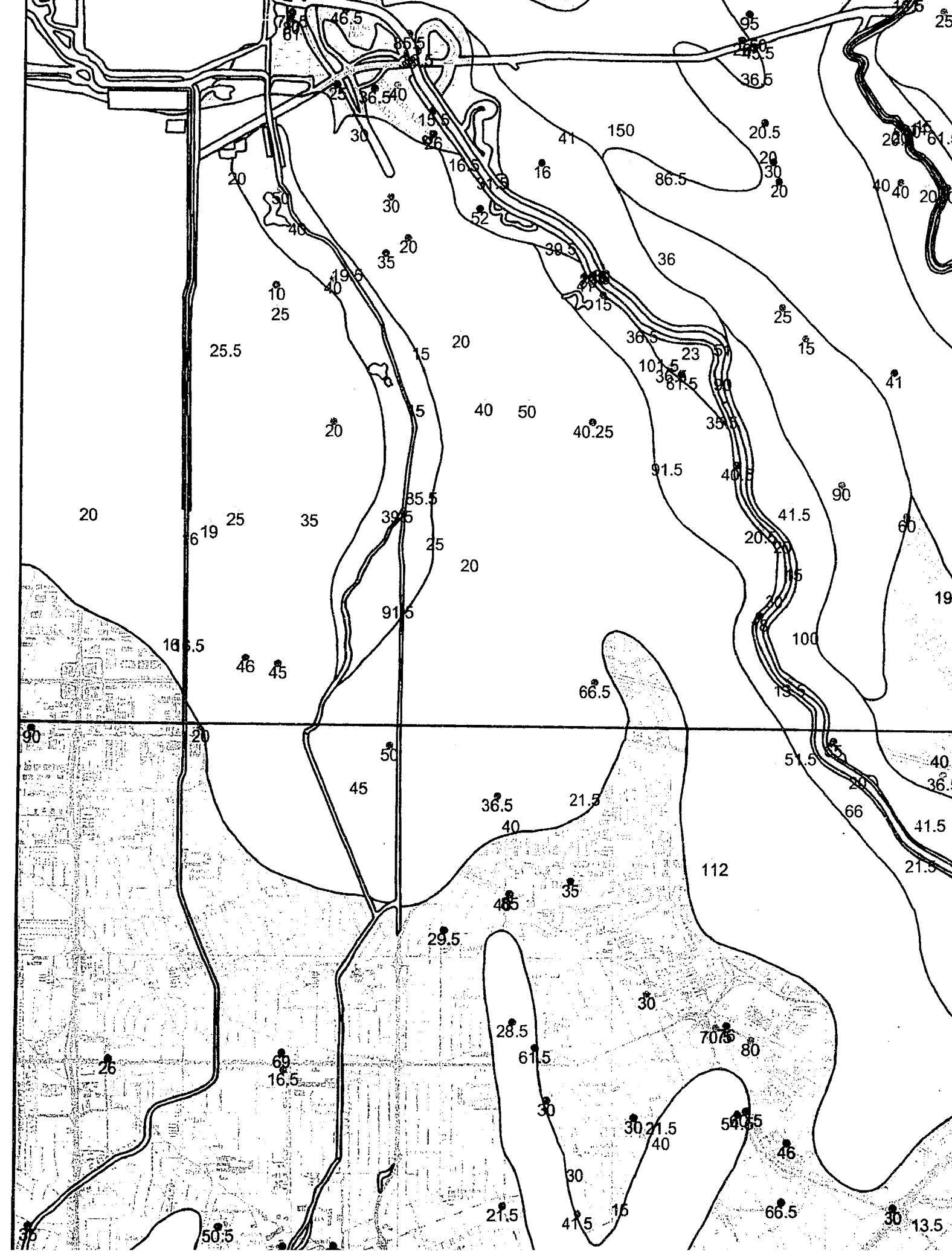
SIDE STUDY AREA

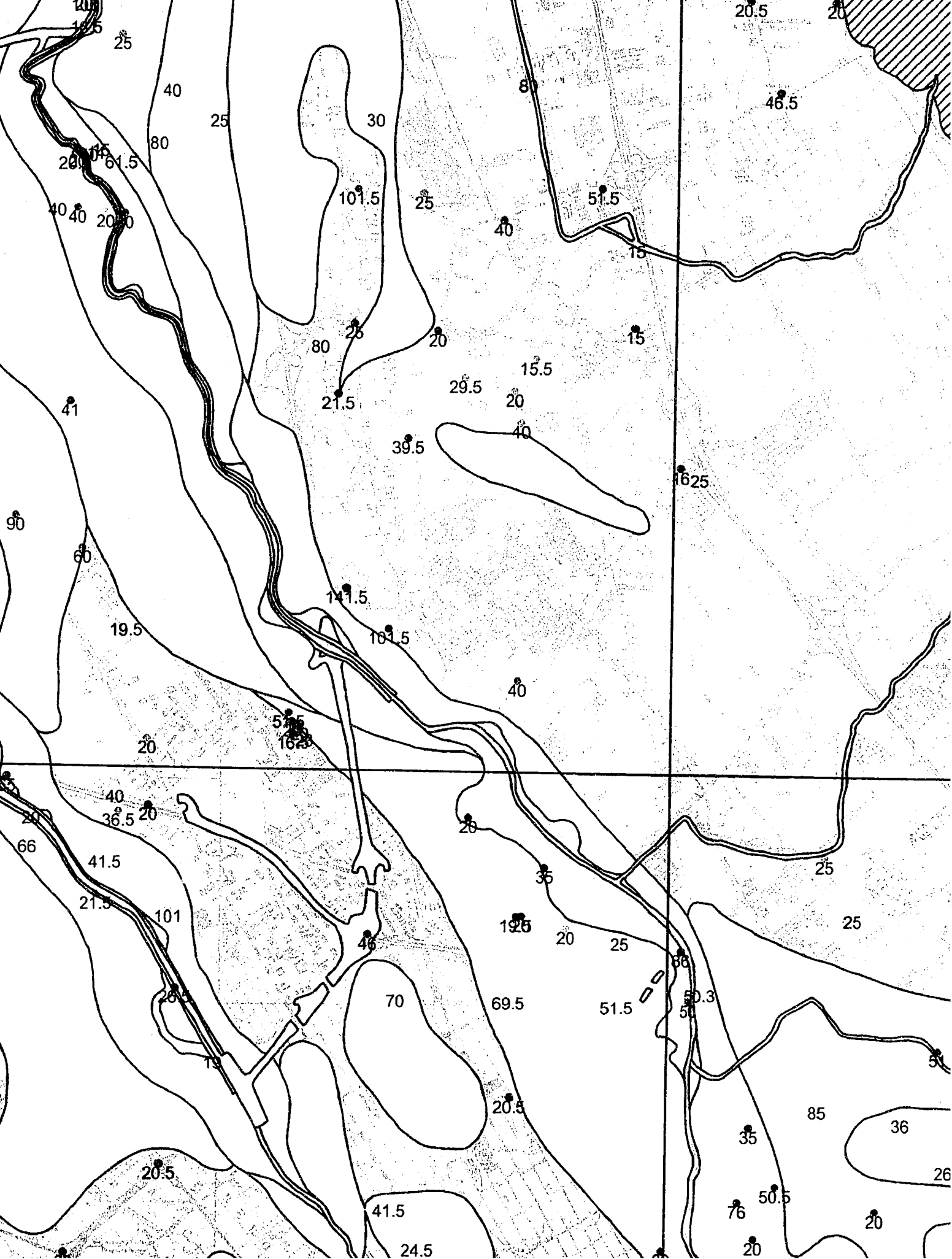


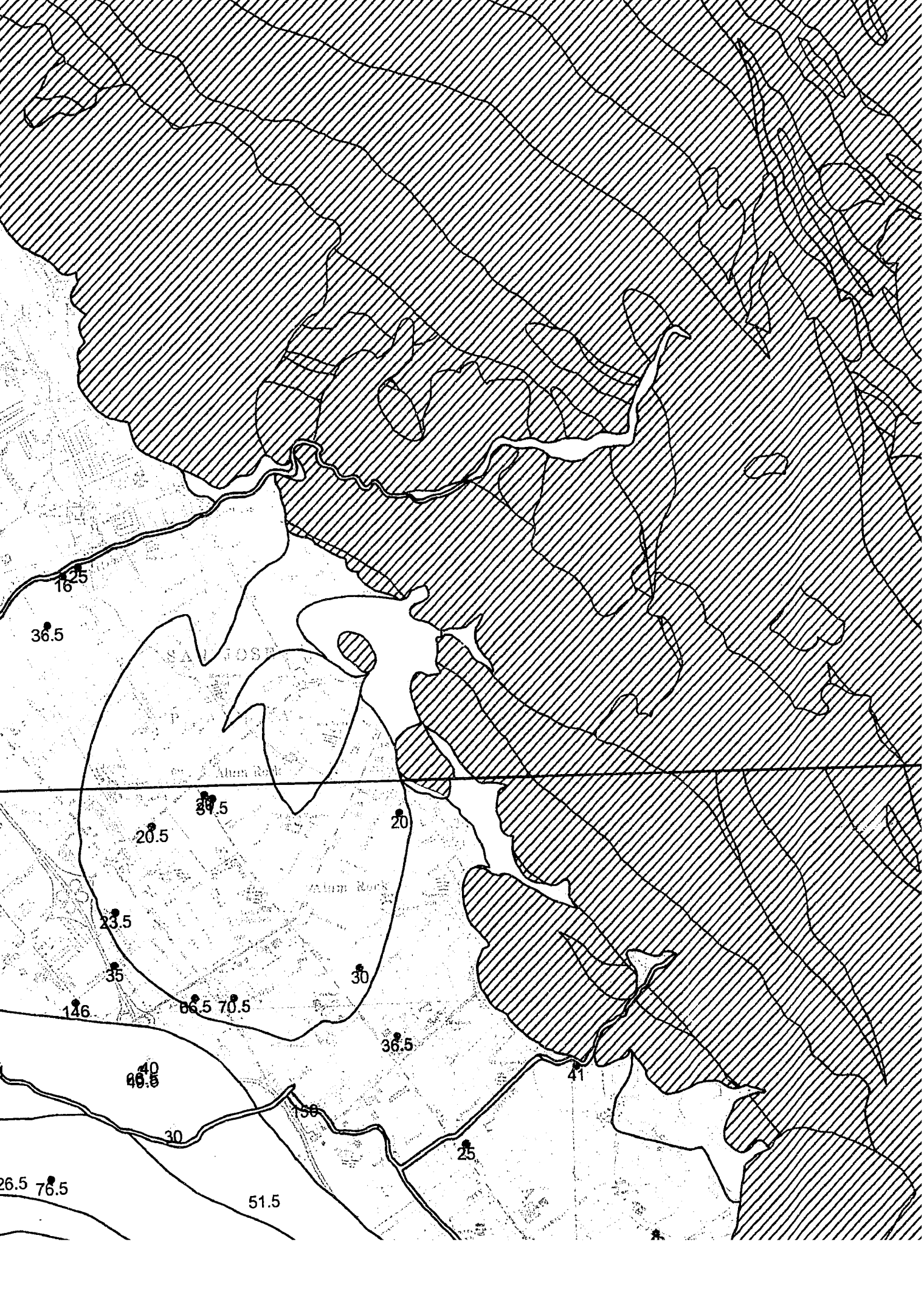
121° 45'
37° 3'

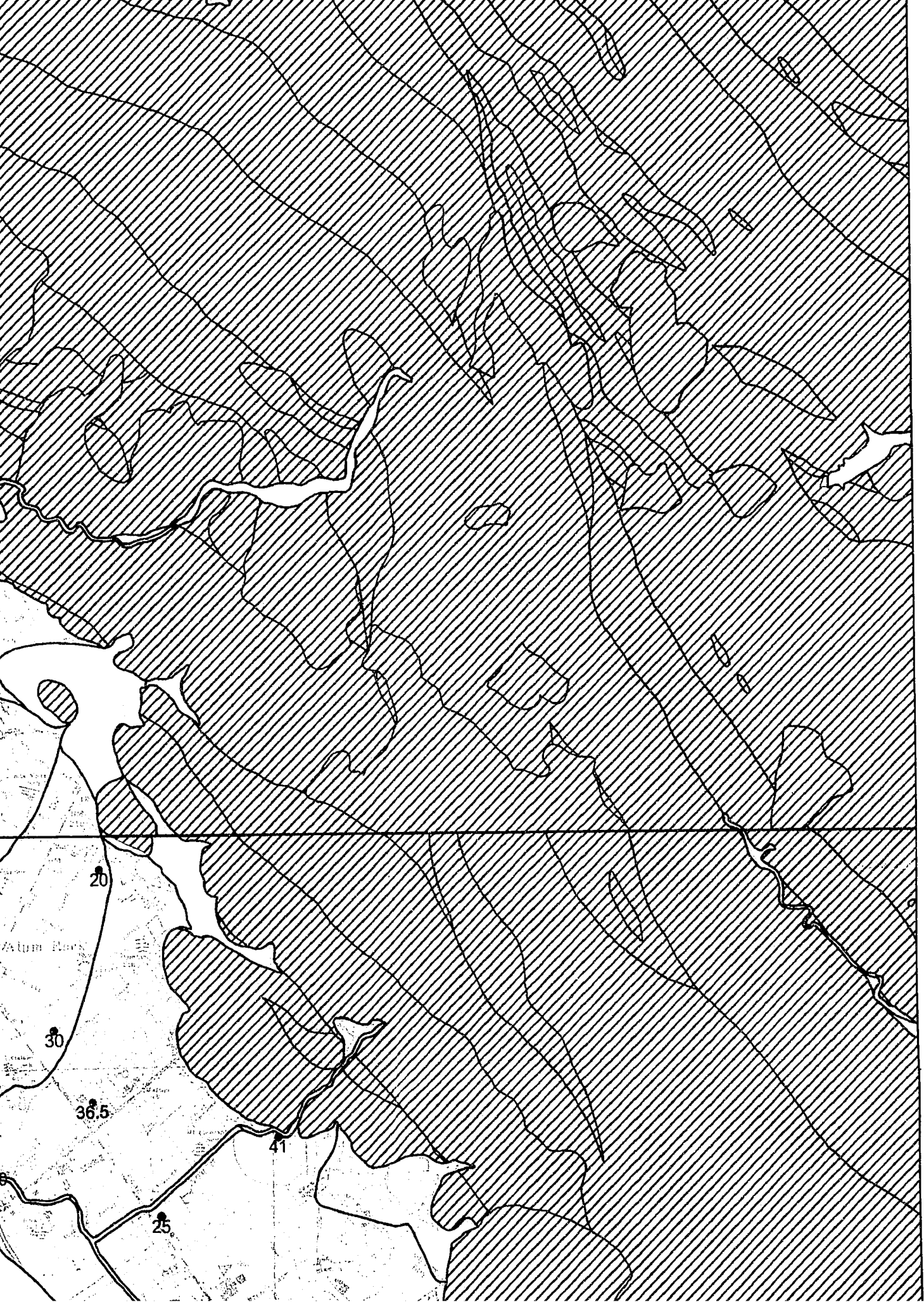
REA

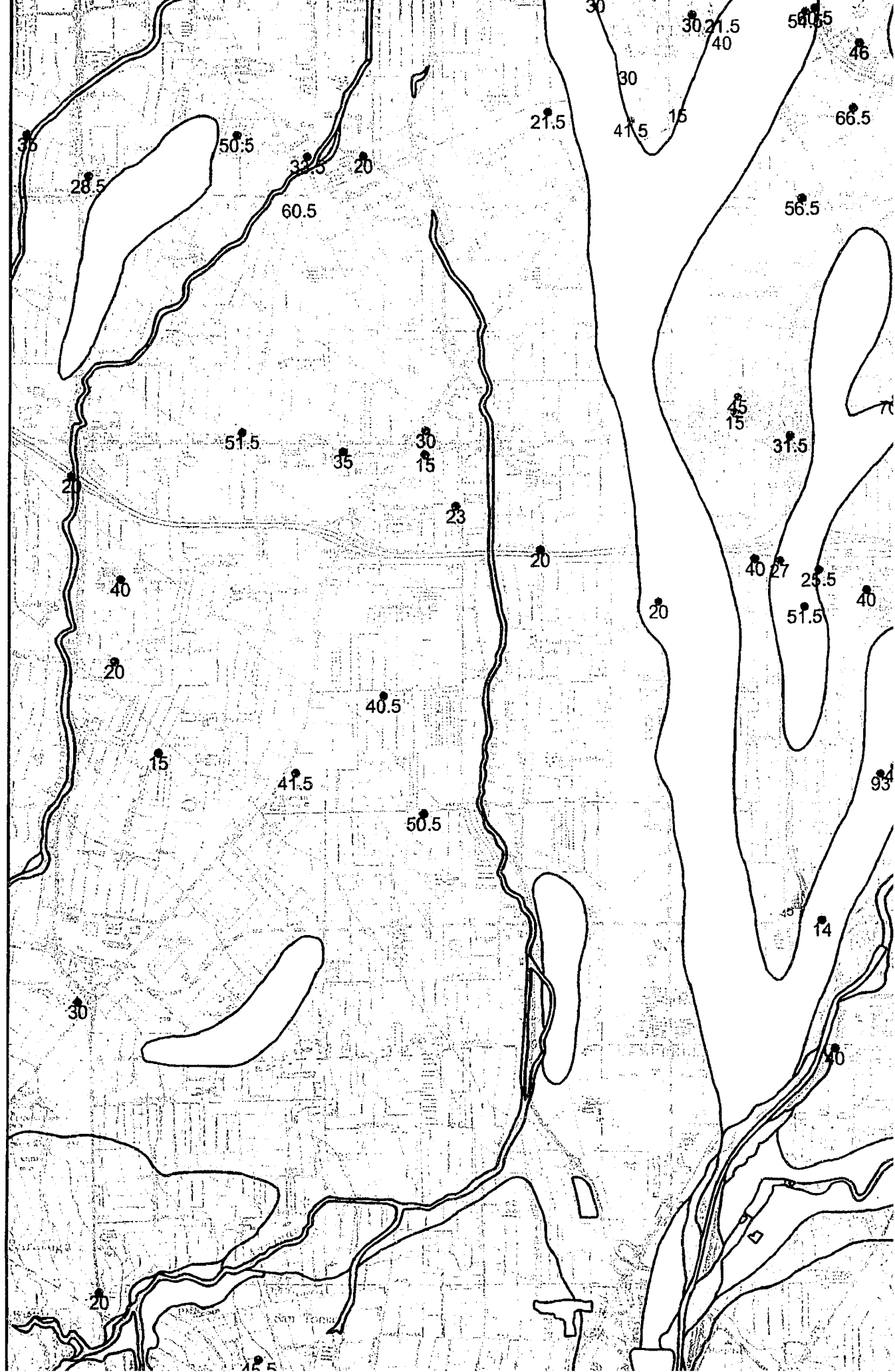


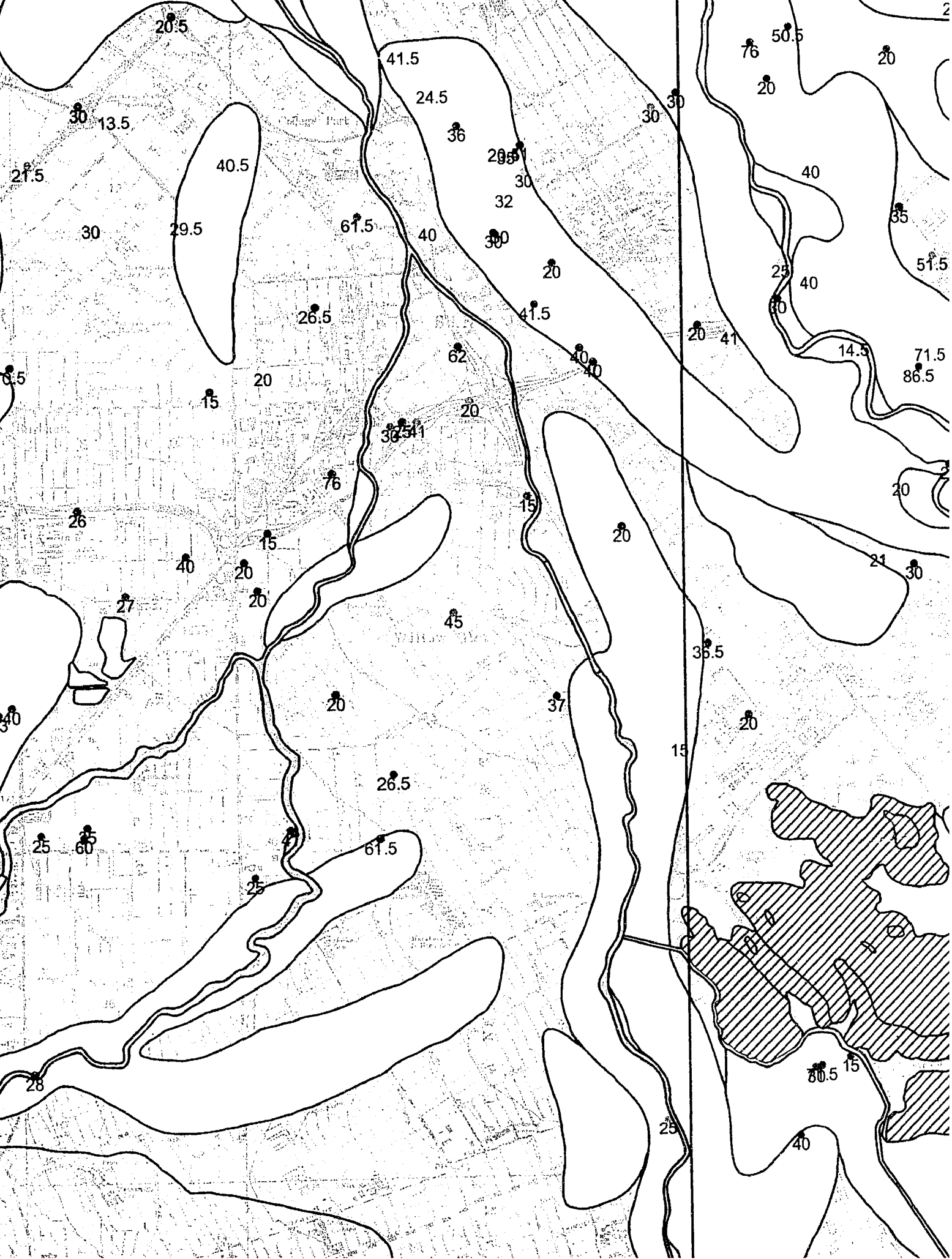


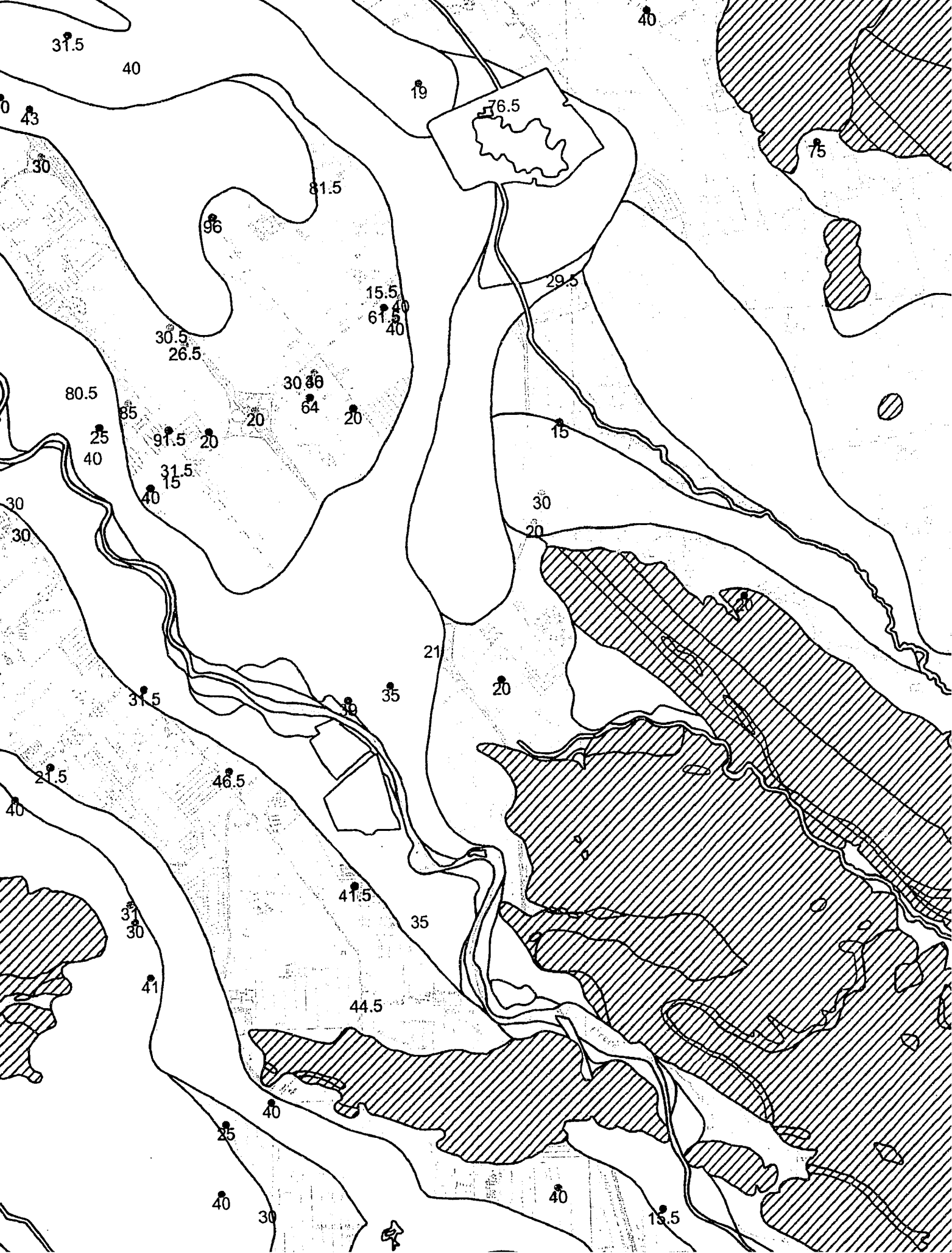




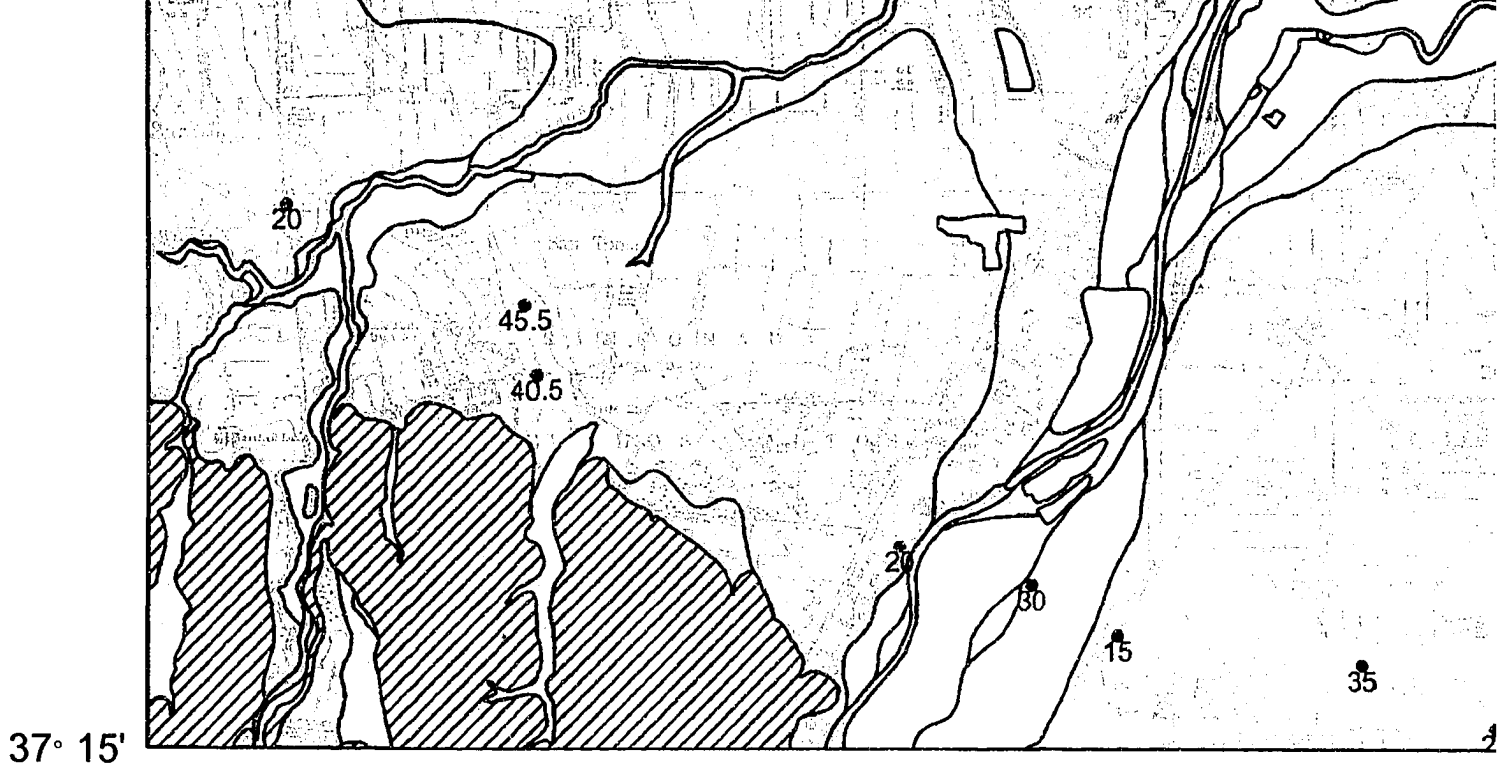












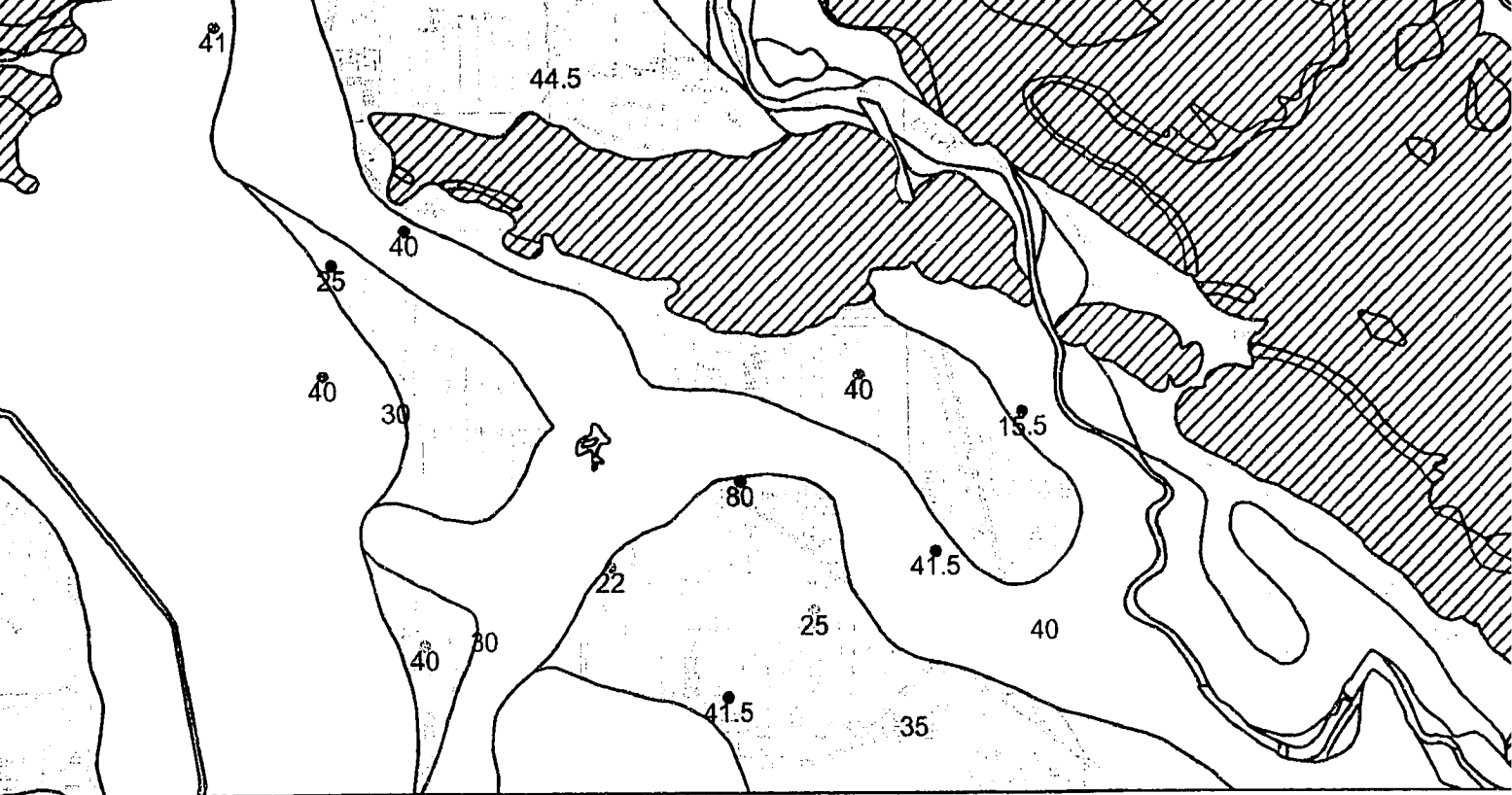
Milpitas base map prepared by the U. S. Geological Survey, 1961, photorevised 1980.
 Calaveras Reservoir base map prepared by the U. S. Geological Survey, 1961, photorevised 1980.
 San Jose East base map prepared by the U. S. Geological Survey, 1961, photorevised 1980.
 San Jose West base map prepared by the U. S. Geological Survey, 1961, photorevised 1980.

REFERENCE:

Quaternary geologic maps of the Milpitas, Calaveras Reservoir, San Jose East and San Jose West Quadrangles modified after Witter et al., (2006)

Milpitas	Calaveras Reservoir
San Jose West	San Jose East

THESIS PLATE 6 - Volumetric Strain Summed for Each Boring and C



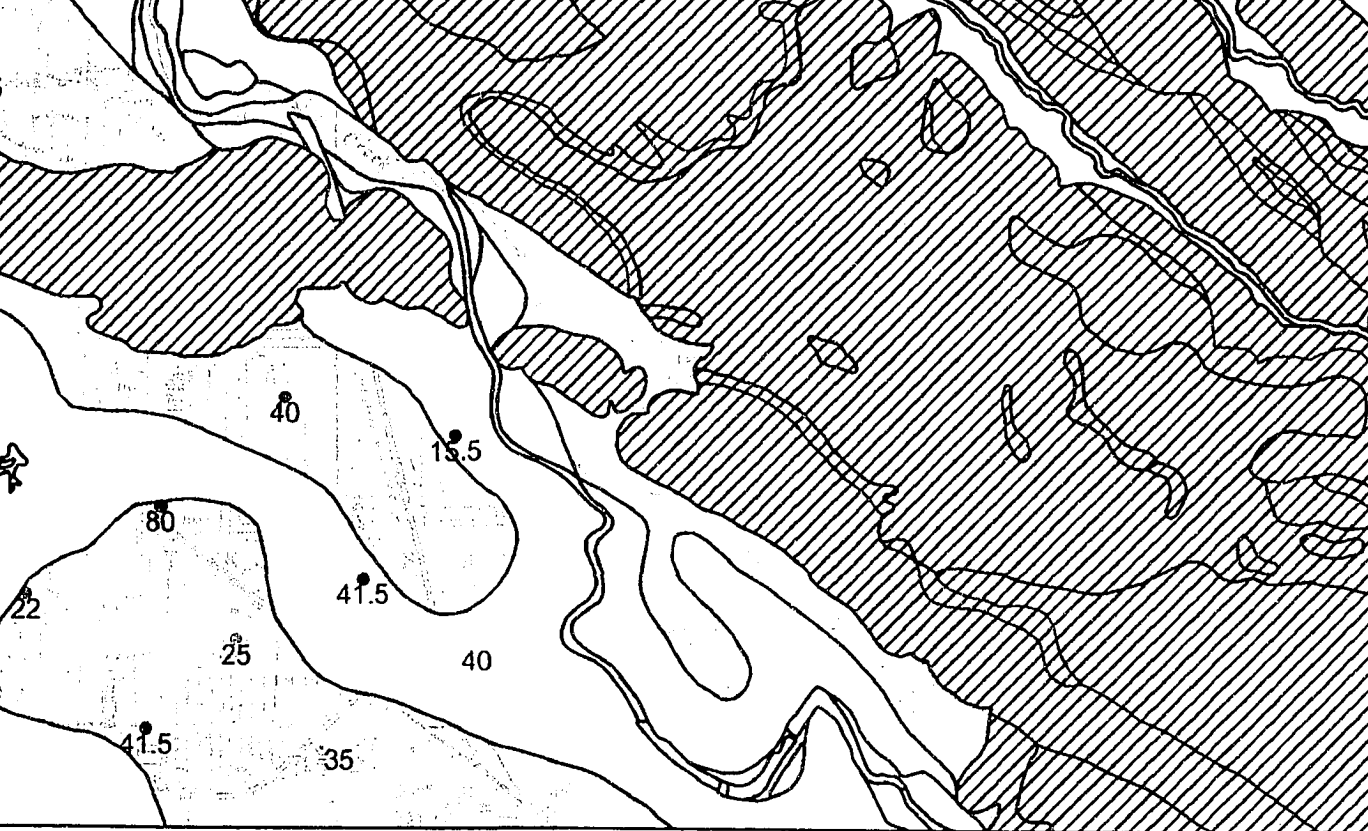
Volumetric strain summed for boring

- 4% to 10%
- 3% to 4%
- 2% to 3%
- 1% to 2%
- 0% to 1%

36 Boring total depth

Geologic Map Units Grouped by Median Volumetric Strain

- HIGH: afbm, Qhfe
- MODERATE-HIGH: a
- MODERATE: ac, Qhly
- LOW: Qf
- VERY LOW: Qhc, Qhf
- BEDROCK
- WATER
- Quaternary units in the boring data collected: Qt, Qa, Qpb, Qpa, Q



37° 15'


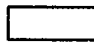
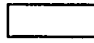

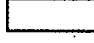
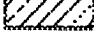
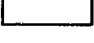

121° 45'

Volumetric strain summed for boring

- 4% to 10%
- 3% to 4%
- 2% to 3%
- 1% to 2%
- 0% to 1%

36 Boring total depth

Geologic Map Units Grouped by Median Volumetric Strain

-  HIGH: afbm, Qhfe
-  MODERATE-HIGH: alf, Qhfy, Qhty
-  MODERATE: ac, Qhly, Qhff, Qhl, Qht
-  LOW: Qf
-  VERY LOW: Qhc, Qhf, Qfp
-  BEDROCK
-  WATER
-  Quaternary units in the study area for which no boring data collected: qq, Qhbm, Qhb, Qha, Ql, Qt, Qa, Qpb, Qpa, Qof, Qoa

NOTE TO USERS

Oversize maps and charts are microfilmed in sections in the following manner:

LEFT TO RIGHT, TOP TO BOTTOM, WITH SMALL OVERLAPS

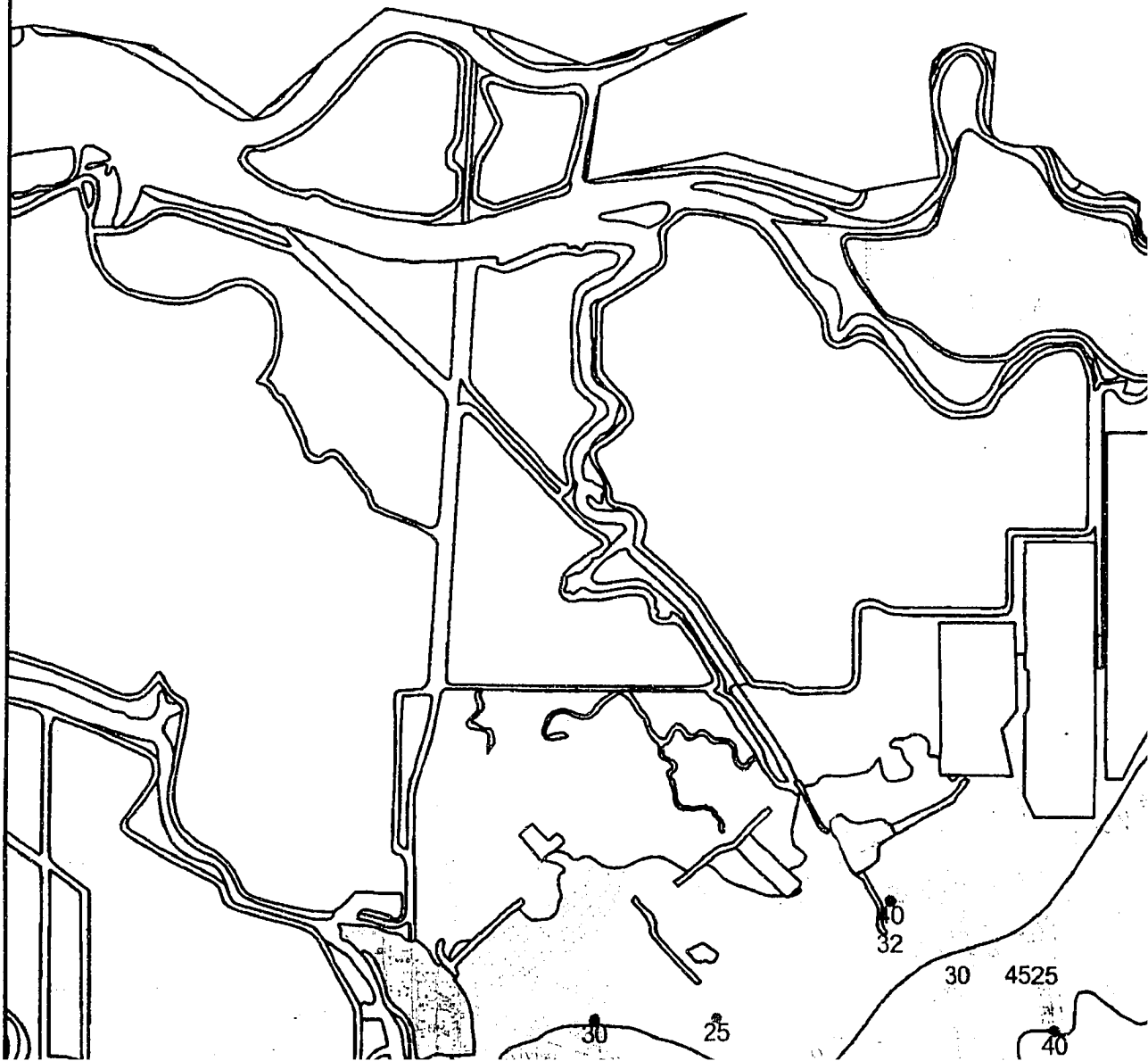
This reproduction is the best copy available.

UMI[®]

122° 00'

37° 30'

N

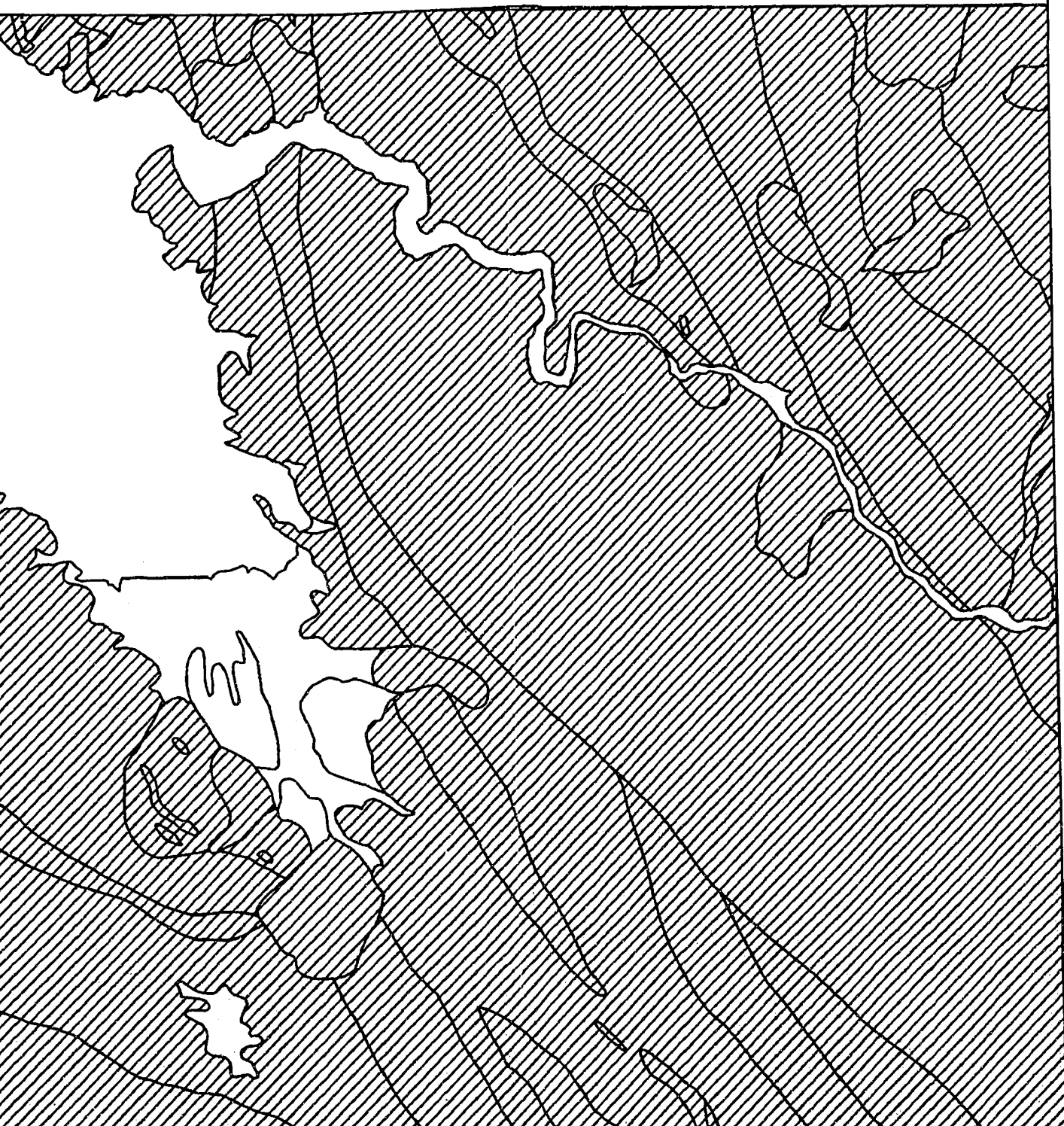


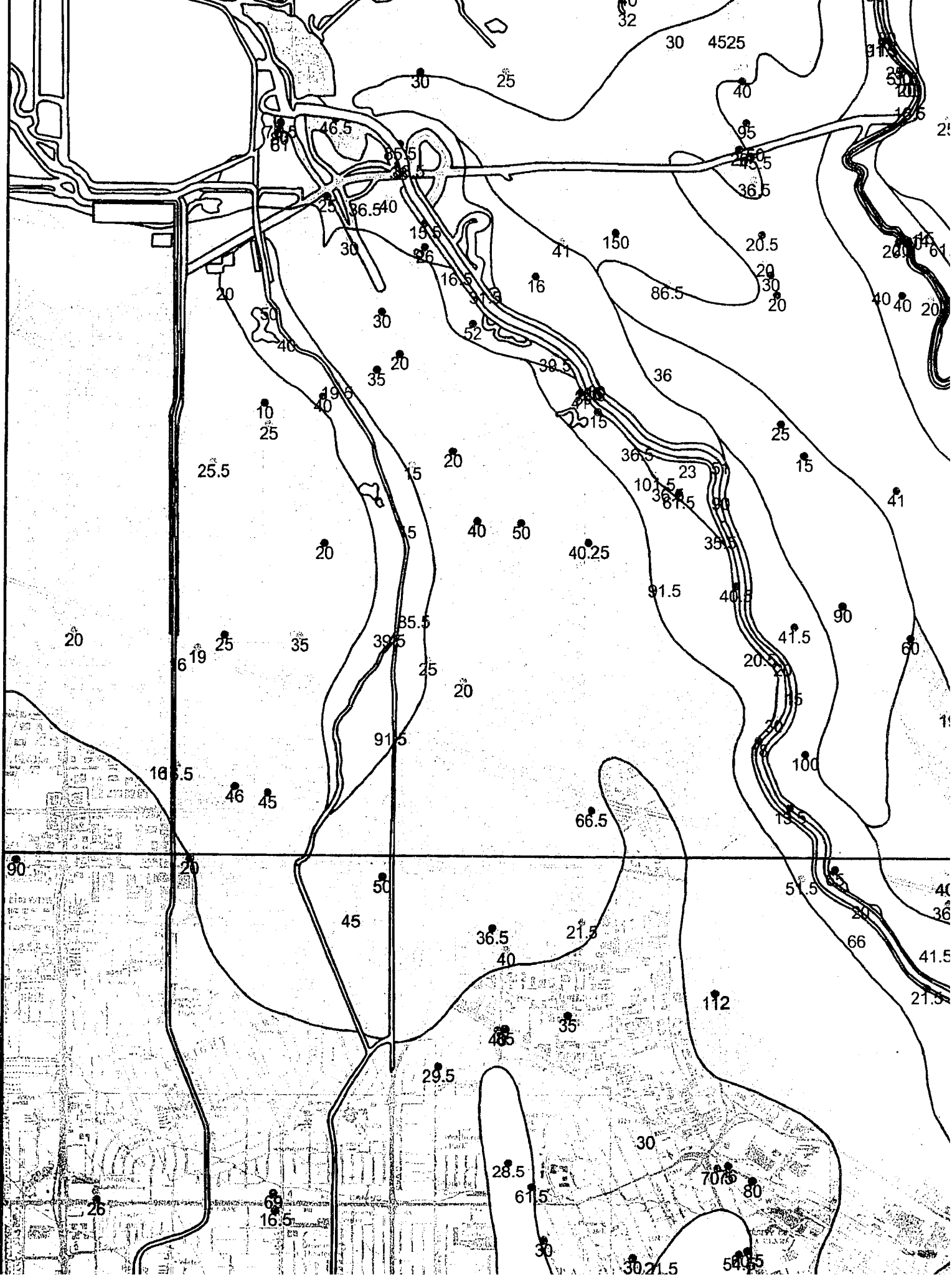
DE STUDY AREA



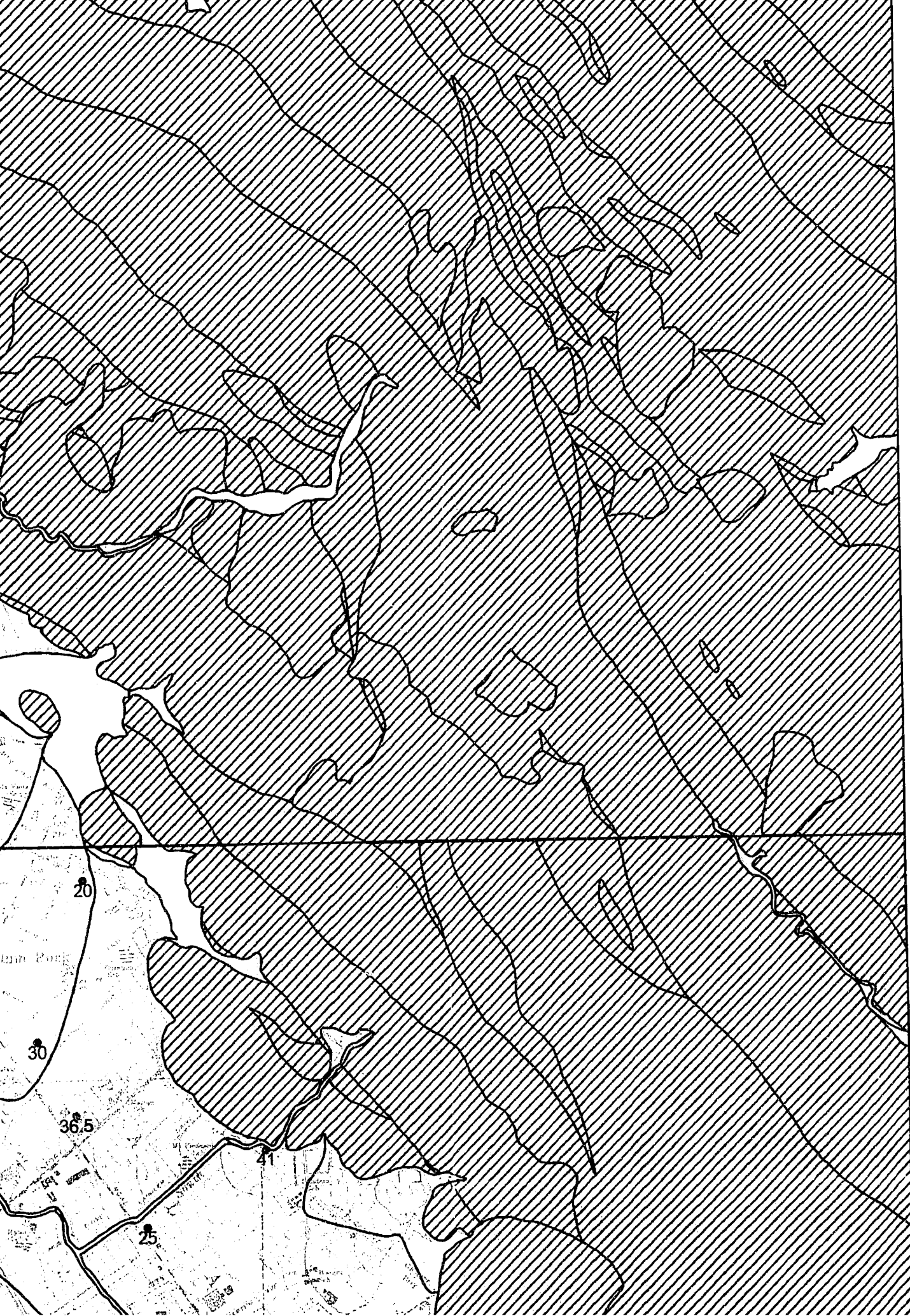
121° 45'
37° 30'

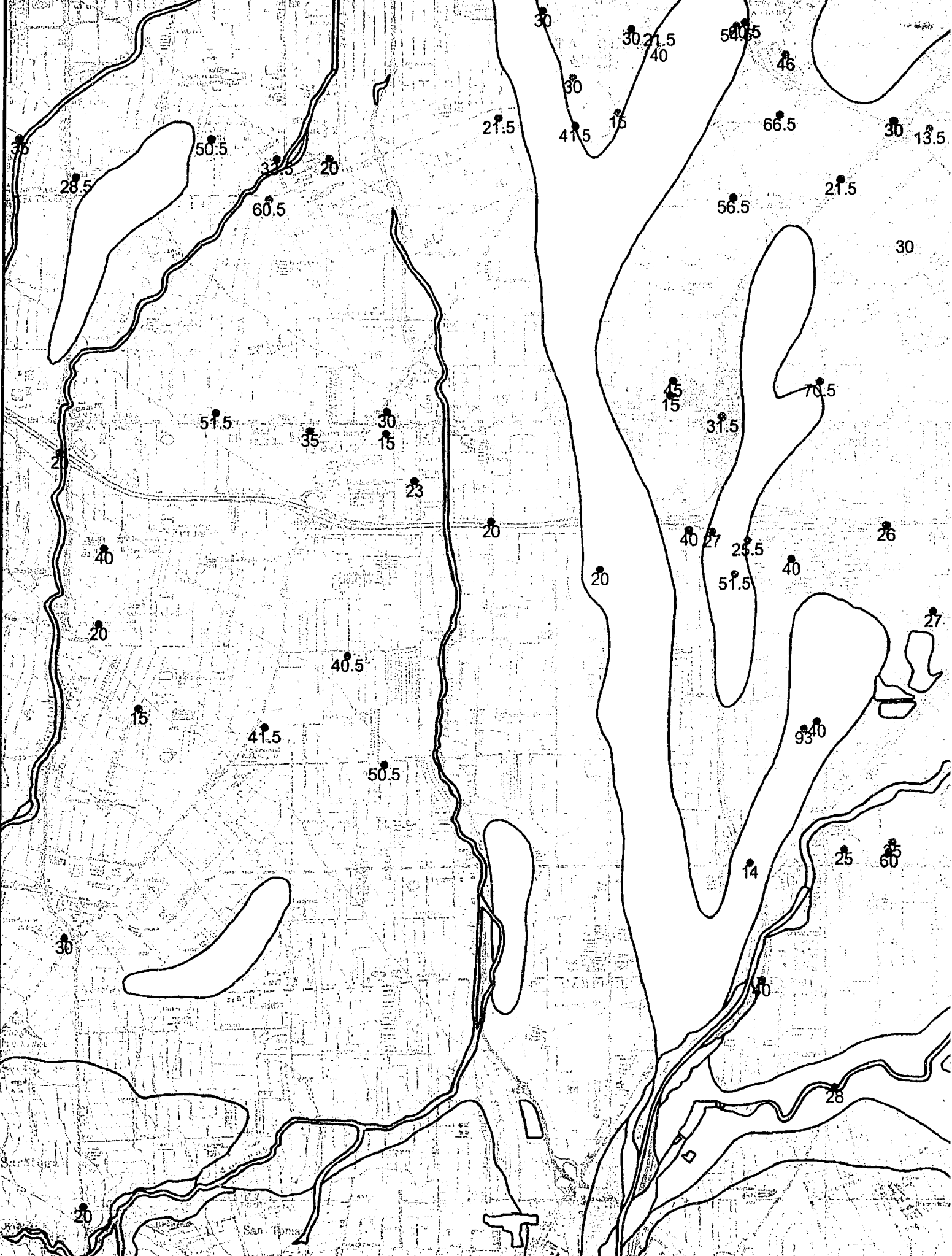
EA

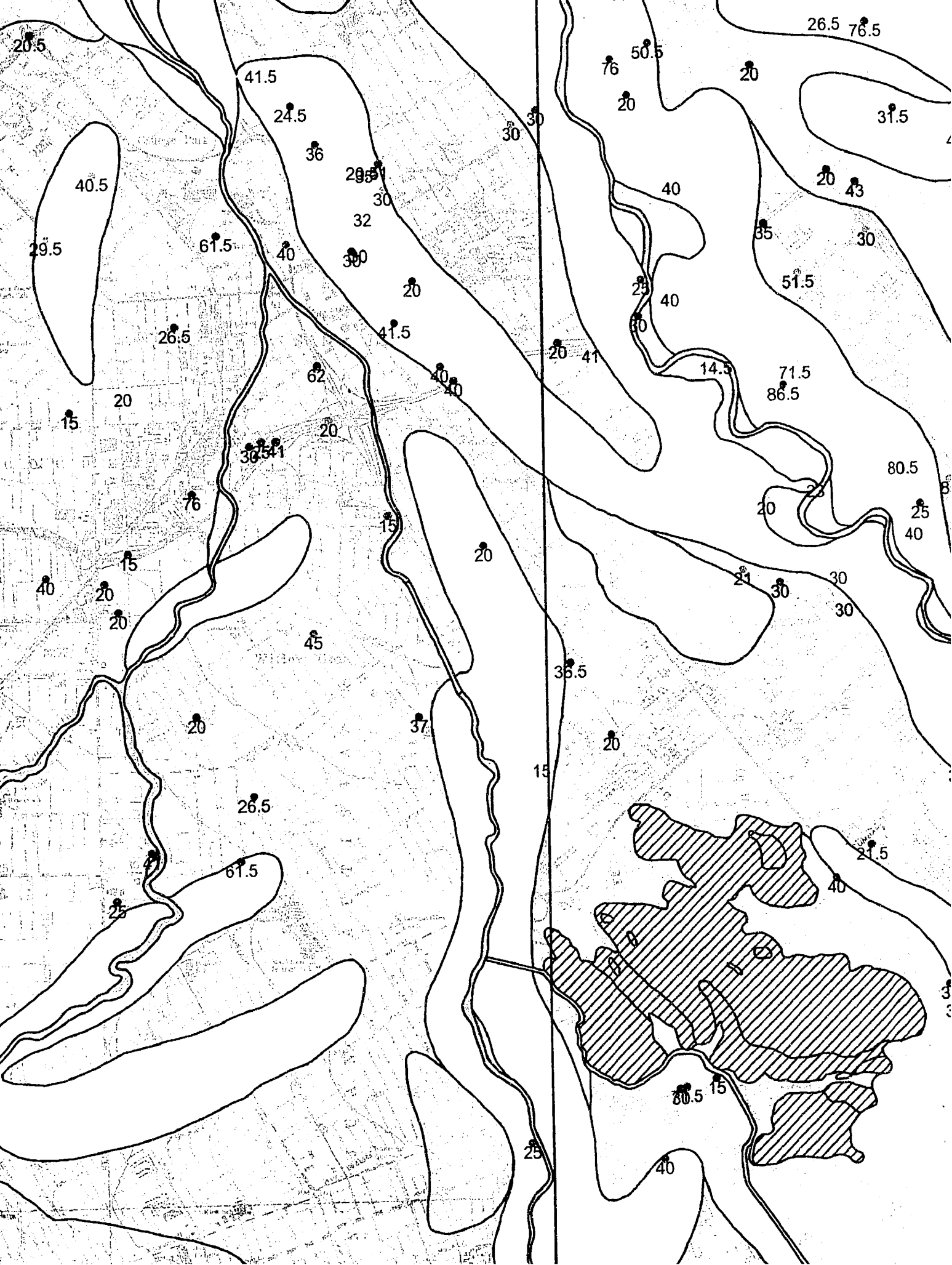


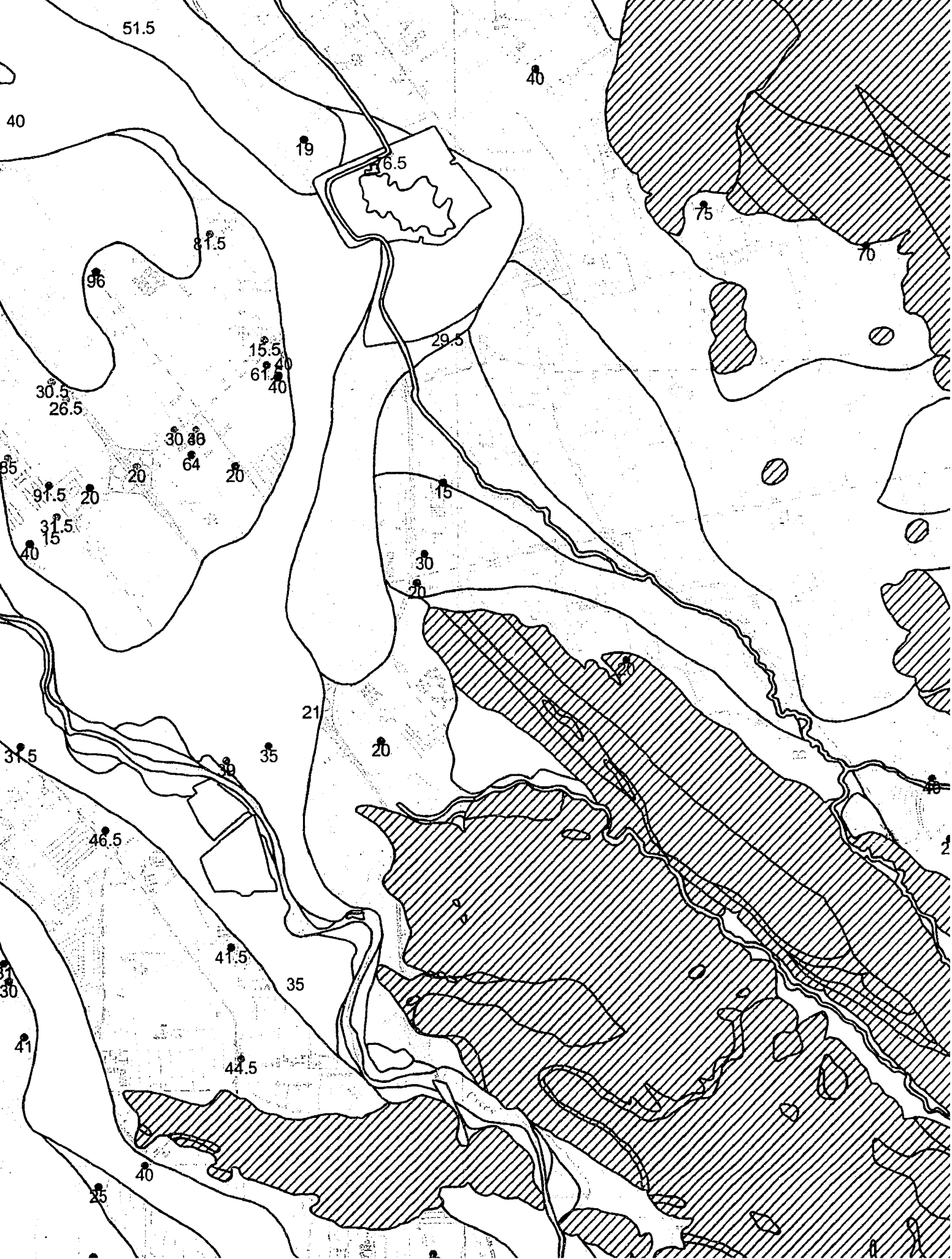


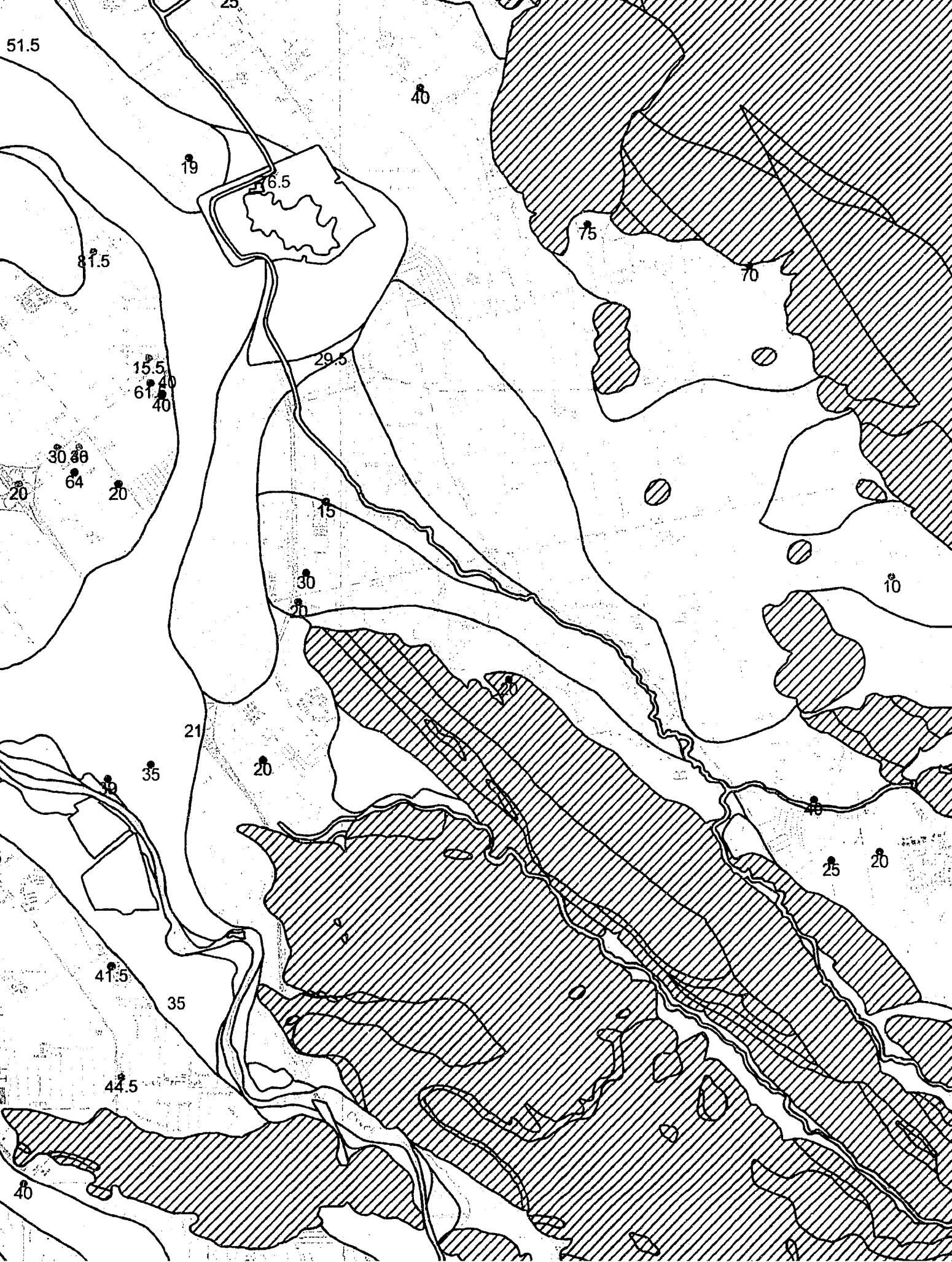


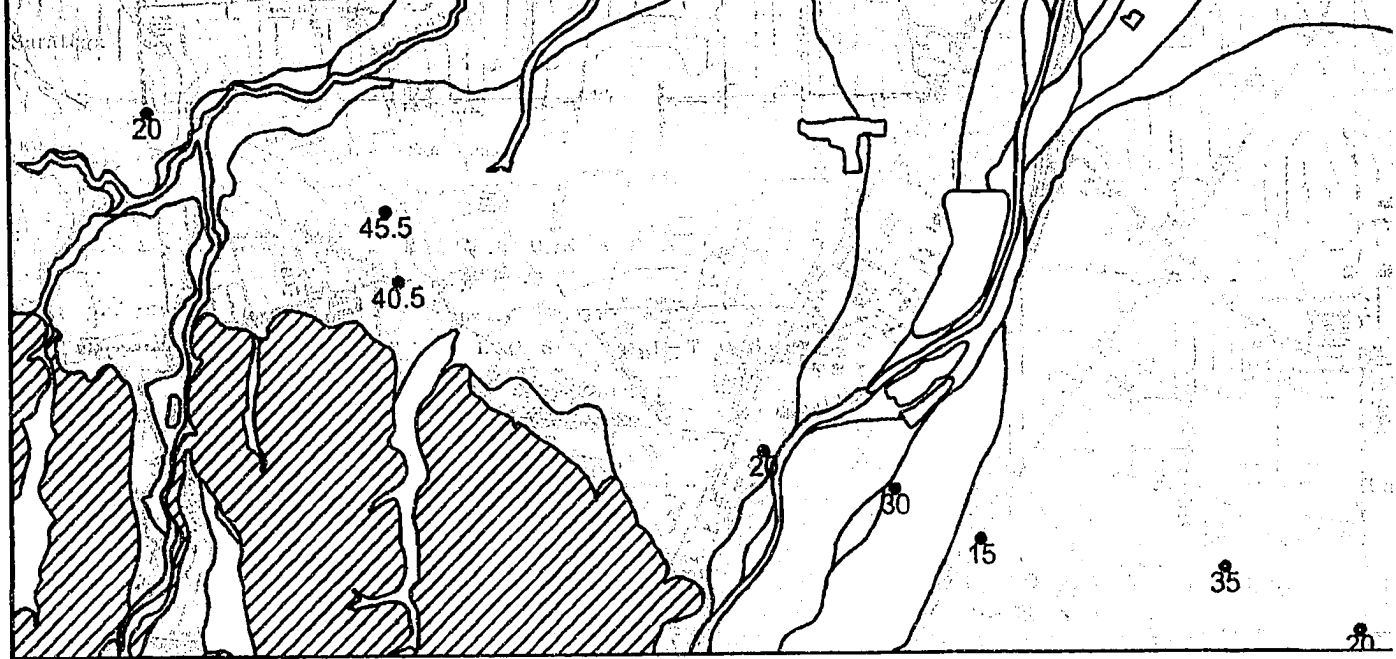












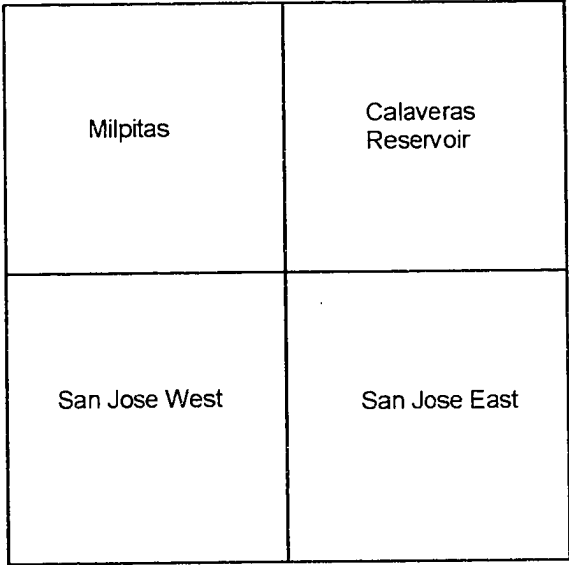
37° 15'

122° 00'

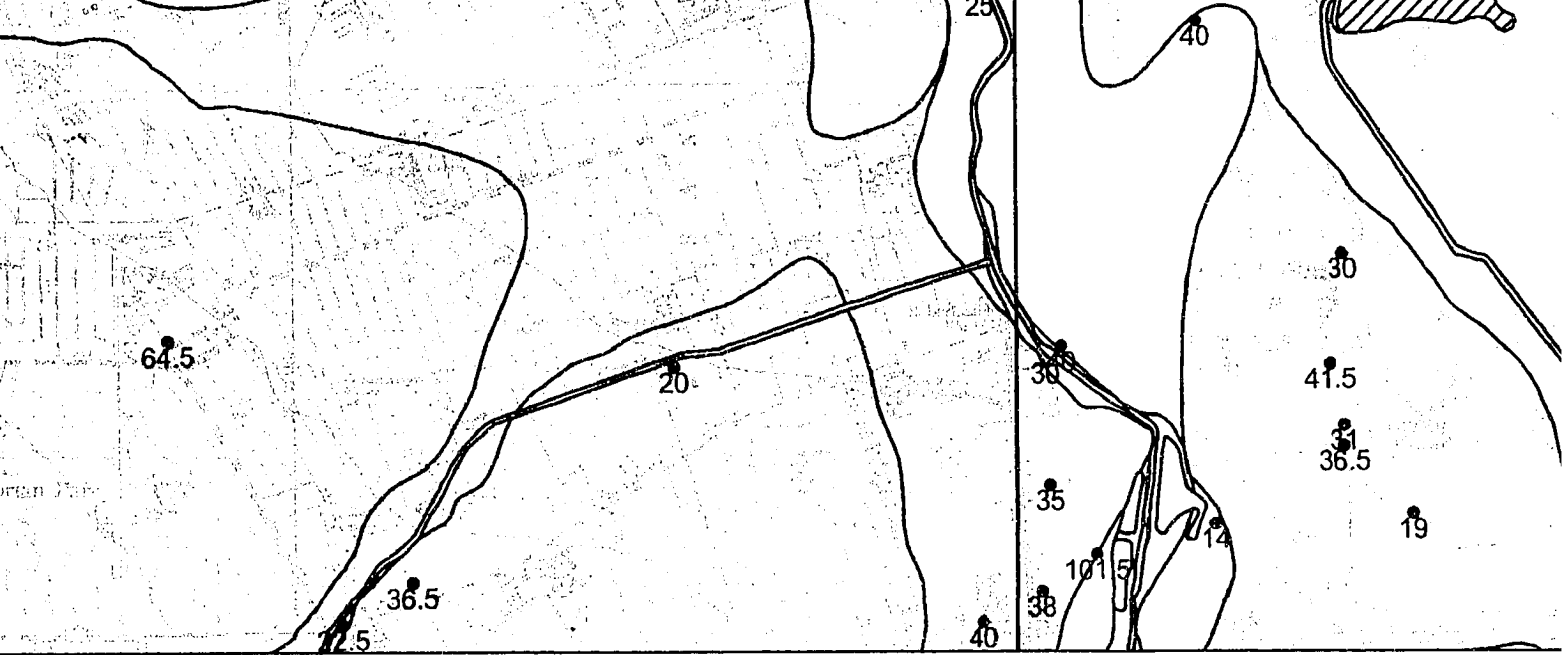
Milpitas base map prepared by the U. S. Geological Survey, 1961, photorevised 1980.
 Calaveras Reservoir base map prepared by the U. S. Geological Survey, 1961, photorevised 1980.
 San Jose East base map prepared by the U. S. Geological Survey, 1961, photorevised 1980.
 San Jose West base map prepared by the U. S. Geological Survey, 1961, photorevised 1980.

REFERENCE:

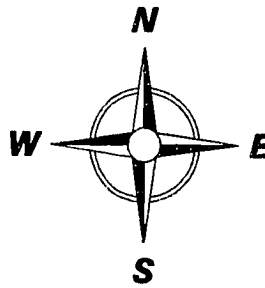
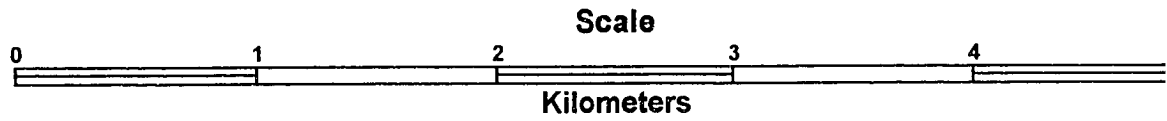
Quaternary geologic maps of the Milpitas, Calaveras Reservoir, San Jose East and San Jose West
 Quadrangles modified after Witter et al., (2006)

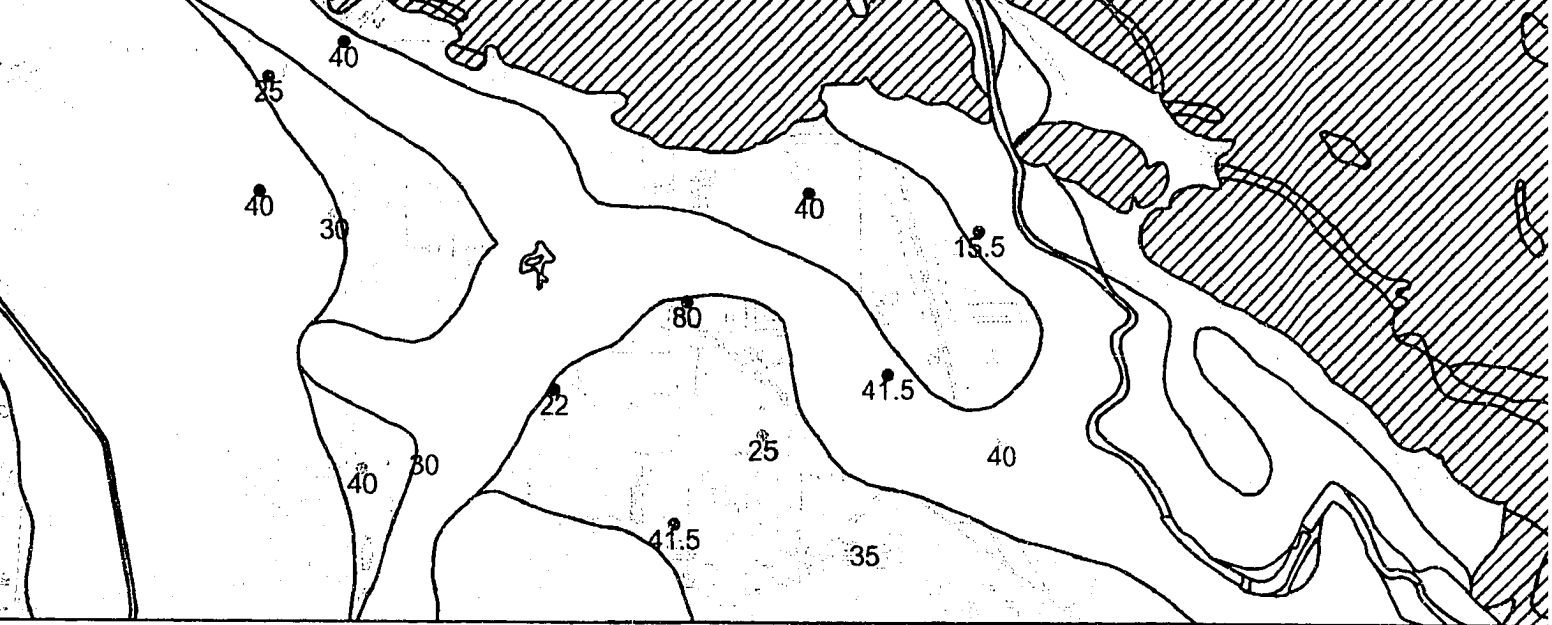


THESIS PLATE 7 - Shear Strain Summed for Each Boring and Geology



Shear Strain


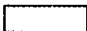
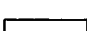
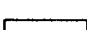








5

Shear strain summed for boring

Geologic Map Units Grouped by Median Shear Strain

•	40% to 50%		HIGH: afbm
•	30% to 40%		MODERATE-HIGH: Qhfe
•	20% to 30%		MODERATE: alf, ac, Qhfy, Qhly, Qhty, Qhl
•	10% to 20%		LOW: Qhff, Qht
•	0% to 10%		VERY LOW: Qhc, Qhf, Qf, Qpf
36 Boring total depth			Bedrock
			Water
			Quaternary units in the study area for which no boring data collected: qq, Qhbm, Qhb, Qha, Ql, Qt, Qa, Qpb, Qpa, Qof, Qoa.



Shear strain summed for boring

Geologic Map Units Grouped by Median Shear Strain

<ul style="list-style-type: none"> • 40% to 50% • 30% to 40% • 20% to 30% • 10% to 20% • 0% to 10% 	<ul style="list-style-type: none"> 	<ul style="list-style-type: none"> HIGH: afbm MODERATE-HIGH: Qhfe MODERATE: alf, ac, Qhfy, Qhly, Qhty, Qhl LOW: Qhff, Qht VERY LOW: Qhc, Qhf, Qf, Qpf
<p>36 Boring total depth</p>	<ul style="list-style-type: none"> 	<ul style="list-style-type: none"> Bedrock Water Quaternary units in the study area for which no boring data collected: qq, Qhbm, Qhb, Qha, Ql, Qt, Qa, Qpb, Qpa, Qof, Qoa.